TKK Dissertations 97
Espoo 2007

NOVEL MODELING AND CONTROL APPROACH FOR PERFORMANCE IMPROVEMENT OF AN INDUSTRIAL COPPER SOLVENT EXTRACTION PROCESS

Doctoral Dissertation

Tiina M. Komulainen

Helsinki University of Technology
Department of Chemical Technology
Laboratory of Process Control and Automation

TKK Dissertations 97
Espoo 2007

NOVEL MODELING AND CONTROL APPROACH FOR PERFORMANCE IMPROVEMENT OF AN INDUSTRIAL COPPER SOLVENT EXTRACTION PROCESS

Doctoral Dissertation

Tiina M. Komulainen

Dissertation for the degree of Doctor of Science in Technology to be presented with due permission of the Department of Chemical Technology for public examination and debate in Auditorium V1 at Helsinki University of Technology (Espoo, Finland) on the 30th of November, 2007, at 12 noon.

Helsinki University of Technology
Department of Chemical Technology
Laboratory of Process Control and Automation

Teknillinen korkeakoulu
Kemian tekniikan osasto
Prosessien ohjauksen ja automaation laboratorio

Distribution:
Helsinki University of Technology
Department of Chemical Technology
Laboratory of Process Control and Automation
P.O. Box 6100
FI - 02015 TKK
FINLAND
URL: http://kepo.tkk.fi/
Tel. +358-9-451 3852
Fax +358-9-451 3854
E-mail: tiina.komulainen@iki.fi

ISBN 978-951-22-9055-0
ISBN 978-951-22-9056-7 (PDF)
ISSN 1795-2239
ISSN 1795-4584 (PDF)
URL: http://lib.tkk.fi/Diss/2007/isbn9789512290567/

TKK-DISS-2370

Yliopistopaino
Helsinki 2007

ABSTRACT OF DOCTORAL DISSERTATION	HELSINKI UNIVERSITY OF TECHNOLOGY P.O. BOX 1000, FI-02015 TKK http://www.tkk.fi

Author Tiina Marjatta Komulainen

Name of the dissertation
Novel modeling and control approach for performance improvement of an industrial copper solvent extraction process

Manuscript submitted 21.5.2007	Manuscript revised 9.10.2007

Date of the defence 30.11.2007

☒ Monograph ☐ Article dissertation (summary + original articles)

Department KE
Laboratory Process control and automation
Field of research Process control
Opponent(s) Prof. Maria Teresa Carvalho and Prof. Aldo Cipriano
Supervisor Prof. Sirkka-Liisa Jämsä-Jounela
Instructor

Abstract

More than 20% of the cathode copper is annually produced by copper leaching, solvent extraction and electrowinning processes. The focus in process technology has been on research and capital intensive development of the process equipment and chemicals. However, the financial benefits gained through an advanced control system would be significant. An advanced control system would maximize the total production and increase the fraction of the first quality copper cathodes by running the process closer to the optimal operating point, and by decreasing the variation in the key process variables. The lack of adequate dynamic process models for industrial applications has, to date, prevented the development of advanced process control systems. Therefore, the first aim of this thesis is to develop dynamic models to describe the behaviour of an industrial copper solvent process and to facilitate control system development. The second aim of this thesis is to develop an advanced control system for the copper solvent extraction process, and to verify that the performance and profitability of an industrial copper solvent extraction process can be significantly increased by utilizing the advanced process control system. In the process model, the mass transfer of copper in the mixer-settler units is described by means of dynamic, modified ideal mixing and plug flow models. The equilibrium value for the ideal mixing model is calculated on the basis of the steady state McCabe-Thiele diagram. The unit process models are combined according to the case plant flowsheet and implemented into a process simulator. Based on the process models, control hierarchy is developed. The optimization level consists of an optimization algorithm and the stabilizing control level consists of a single input-single output control strategy employing two PI controllers or, alternatively, a multi input-multi output control strategy using the model predictive control (MPC). The dynamic models are tested with two data sets representing the normal operation of the industrial case copper solvent extraction plant. The models follow the output copper concentration trends smoothly for the major input changes in the flow rates and copper concentrations, and the residuals between the simulated data and the industrial measurements are sufficiently small, on average 1-3%. The performance of the control system is tested in simulation environment using the industrial data as input. Compared to manual control, the variation in the rich electrolyte copper concentration was decreased by 70 – 80 % with the PI controllers and 80 – 90 % with the model predictive controller. The copper mass production was increased by about 3 – 5 % with both control strategies. The modeling and control results are very encouraging for the further testing of the control system in an industrial copper solvent extraction plant.

Keywords Process Modeling, Process Control, Industrial Application, Copper Solvent Extraction, Hydrometallurgy, Model Predictive Control (MPC), Optimization, Simulation.

ISBN (printed) 978-951-22-9055-0	ISSN (printed) 1795-2239
ISBN (pdf) 978-951-22-9056-7	ISSN (pdf) 1795-4584
Language English	Number of pages 188

Publisher Helsinki University of Technology, Laboratory of Process Control and Automation

Print distribution Helsinki University of Technology, Laboratory of Process Control and Automation

☒ The dissertation can be read at http://lib.tkk.fi/Diss/2007/isbn9789512290567

VÄITÖSKIRJAN TIIVISTELMÄ	TEKNILLINEN KORKEAKOULU PL 1000, 02015 TKK http://www.tkk.fi

Tekijä Tiina Marjatta Komulainen

Väitöskirjan nimi
Novel modeling and control approach for performance improvement of an industrial copper solvent extraction process

Käsikirjoituksen päivämäärä 21.5.2007	Korjatun käsikirjoituksen päivämäärä 9.10.2007

Väitöstilaisuuden ajankohta 30.11.2007

☒ Monografia	☐ Yhdistelmäväitöskirja (yhteenveto + erillisartikkelit)

Osasto	KE
Laboratorio	Prosessien ohjauksen ja automaation laboratorio
Tutkimusala	Prosessien ohjaus
Vastaväittäjä(t)	Prof. Maria Teresa Carvalho ja Prof. Aldo Cipriano
Työn valvoja	Prof. Sirkka-Liisa Jämsä-Jounela
Työn ohjaaja	

Tiivistelmä

Katodikuparista vuosittain yli 20 % tuotetaan kuparin liuotus - uutto - elektrolyysi - menetelmällä. Prosessiteknologian painopisteenä on ollut prosessilaitteiden ja -kemikaalien kehittäminen, joka vaatii paljon tutkimusta ja runsaasti taloudellista pääomaa. Kehittyneitä säätömenetelmiä soveltamalla voitaisiin saavuttaa merkittäviä taloudellisia hyötyjä kuluttamalla huomattavasti vähemmän resursseja. Kehittyneellä säätöjärjestelmällä kuparin uuttoprosessin tuotantoa sekä parhaan katodilaadun osuutta koko tuotannosta voidaan kasvatettaa, koska prosessia voidaan ajaa lähempänä optimaalista operointipistettä ja prosessin laatuparametrien vaihtelua voidaan pienentää. Kuparin uuttoprosessille soveltuvien dynaamisten mallien puute on tähän mennessä estänyt ylemmän tason säätöjärjestemien kehityksen.

Tämän työn ensimmäinen tavoite oli kehitettää dynaaminen malli, joka kuvaa teollisen kuparin uuttoprosessin käyttäytymistä ja mahdollistaa säätöjärjestelmän kehityksen. Työn toisena tavoitteena oli kehittää säätöjärjestelmä ja todistaa että sen avulla kuparin uuttoprosessin tehokkuutta ja tuottavuutta voidaan merkittävästi parantaa.

Dynaaminen prosessimalli perustuu kuparin massansiirrolle vesi- ja orgaanisen faasin välilla sekoitus-selkeytys-prosessilaitteissa. Sekoittimen malli perustuu modifioituun ideaalisekoitin malliin, jossa tasapaino lasketaan McCabe-Thiele diagrammista. Selkeyttimen malli perustuu tulppavirtaukseen. Prosessimalli laadittiin yhdistelemällä sekoitin-selkeytin-yksikkömalleja teollisen sovellusprosessin virtauskaavion mukaisesti. Tämän mallin perusteella implementoitiin prosessisimulaattori. Prosessimalliin perustuen prosessille kehitettiin säätöhierarkia, joka koostuu optimointitason optimointialgoritmista ja stabiloivan säädön tason yksikkösäätöstrategiasta (PI- ja myötäkytkentäsäätimet) tai monimuuttujasäätöstrategiasta (MPC-säädin). Dynaamisten malleilla saatua simulointidataa verrattiin teolliseen prosessidataan hyvin tuloksin. Simuloitu data seurasi kuparikonsentraatioiden ja virtausten vaihteluista johtuvia muutoksia ja keskimääräinen ero simuloidun ja oikean datan valilla oli noin 1-3% testatuissa kahdessa datajoukossa.

Säätösysteemiä testattiin prosessisimulaattorilla, jonka sisääntuloina käytettiin prosessidataa. Manuaaliseen säätöön verrattuna, rikkaan elektrolyytin kuparikonsentraation vaihtelu pienentyi 70-80% PI-säätimillä ja 80-90% MPC-säätimellä. Kuparin tuotanto kasvoi 3-5% käyttämällä kumpaakin säätöstrategiaa. Mallitus - ja säätötulokset luovat vahvan pohjan säätösysteemin testaukselle teollisella kuparin uuttolaitoksella

Asiasanat Prosessien mallitus, Prosessien ohjaus, Teollinen sovellus, Kuparin Uuttoprosessi, Hydrometallurgia, Malli Prediktiivinen Säätö (MPC), Optimointi, Simulointi.

ISBN (painettu) 978-951-22-9055-0	ISSN (painettu) 1795-2239
ISBN (pdf) 978-951-22-9056-7	ISSN (pdf) 1795-4584
Kieli Englanti	Sivumäärä 188

Julkaisija Teknillinen korkeakoulu, Prosessien ohjauksen ja automaation laboratorio

Painetun väitöskirjan jakelu Teknillinen korkeakoulu, Prosessien ohjauksen ja automaation laboratorio

☒ Luettavissa verkossa osoitteessa http://lib.tkk.fi/Diss/2007/isbn9789512290567

PREFACE

The research work presented in this thesis has been carried out in the Laboratory of Process Control and Automation, Helsinki University of Technology, between August 2003 and November 2006. I would like to thank my supervisor Sirkka-Liisa Jämsä-Jounela for encouraging me to start PhD studies, giving me the opportunity to work independently in an industrially related research project, and for her help with the writing. Professor Raimo Ylinen and Dr. Mats Nikus are thanked for all their valuable advice and discussions.

I'm very grateful to Professor Frank J. Doyle III for welcoming me into his research group in University of California at Santa Barbara. Professor Doyle's supervision and collaboration with the group was really inspiring and productive. I wish to thank the group for the great atmosphere during the unforgettable year (2005).

I would like to thank the pre-examiners of this thesis, Prof. Aldo Cipriano and Prof. Erkki Paatero for their thorough review of the thesis and for their stimulating comments.

The thesis work was done in collaboration with Outotec Oy. I would like to thank Ari Rantala, Ville Suontaka and Dr. Kari Saloheimo for their support with the project and help with the industrial aspects of the work. I wish to thank the personnel of Phelps Dodge Morenci Inc. for great co-operation during my visits on the plant.

The thesis work was mainly funded by the Finnish Graduate School in Chemical Engineering (GSCE). Additional funding for the research in UCSB was provided by Jenny and Antti Wihuri foundation, Tekniikan Edistämissäätiö, Alexander and Lucie Lampén foundation and the Foundation of Helsinki University of Technology. All these contributions are gratefully acknowledged.

I would like to thank all my colleagues in "KEPO labra", especially Jerri Kämpe, Antti Remes, Ville Suontaka and Nikolai Vatanski, for keeping up the spirits through thick and thin. I warmly thank my parents, siblings and friends for all their support and caring over these years. Finally, my special thanks go to my fiancé Espen Storkaas for keeping a smile on my face and encouraging me to finish this thesis.

Oslo 25.10.2007

Tiina Komulainen

ABSTRACT

More than 20% of the cathode copper is annually produced by copper leaching, solvent extraction and electrowinning processes. The focus in process technology has been on research and capital intensive development of the process equipment and chemicals. However, the financial benefits gained through an advanced control system would be significant. An advanced control system would maximize production by running the process closer to the optimal operating point, and increase the production of the first quality copper cathode by decreasing the variation in key process variables. The lack of adequate dynamic process models for industrial applications has, to date, prevented the development of advanced process control systems.

Therefore, the first aim of this thesis is to develop dynamic models to describe the behaviour of an industrial copper solvent process and to facilitate control system development. The second aim of this thesis is to develop an advanced control system for the copper solvent extraction process, and to verify that the performance and profitability of an industrial copper solvent extraction process can be significantly increased by utilizing the advanced process control system.

In the process model, the mass transfer of copper in the mixer-settler units is described by means of dynamic, modified ideal mixing and plug flow models. The equilibrium value for the ideal mixing model is calculated on the basis of the steady state McCabe-Thiele diagram. The model utilizes industrial online and offline measurements. The unit process models are combined according to the case plant flowsheet. Based on the process models, a control hierarchy is developed for the case copper solvent extraction process. The optimization level in the hierarchy consists of an optimization algorithm that maximizes the production of the copper solvent extraction process and provides setpoints for the stabilizing control level. The stabilizing control level consists of a single input-single output control strategy employing two PI controllers or, alternatively, a multi input-multi output control strategy using the model predictive control (MPC).

The dynamic models are tested by comparing the simulated data with the industrial data. The controller performances are tested for setpoint tracking and disturbance rejection in the simulation environment with step input changes. The benefits of the control system are assessed by comparing the variation in the controlled variables and the total copper production to the data collected from the process under manual control.

The dynamic models are tested with two data sets representing the normal operation of the industrial case copper solvent extraction plant. The models follow the output copper concentration trends smoothly for the major input changes in the flow rates and copper concentrations, and the residuals between the simulated data and the industrial measurements are sufficiently small. The average absolute error is 1-3% of the mean value of the output copper concentrations.

The performance of the control system for setpoint tracking and disturbance rejection is very good. As expected, the model predictive controller performs better than the PI controllers. The disturbance rejection capabilities are further improved by adding four feedforward compensators to the control strategies. Compared to manual control, the variation in the rich electrolyte copper concentration was decreased by 70 – 80 % with

the PI controllers and 80 – 90 % with the model predictive controller. The copper mass production was increased by about 3 – 5 % with both control strategies.

The modeling and control results are very encouraging for the further testing of the control system in an industrial copper solvent extraction plant.

TABLE OF CONTENTS

LIST OF THE SYMBOLS

a_{ij}, b_{ij},c_{ij}	parameters of the transfer function model	
a,b	parameters of the operating line	
A,B	parameters of extraction equilibrium isotherm	
C,D	parameters of stripping equilibrium isotherm	
A_i,B_i	parameters of linearized extraction equilibrium isotherm, i=E1,E2,EP	
c	Concentration of copper if not otherwise specified	(g/l)
c^*	Equilibrium concentration	(g/l)
c^{aq}	Copper concentration of aqueous solution	(g/l)
c^{org}	Copper concentration of organic solution	(g/l)
cf_i	recycle correction coefficient, i=E1,E2,EP,S	
f	general function	
F	Flow rate	(m^3/min)
g_m	percentage of the entrained flow between the units	
g_s	percentage of the well mixed volume in the settler	
$G_{p,tot}$	total transfer function of the process	
I	electric current	(A)
k_f	rate constant for the forward reaction	
k_r	reaction rate constant	
k^{aq}, k^{org}	phase specific film theory coefficients	
K_i	mass transfer coefficient, i=E1,E2,EP,S	(1/min)
m	mass	(kg)
M_{Cu}	atomic weight of copper	(g/mol)
M_i	matrix	
N	number of samples	
P	profit function of the optimization problem	
r_i	steady state gain of a transfer function	
s	Laplace transform variable	
t	time	(min)
V	volume	(m^3)
V_m	volume of the mixer	(m^3)
V_s	volume of the settler	(m^3)
V_{tank}	volume of the organic storage tank	(m^3)
w_i	steady state gain of a transfer function	
X,x	theoretical equilibrium value of the aqueous copper concentration	(g/l)

Y,y	theoretical equilibrium value of the organic copper concentration (g/l)
$y(t)$, $u(t)$	output and input of a process at time t
Y_{meas}	measured value
Y_{model}	model prediction
z	ion charge

α_i	Extraction / stripping efficiency, i=E1,E2,EP,S
α_d	dead time of the controlled variable-disturbance variable pair (min)
α_p	dead time of the controlled variable–manipulated variable pair (min)
β_1 , β_2	the organic to aqueous flow ratio constraints
ε	estimation error
η	current efficiency
θ	time delay of the organic phase (min)
δ	time delay of the aqueous phase (min)
κ_i	Equilibrium constant, i=E1,E2,EP,S
τ_d	dead time of the controlled variable-disturbance variable pair (min)
τ_p	dead time of the controlled variable–manipulated variable pair (min)
ν	phase hold up (m^3)
ω	frequency (1/s)
ζ, φ, ψ, ω	constants of the equilibrium isotherm parameters

aq	aqueous
el	electrolyte
entr	entrainment
in	into a mixer
int	interface between aqueous and organic solutions
max	maximum value
min	minimum value
o, op	operating point
opt	optimum value
org	organic
out	out of mixer / unit
outs	out of settler

ABBREVIATIONS

AAE	average absolute error
acid	acidity of the electrolyte solution
BO	Barren organic solution
c(BO)	copper concentration of the barren organic solution
c(LE)	copper concentration of the lean electrolyte solution
c(LO)	copper concentration of the loaded organic solution
c(PLS)	copper concentration of the pregnant leach solution
c(Raff)	copper concentration of the raffinate solution
c(RE)	copper concentration of the rich electrolyte solution
CV	controlled variable
DP1,DP4	operating points of the industrial process
DV	disturbance variable
E	extraction step
E1,E2,EP	Series 1 and 2 and parallel extraction steps
E1S,E2S,E1P	Series 1 and 2 and parallel extraction steps
EW	electrowinning
F(LE)	flow rate of the electrolyte solution
F(LO)	flow rate of the organic solution
F(PLS)	flow rate of the pregnant leach solution
FB	feedback
FF	feedforward
FOPTD	first order plus time delay model
IAE	integral of the absolute error index
ISE	integral of the square error index
LE	Lean electrolyte solution
LO	Loaded organic solution
MIMO	Multi input – multi output
MPC	Model predictive control
MV	manipulated variable
OL	open loop
pH	pH level of the pregnant leach solution
PI	PI (proportional, integral) controller
PID	PID (proportional, integral, derivative) controller
PLS	Pregnant leach solution
R	reagent molecule in acid form

Raff	Raffinate solution of the extraction step
RaffS	Raffinate solution from series extraction step
RaffP	Raffinate solution from parallel extraction step
RE	Rich electrolyte solution
RGA	relative gain array method
S/ S1H	Stripping step
SISO	single input – single output
SS	state space model
SX	solvent extraction
TF	transfer function model
vol	reagent volume percent in the organic solution

1 INTRODUCTION

Copper (Cu) and its alloys are widely utilized in a great variety of industrial machinery and equipment, infrastructure tubes and cables, and a range of consumer products such as cars and cell phones. Copper mainly occurs in copper-iron sulphide and copper sulphide mineral form. The largest producers of copper ore are Chile, the USA, Indonesia, Peru, Australia, Russia and China. (Moskalyk and Alfantazi, 2003, Norton and Leahy, 2006)

The world production of copper in 2004 was about 15.800 metric tons, of which 88 % was from primary copper refining and 12% from the treatment of copper-containing scrap. The main refining options are hydrometallurgical and pyrometallurgical processes. Currently, around 20 % of the copper ores are processed by hydrometallurgical methods, with copper cathode production accounting for over 2.700 metric tons annually. The largest producers of copper by leaching, solvent extraction and electrowinning processes are Chile (1.636 metric tons), the USA (584 metric tons), Peru (167 metric tons) and Zambia (83 metric tons) (Edelstein 2004)

Hydrometallurgical treatment is preferred for oxidized copper ores such as cuprite (Cu2O) and low grade secondary ores such as chalcocite (Cu2S). In the future, the most common copper ore, chalcopyrite (CuFeS2), can also be industrially processed by hydrometallurgical methods with improved leaching techniques, such as pressure leaching and bio-oxidation leaching. The oxidized copper ores are found in South America, the southwest of North America, Australia and Southern Africa. A typical hydrometallurgical processing chain for copper ore consists of leaching, solvent extraction and electrowinning. Copper rich slag from other metallurgical processes can also be treated by hydrometallurgical methods. (Habashi, 1999, Seward, 1999, Kordosky, 2002, Munnik et al., 2003, Rydberg et al., 2004, Hyvärinen and Hämäläinen, 2005).

The importance of hydrometallurgical copper production is increasing strongly: between 2000 and 2004 hydrometallurgical copper production increased in Chile by 19%, in the USA by 5%, in Peru by 31% and in Zambia by 27%. Since the industrial production of copper by the leaching-solvent extraction and the electrowinning process started in the USA in around 1970, the proportion of hydrometallurgical copper production out of the total mined copper production has increased from 1,2 % to 38% in 30 years. The reason for this is the depletion of the rich, copper ore bodies that provide suitable raw material for pyrometallurgical processing, and the tightening of environmental requirements which favour hydrometallurgical processing over pyrometallurgical processing. (Bartos, 2002, Kordosky, 2002, Edelstein 2004)

Therefore, the development of new technologies to increase the performance and profitability of industrial copper leaching, solvent extraction and electrowinning processes is very important. During the past decade, the development has focused has on process technology. The leaching efficiency has been increased by the new leaching processes, for example pressure leaching (Hyvärinen and Hämäläinen, 2005) and bioleaching. New chemicals and equipment have also enhanced the performance of the solvent extraction and electrowinning processes. (Habashi, 1999, Kordosky, 2002).

However, the major challenge in the field of copper leaching-solvent extraction-electrowinning, the development of an advanced control system for industrial plants,

has still not been resolved (Bergh et al., 2001, Bergh and Yianatos, 2001, Jämsä-Jounela, 2001, Hodouin et. al., 2001). Basic control level PID controllers and basic measurements, possibly with online copper and impurity concentration analyzers, are currently used in most plants (Flintoff, 1993, Hughes, D., Saloheimo, K., 2000, Bergh and Yianatos, 2001). However, the lack of suitable dynamic models for industrial applications has prevented the development of advanced process control systems for the copper solvent extraction process. A considerable amount of work was carried out on the modeling laboratory-scale solvent extraction mixer-settler cascades in the 1970s and 1980s but, due to computational restrictions and inadequate industrial online measurements, model development did not reach the stage of industrial applications (Wilkinson and Ingham, 1983, Ingham et al., 1994). Recently, Aminian et al. (2000) published a steady-state model for a copper solvent extraction and electrowinning pilot plant, and Komulainen et al. (2005, 2006) a dynamic model for an industrial copper solvent extraction process.

The primary control aims are the maximization of production, rejection of disturbances in the leach solution copper concentration and pH level, a reduction of process variation, and fast adaptation to the most optimal operating point. An advanced control system with higher level optimizer should be developed in order to meet these aims.

Due to the long time delays and complex interactions in the copper solvent extraction-electrowinning process, one possible multi-input multi-output (MIMO) approach would be model predictive control (MPC). MPC is effective in handling time delays and constraints, and the future process outputs, calculated on the basis of the process model, can be easily visualized for the process operators. MPC is widely used in several application areas in the process industries, including the refining, chemical, and papermaking industries (Qin and Badgwell, 2003). MPC applications have recently emerged in the metal and mineral industries, for example for the control of a flotation bank (Hodouin et al., 2000) and the control of a pilot flotation column (Nunez et. al. 2006).

The economic benefits of maximizing the total copper production and minimizing the production costs by process control methods would be significant for industrial copper solvent extraction plants. Assuming that the control system does not increase production costs and the copper price is 1,67$/lbs (average LME 2005), a production increase of 5% would be equivalent to 60 million dollars per year for a copper solvent extraction-electrowinning plant with an annual production of 365000 tonnes.

1.1 Research problem and asserted hypothesis

The production of copper by leaching, solvent-extraction and electrowinning processes is increasing considerably due to the depletion of rich copper ore bodies and the tightening of environmental restrictions. Since industrial utilization of the technique began in the late 1960s, process technology development has focused on the process chemicals and equipment. Industrial plants do have basic level automation systems but, to date, advanced process control systems for industrial copper solvent extraction processes have not been reported in the literature. However, the financial benefits gained with an advanced control system would be considerable. The use of process control methods in copper solvent extraction-electrowinning plants would maximize the throughput, enable the process to be run closer to the optimal operating point, provide fast adaptation to the most optimal operating point, and reject

disturbances from the leach solution. Thus, an advanced process control system would maximize total production, increase the production of the best (grade A) quality copper cathodes, while minimizing the consumption of chemicals and energy per produced copper tonne.

The focus in this thesis is on performance improvement of the copper solvent extraction process through the utilization of process control methods. In order to investigate the benefits of a process control system for an industrial copper solvent extraction process, this thesis aims at developing dynamic process models and, based on these, an advanced control system for the copper solvent extraction process.

The hypotheses of the thesis are:

1. Dynamic process models utilizing only industrial online process measurements are able to describe the behaviour of an industrial copper solvent extraction process. The dynamic models enable development of an advanced process control system for the copper solvent extraction process.

2. Utilization of the advanced process control strategy significantly increases the performance and profitability of an industrial copper solvent extraction process compared to the utilization of a manual control strategy.

In order to prove the hypotheses, the following tasks have to be performed:

1. To develop static and dynamic models of the copper solvent extraction process.

2. To construct a process simulator on the basis of the process models, and to verify the modeling accuracy with industrial data.

3. To linearize the dynamic models, and to design the control strategy on the basis of these linear models.

4. To develop an optimization algorithm for maximizing the copper production

5. To design single input-single output (SISO) controllers for set-point tracking and disturbance rejection.

6. To design a multi input-multi output (MIMO) controller, and to compare the SISO and MIMO control strategies on set-point tracking and disturbance rejection.

7. To test the controller performance with industrial data. In order to assess the benefits of the control system, the controller performances in the simulation environment are compared to the data from an industrial plant under manual control.

The first and second tasks increase our understanding of the dynamic process phenomena, enable control system development, and provide a test bench for the control strategies. The third to sixth tasks provide the optimizer and the SISO and MIMO control strategies for the industrial copper solvent extraction process. The profitability and performance of the control system are asserted within the seventh task.

1.2 Scope and content of the thesis work

The scope of this thesis is dynamical modeling, simulation, optimization and control of an industrial copper solvent extraction plant.

An overview of hydrometallurgical processing, with the focus on industrial hydrometallurgical processing of copper with leaching, solvent extraction and electrowinning, is given in Chapter 2. A literature review of the state of the art in modeling and control of the industrial copper solvent extraction process is presented in Chapter 3.

The development of steady state and dynamic models that fulfill the requirements and restrictions of an industrial copper extraction plant, is described in Chapter 4. The dynamic model of a unit process consists of a plug flow part and a mixing part in which the equilibrium value is calculated on the basis of the steady state McCabeThiele diagram model. The dynamic models are illustrated with a copper solvent extraction process consisting of one mixer-settler pair for both extraction and stripping.

The industrial case process is introduced in Chapter 5. The current control strategy and a preliminary analysis of the plant operation are described. The dynamic models of the unit processes are combined according to the case process flow sheet in Chapter 6. The process simulator, based on this model structure, is also described at the end of Chapter 6.

In Chapter 7, the steady state model is parametrized with the case process offline data, and the accuracy of the dynamic models is verified against the industrial online measurements.

Linearization of the dynamic process models is presented in Chapter 8. The control hierarchy for the case copper solvent extraction process is developed in Chapter 9. The optimization algorithm and a single input-single output (SISO) control strategy and a multi-input-multi-ooutput control strategy are developed on the basis of the linearized dynamic models in Chapter 9.

The two PI-controllers and four feedforward compensators are tuned on the basis of the transfer function models, and the control performance for setpoint tracking and disturbance rejection is tested in the simulation environment in Chapter 10. The multi input-multi output (MIMO) controller is tuned on the basis of the state space models of the process, and the performance is compared to the SISO strategy in Chapter 11. The SISO and MIMO strategies are compared to manual operation of the case process in the simulation environment in Chapter 12.

Finally, the results of the dynamic modeling and control system development are summarized in Chapter 13. The conclusions and suggestions for future research are presented in Chapter 14.

The first hypothesis of the thesis is asserted in Chapters 4 to 7; and the second hypothesis in Chapters 8 to 12.

1.3 Contribution of the author

In order to meet the challenges of dynamic modeling and control development for an industrial copper solvent extraction process, a research project has been carried out in the Laboratory of Process Control and Automation at the Helsinki University of Technology. The author has worked under the supervision of Professor Sirkka-Liisa Jämsä-Jounela and Professor Francis J. Doyle III (during 2005 at the University of California at Santa Barbara). The results achieved in the project by the author are presented in this thesis.

This thesis presents novel dynamic modeling, a novel process simulator and novel control strategies for an industrial copper solvent extraction process. The three main contributions of the author are more specifically the following:

Development of the novel model combination for the industrial copper solvent extraction process. The dynamic model is based on plug flow and ideal mixing models, in which the equilibrium concentration is calculated on the basis of the plant specific McCabe-Thiele diagram. The dynamic models utilize only industrial measurements.

Development of the novel copper solvent extraction process simulator. The unit process models are combined in the simulation model according to the plant flow sheet. The parameters of the simulator are tuned with the offline process data. The simulator is verified with industrial data.

Development of the novel control strategies for the industrial copper solvent extraction process. The single input – single output and multi input- multi output control strategies and the optimization algorithm are developed on the basis of the linearized process models.

2 DESCRIPTION OF THE COPPER SOLVENT EXTRACTION PROCESS

The copper solvent extraction process is described in this chapter. First, the hydrometallurgical processing chain is briefly introduced in Section 2.1. Next, the copper leaching- solvent extraction- electrowinning process is described in Section 2.2. Finally, the most important physico-chemical phenomena, chemicals, equipment and plant configurations of the industrial copper solvent extraction processes are described in Section 2.3.

2.1 Hydrometallurgical processes

The role of hydrometallurgical processing has become very important during the past two decades owing to the tightening of economic and environmental demands. Hydrometallurgical processes are widely used to treat low grade ores, recycled materials, wastewaters and hazardous waste. Several regeneration processes in the metal industries also rely on hydrometallurgical technologies.

A typical hydrometallurgical unit process operates with liquid/solid or liquid/liquid reactions, in dilute process streams (less than 1 mol/l) at temperatures lower than 50°C. Hydrometallurgical processing is very selective for the desired metal, and the ore type can be rather complex and contain very low metal grades. Hydrometallurgical processing is often more environmentally friendly than the competing processing options. Hydrometallurgical processing of copper is often compared to pyrometallurgical treatment, which consists of the concentration of grinded ore, smelting, converting, fire refining and electrorefining. For example, in the copper leaching-solvent extraction-electrowinning process chain, part of the sulphur can be recovered in an elementary form and there are no emissions of sulphur dioxide gas, whereas the pyrometallurgical processing of copper ore produces significant amounts of sulphur dioxide emissions.

In hydrometallurgical processing the amounts of raw material are massive, and the flow volumes are large due to the slow chemical reactions or mass transport rates. Therefore, the capital costs related to the process solutions and raw materials are substantial. Also the treatment and storage of large amounts of liquid and solid waste materials can be a concern in some hydrometallurgical operations. (Ritcey and Ashbrook, 1988, Aromaa, 1990, Hayes, 1993, Biswas and Davenport, 1994, Moskalyk and Alfantazi, 2003)

Hydrometallurgical processing from ore to product consists of four basic steps: size reduction, leaching, solution purification and precipitation. Additionally the grinded ore can be concentrated and activated and, after leaching, the solid particles can be separated from the liquid. The processing chain is presented in Figure 2-1.

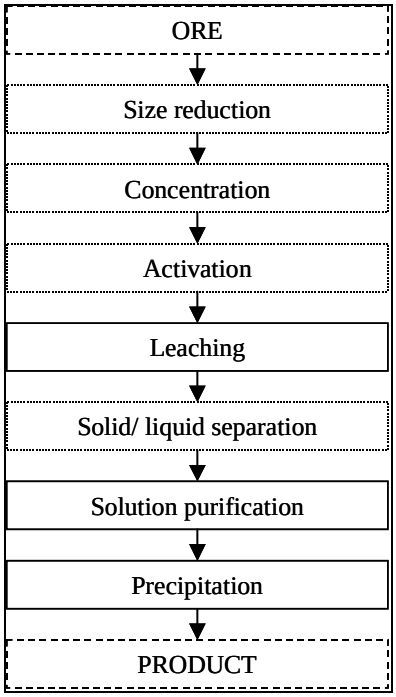

Figure 2-1: General flowsheet of hydrometallurgical processing [Aromaa, 1990, Hayes, 1993].

The mined ore, or other feed material, is first pretreated by crushing, concentrating (e.g. flotation), activation by chemical changes and physical modifications (e.g. agglomeration) or roasting. Next, the process options in the leaching stage are oxidative leaching, acid leaching, alkaline leaching, metathetic leaching, irrigation leaching (in situ, dump and heap), percolation leaching, and bacterial leaching. If the liquid contains solid particles after leaching, separation can be done by filtration, thickening and clarification (including coagulation, flocculation), counter-current decantation or with other equipment like centrifuges and hydrocyclones. Solution purification techniques include precipitation of impurities (pH controlled, hydrothermal, crystallization, cementation and electrolytic processes), solvent extraction, adsorption and ion exchange, membrane processes (reverse osmosis, ultrafiltration and electrodialysis), and chemical reactions (oxyhydrolysis). Process options for metal recovery are electrowinning, chemical reduction, precipitation and crystallization. The hydrometallurgical processing chain of the different unit processes and conditions are designed on the basis of the type of raw material. Each type of ore, slag matte and recycled material requires a tailored processing option. (Ray et al., 1985, Aromaa, 1990, Hayes 1993, Mooiman et al. 2005)

2.2 Copper leaching – solvent extraction – electrowinning process

Copper leaching – solvent extraction and the electrowinning process is the main hydrometallurgical processing chain for oxidized and low grade copper ore.

The first phase in the hydrometallurgical treatment of copper ore is leaching. In leaching, the crushed, oxidized copper ore is irrigated with a weak sulphuric acid solution. The copper rich leach solution is collected and clarified by removing the heaviest impurity particles, for example sand, in large settling tanks, called thickeners. The resulting pregnant leach solution (PLS) is then lead to the solvent extraction process. The composition of the pregnant leach solution depends on the raw material.

The copper concentration varies from less than 1 g/l to 35 g/l, and the pH varies between 0,8 and 2,5. The main impurities are iron, manganese, chloride and nitrate.

The second phase in the hydrometallurgical treatment of copper ore is solvent extraction. In copper solvent extraction, the aqueous copper leach solution is concentrated and purified using a copper-selective organic solution. The solvent extraction process consists of extraction and stripping processes, both of which may contain parallel and series unit processes. Currently, all the industrial operations use mixer-settler type of equipment, in which the solutions flow in a counter current direction. In mixer units, the phase with the smaller volume is dispersed into the continuous phase in order to ensure a maximal mass transfer interface. The mixer units consist of pumping and mixing parts, with axial impellers designed to maintain the dispersion. The aqueous and organic phases are separated in settlers. Settlers are long and shallow in oder to ensure proper phase separation, thus minimizing entrainment. The organic solution is a mix of an organic solvent such as kerosene and the copper selective extractant. Industrially used extractants are ketoximes and aldoximes, possibly with modifiers, and mixtures of these. The extractant blend is chosen according to the leach solution, operating conditions and plant design. (Kordosky, 2002, Robinson, 2003, Vancas, 2003, Rydberg et al., 2004)

The third phase in the hydrometallurgical treatment of copper ore is electrowinning. In this process, the concentrated aqueous copper solution, the rich electrolyte, is electrowon to form 99,999% pure copper cathodes. In electrowinning, the copper concentration of the electrolyte is typically between 32 and 37 g/l, the sulphuric acid concentration between 160 to 180 g/l, and the current density around 240 – 320 A/m2. The current efficiency can be up to 95%. Most electrowinning operations use rolled anodes of Pb-Ca or Pb-Sr-Sn due to their low corrosion rate and dimensional stability. Stainless steel blanks are used as starter cathodes to improve current efficiency and copper quality. In the larger plants, the copper cathodes are mechanically stripped from the steel blanks. (Bergh and Yianatos, 2001, Kordosky, 2002)

Examples of the copper solvent extraction and elecrowinning processes can be found in Sole et al. (2005), Munnik et al. (2003) and Whyte et al. (2001), Jenkins et al. (1999).

2.3 Copper solvent extraction process

The copper solvent extraction process has two input flows, the leach solution and the lean electrolyte solution, and one recycling flow, the organic solution. In the extraction stage, the copper is extracted from the leach solution into the organic solution. In the stripping stage, copper is stripped from the loaded organic solution into the electrolyte solution. The result of stripping, the rich electrolyte, is blended and fed to the electrowinning process, where 99,999% pure copper cathodes are produced. A general flow diagram of the process chain is illustrated in Figure 2-2. (Biswas and Davenport, 1994, Rydberg et al., 2004)

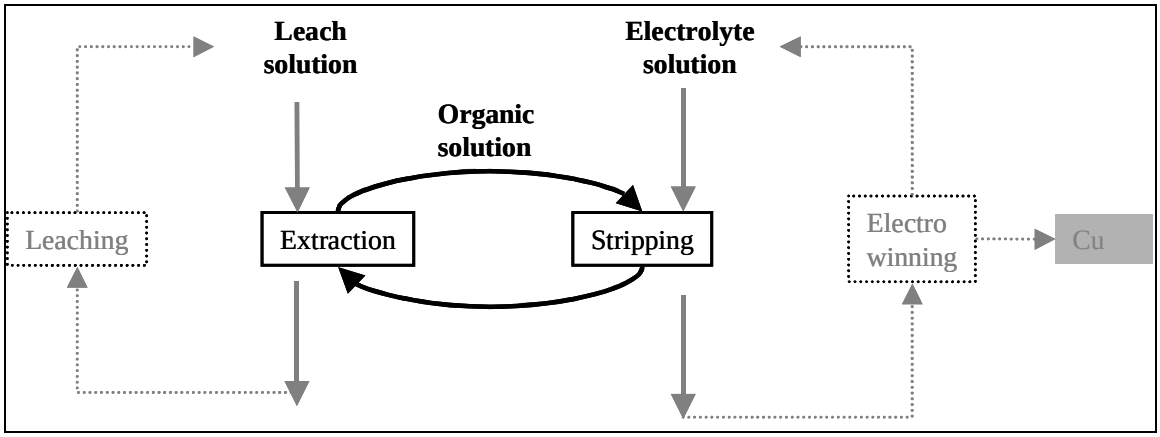

Figure 2-2: General flow diagram of copper solvent extraction process.

The main chemical reaction taking place in the copper solvent extraction process is described in Section 2.3.1, and the chemical and physical side reactions of the copper solvent extraction process in Section 2.3.2. The process chemicals, equipment and plant configurations used in industrial copper solvent extraction plants are discussed in Section 2.3.3.

2.3.1 The main chemical reaction in the copper solvent extraction process

In the copper solvent extraction process, the main phenomenon is the mass transfer of copper between the aqueous and organic solutions. The mass transfer of copper is based on cation exchange reaction, where the copper ions are forming chelates with copper selective reagent molecules. The equilibrium of this cation exchange reaction can be affected by adjusting the acidity of the aqueous solution.

The equilibrium reaction is as follows:

$$Cu^{2+}(aq) + SO_4^{2-}(aq) + 2RH(org) \leftrightarrow CuR_2(org) + 2H^+(aq) + SO_4^{2-}(aq) \quad \textbf{(2-1)}$$

In the extraction units, the copper ions form complexes with reagent molecules in an acid (pH ~1.8, ~5 g/l H_2SO_4 in PLS solution (Kordosky, 2002) over the temperature range 15 – 25 °C (Kordosky, 2006). The copper chelate is very stable in as low pH as 1.8. The proper pH range for extraction depends on the reagent characteristics, ferric concentration and the other impurities in the leach solution. Each reagent has an optimal pH for the most selective extraction of copper from the other metals present in the leach solution. Too low a pH can change the equilibrium reaction to prefer breaking of the chelate.

The copper-rich organic solution is led from extraction to the stripping units, where the strongly acid environment (~160 – 180 g/l H_2SO_4, Kordosky, 2002) catalyses disruption of most of the organic copper complexes. The chelate breaking reaction can be presented as follows:

$$CuR_2(org) + 2H^+(aq) + SO_4^{2-}(aq) \rightarrow Cu^{2+}(aq) + SO_4^{2-}(aq) + 2RH(org) \quad \textbf{(2-2)}$$

In the stripping units, high acidity is preferred in order to achieve fast mass transfer. However, due to the increased amount of acid mist in the downstream electrowinning facilities and the corrosive effect on the equipment in the electrowinning process, the acidity should remain under 200 g/l.

In the copper solvent extraction process it is essential to maintain the optimum within the copper mass balance; the amount of copper extracted from the leach solution in the extraction units has to be stripped into the electrolyte solution in the stripping units.

The exact equilibrium for the liquid-liquid extraction system can be calculated from the ternary phase data or equilateral-triangular diagrams (Robbins, 1984). Assuming the solubility of organic and aqueous phases can be neglected, simpler methods can be utilized. Thus, in industrial practice methods, such as the McCabeThiele diagram, also known as the Fenske diagram, are widely used (Mills, 1983, Robbins, 1984, Hayes, 1993).

The equilibrium copper solvent extraction unit processes can be studied by formulating an equilibrium constant κ for the system:

$$\kappa = \frac{\left[CuR_2\right] \cdot \left[H^+\right]^2}{\left[Cu^{2+}\right] \cdot \left[RH\right]^2} \qquad \textbf{(2-3)}$$

where $[CuR_2]$ is the copper complex concentration in the organic phase, [H+] the hydrogen concentration in the aqueous phase, $[Cu^{2+}]$ the copper concentration in the aqueous phase and [RH] the reagent concentration in the organic phase. (Hayes, 1994)

The kinetics of the solvent extraction includes both the mass transfer and the chemical reaction in the heterogeneous system. The extraction is controlled by the diffusion or chemical reaction rate. Diffusion is affected by the mass transfer surface area and concentration of the slowly diffunded reagents. The rate of the chemical reactions on the phase surface is affected by the surface area, the activity of the reacting components, and the molecular geometry.

In the copper solvent extraction process, the chemical reaction rate is affected by the solubility of both phases, the distribution and ionization coefficients, and the volumes of both phases. The reaction rate is defined by:

$$r = \frac{k_f \left[Cu^{2+}\right]^x \left[R^-\right]^y}{\left[H^+\right]^z} \qquad \textbf{(2-4)}$$

, where k_f is the rate constant for the forward reaction, $[H^+]$ the hydrogen concentration in the aqueous phase, $[Cu^{2+}]$ the copper concentration in the aqueous phase and $[R^-]$ the reagent concentration in the organic phase.

2.3.2 The chemical and physical side reactions in the copper solvent extraction process

The main chemical side reaction is the extraction of iron from the leach solution into the organic solution in the extraction units. Only ferric (Fe^{3+}) iron forms complexes with the organic solution, and it can therefore be transferred chemically from the leach solution via the organic solution to the electrolyte solution. The reaction rate is dependent on the acidity of the leach solution and the selectivity of the organic solution. The ferrous and ferric ions accumulate in the electrolyte and prevent maximum possible copper transfer from the organic solution to the electrolyte

solution. To prevent ferrous and ferric loading of the electrolyte, small amounts of the electrolyte are bled to the extraction units.

The main physical side phenomena are the transfer of impurities with entrainment and the accumulation of crud. Ferrous (Fe^{2+}), manganese (Mn^{2+}), and other impurities can pass from the leach solution to the electrolyte solution only as aqueous entrainment, i.e. in aqueous droplets within the imperfectly separated organic solution from the extraction units to the stripping units. In electrolysis, the presence of iron reduces current efficiency and decreases copper production. Manganese is converted to permanganate, which circulates back to stripping, and disrupts the reagent in the organic phase. Since the reagent is the most expensive chemical in the plant, this causes severe financial losses. In order to minimize such losses, a mixer-settler unit, called the washing or scrubbing stage, is added between the extraction and stripping processes. The aim of the washing stage is to remove the entrained PLS solution containing impurities and to strip the ferric ions from the organic solution. A concurrent strategy is to bleed small portions of the electrolyte solution from the electrowinning process to the washing stage or one of the extraction stages in order to remove the excess iron. The choice of reagent, copper and acid concentration in the wash stage aqueous solution, and the mixer retention time, also affect the transfer of impurities in the solvent extraction process. (Kordosky et. al., 2000, Virnig and Olafson, 2002)

All the solvent extraction plants contain at least small amounts of crud, gelatinous or crystalline emulsions of solid particles, in the aqueous and organic solutions. The solid particles and biological material in the leach solution, as well as precipitates and silica generated during changes in the pH in the mixers, are sources of crud formation. Crud formation is especially fast in a low pH range. A small amount of crud improves separation of the dispersion of the organic and aqueous phases in the settler, but excess crud causes severe problems. (Biswas and Davenport, 1994, Kordosky, 2002, Ritcey, 2002, Tetlow 2003)

2.3.3 Process chemicals, equipment and plant configurations of the copper solvent extraction process

The organic solution in the copper solvent extraction process consists of a solvent and a reagent. The high viscosity of the reagents means that they have to be diluted in the organic solvents. The preferred solvent characteristics are a flash point of over 60 °C, difficultly vaporizable, and a specific gravity of around 0,8 in order to ensure good separation from the aqueous solution. The solvents are usually different mixtures of paraffin, and aromatic and naphthalene hydrocarbons like kerosene. The aromatic compounds increase copper solubility to the organic solution, but slow the kinetics of extraction and stripping. (Biswas and Davenport 1994, Kordosky, 2002)

The reagents are typically hydroxy oximes: salicyl aldoximes, ketoximes and their mixtures. Ketoximes are readily soluble in kerosene, resistant to heating and do not require modifiers. Compared to the aldoximes, a lower acidity can be used in stripping ,and small amounts of particles, like colloid silicates and flocculents, are allowed in the pregnant leach solution. However, the extraction strength, kinetics and selectivity for ferric are inferior to those with aldoximes. The salicyl aldoximes are strong extraction chemicals with good extraction kinetics and selectivity against ferric. The aldoximes dissolve easily in kerosene, and separate rapidly from the acid aqueous solutions. Stripping requires such a high acidity that equilibrium modifiers, such as tridecanol and nonylphenol, are necessary. Modifiers prevent decomposition

of the aldoximes and form stable complexes with silicates possibly present in the leach solution. Possible side effects are crud formation, organic losses due to entrainment in the raffinate leach solution, and aqueous entrainment to stripping. Mixtures of ketoximes and aldoximes combine the strengths of these hydroxyl oximes, good extraction capability, fast kinetics, selectivity, stability and an even better stripping ability. In mixtures ketoximes replace aldoxime modifiers. Commercial ketoximes include LIX64N, LIX65N, LIX84, and aldoximes LIX860, LIX612N-LV, acorga P5100, acorga PT5050 and the mixture LIX 984. (Kordosky et al., 1987, Biswas and Davenport, 1994)

Typical process instrumentation in industrial copper solvent extraction plants includes the measurement of flow rate, temperature, and level. Conductivity measurements in mixers, pH-meters, and online measurements of the copper and impurity concentrations may exist. The copper and impurity assays, phase ratio, breaking time, and other diagnostic measurements are performed by the process operators and the laboratory. (Bergh and Yianatos, 2001)

The only equipment in industrial copper solvent extraction plants is the mixer-settler. Copper transfer between the aqueous and organic phases takes place in mixers, and the phases are separated in settlers. Different mixer designs are utilized, for example, in the Outokumpu VSF technology the organic and aqueous flows are combined in a dispersion pumping unit followed by two mixers (Nyman et. al. 2003). Most of the modern settlers are large and shallow. (Kordosky 2002, Robinson, 2003)

The unit process configurations of the industrial plants vary from a simple 2 series extraction steps with one stripping step to more complex configurations with 1 parallel extraction step, 2 series extraction steps, 1 washing step and 2 stripping steps (Kordosky, 2002, Sole et al., 2005). The relationship between the extraction and stripping units and the copper concentrations can be visualized using the McCabe-Thiele diagram. (Mills, 1983, Robbins, 1984, Hayes, 1993 (p. 277))

Different design aspects of solvent extraction operation using mixer-settlers have been studied by Galvez et al. (2004) and Pinto et al. (2004). Galvez et al. (2004) developed a graphical method to study the different flow configurations between the unit processes, including the organic and aqueous recycles inside the mixer-settler pairs and bypass flows. In their approach, the slopes of the operating lines in extraction and stripping are first transformed so as to be the same and are therefore presentable at the same scale (e.g. 0 – 8 g/l Cu), and the analysis is then performed with the experimentally determined equilibrium curves. The method enables easy design and comparison of the different flowsheets.

Pinto et al. (2004) developed a complex steady state simulation model to test the selectivity of the similarly extracted metal species under different mixing conditions. The studied parameters included the mean residence time, the dispersion phase hold up and the agitation speed. The optimal parameters were found using multiobjective optimization, illustrated with a case study of zinc and cadmium extraction in a sulphuric acid environment. This method helps in optimizing the process conditions, but requires detailed models of the process and industrial measurements of the phase hold up and residence time.

Cognis has developed a statistical program for designing copper solvent extraction plants with different reagents and varying temperatures and copper and acid concentrations. The accuracy of the statistical model was tested by comparing

measured and predicted stripped organic values obtained with the reagents LIX 612N-LV, LIX 860N-I and LIX 8180, as described by Kordosky et al. (2006). The agreement between the predictions and measurements under varying copper concentrations (30-55 g/l), acid concentrations (130-180g/l) and temperatures (35 - 41°C) was very good. The copper recovery was also analyzed using the Cognis Isocalc model for the extraction circuit. An increase in temperature increased copper production under the assumption that the extraction efficiency is higher at higher temperatures.

3 MODELING AND CONTROL OF THE COPPER SOLVENT EXTRACTION PROCESS – STATE OF THE ART

A state of the art review of the modeling approaches and the control challenges for copper solvent extraction process are presented and discussed in this chapter. First, the steady state models of the mixer-settler cascades are reviewed in Section 3.1. Next, the dynamic models of the mixer-settler cascades are presented in Section 3.2. Finally, the control challenges are discussed in Section 3.3.

3.1 Steady state models of the mixer-settler cascades

The steady state of a copper solvent extraction process can be studied using mass balance equations and equilibrium diagrams, for example, equilateral-triangular diagrams and McCabeThiele diagrams. McCabe-Thiele diagram is widely used in the industry for plant design and production optimization. (Mills, 1983, Robbins, 1984, Hayes, 1993 (p. 277), McCabe et al., 1993, Anon, 2000)

In the McCabe-Thiele method, the theoretical equilibrium values for extraction and stripping are determined on the basis of the incoming copper concentrations, the ratio between the aqueous and organic flow rates, and the curved equilibrium isotherms. The basic assumptions of the method are a steady state and immiscibility of the solutions under normal process conditions. The plant is approximately in a steady state if the flow rates are constant and the input concentrations and reagent volume per cent in the organic solvent are not changing. (Robbins, 1984)

An example of the McCabeThiele diagram is presented in Figure 3-1, where each triangular step, presenting one unit process, i.e. mixer-settler pair, is iterated to fit the equilibrium isotherms and the operating lines. The slope of the operating line for one mixer is the aqueous to organic ratio between the incoming flows.

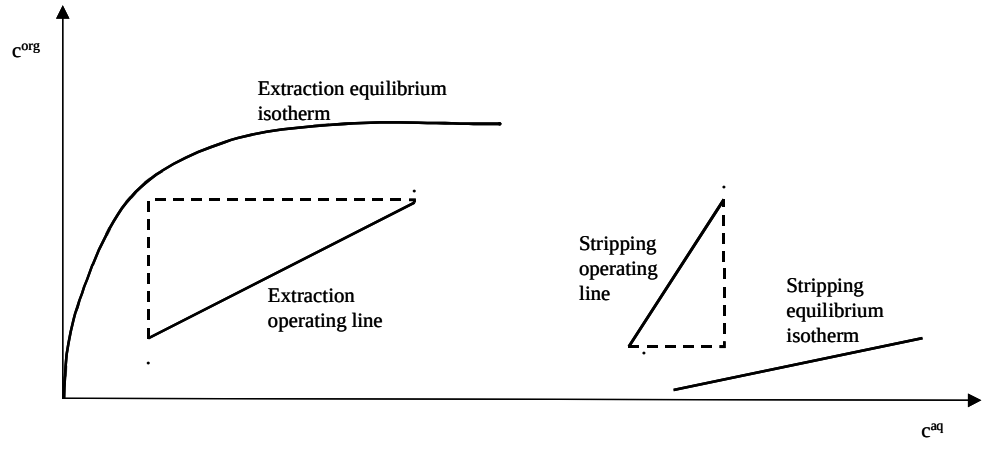

Figure 3-1: The McCabe-Thiele diagram for a process with one unit process for both extraction and stripping, marked with the dashed triangles. The extraction and stripping equilibrium isotherms and operating lines are marked with solid lines. The horizontal axis is the copper concentration in the aqueous phase and the vertical axis the copper concentration in the organic phase.

The extraction equilibrium isotherm is determined as a nonlinear function between the copper concentrations of the organic and aqueous solutions with constants *A* and *B* as follows:

$$c^{org} = \frac{Ac^{aq}}{c^{aq} + B} \quad \textbf{(3-1)}$$

The equilibrium isotherm for stripping can be approximated with a linear function between the copper concentrations of the organic and aqueous solutions with constants *C* and *D* as follows:

$$c^{org} = C \cdot c^{aq} + D \quad \textbf{(3-2)}$$

The constants, *A*, *B*, *C* and *D*, depend on the reagent concentration in the organic solution, acidity of the aqueous phases, temperatures of the solutions, and the other metals (impurities) that could be extracted, like ferric. The copper concentrations of the input flows and the flow ratios also affect the equilibrium isotherm curves. The following articles by Doungdeethaveeratana and Sohn (1998), Aminian and Bazin (2000) and Bazin et al. (2005), are referred to as examples of the parameter estimation techniques for the copper solvent extraction process.

Doungdeethaveeratana and Sohn (1998) determined the extraction equilibrium parameters for a $CuSO_4$-H_2SO_4- LIX860 (2%)-kerosene solution by contacting aqueous copper solution with the organic solution at various organic to aqueous volume ratios. The resulting equilibrium isotherm parameters were *A* = 1,071 and *B* = 0,037. With the same data the equilibrium constant, *K* (see Equation 2-3), was estimated to be 297 ± 5.

The equilibrium constants with different $CuSO_4$-H_2SO_4 –reagent-solvent combinations were summarized by Aminian and Bazin (2000). The equilibrium constant varied between 3,7 and 297 depending on the organic reagents and solvents used. Aminian and Bazin studied the equilibrium constant with a aqueous solution containing both copper (II) and iron (III) with organic solution LIX984-Orform SX-1. The resulting equilibrium constant was 15,0 ± 4,2.

A data reconciliation method with equilibrium constant estimation for batch solvent extraction data was developed by Bazin et al. (2005). The experimental data were created by mixing the organic LIX-Orform SX-11 solution and the aqueous copper solution in separation funnels for 15 minutes at a temperature of 25 °C and measuring the initial and final copper and acid concentrations of both phases. The initial copper and acid concentration of the aqueous phase and the organic to aqueous ratios were varied. The data reconciliation algorithm was based on the mass conservation and chemical equilibrium equations. In comparison to the utilization of raw measurements for calculating the copper recovery and performance indices, when the data reconciliation method was used the standard deviations of the indices were decreased. Data reliability and the performance indices are essential for process optimization and control. Thus, a data reconciliation algorithm, implemented in Microsoft Excel using Solver for the nonlinear optimization, has been found to be an excellent tool for data preprocessing for steady state models.

A steady state model of an industrial copper leaching – solvent extraction and electrowinning plant was developed by Saarenpää (1992). The aim of the model is to

estimate the building and operational costs and the equipment dimensions of the plant. The heap leaching model is a linear function based on the amount and grade of the copper rich ore, leaching time and leaching yield. The solvent extraction model is based on the McCabe Thiele diagram. The inputs are the PLS copper concentration and flow rate, electrolyte copper concentration, organic to aqueous ratios in the mixers, and mixer efficiencies. The electrowinning model is based on the cathode area, current efficiency and growing period. The model was developed in the Microsoft Excel environment and illustrated with the flow sheet calculation and the cost estimate of the industrial copper leaching-solvent extraction –electrowinning plant in Zaldivar, Chile.

A multivariable model of the electrowinning process of the Zaldivar copper leaching, solvent extraction and electrowinning plant was developed by Katajainen (1998). The lean electrolyte copper concentration was modeled with a linear combination of the lagged variables of rich electrolyte copper concentration and flow rate, cathode currents, acidity of the rich and lean electrolyte solutions, chloride concentration and temperature of the electrolyte solution. The model fit to the operational data was good within similar operating conditions as in the modeling data set, with a standard deviation of 0,23. With the other data sets the standard deviation increased to 0,66. The model gives a good starting point for dynamical model development for the electrowinning process.

A steady state model of an industrial copper solvent extraction and electrowinning plant was developed by Aminian et al. (2000). The model for the solvent extraction considers mass transfer in the mixers. The inputs of the model are the copper, iron and acid concentrations, and the aqueous and organic flow rates. The mixer model is based on mass conservation and it includes both transfer to the interfacial surface of the phases and the reaction rate over the surface. The equilibrium curves are experimentally defined. The output copper concentration of the mixer unit is modeled as:

$$c_{out}^{org} = c_{in}^{org} + \frac{6V^{org}}{d_B F^{org}} k_r \left\{ \kappa \frac{\left[RH_{\text{int}}\right]^n}{\left[H_{\text{int}}^+\right]^p} \left[c_{\text{int}}^{aq}\right]^m - \frac{\left[H_{\text{int}}^+\right]^{2-p}}{\left[RH_{\text{int}}\right]^{2-n}} \frac{\left[c_{\text{int}}^{org}\right]}{\left[c_{\text{int}}^{aq}\right]^{1-m}} \right\} \qquad \textbf{(3-3)}$$

where V^{org} is the mixer volumefor the organic solution, F^{org} the organic flow rate, d_B the mean diameter of the organic droplets, k_r the reaction rate constant, κ the equilibrium constant, RH the reagent concentration and H^+ the hydrogen ion concentration at the interface. The indices n,p, and m are partial reaction orders.

The input variables of the electrowinning model are the copper, iron and acid concentrations, electrolyte flow rates, temperatures and voltages. The steady state model predicting the output copper concentration of the electrowinning has the following form:

$$c_{out}^{el} = \frac{F_{in}^{el}}{F_{out}^{el}} c_{in}^{el} - \frac{1}{F_{out}^{el}} \frac{M_{Cu}}{zF} \eta I \qquad \textbf{(3-4)}$$

where concentrations are marked with c, electrolyte flow rates with F^{el}, z (=2) the charge of copper ion, F the Faraday constant, M_{Cu} the atomic weight of copper, η the current efficiency, and I the total electric current.

The models were combined to agree with the flow sheet of the pilot plant consisting of two series extraction units, one stripping unit and an electrowinning process. The model parameters were first calibrated with one data set and the model was then tested with other data set. The measurements and steady state model predictions were compared and had good agreement. The simulator can be used to increase understanding of the steady state process and to perform the optimization of copper solvent extraction and electrowinning plants. The steady state models also provide a good starting point for the development of the dynamic process models necessary for the control studies.

A mass balance monitoring prototype with data reconciliation for an industrial copper solvent extraction and electrowinning process has been reported by Suontaka et al. (2004, 2003). The inputs to the monitoring model were the flow rate and copper concentration measurements. In order to filter the measurement noise, a static data reconciliation based on the mass conservation equations was used. The mass balance model assumed steady state operation and constant equilibrium isotherms. The predictions of the mass balance model were compared to the output copper concentrations in order to monitor performance of the process. The prototype was tested with plant history data and the operational principle of the application was found to be successful. The aim of the monitoring system was to assist operators with process control, and was implemented in the Microsoft Excel environment. The system can be used to monitor other copper solvent extraction and electrowinning plants with only small plant-specific modifications.

Since relatively few articles have been published on steady state modeling of the copper solvent extraction process, three papers describing approaches to modeling solvent extraction with mixer-settler equipment are referred to here. Abdeltawab et al. (2002) studied the effect of agitation speed and aqueous to organic flow ratio on the extraction of rare earth metals in a laboratory scale mixer-settler column (with 5 extractions, no stripping stages). The basic formulation of the steady state output concentrations sums the input concentration with a stage efficiency weighted difference between the equilibrium and input concentrations as follows:

$$c_{out}^{org} = c_{in}^{org} + \alpha\left(c_{out}^{org} * - c_{in}^{org}\right) = c_{in}^{org} + \frac{K_o a V}{F^{org} + K_o a V}\left(\kappa_e\left(\frac{\left[R^{\text{int}}\right]}{\left[H^{+\text{int}}\right]}\right)^3 c_{in}^{aq} - c_{in}^{org}\right) \quad \textbf{(3-5)}$$

The equilibrium curve between the aqueous and organic concentrations is linear, where the coefficient consists of the equilibrium constant κ_e times the third order term of the ratio between the reagent [R^{int}] and the hydrogen ion [H^{+int}] concentrations at the droplet interface. The interface concentrations lead to detailed models of the mass transfer coefficients and the interfacial areas. The stage efficiency α is defined with an overall mass transfer coefficient K_o, organic flow rate F^{org}, interfacial area, a, and mixer volume V. The model was very successful in predicting the steady state effects of agitation speed, aqueous feed solution pH, and the number of stages.

Nishihama et. al. (2003) developed a steady-state model for the extraction of rare earth ions with EHPNA (2-ethylhexyl phosphonic acid mono-2-ethylhexyl ester) in the presence of EDTA. The model, based on material balance equations and the experimentally verified equilibrium curves, at different pHs and reagent loadings, was developed to design a separation process with a counter-current mixer-settler cascade. The emphasis in this steady state model was more on the process equipment design

than on further dynamic model development. Testing clearly implied that there was an increase in extraction with an added scrubbing stage, and a mixer-settler cascade of 10 extraction steps and 1 washing (scrubbing) step was proposed for this system. As was the case for the steady state model described by Takahashi et al. (2002), the lack of stripping steps for the process partly prevents comparison with the industrial copper solvent extraction process, in which the total performance is strongly connected to the effects of organic solution recycling between the extraction and stripping steps.

3.2 Dynamic models of the mixer-settler cascades

The basic structure of a continuous dynamical model for a mixer-settler cascade was summarized by Wilkinson and Ingham (1983). The model for one extraction step consisted of an ideal mixing model describing a mixer and a plug flow model describing a settler. The assumptions were: (1) perfect mixing in the mixer, (2) equilibrium is immediately achieved in the mixer, (3) the aqueous and the organic solutions are immiscible, (4) flow rates for both phases are constant, (5) plug flow separately for both phases in the settler, and (6) no mass transfer in the settler. The mixer model structure was expressed as follows:

$$\frac{dc_{out}^{org}\upsilon^{org}}{dt} = F^{org}\left(c_{in}^{org}(t) - c_{out}^{org}(t)\right) + \kappa a\left(c_{out}^{aq}*(t) - c_{in}^{aq}(t)\right) \qquad \textbf{(3-6)}$$

where υ is the stage specific organic solution hold-up in the mixer, κ the stage specific mass transfer coefficient and a is the interfacial area of the extraction stage. In equilibrium the driving force $(c_{out}^{aq}*(t) - c_{in}^{aq}(t))$ was recommended to be close to zero, which implies that the term will have an arbitrary high value. The equilibrium equation used to calculate c^* was assumed to be linear and the parameters constant. The settler output value $c_{out,settler}^{org}$ was a time-delayed value of the mixer output value, defined as follows:

$$c_{out,settler}^{org} = c_{out,mixer}^{org}(t - t_n) \qquad \textbf{(3-7)}$$

where the time delay (t- t_n) is calculated by dividing the phase volume in the settler with the flow rate (see equation 4-39).

A more exact approach was to model the hydrodynamic effect between the mixer and settler, and to model the settler with a series of ideal mixers. In the detailed settler model the settling volume was divided into perfectly mixed stages with back mixing streams, separately for both phases.

In Ingham et al. (1994), the mixing model was further modified by adding an entrainment flow, c_{entr}, which is the total flow of the organic droplets in the incoming aqueous flow, as presented in Equation (3-8). The hold-up volume υ was assumed to be proportional to the flow rate of the phase, and the hold-up was replaced by the mixing volume, V_m. The equation for mixing was presented as follows:

$$V_m^{org}\frac{dc_{out}^{org}}{dt} = F^{org}\left(c_{in}^{org}(t) + g_m c_{entr}^{org}(t) - (1+g_m)c_{out}^{org}(t)\right) + \kappa a\left(c_{out}^{aq}{}^*(t) - c_{in}^{aq}(t)\right)V_m^{aq} \quad \textbf{(3-8)}$$

where V^{org} and V^{aq} are the organic and aqueous volumes in the mixer, and g_m the percentage of the entrained flow. The mass transfer coefficient κ was derived from two film theory using the phase specific film coefficients k^{org} and k^{aq}, and the derivative of the equilibrium curve $c^{org}* = f(c^{aq}*)$.

$$\kappa^{aq} = \frac{k^{aq}k^{org}}{k^{org} + k^{aq}\cdot f'(c^{aq}*)} \quad \textbf{(3-9)}$$

Instead of the mass transfer coefficient term κa, the Murphree stage efficiency can be used. However, as indicated by Wilkinson and Ingham (1983), the Murphree efficiency coefficient changes considerably more during operating point changes than the coefficients in the previous approach. The Murphree efficiency was determined as:

$$E = \frac{c_{in}^{aq} - c_{out}^{aq}}{c_{in}^{aq} - c_{out}^{aq*}} \quad \textbf{(3-10)}$$

The settler model consisted of plug flow and mixed flow regions, where the latter represents the turbulent flow region and the backmixing phenomena in the settler. The output organic concentration from the plug flow model was a time-delayed value of the mixer output organic concentration, as in Equation (3-5). The output concentration for the well-mixed region was calculated as follows:

$$V_s^{org}\frac{dc_{out,s}^{org}}{dt} = g_s\cdot F^{org}\cdot\left(c_{out,s}^{org}(t) - c_{out,m}^{org}(t)\right) \quad \textbf{(3-11)}$$

where g_s is the percentage of the well mixed region of the settler.

A dynamic model describing the transfer mechanism of copper extraction in mixer-settler is described by Hoh et al. (1989). The continuous-flow stirred tank reactor model is chosen to represent the process unit, and the reaction is described with the following equations:

$$\frac{dc_{out}^{aq}}{dt}V = F^{aq}\left(c_{in}^{aq}(t) - c_{out}^{aq}(t)\right) - \frac{k_r S}{F^{aq}}\cdot \left(\frac{\kappa c_{out}^{aq}(t)\left(c(RH)_{in}(t) - 2F^{aq}/F^{org}\cdot\left(c_{in}^{aq}(t) - c_{out}^{aq}(t)\right)\right)}{c(H^+)_{in}(t) + 2\left(c_{in}^{aq}(t) - c_{out}^{aq}(t)\right)} - \frac{\left(c_{in}^{org}(t) + F^{aq}/F^{org}\cdot\left(c_{in}^{aq}(t) - c_{out}^{aq}(t)\right)\right)\cdot\left(c(H^+)_{in}(t) + 2\left(c_{in}^{aq}(t) - c_{out}^{aq}(t)\right)\right)}{\left(c(RH)_{in}(t) - 2F^{aq}/F^{org}\cdot\left(c_{in}^{aq}(t) - c_{out}^{aq}(t)\right)\right)}\right) \quad \textbf{(3-12)}$$

where k_r is the reaction rate constant, S the interfacial area, κ is the equilibrium constant (=4.0), c(RH) the organic reagent concentration and c(H^+) the hydrogen ion

concentration. If one of the phases is recycled from the settler back to the mixer, then the k_rS term becomes dependent on the aqueous phase hold up ν with a polynomial correlation, as follows:

$$k_rS = 3.78 - 16.6\nu + 28.1\nu^2 - 16.2\nu^3, \nu \in [1/3, 0.8] \quad \textbf{(3-13)}$$

where the aqueous hold up with the recycle flow rates, $F_{recycle}$, is determined as follows:

$$\nu` = \frac{F_{in}^{aq} + F_{recycle}^{aq}}{F_{in}^{aq} + F_{recycle}^{aq} + F_{in}^{org} + F_{recycle}^{org}} \quad \textbf{(3-14)}$$

The output concentrations of the mixer-settler unit are lagged with a time delay *t* calculated by dividing the total volume by the sum of the flow rates.

The model was configured for an experimental system with one extraction step, one washing step and five stripping steps. The input pregnant leach solution contained 1.6 g/l copper and 0.016M H_2SO_4, the organic solution contained 12.5% LIX64N reagent in kerosene, and the aqueous stripping solution 150 g/l H_2SO_4. The model fit to the experimental data was very good. On the basis of the experiments the authors suggest that the organic to aqueous ratio be kept near 2.0, by adjusting the flow rates or the recycle flow rates.

An example of applying Murphree efficiency to modeling solvent extraction with mixer-settler equipment is described by Salem and Sheirah (1990). They applied a dynamic model to describe the dynamic behaviour of the mixer-settler cascade. In the model, a linear equilibrium isotherm dependent on the temperature and aqueous equilibrium concentration was assumed. The experimental laboratory system consisted of a mixer-settler cascade with four extraction steps and a water-toluene-acetic acid medium. With the model, the effects of agitation speed, temperature and holdups and the optimal number of extraction stages were studied. The dynamic model gave adequate fit to the experimental data.

Aminian et al. (1998) used the previously presented dynamic mixer-settler model to study the residence times of an extraction cascade pilot plant with two extraction and one stripping stages. The tracer experiment for data collection was carried out with lithium chloride. The best model structure to describe the residence time distribution of the lithium chloride impulse response was a mixer model with two ideal mixers, and a settler model with two parallel models, minor flow to the ideal mixing series, and most of the flow to the plug flow in series with two ideal mixers. The electrowinning model consisted of one perfect mixer with a very small bypass of plug flow and two perfect mixers in series. The simulation results were very consistent with the experimental data.

A discrete, pulsed flow model for a rare-earth solvent extraction cascade was developed by Wichterlowa and Rod (1999). The model for one mixer-settler pair was separated into one mixing and several settling steps, in which each of the steps had equal time intervals. In the mixing step, the metal was transferred between the aqueous and organic phases according to the linear equilibrium relationship. The settling steps were modeled as ideal mixers, separately for each phase. The discrete output concentration in the ideal mixing step with mass transfer was presented as follows:

$$c_{out}^{org}(t+1) = (1-\hat{\alpha})c_{\text{int}}^{org} + \hat{\alpha}\cdot c_{\text{int}}^{org*} = (1-\hat{\alpha})c_{\text{int}}^{org} + \frac{\hat{\alpha}\cdot m}{V^{aq}+mV^{org}}\left(V^{aq}c_{\text{int}}^{aq} + V^{org}c_{\text{int}}^{org}\right)$$

$$= (1-\hat{\alpha})\frac{v^{org}c_{out}^{org}(t) + F^{org}\Delta t\cdot c_{in}^{org}(t)}{V^{org}} \qquad \textbf{(3-15)}$$

$$+ \frac{\hat{\alpha}\cdot m}{V^{aq}+mV^{org}}\left(v^{aq}c_{out}^{aq}(t) + F^{aq}\Delta t\cdot c_{in}^{aq}(t) + v^{org}c_{out}^{org}(t) + F^{org}\Delta t\cdot c_{in}^{org}(t)\right)$$

where $F\Delta t$ is the pulsed volume entering each ideal mixing step, V^{aq} and V^{org} the ideal mixer volumes for the aqueous and organic phases with half of the entering pulsed phase volumes, and v^{aq} and v^{org} the ideal mixer phase volumes minus half of the entering pulsed phase volume. m is the linear slope of the equilibrium curve, and $\hat{\alpha}$ the efficiency. The equilibrium curve is a nonlinear function of the steady state efficiency, concentrations and volumes. The model was applied to neodymium and praseodymium extraction with DEHPA in a mixer-settler cascade of 6 extraction and 6 stripping stages. The system was tested on laboratory scale extraction equipment with 30 mixer-settlers, each having a volume of 2,5 liters. The model could be used for the industrial copper solvent extraction process, and was characterized by relatively stable mixer and settler volumes, flow rates and flow ratios. However, division of the mixers and settlers into ideal mixing steps should be done carefully.

3.3 Control of the copper solvent extraction process

The control of the copper solvent extraction and electrowinning processes relies on the operators actively manipulating the setpoints for the basic controllers. This means that the control loops are decentralized, with manual setpoints for flow rates, levels, motor speeds, stirring speeds, pumps and valves. Since the process includes long time delays and complex interactions between the variables, optimal performance and productivity of the plant is seldom achieved. (Bergh, 2006, Bergh and Yianatos, 2001).

The measured variables for the control system typically consist of sensors for flow rates, levels, temperatures, pressures, pH and conductivity. Online concentration analyzers have recently become more common (Hughes, D. and Saloheimo, K.,2000). The manipulated variables in solvent extraction are the flow rates, levels, stirring speeds and addition of extraction chemicals. In electrowinning the manipulated variables are voltage, current density, temperature and the addition concentration of chemical compounds. In solvent extraction the main problems, which can be formulated as measured disturbance variables for a control system, are changes in the PLS pH level and copper concentration (Bergh And Yianatos, 2001). Bergh et al. (2006) suggested dividing the control structure of a copper solvent extraction pilot plant into three levels. The first level consists of basic local controllers of flows and levels. The second level, hydrodynamic supervisory control, controls the flow rates between the process units, the recycle flow rates of the process units, and the stock solution levels. The aim of the second level is to minimize aqueous and organic entrainments by adjusting the setpoints of the first level controllers. The third level, metallurgic supervisory control, adjusts the organic to aqueous flow ratios according to the metallurgical model of the process. The organic to aqueous flow ratios are given as setpoints for the second level control.

The control system for the solvent extraction and electrowinning plant has several tasks, such as keeping the operation within the safety limits, maximizing throughput and rejecting disturbances. These tasks, with the exception of safety-related issues, can be formulated into a set of control objectives. Bergh and Yianatos (2001) proposed that the main control objectives for copper solvent extraction and electrowinning processes are maximization of the production rate while fulfilling the product quality constraints, for example high quality of the copper cathodes.

There are several challenges associated with achieving these control objectives. Bergh and Yianatos (2001) state that, to date, the lack of adequate mathematical models applicable for industrial plants has prevented the development of control systems for copper solvent extraction and electrowinning processes. However, development of the dynamical models and the control system should not be too complicated. The responses in extraction, with mixer-settler type of equipment, are sluggish and rather stable due to the relatively low throughputs and large hold-up volumes (Wilkinson and Ingham, 1983). The steady state effect of mass flow rate changes can be easily calculated from the equilibrium scheme, for example a change in the aqueous to organic flow rate changes the slope of the operating line in the McCabe Thiele diagram, and subsequently also the output of the corresponding unit process.

Aqueous and organic entrainments, crud formation and phase separation times are problems that could be solved with appropriate operating practices, separation equipment, chemicals or with control strategies, as proposed by Bergh et al. (2006). However, entrainments could pose a possible control problem if measurements of the emulsion band and dispersion characteristics exist, and the phenomenon could be modeled. In eletrowinning, problems such as operation of the baths are more of maintenance/equipment development issues. (Bergh and Yianatos, 2001).

4 MODEL DEVELOPMENT FOR THE COPPER SOLVENT EXTRACTION PROCESS

The first aim of this thesis is to develop dynamical models for an industrial copper solvent extraction process in order to facilitate dynamical behaviour studies and control system design and testing. In this chapter, a copper solvent extraction process with one extraction unit and one stripping unit is first described in Section 4.1. Next, the equilibrium state models (Section 4.2) and dynamic models (Section 4.3) with parameter estimations are developed for a copper solvent extraction plant.

4.1 Description of a copper solvent extraction process

The copper solvent extraction process to be modeled consists of two processes. In the extraction process copper is extracted from the aqueous phase into the organic phase, and in the stripping process copper is stripped from the organic solution into the electrolyte solution. Both the extraction and stripping processes consist of one or more unit processes; at the industrial scale, the unit processes are solely mixer-settlers (Robinson, 2003). In the mixer the minor phase is dispersed and mixed with the continuous phase in order to maximize the interfacial area for the mass transfer of copper. In the settler the organic and aqueous phases are separated by gravity.

The process to be modeled consists of three main streams, the PLS solution to the extraction unit, the lean electrolyte solution to the stripping unit, and the organic solution recycling between the extraction and stripping units (Figure 4-1). The controlled variables are the copper concentrations of the raffinate, the rich electrolyte and the organic solutions, the manipulated variables are the flow rates, and the disturbance variables are the incoming copper concentrations of the PLS solution and lean electrolyte solution. A summary of the variables is given in Table 4-1.

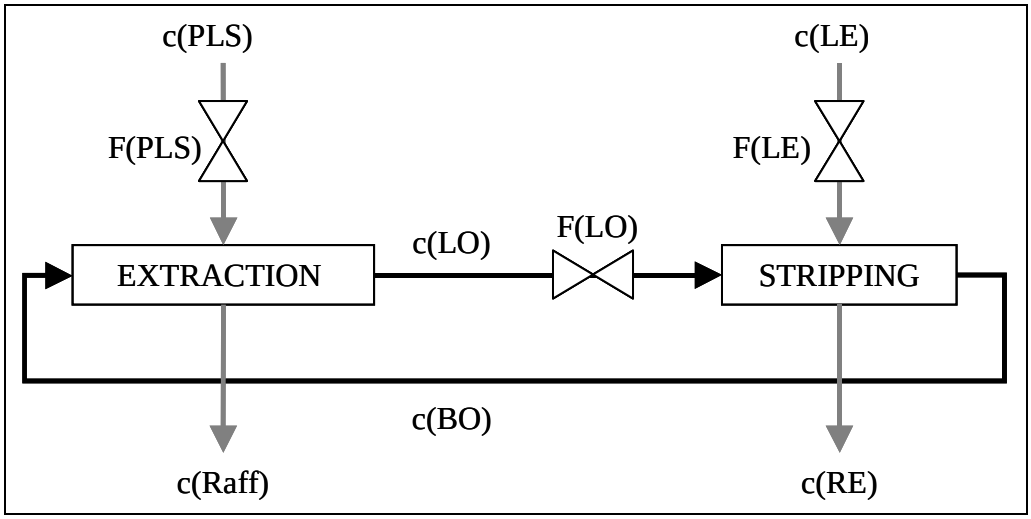

Figure 4-1: The solvent extraction process. The inputs are the copper concentration of the PLS, c(PLS), and lean electrolyte, c(LE), and the flow rates of PLS, F(PLS), organic, F(LO), and lean electrolyte, F(LE). The controlled variables are the copper concentration of the raffinate, c(Raff), rich electrolyte, c(RE); and the copper concentrations of the recycled organic stream after stripping, barren organic, c(BO), and after extraction, loaded organic, c(LO).

Table 4-1: Controlled, manipulated and disturbance variables of the copper solvent extraction process.

Classification	Variable name	Abbreviation
Controlled variables	Raffinate copper concentration	c(Raff)
	Loaded organic coppe concentration	c(LO)
	Rich electrolyte copper concentration	c(RE)
	Barren organic copper concentration	c(BO)
Manipulated variables	PLS flow rate	F(PLS)
	Electrolyte flow rate	F(LE)
	Organic flow rate	F(LO)
Disturbance variables	PLS copper concentration	c(PLS)
	Lean electrolyte copper concentration	c(LE)

4.2 Equilibrium state model of the copper solvent extraction process

The equilibrium state model of the copper solvent extraction process is based on the McCabe-Thiele diagram. The McCabe-Thiele diagram is the design flowsheet of the industrial copper solvent extraction processes, and the necessary equilibrium isotherms are measured offline. The information needed for the equilibrium state model are the copper concentrations after each unit process, the flow rates, efficiencies of each extraction and stripping steps, and the equilibrium isotherms for extraction and stripping. The theoretical equilibrium values for extraction and stripping are determined from the McCabe-Thiele diagram, as presented in Figure 4-2. Each step in the diagram represents one mixer-settler pair.

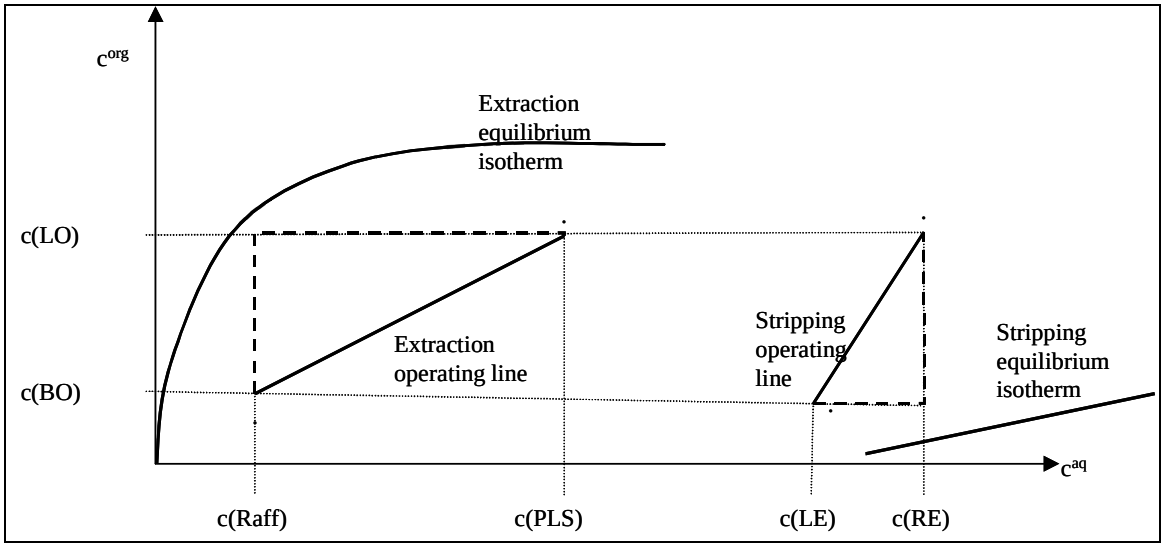

Figure 4-2: The McCabe-Thiele diagram for the modeled process with one unit process for both extraction and stripping, marked with dashed triangles. The input and output variables are presented in Table 4-1. Extraction and stripping equilibrium isotherms and operating lines are marked with solid lines. The horizontal axis is the copper concentration in the aqueous phase and the vertical axis the copper concentration in the organic phase.

The equilibrium isotherm for extraction is nonlinear and for stripping it is linear, as presented in Equations (3-1) and (3-2). In order to calculate the equilibrium output copper concentrations from each unit process, the point where the equilibrium isotherm and the inverse operating line overlap has to be determined. The calculation is illustrated in Figure 4-3. The inverse operating line is first determined, and the equation for the theoretical equilibrium point x^* in the extraction is then derived. The equilibrium points $c^{aq}*$ and $c^{org}*$ for extraction are calculated on the basis of this theoretical variable. The theoretical equilibrium point and the equilibrium points are then derived for the stripping process and, finally, the steady state equations are simplified and presented for the solvent extraction plant with one extraction unit and one stripping unit.

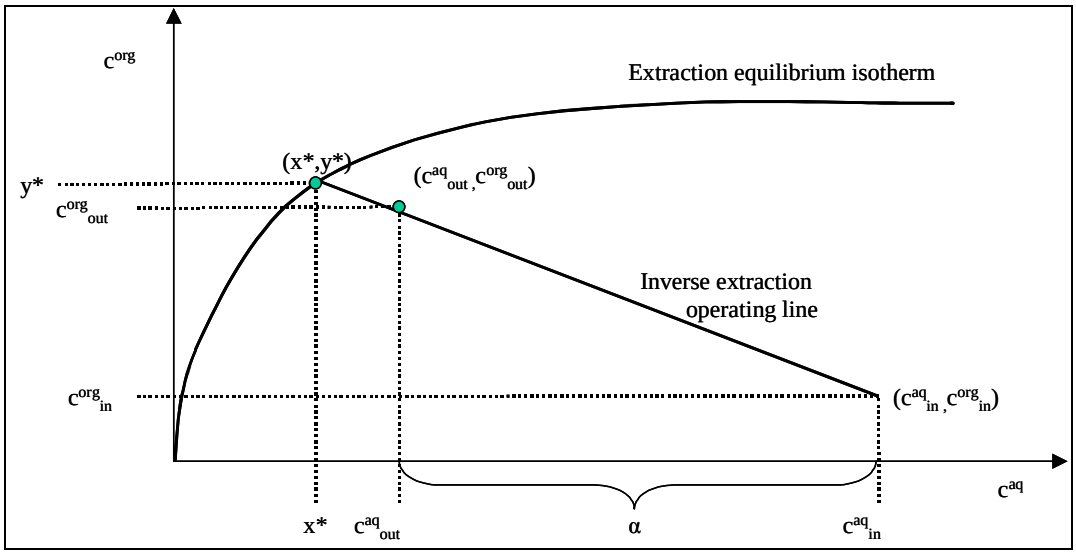

Figure 4-3: Calculation of the output concentrations (c_{out}) for extraction with the nonlinear extraction equilibrium isotherm and the efficiency coefficient α. The input copper concentrations are marked with c_{in}, and the equilibrium copper concentrations with c_{eq}.

The slope of the inverse operating line is the negative ratio between the aqueous and the organic flow rates to the mixer, $-F^{aq} / F^{org}$. The inverse operating line is drawn through the input copper concentrations $(c^{aq}_{in}, c^{org}_{in})$. The inverse operating line is determined as follows:

$$c^{org} = -F^{aq} / F^{org} \cdot c^{aq} + \left(c^{org}_{in} + c^{aq}_{in} \cdot F^{aq} / F^{org} \right) \qquad \textbf{(4-1)}$$

In the extraction, the theoretical equilibrium value for the aqueous copper concentration, x^*, is calculated by setting the equilibrium isotherm and the inverse operating line (Equation 4-1) equal, as follows:

$$c^{org} = \frac{Ac^{aq}}{c^{aq} + B} = -F^{aq} / F^{org} \cdot c^{aq} + \left(c^{org}_{in} + F^{aq} / F^{org} \cdot c^{aq}_{in} \right) \qquad \textbf{(4-2)}$$

For clarity, the coefficients of the inverse operating line are replaced with a and b, and the second order equation is solved in relation to the aqueous copper concentration c^{aq}, as follows:

$$\begin{aligned} & c^{org} = \frac{Ac^{aq}}{c^{aq} + B} = ac^{aq} + b \\ & \Leftrightarrow a(c^{aq})^2 + (Ba - A + b)c^{aq} + Bb = 0 \qquad \textbf{(4-3)} \\ & \Rightarrow c^{aq} = 1/2a \left(-(Ba - A + b) \pm \sqrt{(Ba - A + b)^2 - 4aBb} \right) \end{aligned}$$

The negative square root is chosen because the positive square root produces unfeasible solutions (due to multiplication with *1/2a* term, where *a* has negative value. This follows from the assumption that flow rates are positive in Equation 4-2). The coefficients of the inverse operating line, *a* and *b*, are replaced back to the original variables. The theoretical equilibrium aqueous copper concentration is now:

$$x^{*}=\left(\frac{-1}{2F^{aq}/F^{org}}\right)\cdot\left(-\left(-B\cdot F^{aq}/F^{org}-A+\left(c_{in}^{org}+c_{in}^{aq}\cdot F^{aq}/F^{org}\right)\right)\right.$$
$$\left.-\sqrt{\left(-B\cdot F^{aq}/F^{org}-A+\left(c_{in}^{org}+c_{in}^{aq}\cdot F^{aq}/F^{org}\right)\right)^{2}+4B\cdot F^{aq}/F^{org}\left(c_{in}^{org}+c_{in}^{aq}\cdot F^{aq}/F^{org}\right)}\right) \quad \textbf{(4-4)}$$

The output copper concentrations for the aqueous and organic phases are the theoretical values weighted with the efficiency α:

$$c_{out}^{org}=\alpha_i x^{*}+(1-\alpha_i)\cdot c_{in}^{aq} \quad \textbf{(4-5)}$$

$$c_{out}^{org}=-c_{out}^{aq}\cdot F^{aq}/F^{org}+\left(c_{in}^{org}+c_{in}^{aq}\cdot F^{aq}/F^{org}\right) \quad \textbf{(4-6)}$$

For clarity, the extraction equilibrium isotherm is linearized around the operating point (op1), represented by the aqueous copper concentration ($c_{op1}^{aq}, c_{op1}^{org}$). The slope of the linearized curve is the derivate of the equilibrium curve evaluated at the linearization point (Taylor series expansion). The linearized extraction equilibrium isotherm is defined as follows:

$$c^{org}=\frac{AB}{(B+c_{op1}^{aq})^{2}}c^{aq}+\frac{A\left(c_{op1}^{aq}\right)^{2}}{(B+c_{op1}^{aq})^{2}}=\hat{A}_i c^{aq}+\hat{B}_i \quad \textbf{(4-7)}$$

The theoretical equilibrium point is calculated by setting the inverse operating line (Equation 4-1) equal to the linearized extraction equilibrium isotherm, and solving this in relation to aqueous copper concentration c^{aq}. The theoretical equilibrium point x^{*} is now defined as follows:

$$c^{org}=\hat{A}_i c^{aq}+\hat{B}_i=-c_{in}^{aq}\cdot F^{aq}/F^{org}+\left(c_{in}^{org}+c_{in}^{aq}\cdot F^{aq}/F^{org}\right)$$
$$\Rightarrow x^{*}=\frac{\left(c_{in}^{org}+c_{in}^{aq}\cdot F^{aq}/F^{org}\right)-\hat{B}_i}{\hat{A}_i+F^{aq}/F^{org}} \quad \textbf{(4-8)}$$

The output copper concentrations in the extraction, with the linearized equilibrium isotherm curve, are formulated explicitly as a combination of the input concentrations. The aqueous output copper concentration can be expressed by combining Equations (4-4) and (4-7) as follows:

$$c_{out}^{aq}=\alpha_i\frac{c_{in}^{org}+c_{in}^{aq}\cdot F^{aq}/F^{org}-\hat{B}_i}{\hat{A}_i+F^{aq}/F^{org}}+(1-\alpha_i)\cdot c_{in}^{aq}$$
$$=c_{in}^{aq}\left[\frac{(1-\alpha_i)\hat{A}_i F^{org}+F^{aq}}{\hat{A}_i F^{org}+F^{aq}}\right]+c_{in}^{org}\left[\frac{\alpha_i F^{org}}{\hat{A}_i F^{org}+F^{aq}}\right]-\left[\frac{\alpha_i\hat{B}_i F^{org}}{\hat{A}_i F^{org}+F^{aq}}\right] \quad \textbf{(4-9)}$$

The organic output copper concentration is calculated as a combination of Equations (4-5) and (4-9), as follows:

$$c_{out}^{org} = c_{in}^{org} + \alpha_i \cdot \left(F^{aq} / F^{org} \right) \cdot \left(\frac{\hat{B}_i - c_{in}^{org} - c_{in}^{aq} \cdot F^{aq} / F^{org}}{\hat{A}_i + F^{aq} / F^{org}} + c_{in}^{aq} \right)$$
$$= c_{in}^{aq} \left[\frac{\alpha_i \hat{A}_i F^{aq}}{\hat{A}_i F^{org} + F^{aq}} \right] + c_{in}^{org} \left[\frac{\hat{A}_i F^{org} + (1-\alpha_i) F^{aq}}{\hat{A}_i F^{org} + F^{aq}} \right] + \left[\frac{\alpha_i \hat{B}_i F^{aq}}{\hat{A}_i F^{org} + F^{aq}} \right] \quad \textbf{(4-10)}$$

In stripping, the parameters of the linear equilibrium isotherm are *C* and *D*. The theoretical equilibrium point *x** is solved as in extraction. The inverse operating line is set equal to the equilibrium isotherm, and the aqueous copper concentration *x** is solved as follows:

$$c^{org} = C \cdot c^{aq} + D = -F^{aq} / F^{org} \cdot x + \left(c_{in}^{org} + c_{in}^{aq} \cdot F^{aq} / F^{org} \right)$$
$$\Rightarrow x^* = \frac{\left(c_{in}^{org} + c_{in}^{aq} \cdot F^{aq} / F^{org} \right) - D}{C + F^{aq} / F^{org}} \quad \textbf{(4-11)}$$

The output copper concentrations for stripping can now be expressed as a combination of the input concentrations. The aqueous output copper concentration in stripping is a combination of (4-4) and (4-10):

$$c_{out}^{aq} = \alpha_i \frac{c_{in}^{org} + c_{in}^{aq} \cdot F^{aq} / F^{org} - D}{C + F^{aq} / F^{org}} + (1-\alpha_i) \cdot c_{in}^{aq}$$
$$= c_{in}^{aq} \left[\frac{(1-\alpha_i) C F^{org} + F^{aq}}{C F^{org} + F^{aq}} \right] + c_{in}^{org} \left[\frac{\alpha_i F^{org}}{C F^{org} + F^{aq}} \right] - \left[\frac{\alpha_i D F^{org}}{C F^{org} + F^{aq}} \right] \quad \textbf{(4-12)}$$

The organic output copper concentration in stripping is a combination of Equations (4-5) and (4-11), as follows:

$$c_{out}^{org} = -\left(F^{aq} / F^{org} \right) \cdot \left[c_{in}^{aq} \left[\frac{(1-\alpha_i) C F^{org} + F^{aq}}{C F^{org} + F^{aq}} \right] + c_{in}^{org} \left[\frac{\alpha_i F^{org}}{C F^{org} + F^{aq}} \right] - \left[\frac{\alpha_i D F^{org}}{C F^{org} + F^{aq}} \right] \right]$$
$$+ \left(c_{in}^{org} + c_{in}^{aq} \cdot F^{aq} / F^{org} \right)$$
$$= c_{in}^{aq} \left[\frac{\alpha_i C F^{aq}}{C F^{org} + F^{aq}} \right] + c_{in}^{org} \left[\frac{C F^{org} + (1-\alpha_i) F^{aq}}{C F^{org} + F^{aq}} \right] + \left[\frac{\alpha_i D F^{aq}}{C F^{org} + F^{aq}} \right] \quad \textbf{(4-13)}$$

The equilibrium state model for the plant is derived using these equations. The steady state concentrations from each mixer-settler can be expressed as a function of the incoming concentrations (c_{in}), flow rates (F), stage efficiencies (α), and equilibrium isotherm parameters (A_i,B_i,C,D). For the extraction step E, the aqueous and organic output copper concentrations are derived from Equations (4-9) and (4-10) with the variables listed in Table 4-1:

$$c(Raff) = c(PLS)\left[\frac{(1-\alpha_E)\hat{A}_E F(LO) + F(PLS)}{\hat{A}_E F(LO) + F(PLS)}\right] + c(BO)\left[\frac{\alpha_E F(LO)}{\hat{A}_E F(LO) + F(PLS)}\right] - \left[\frac{\alpha_E \hat{B}_E F(LO)}{\hat{A}_E F(LO) + F(PLS)}\right] \quad \textbf{(4-14)}$$

$$c(LO) = c(PLS)\left[\frac{\alpha_E \hat{A}_E F(PLS)}{\hat{A}_E F(LO) + F(PLS)}\right] + c(BO)\left[\frac{\hat{A}_E F(LO) + (1-\alpha_E)F(PLS)}{\hat{A}_E F(LO) + F(PLS)}\right] + \left[\frac{\alpha_E \hat{B}_E F(PLS)}{\hat{A}_E F(LO) + F(PLS)}\right] \quad \textbf{(4-15)}$$

For the stripping step S, the aqueous and organic output copper concentrations are derived from Equations (4-12) and (4-13) using the variables listed in Table 4-1:

$$c(RE) = c(LE)\left[\frac{(1-\alpha_S)CF(LO) + F(LE)}{CF(LO) + F(LE)}\right] + c(LO)\left[\frac{\alpha_S F(LO)}{CF(LO) + F(LE)}\right] - \left[\frac{\alpha_S DF(LO)}{CF(LO) + F(LE)}\right] \quad \textbf{(4-16)}$$

$$c(BO) = c(LE)\left[\frac{\alpha_S CF(LE)}{CF(LO) + F(LE)}\right] + c(LO)\left[\frac{CF(LO) + (1-\alpha_S)F(LE)}{CF(LO) + F(LE)}\right] + \left[\frac{\alpha_S DF(LE)}{CF(LO) + F(LE)}\right] \quad \textbf{(4-17)}$$

The steady state of the system can be solved from these equations by substitution. Estimation of the equilibrium isotherm parameters, the efficiencies and recycle corrections are explained in more detail in the following sections.

4.2.1 Estimation of the equilibrium isotherms

The isotherm curves for extraction and stripping are assumed to be almost constant, or to change at a significantly slower rate than the other process dynamics, e.g. the flow ratios determining the operating lines.

The extraction and stripping equilibrium isotherms are nonlinear functions of various process variables, such as temperature, pH and reagent strength. However, only offline measurements of the pH level of the leach solution, acidity of the electrolyte solution and reagent volume in the organic solvent are usually available. Therefore, the extraction and stripping equilibrium isotherms are approximated by manipulating the equilibrium Equation (2-3), as described in Hayes (1993, p.227 – 228).

Assume that total volume of the organic phase [R] and the concentration of hydrogen ions [H^+] do not change throughout the equilibrium reaction. Therefore, in equilibrium, the sum of the organic reagent molecules with copper ions [CuR_2] and the organic reagent molecule with hydrogen ion [RH] is assumed to be constant and described as follows:

$$[CuR_2] + [RH]^2 = [R]^2 = \text{constant} \quad \textbf{(4-18)}$$

By rearranging this, we get:

$$[RH]^2 = [R]^2 - [CuR_2] \quad \textbf{(4-19)}$$

Assume that the concentration of [CuR_2] can be approximated by the organic copper concentration c^{org} and the copper ion concentration by the aqueous copper

concentration c^{aq}. Now by replacing Equation (4-19) to the equilibrium Equation (2-3), the following equation for the equilibrium constant is formulated:

$$\kappa = \frac{\left[CuR_2\right]\cdot\left[H^+\right]^2}{\left[Cu^{+2}\right]\cdot\left(\left[R\right]^2-\left[CuR_2\right]\right)} \approx \frac{c^{org}\cdot c\left(H^+\right)^2}{c^{aq}\cdot\left(c(R)^2-c^{org}\right)} \qquad \textbf{(4-20)}$$

and by rearranging this equation we get the form of the extraction equilibrium isotherm with the extraction equilibrium constant κ_E :

$$c^{org} = \frac{\kappa_E\cdot c(R)^2\cdot c^{aq}}{c(H^+)^2+\kappa_E\cdot c^{aq}} = \frac{c(R)^2\cdot c^{aq}}{c(H^+)^2/\kappa_E + c^{aq}} \qquad \textbf{(4-21)}$$

For the stripping equilibrium isotherm the equation is the same with the stripping equilibrium constant κ_S but, since the acidity is much higher, the hydrogen ion concentration becomes the determining term, and the equation simplifies into a linear form with the estimation error term ε:

$$c^{org} = \frac{\kappa_S\cdot c(R)^2\cdot c^{aq}}{c(H^+)^2+\kappa_S\cdot c^{aq}} \approx \frac{\kappa_S\cdot c(R)^2\cdot c^{aq}}{c(H^+)^2} + \varepsilon \qquad \textbf{(4-22)}$$

4.2.2 Estimation of the extraction and stripping efficiencies

The efficiency of extraction and stripping is affected by the reagent concentration in the organic solution and the acidity of the aqueous solution. The retention time in the mixers and settlers also have an effect, especially if they are too short. (Ritcey and Ashbrook, 1988)

The efficiency for each unit process is estimated on the basis of the theoretical equilibrium value x (aqueous) and y (organic), the input concentration c_{in} and the actual equilibrium value c_{out}, as follows:

$$\alpha_E = \frac{c_{in}^{aq}-c_{out}^{aq}}{c_{in}^{aq}-x} = \frac{c_{in}^{org}-c_{out}^{org}}{c_{in}^{org}-y} \qquad \textbf{(4-23)}$$

Calculation of the efficiency for the extraction unit is presented in Figure 4-3. The output concentrations c_{out} are determined by drawing an inverse operating line from the input concentrations c_{in} towards the extraction equilibrium isotherm. The point where this line and the equilibrium isotherm overlap is the theoretical equilibrium value for the aqueous X and organic Y concentrations. These values are then weighed with the efficiency parameter α to obtain the output values c_{out}. The efficiency parameter typically has values close to 1; values above 1 are possible for real plants because the efficiency is a theoretical measure. (Ingham et al., 1994)

4.2.3 Estimation of the recycle corrections

It is often possible within the mixer-settler units to recycle one of the phases in order to change the aqueous to organic phase ratio without changing the flow rates. If the recycle flow rates are not measured, then the aqueous to organic flow ratios in the mixer have to be estimated from the steady state data of the plant. The recycle correction is based on the mass balance of copper in the mixer. The aqueous copper

mass is multiplied by the recycle correction coefficient, *cf*, to equal with the organic copper mass as follows:

$$cf \cdot F^{aq}\left(c_{in}^{aq} - c_{out}^{aq}\right) = -F^{org}\left(c_{in}^{org} - c_{out}^{org}\right) \quad \textbf{(4-24)}$$

The correction coefficient can now be estimated from the steady state data of the plant as follows:

$$cf = \frac{-F^{org}\left(c_{in}^{org} - c_{out}^{org}\right)}{F^{aq}\left(c_{in}^{aq} - c_{out}^{aq}\right)} \quad \textbf{(4-25)}$$

4.3 Dynamic models of the copper solvent extraction process

A mechanistic model approach was preferred for the dynamic model in order to be able to describe the detailed process phenomena. The dynamic model development was started from the basic formulation for mixer-settlers presented in Wilkinson and Ingham (1983). This approach was chosen due to the successful earlier studies described in Chapter 3. The dynamic models are based on ideal mixing and plug flow models. In this work, the ideal mixing model is modified to utilize the equilibrium values calculated with the equilibrium state model. The assumptions used by Wilkinson and Ingham (1983) that are applicable to the developed dynamic model are: (1) perfect mixing in the mixer, (2) immiscibility of the two phases, and (3) no mass transfer or back-mixing in the settler (plug flow). In this work, the following assumptions are added: (4) the equilibrium curve in the mixer is a plant specific non-linear equilibrium isotherm, (5) the mass transfer coefficients K_i, the equilibrium isotherm parameters *A* and *B* for extraction, and *C* and *D* for stripping, and the efficiency coefficients α_i, are not constant, but estimated from the offline plant measurements. (6) The phase volumes are calculated on the basis of the phase flow rates and total equipment volumes, and (7) hydrodynamic effects are neglected. (8) The equilibrium and the phase ratio in the mixer are reached gradually, not immediately as in Wilkinson and Ingham (1983).

The copper mass transfer is calculated from the ideal mixing Equation (3-6), where the equilibrium value *c** is determined on the basis of the equilibrium state model described in the previous section. The variables are marked as follows: flow rates F, the mixing volumes V_m, organic concentrations c^{org}, aqueous concentrations c^{aq}, mass transfer coefficients K_i, efficiency parameters α_i. The settler, which always follows the mixer, is described by a pure time delay t_i .

In extraction, copper is transferred from the aqueous to the organic phase. The extraction unit operation is modelled by differential equations of the concentrations for both the organic ($dc_1^{org}(t)/dt$) and aqueous phases ($dc_1^{aq}(t)/dt$), where the equilibrium output value *c** is calculated from the equilibrium state model:

$$\frac{dc_1^{org}(t)}{dt} = \frac{F_1^{org}(t)}{V_m} \cdot \left[c_0^{org}(t-t_0) - c_1^{org}(t) \right] + K_1 \left[c_1^{org}(t) - c_1^{org*}(t) \right] \quad \textbf{(4-26)}$$

$$\frac{dc_1^{aq}(t)}{dt} = \frac{F_1^{aq}(t)}{V_m} \cdot \left[c_0^{aq}(t) - c_1^{aq}(t) \right] - K_1 \left[c_1^{org}(t) - c_1^{org*}(t) \right] \quad \textbf{(4-27)}$$

$$c_1^{org*}(t) = g\left(c_0^{org}(t-t_0), c_0^{aq}(t), F_1^{org}(t), F_1^{aq}(t), \alpha_1, A, B \right) \quad \textbf{(4-28)}$$

where the incoming copper concentrations are marked with subscript 0 and the copper concentrations in the mixer with subscript 1. The settler is taken into account by delaying the mixer output concentrations for the aqueous phasewith a time delay t_1 and for the organic phase with a time delay t_2:

$$c(Raff)(t) = c_1^{aq}(t-t_1) \quad \textbf{(4-29)}$$

$$c(LO)(t) = c_1^{org}(t-t_2) \quad \textbf{(4-30)}$$

In stripping, copper is transferred from the organic to the electrolyte solution. The stripping unit operation is modeled by differential equations of the concentrations for both electrolyte ($dc_1^{el}(t)/dt$) and organic ($dc_2^{org}(t)/dt$) phases, taking into account the equilibrium concentration c^* calculated from the equilibrium state model:

$$\frac{dc_1^{el}(t)}{dt} = \frac{F_1^{el}(t)}{V_m} \cdot \left[c_0^{el}(t) - c_1^{el}(t) \right] - K_2 \left[c_1^{el}(t) - c_1^{el*}(t) \right] \quad \textbf{(4-31)}$$

$$\frac{dc_2^{org}(t)}{dt} = \frac{F_2^{org}(t)}{V_m} \cdot \left[c_1^{org}(t-t_2) - c_2^{org}(t) \right] - K_2 \left[c_1^{el}(t) - c_1^{el*}(t) \right] \quad \textbf{(4-32)}$$

$$c_1^{el*}(t) = h\left(c_1^{org}(t-t_2), c_0^{el}(t), F_2^{org}(t), F_1^{el}(t), \alpha_2, C, D \right) \quad \textbf{(4-33)}$$

where the incoming electrolyte copper concentrations are marked with subscript 0, and the electrolyte copper concentrations in the mixer with subscript 1. Since the organic solution comes from the extraction unit, the incoming organic copper concentrations are marked with subscript 1 and the organic copper concentrations in the mixer with subscript 2. Rich electrolyte concentration (c(RE)) is the time delayed (t_3) value of the electrolyte concentration, and barren organic (c(BO)) is the time delayed (t_4) value of the organic concentration in the stripping unit.

$$c(RE)(t) = c_1^{el}(t-t_3) \quad \textbf{(4-34)}$$

$$c(BO)(t) = c_2^{org}(t-t_4) \quad \textbf{(4-35)}$$

Since the organic solution is recycled from the stripping unit back to the extraction unit, c(BO) is c_0^{org} and t_4 is same as t_0 in Equation (4-26) and Equation (4-28).

These four equations (4-26, 4-27, 4-31, 4-32) are ordinary differential equations that can be solved with standard techniques. These time variant models have four states, copper concentrations of aqueous and organic phases in both extraction and stripping units.

4.3.1 Calculation of the mass transfer coefficients

The mass transfer coefficient K describes the speed of the concentration change in the mixers. It is inversely related to the process time constant: the higher the *K* value, the shorter the time constant. The mass transfer coefficient *K* is approximated from the process model by setting it to a steady state and giving a small value (a tuning coefficient 0.01 was found that gave appropriate time dynamics) to the difference term $(c_{out} - c_{out}^*)$.

$$V\frac{dc_{out}}{dt} = F(c_{in} - c_{out}) - K(c_{out} - c_{out}^*)V = 0$$
$$\Leftrightarrow K = \frac{F(c_{in} - c_{out})}{V(c_{out} - c_{out}^*)} = \frac{F(c_{in} - c_{out})}{V \cdot \varepsilon} \quad \textbf{(4-36)}$$

Using this procedure the K values are between 50 – 400 1/s for the studied process. Wilkinson and Ingham (1983) suggested giving an arbitrary high value for the $K{\cdot}V$ term. The modelling approach in Ingham et. al. (1994) is slightly different; they use a constant mass transfer coefficient K = 25 1/s.

4.3.2 Estimation of the mixer and settler phase volumes

The mixing model includes the mixer volume, V_m, and the settling model settler volume, V_s, both for the aqueous and organic phases. Since there are no measurements of the volumetric ratio between the organic and the aqueous phases in the mixer and the settler, the ratio is assumed to follow the incoming flow ratio to the mixer, as suggested by Ingham et al. (1994, p 186). Considering that *V* represents the total volume of the equipment, the volume of the organic phase can be represented as:

$$V^{org} = V\frac{F^{org}}{F^{org} + F^{aq}} \quad \textbf{(4-37)}$$

and the volume of the aqueous phase as:

$$V^{aq} = V\frac{F^{aq}}{F^{org} + F^{aq}} \quad \textbf{(4-38)}$$

4.3.3 Estimation of the time delay for the plug flow model

The plug flow model describing the settler has one parameter, a time delay *t*. The organic mean residence time (delay) is the total organic volume divided by the organic flow rate, which simplifies into the total volume divided by the total flow rate:

$$t^{org} = \frac{V^{org}}{F^{org}} = \frac{V_s \cdot \frac{F^{org}}{F^{org} + F^{aq}}}{F^{org}} = \frac{V_s}{F^{org} + F^{aq}} \quad \textbf{(4-39)}$$

and the aqueous mean residence time (delay) is the total aqueous volume divided by the aqueous flow rate, simplifying into the same form as the organic time delay:

$$t^{aq} = \frac{V^{aq}}{F^{aq}} = \frac{V_s \cdot \frac{F^{aq}}{F^{org} + F^{aq}}}{F^{aq}} = \frac{V_s}{F^{org} + F^{aq}} \quad \textbf{(4-40)}$$

Thus, the time delay for the aqueous phase and organic phase in the settler are equal. The result is justified by the operating practice of the case industrial copper solvent plant: The flow rates organic and aqueous phases in the settler are maintained on equally levels in order to minimize problems on the organic/aqueous interphase layer such as entrainment and thickening of the emulsion layer.

5 DESCRIPTION AND THE PRELIMINARY ANALYSIS OF THE INDUSTRIAL CASE PROCESS

The industrial case process is described and a preliminary analysis of the process is performed in this chapter. The industrial case process and a preliminary analysis of the control structure are presented in Section 5.1. A data filtering method is developed for the case process data in Section 5.2.1. Process characterization is performed with the case process data in Section 5.2: The typical operating points are determined using a clustering technique, and the maximum variations of the controlled, disturbance and manipulated variables are calculated.

5.1 Description of the industrial case copper solvent extraction process

The studied solvent extraction process consists of four unit processes, one parallel (E1P) and two series (E1S, E2S) mixer-settler units for extracting copper from the aqueous phase into the organic phase, and one mixer-settler unit (S1H) for stripping copper from the organic solution into the electrolyte solution, as illustrated in Figure 5-1. Between the third extraction unit (E2S) and the stripping unit (S1H) there is a washing mixer-settler unit and an organic storage tank, marked as ‘Tank’ in Figure 5-1. In the washing unit, the organic solution is scrubbed with water to remove most of the iron. The copper concentration of the organic solution does not change significantly in the washing unit.

The inputs of the process are the pregnant leach solution (PLS) flow rate and copper concentration, the lean electrolyte flow rate and copper concentration, and the flow rate of the organic solution. The organic solution is recycled in the process, but the flow rate can be manipulated through the organic storage tank.

The outputs of the process are the raffinate and organic copper concentrations from the extraction units, and the rich electrolyte and barren organic copper concentrations from the stripping unit. The measured state variables are the partial organic copper concentration, c(BO1) and c(BO2), and the partial PLS copper concentration, c(PLS1), together with all the output copper concentrations.

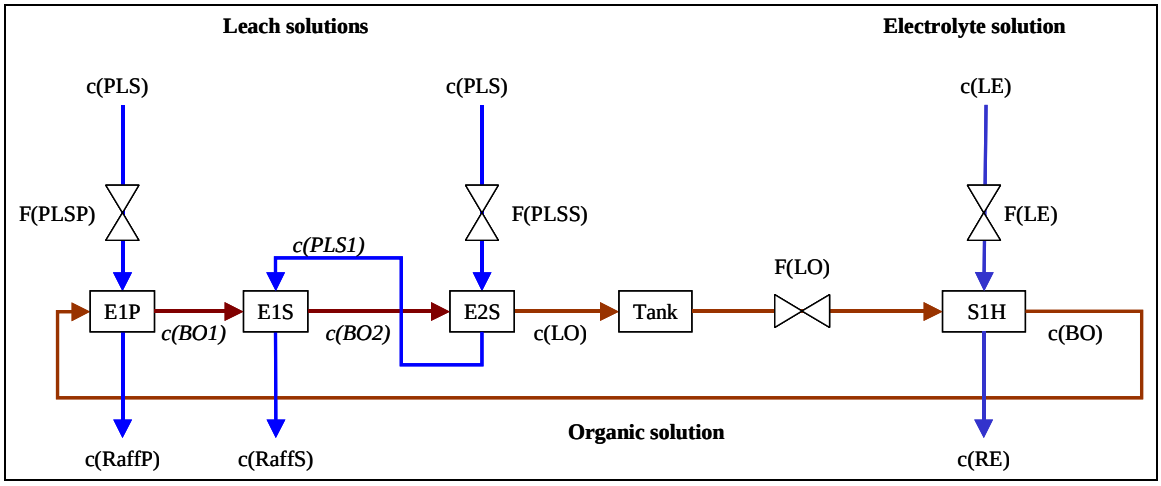

Figure 5-1: The copper solvent extraction process. The output variables are the copper concentrations of the raffinates c(RaffP) and c(RaffS), rich electrolyte, c(RE), and the copper concentrations of the recycled organic stream, barren organic, c(BO) and loaded organic c(LO). The input variables are the flow rates of PLS, F(PLSS) and F(PLSP), organic, F(LO), and lean electrolyte, F(LE), and the copper concentration of PLS, c(PLS) and lean electrolyte, c(LE).

The online measurements consist of two organic and five aqueous copper concentrations and four flow rates. The offline measurements include pH of the PLS solution (pH), acidity of the electrolyte solution (acid), the reagent volume per cent in the organic solvent (vol) (for description of the reagent, see Section 2.3.3). The offline measurements also include four organic and five aqueous copper concentrations. The measurements with information about the measurement type (online/offline) are listed in Table 5-1.

In the copper solvent extraction and electrowinning plant there are no advanced control systems. The process operators change the flow rates in the solvent extraction process and current amperages in the electrowinning process in order to keep the lean electrolyte copper concentration within the target value. The lean electrolyte copper concentration target value is set in order to maximize the production of copper cathodes by the plant management. The control structure and strategy are further discussed in Chapter 9.

A preliminary classification of the controlled, manipulated and disturbance variables of the copper solvent extraction plant was performed on the basis of the operational and process knowledge. The possible controlled variables are the outputs of the extraction and stripping processes; rich electrolyte concentration, c(RE), raffinate concentrations c(RaffS) and c(RaffP), and organic concentrations c(LO) and c(BO). The manipulated variables are the four flow rates of the leach, organic and electrolyte solutions. The measured disturbance variables are the leach and electrolyte solution concentrations. This classification is presented in Table 5-1.

Table 5-1: Controlled, manipulated, disturbance and state variables of the industrial copper solvent extraction process. The measurement type, online/offline, is indicated on fourth and fifth column, with an indication of the online and offline measurements.

Classification	Variable name	Abbreviation	Online	Offline
Controlled variables	Rich electrolyte copper concentration	c(RE)	X	X
	Loaded organic copper concentration	c(LO)	X	X
	Raffinate series copper concentration	c(RaffS)	X	X
	Raffinate parallel copper concentration	c(RaffP)	X	X
	Barren organic copper concentration	c(BO)	X	X
Manipulated variables	PLS series flow rate	F(PLSS)	X	
	PLS parallel flow rate	F(PLSP)	X	
	Organic flow rate	F(LO)	X	
	Electrolyte flow rate	F(LE)	X	
Disturbance variables	PLS copper concentration	c(PLS)	X	X
	Lean electrolyte copper concentration	c(LE)	X	X
	Reagent volume percent in organic solution	Vol		X
	pH level of the PLS solution	PH		X
	Acidity of electrolyte solution	Acid		X
State variables	Partial PLS copper concentration	c(PLS1)		X
	Partial organic copper concentration after E1P step	c(BO1)		X
	Partial organic copper concentration after E1S step	c(BO2)		X

5.2 Preliminary analysis of the case copper solvent extraction process

The aim of this preliminary analysis is to develop a data filtering method, and to define the typical operating points and the maximum variations of the process variables for the further modeling and control studies. The analysis is performed on the basis of the two online and offline industrial data sets. The data filtering method is described in Section 5.2.1, the typical operating points are determined in Section 5.2.2, and the maximum variation of the process variables is analyzed in Section 5.2.3.

5.2.1 Data preprocessing

Filtering of the industrial data is necessary due to measurement noise and outliers (Ray, 1989, p.28-30). In the copper solvent extraction process, because all the measurements contained frequent outliers and most of the online copper concentrations differed from those given by reliable laboratory analysis, bias correction for the online copper concentrations was justified. The filtering method is described in detail in Section 5.2.1.1, and the bias correction in Section 5.2.1.2.

5.2.1.1 Noise filtering for the online measurements

The clear outliers, i.e. those over or under the minimum limit of each variable, were first removed. A zero-phase digital filtering method was then applied: because the dynamic model structure is of the first order, only the main trends in the process data were of interest for comparison to the simulated data. The Matlab filtfilt –algorithm (The MathWorks, 2006), which applies first order filtering to forward and backward directions of the data vector (Matlab Help manual, Orfanidis, 1990), was used.

Averaging periods from 3 to 30 sample times were tested and compared on the basis of the sum of squared errors (SSE) index and visual examination. The average sum of squared errors (*aSSE*) between the measurements y_m and the filtered measurements y is defined as follows:

$$aSSE = \frac{1}{N}\sum_{i=1}^{N}\left(y_{m,i} - y_i\right)^2 \qquad \textbf{(5-1)}$$

The average sum of squared errors for the online measurements are presented in Table 5-2. The averages of the squared error sums are higher for the variables with higher values. The squared errors between the measurements and filtered signals are considerable for all the variables with all the filtering periods. This suggests that there is significant measurement noise, and filtering is therefore necessary.

Table 5-2: Average sum of squared errors for the online measurements with different averaging periods (3, 6, 12, 18, 24 and 30 sampling times).

period	3	6	12	18	24	30
c(PLS)	0.1606	0.1609	0.1612	0.1614	0.1615	0.1617
c(RaffS)	0.0065	0.0065	0.0066	0.0066	0.0067	0.0067
c(RaffP)	0.0010	0.0011	0.0011	0.0011	0.0011	0.0011
c(LE)	20.2950	20.2985	20.3151	20.3113	20.2982	20.2882
c(RE)	35.8249	35.8738	35.9320	35.9615	35.9863	36.0086
c(LO)	2.6428	2.6464	2.6477	2.6505	2.6553	2.6608
c(BO)	0.2534	0.2535	0.2536	0.2538	0.2539	0.2540
F(PLSS)	0.5618	0.5665	0.5716	0.5744	0.5774	0.5805
F(PLSP)	0.5110	0.5225	0.5304	0.5347	0.5381	0.5412
F(LE)	0.1329	0.1396	0.1537	0.1648	0.1739	0.1823
F(LO)	0.3092	0.3117	0.3160	0.3198	0.3237	0.3276

For the PLS copper concentration an averaging period of 6 sample times or less gave relatively noisy signals, whereas the period of 30 sample times removed too much variation from the data for modeling purposes. An averaging period of 12 sample

times produced low residuals (aSSE 0,16), and visual examination of the data confirmed that the filtered signal followed smoothly the raw data. As can be seen from Figure 5-2 for the PLS copper concentration, the dynamic changes in the data are still present and the noise has been removed. The PLS copper concentration residuals are approximately white noise, as can be seen from Figure 5-3.

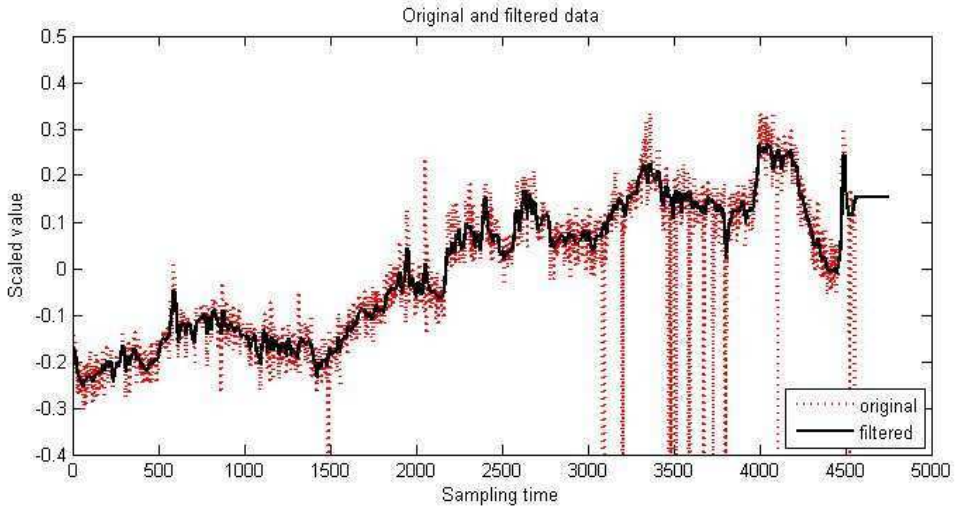

Figure 5-2: The original data with the outliers (dotted, red) and filtered data (solid, black) measurements of the PLS copper concentration.

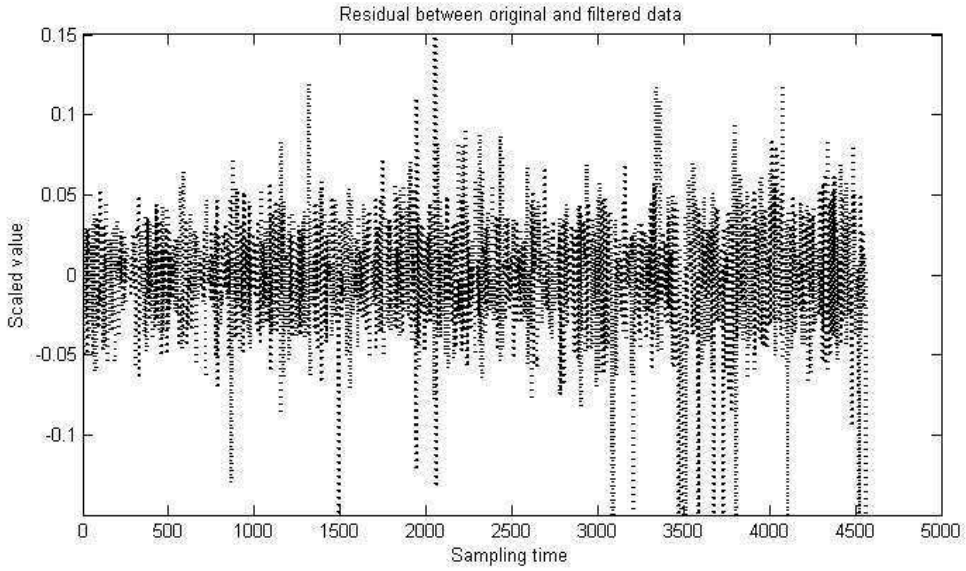

Figure 5-3: Residuals between the original measurement data with the outliers and filtered measurements of the PLS copper concentration.

5.2.1.2 Bias correction for the online copper concentration measurements

Due to severe bias between the online and the offline copper concentrations, it was necessary to apply bias correction. Recursive auto-regression with an external output

algorithm was chosen for the bias correction. The algorithm with a forgetting factor of 0.95 was used to estimate the bias coefficient *b* between the online *y(t)* and offline *u(t)* measurements with the recursive least squares method, as follows:

$$y(t) = b \cdot u(t) + e(t) \quad \textbf{(5-2)}$$

, where *e(t)* is the residual term.

The averages of the online concentration measurements and the laboratory assays were used for the calculations. The inverse of the correction coefficient (1/b) was applied to correct the online copper concentration measurements. The method successfully corrected the level difference between the online and offline measurements. For example, the bias coefficient of the PLS copper concentration measurements was around 1.05. For the noise-filtered and bias-corrected PLS copper concentration measurement (ff+bias), the copper concentration level corresponds to the laboratory measurements (laboratory) and the main trends of the original measurement data (original) are more clear, as illustrated in Figure 5-4.

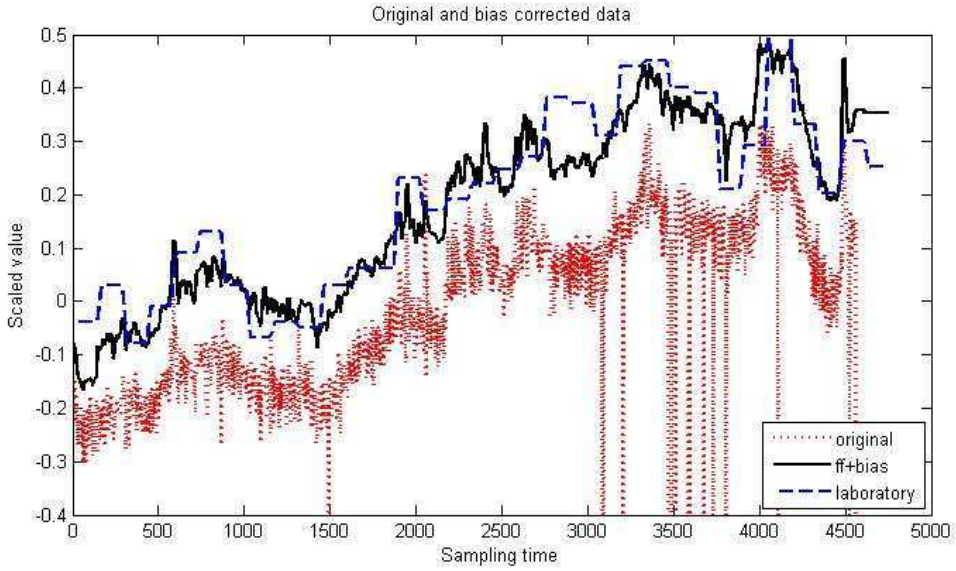

Figure 5-4: The original PLS online concentration measurement (dotted, red), bias corrected concentration measurements (solid, black) and the laboratory measurements (dashed, blue).

5.2.2 Operating points of the case process

The aim was to find the typical operating points from the industrial plant data. The studied variable set included offline measurements of the PLS, raffinate, barren organic, loaded organic, rich electrolyte and lean electrolyte copper concentrations, and the averages of the online measurements of the PLS parallel and series, organic and electrolyte flow rates.

The operational data were clustered with the Matlab kmeans algorithm using the squared Euclidean distance measure. The number of clusters was chosen according to the distance sums and the cluster means illustrated on the process data. The number of clusters should be as small as possible, while having a small distance sum between the data points and the cluster centres, and giving a good representation of the whole data set. Silhouette plots are used to illustrate how well-separated the resulting clusters are. The silhouette plot displays a measure of how close each point in one cluster is to

points in the neighbouring clusters. Points that are very distant from the neighbouring clusters have the value 1. If a point is not especially close to any of the clusters, the silhouette value is –1.

On the basis of the distance sums and cluster means plotted into the process data, the cases with 3,6 and 9 were examined in more detail. The corresponding silhouettes are illustrated in Figure 5-5, Figure 5-6 and Figure 5-7. The case with three clusters separates one extreme point and clusters the rest of the data points into two well separated large clusters. The case with six clusters separates two extreme points, while clustering the rest of the points into three smaller groups and one well separated large group. The case with nine clusters separates three extreme points, one large group and five smaller groups, two of which are not well separated.

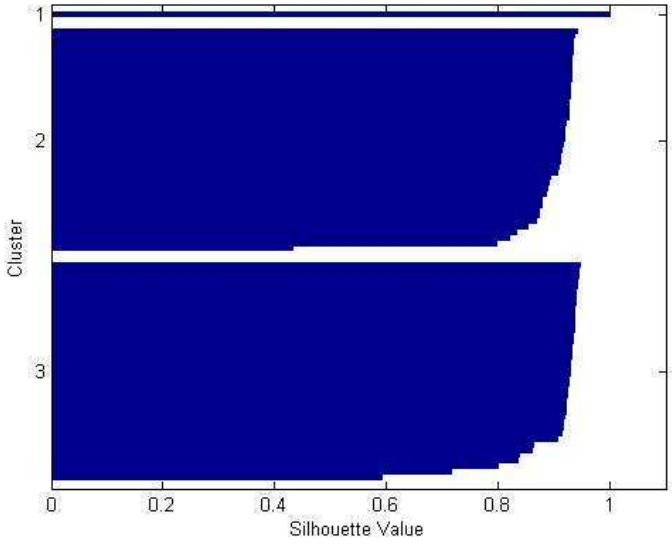

Figure 5-5: Silhouette of three clusters.

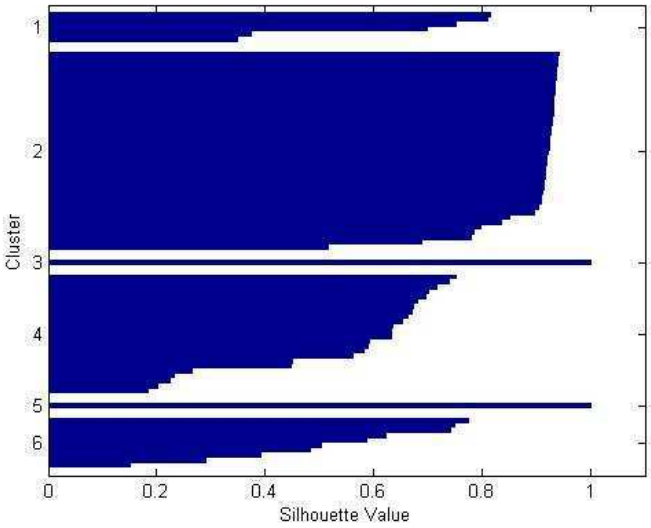

Figure 5-6: Silhouette of six clusters.

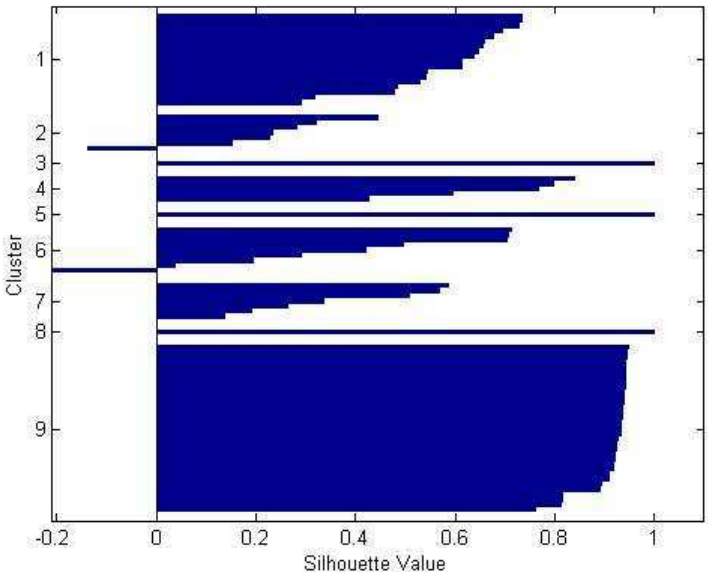

Figure 5-7: Silhouette of nine clusters

The cluster centers were illustrated by plotting them into the process data, as shown in Figure 5-8 for the six-cluster case. Three clusters were not enough to cover the different operating points, whereas with 9 clusters some of the cluster centres were almost the same. With six clusters the four normal and two of the extreme operating points were covered well, as illustrated in Figure 5-8 and Figure 5-9. The distances between the closest data points and the mathematical cluster centres were small. Only the two normal operating points from the start of each data set (first and fourth circle in both Figure 5-8 and Figure 5-9 were considered for further study. In the following, these two operating points are called the first operating point (DP1) and the second operating point (DP4).

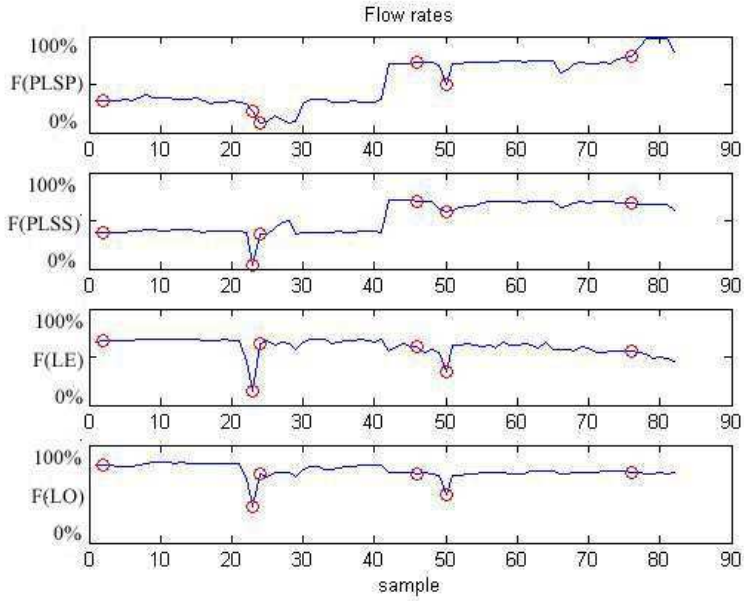

Figure 5-8: The flow rates of the PLS parallel, PLS series, lean electrolyte and loaded organic. The data points closest to the cluster centres are circled. The first and fourth circles (around samples 2 and 46) are operating points DP1 and DP4 chosen for further study.

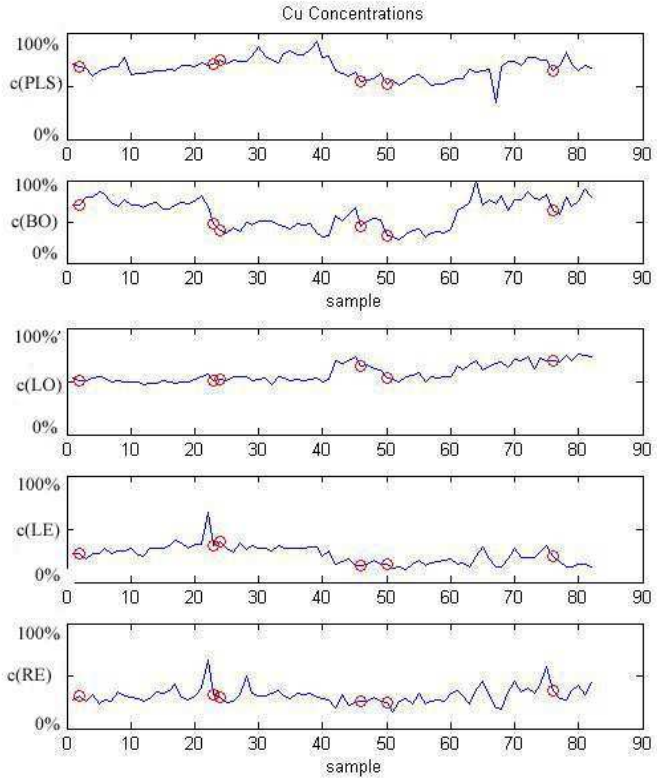

Figure 5-9: Copper concentrations of the PLS, barren organic, loaded organic, lean electrolyte and rich electrolyte. The data points closest to the cluster centres are circled. The first and fourth circles (around samples 2 and 46) are operating points DP1 and DP4 chosen for further study.

5.2.3 Analysis of the process variation

The online process data were studied in order to determine the maximum and normal variation in the controlled, manipulated and disturbance variables. The studied data set included filtered online measurements of the PLS, loaded organic, rich electrolyte and lean electrolyte copper concentrations, and the PLS parallel and series, organic and electrolyte flow rates. The data filtering method is described in Section 5.2.1. . The variation was determined as the average of the absolute errors between the filtered online measurement data *y* and the moving daily average $\overline{y}$, as follows:

$$Variation = \frac{1}{n} \cdot \sum_{i=1}^{n} \left| y_i - \overline{y}_i \right| = \frac{1}{n} \cdot \sum_{i=1}^{n} \left| y_i - \frac{1}{2p+1} \sum_{j=i-p}^{i+p} y_j \right| \qquad \textbf{(5-3)}$$

where *y* is the filtered online measurement at time (i), *n* is the number of data points in one week, and *p* is the number of data points in one day. The variation index is scaled by dividing it with the nominal value of the variable.

The data set included 18 weeks of operational online measurements of the controlled, manipulated and disturbance variables. The variations in the possible controlled variables (CV), manipulated variables (MV) and disturbance variables (DV) are presented in Table 5-3.

Table 5-3: Variations of the online measured controlled (CV), manipulated (MV) and disturbance (DV) variables.

	CV	**CV**	**CV**	**CV**	**CV**	**MV**	**MV**	**MV**	**MV**	**DV**	**DV**
	c(RE)	**c(LO)**	**c(RaffS)**	**c(RaffP)**	**c(BO)**	**F(PLSS)**	**F(PLSP)**	**F(LE)**	**F(LO)**	**c(PLS)**	**c(LE)**
	%	%	%	%	%	%	%	%	%	%	%
W1	1.30	3.20	15.30	10.31	2.92	1.99	3.04	1.25	1.77	2.30	1.58
W2	0.79	0.56	1.87	3.54	0.75	1.35	1.14	1.87	1.10	0.92	1.00
W3	0.84	1.53	7.64	3.30	0.69	1.06	0.95	1.12	0.65	3.57	1.16
W4	1.29	1.80	9.33	6.18	2.41	2.67	2.68	2.24	1.31	2.61	1.52
W5	0.97	2.45	9.03	6.54	3.03	0.90	1.22	2.47	0.95	2.37	1.18
W6	1.10	2.84	8.99	9.25	2.72	0.50	0.49	0.61	1.00	0.78	1.47
W7	0.88	1.98	6.36	5.15	1.96	0.83	0.43	0.38	0.84	0.87	0.95
W8	0.82	1.45	11.47	9.23	2.62	0.31	0.20	1.81	0.85	0.89	0.96
W9	0.93	1.44	8.21	9.62	1.78	0.11	0.17	2.72	0.75	0.87	1.47
W10	0.86	1.18	6.54	7.55	2.06	1.06	0.36	2.28	0.96	0.95	1.13
W11	1.35	3.00	8.15	7.33	2.01	0.59	0.34	2.80	0.75	0.84	1.71
W12	1.19	2.35	10.12	12.62	2.22	2.69	0.65	3.11	1.52	1.37	1.71
W13	1.18	0.70	6.62	7.47	1.68	1.50	0.25	2.62	1.05	1.39	1.81
W14	0.84	1.62	5.91	5.47	2.49	0.54	0.42	2.11	0.93	1.04	1.01
W15	2.44	1.30	13.02	9.48	1.93	1.64	1.54	2.73	1.10	1.13	3.09
W16	1.51	0.96	9.32	7.82	2.62	0.67	1.71	1.38	1.10	0.93	2.29
W17	1.59	1.22	17.06	10.47	2.58	1.55	2.38	2.63	1.05	1.78	2.64
W18	1.42	0.93	7.69	6.75	2.48	0.50	0.41	2.94	0.45	0.67	2.27
Min	0,79	0,56	1,87	3,30	0,69	0,11	0,17	0,38	0,45	0,67	0,95
Max	2,44	3,20	17,06	12,62	3,03	2,69	3,04	3,11	1,77	3,57	3,09
Mean	1,18	1,70	9,04	7,67	2,16	1,14	1,02	2,06	1,01	1,40	1,61

The maximum variation in the rich electrolyte, c(RE), loaded organic, c(LO) and barren organic c(BO) copper concentrations was between 2,5 – 3,2 %. The variations

in the raffinate copper concentrations, c(RaffS) and c(RaffP), are significantly higher (between 12 – 17%) than for the other controlled variables. The average variation in the raffinate copper concentrations is 7,7 – 9,0%, which is very large compared to that for the other variables. This might imply that the raffinate copper concentration measurements are less accurate than the other copper concentration measurements, and thus should not be used as controlled variables in the further studies.

The maximum variations for the manipulated variables (MV), the PLS series and parallel, organic and electrolyte flow rates, were around 2,8 – 3,1%. The largest average variation was in the electrolyte flow rate F(LE) and the smallest average variations in the organic flow rate F(LO) and PLS parallel flow rate F(PLSP). The disturbance variables (DV), PLS and lean electrolyte copper concentrations, had maximum variations of between 3,1 – 3,6%. On the average the variations were between 1,4 – 1,6%.

The following suggestions for the modeling and control studies are formulated on the basis of this analysis; the maximum realistic changes for the controlled and disturbance variables are less than ±5% around the chosen operating point. The maximum changes in the manipulated variables are less than ±3% around the chosen operating point. This study also suggests that the raffinate copper concentrations should not be used as controlled variables, since the large variations in these variables might indicate serious measurement inaccuracy. Variation starting from 0,5 % in the rich electrolyte copper concentration is significant for the production of the copper cathodes.

5.2.4 Remarks on the quality of the process data

Based on the preliminary analysis of the available online and offline data from the case industrial copper solvent extraction plant, the remarks are given on the process data quality.

Most of the online copper concentration measurements and the flow rate measurements have some noise, but after the data filtering, these measurements can be considered to be reliable. The online raffinate and loaded organic copper concentration measurements have high noise level and at some periods possible measurement inaccuracies. Therefore, the interpretation of these three variables should be done carefully.

The offline measurements of the intermediate copper concentrations, pH, acidity and reagent volume percent are considered to be reliable. The problem with pH, acidity and reagent volume percent measurements is the long sampling interval.

The internal recycle flow rates in the mixer-settler units are adjusted with manual valves, and thus these are not measured on the plant. Therefore in this study, these recycle flow rates have to be approximated.

6 MODELS AND THE DYNAMIC SIMULATOR FOR THE INDUSTRIAL CASE PROCESS

The steady state and dynamic models are presented and the dynamic simulator described in this Chapter.

The steady state and dynamic models, presented in Chapter 4, , are modified to conform with the flowsheet of the industrial case process described in Section 6.1 and Section 6.2 respectively. The dynamic process simulator, based on these modified models, is described in detail in Section 6.3.

The process is illustrated in Figure 5-1 and the available process measurements are listed in Table 5-1.

6.1 The equilibrium state models of the case process

The steady state copper concentrations in each mixer-settler can be expressed as a function of the incoming copper concentrations (c), the flow rates (F), the stage efficiencies (α), and the equilibrium isotherm parameters (A_i,B_i,C,D). For simplicity, the extraction equilibrium isotherm is linearized near to the operating points, represented by three aqueous copper concentrations c_{EP}^{aq}, c_{E2}^{aq}, c_{E1}^{aq}. Equations are determined for the three extraction steps EP, E1, E2 and the stripping step S. The equations are derived from those for a plant with one extraction unit and one stripping unit presented in Chapter 4 in Section 4.2. Note that the full nonlinear equilibrium isotherm is used for the simulations in Chapter 7.

For the parallel extraction unit, EP, the aqueous and organic equilibrium copper concentrations are:

$$c(RaffP) = c(PLS)\left[\frac{(1-\alpha_{EP})\hat{A}_{EP}F(LO)+F(PLSP)}{\hat{A}_{EP}F(LO)+F(PLSP)}\right] + c(BO)\left[\frac{\alpha_{EP}F(LO)}{\hat{A}_{EP}F(LO)+F(PLSP)}\right] - \left[\frac{\alpha_{EP}\hat{B}_{EP}F(LO)}{\hat{A}_{EP}F(LO)+F(PLSP)}\right] \quad (6\text{-}1)$$

$$c(BO1) = c(PLS)\left[\frac{\alpha_{EP}\hat{A}_{EP}F(PLSP)}{\hat{A}_{EP}F(LO)+F(PLSP)}\right] + c(BO)\left[\frac{\hat{A}_{EP}F(LO)+(1-\alpha_{EP})F(PLSP)}{\hat{A}_{EP}F(LO)+F(PLSP)}\right] + \left[\frac{\alpha_{EP}\hat{B}_{EP}F(PLSP)}{\hat{A}_{EP}F(LO)+F(PLSP)}\right] \quad (6\text{-}2)$$

For the first series extraction unit, E1, the aqueous and organic equilibrium copper concentrations are:

$$c(RaffS) = c(PLS1)\left[\frac{(1-\alpha_{E2})\hat{A}_{E2}F(LO)+F(PLSS)}{\hat{A}_{E2}F(LO)+F(PLSS)}\right] + c(BO1)\left[\frac{\alpha_{E2}F(LO)}{\hat{A}_{E2}F(LO)+F(PLSS)}\right] - \left[\frac{\alpha_{E2}\hat{B}_{E2}F(LO)}{\hat{A}_{E2}F(LO)+F(PLSS)}\right] \quad (6\text{-}3)$$

$$c(BO2) = c(PLS1)\left[\frac{\alpha_{E2}\hat{A}_{E2}F(PLSS)}{\hat{A}_{E2}F(LO)+F(PLSS)}\right] + c(BO1)\left[\frac{\hat{A}_{E2}F(LO)+(1-\alpha_{E2})F(PLSS)}{\hat{A}_{E2}F(LO)+F(PLSS)}\right] + \left[\frac{\alpha_{E2}\hat{B}_{E2}F(PLSS)}{\hat{A}_{E2}F(LO)+F(PLSS)}\right] \quad (6\text{-}4)$$

For the second series extraction unit, E2, the aqueous and organic equilibrium copper concentrations are:

$$c(PLS1) = c(PLS)\left[\frac{(1-\alpha_{E1})\hat{A}_{E1}F(LO)+F(PLSS)}{\left[\hat{A}_{E1}F(LO)+F(PLSS)\right]}\right] + c(BO2)\left[\frac{\alpha_{E1}F(LO)}{\left[\hat{A}_{E1}F(LO)+F(PLSS)\right]}\right] - \left[\frac{\alpha_{E1}\hat{B}_{i}F(LO)}{\left[\hat{A}_{E1}F(LO)+F(PLSS)\right]}\right] \quad (6\text{-}5)$$

$$c(LO) = c(PLS)\left[\frac{\alpha_{E1}\hat{A}_{E1}F(PLSS)}{\hat{A}_{E1}F(LO)+F(PLSS)}\right] + c(BO2)\left[\frac{\hat{A}_{E1}F(LO)+(1-\alpha_{E1})F(PLSS)}{\hat{A}_{E1}F(LO)+F(PLSS)}\right] + \left[\frac{\alpha_{E1}\hat{B}_{E1}F(PLSS)}{\hat{A}_{E1}F(LO)+F(PLSS)}\right] \quad (6\text{-}6)$$

For the stripping unit, S, the aqueous and organic equilibrium copper concentrations are:

$$c(RE) = c(LE)\left[\frac{(1-\alpha_{S})CF(LO)+F(LE)}{CF(LO)+F(LE)}\right] + c(LO)\left[\frac{\alpha_{S}F(LO)}{CF(LO)+F(LE)}\right] - \left[\frac{\alpha_{S}DF(LO)}{CF(LO)+F(LE)}\right] \quad (6\text{-}7)$$

$$c(BO) = c(LE)\left[\frac{\alpha_{S}CF(LE)}{CF(LO)+F(LE)}\right] + c(LO)\left[\frac{CF(LO)+(1-\alpha_{S})F(LE)}{CF(LO)+F(LE)}\right] + \left[\frac{\alpha_{S}DF(LE)}{CF(LO)+F(LE)}\right] \quad (6\text{-}8)$$

Calculation of all the copper concentrations in the steady state requires iteration due to organic solvent recycle between the extraction and stripping units [c(BO) - c(BO1) - c(BO2) - c(LO) - c(BO)], and the aqueous recycle between series extraction units E1 and E2 [c(PLS) – c(PLS1) – c(RaffS)]. The steady state equilibrium copper concentrations of the solvent extraction plant can be evaluated using this set of eight equations.

6.2 The dynamic models of the case process

In the extraction process, copper is transferred from the aqueous to the organic phase. Each of the three extraction unit operations are modelled by differential equations of the concentrations for both the organic ($dc_i^{org}(t)/dt$) and aqueous phases ($dc_i^{aq}(t)/dt$). The equations are derived from those for a plant with one extraction unit and one stripping unit presented in Chapter 4 in Section 4.3.

For the parallel extraction unit, EP, the aqueous and organic copper concentrations after the mixer are determined as follows:

$$\frac{dc_1^{org}(t)}{dt} = \frac{F_1^{org}(t)}{V_{mix,1}(t)} \cdot \left[c_0^{org}(t-t_0) - c_1^{org}(t) \right] + K_1 \left[c_1^{org}(t) - c_1^{org*}(t) \right] \quad \textbf{(6-9)}$$

$$\frac{dc_1^{aq}(t)}{dt} = \frac{F_1^{aq}(t)}{V_{mix,1}(t)} \cdot \left[c_0^{aq}(t) - c_1^{aq}(t) \right] - K_1 \left[c_1^{org}(t) - c_1^{org*}(t) \right] \quad \textbf{(6-10)}$$

where the equilibrium value is calculated from the equilibrium state model with the following variables:

$$c_1^{org*}(t) = g\left(c_0^{org}(t-t_0), c_0^{aq}(t), F_1^{org}(t), F_1^{aq}(t), \alpha_1, A, B \right) \quad \textbf{(6-11)}$$

For the first series extraction unit, E1, the aqueous and organic copper concentration after the mixer are determined as follows:

$$\frac{dc_2^{org}(t)}{dt} = \frac{F_2^{org}(t)}{V_{mix,2}(t)} \cdot \left[c_1^{org}(t-t_1) - c_2^{org}(t) \right] + K_2 \left[c_2^{org}(t) - c_2^{org*}(t) \right] \quad \textbf{(6-12)}$$

$$\frac{dc_2^{aq}(t)}{dt} = \frac{F_2^{aq}(t)}{V_{mix,2}(t)} \cdot \left[c_1^{aq}(t) - c_2^{aq}(t) \right] - K_2 \left[c_2^{org}(t) - c_2^{org*}(t) \right] \quad \textbf{(6-13)}$$

where the equilibrium value is calculated from the equilibrium state model with the following variables:

$$c_2^{org*}(t) = g\left(c_1^{org}(t-t_1), c_1^{aq}(t), F_2^{org}(t), F_2^{aq}(t), \alpha_2, A, B \right) \quad \textbf{(6-14)}$$

For the second series extraction unit, E2, the aqueous and organic copper concentration after the mixer are determined as follows:

$$\frac{dc_3^{org}(t)}{dt} = \frac{F_3^{org}(t)}{V_{mix,3}(t)} \cdot \left[c_2^{org}(t-t_2) - c_3^{org}(t) \right] + K_3 \left[c_3^{org}(t) - c_3^{org*}(t) \right] \quad \textbf{(6-15)}$$

$$\frac{dc_3^{aq}(t)}{dt} = \frac{F_3^{aq}(t)}{V_{mix,3}(t)} \cdot \left[c_2^{aq}(t) - c_3^{aq}(t) \right] - K_3 \left[c_3^{org}(t) - c_3^{org*}(t) \right] \quad \textbf{(6-16)}$$

where the equilibrium value is calculated from the equilibrium state model with the following variables:

$$c_3^{org*}(t) = g\left(c_2^{org}(t-t_2), c_2^{aq}(t), F_3^{org}(t), F_3^{aq}(t), \alpha_3, A, B \right) \quad \textbf{(6-17)}$$

The parallel raffinate copper concentration, c(RaffP), after the EP settler is the time delayed value of the aqueous copper concentration from the EP mixer.

$$c(RaffP)(t) = c_1^{aq}(t - t_1) \quad \textbf{(6-18)}$$

The series raffinate copper concentration, c(RaffS), after the E1 settler is the time delayed value of the aqueous copper concentration from the E1 mixer.

$$c(RaffS)(t) = c_2^{aq}(t - t_2) \quad \textbf{(6-19)}$$

The loaded organic copper concentration, c(LO), after the E2 settler is the time delayed value of the organic concentration from the E2 mixer.

$$c(LO)(t) = c_3^{org}(t - t_3) \quad \textbf{(6-20)}$$

In the stripping unit, copper is transferred from the organic to the electrolyte solution. The stripping unit operation is modelled using differential equations of the concentrations for both the electrolyte ($dc_i^{aq}(t)/dt$) and organic ($dc_i^{org}(t)/dt$) phases as follows:

$$\frac{dc_1^{el}(t)}{dt} = \frac{F_1^{el}(t)}{V_{mix,4}(t)} \cdot \left[c_0^{el}(t) - c_1^{el}(t) \right] + K_4 \left[c_1^{el}(t) - c_1^{el*}(t) \right] \quad \textbf{(6-21)}$$

$$\frac{dc_4^{org}(t)}{dt} = \frac{F_4^{org}(t)}{V_{mix,4}(t)} \cdot \left[c_3^{org}(t - t_3) - c_4^{org}(t) \right] - K_4 \left[c_1^{el}(t) - c_1^{el*}(t) \right] \quad \textbf{(6-22)}$$

where the equilibrium copper concentration is calculated from the equilibrium state model with the following variables:

$$c_1^{el*}(t) = h\left(c_3^{org}(t - t_3), c_0^{el}(t), F_4^{org}(t), F_1^{el}(t), \alpha_4, C, D \right) \quad \textbf{(6-23)}$$

The rich electrolyte concentration (c(RE)) is the time delayed value of the electrolyte concentration, and the barren organic concentration (c(BO)) is the time delayed value of the organic concentration in the stripping unit.

$$c(RE)(t) = c_1^{el}(t - t_4) \quad \textbf{(6-24)}$$

$$c(BO)(t) = c_4^{org}(t - t_4) \quad \textbf{(6-25)}$$

The organic tank and wash stage between the extraction and stripping stages are modeled as a lumped time delay.

6.3 Dynamic simulator for the industrial case process

The aim of the simulator is to facilitate studies on the dynamic behaviour of the solvent extraction process, and to provide a test bench for the control system. The simulation model describes the real time behaviour of a continuous copper solvent extraction process, and considers only the mass transfer of copper.

6.3.1 Overall structure of the simulator

The dynamic simulator of the process was constructed on the basis of the dynamic models described earlier in this chapter. The unit operation models were implemented in the Matlab Simulink environment according to the plant flowsheet, as shown in Figure 6-1. The model of the extraction process consists of three mixer-settler unit models, one in parallel (E1P) and two in series (E1S and E2S). The stripping process model consists of one mixer-settler unit model (S1H). The organic storage tank model (Tank) is located between the extraction and stripping processes.

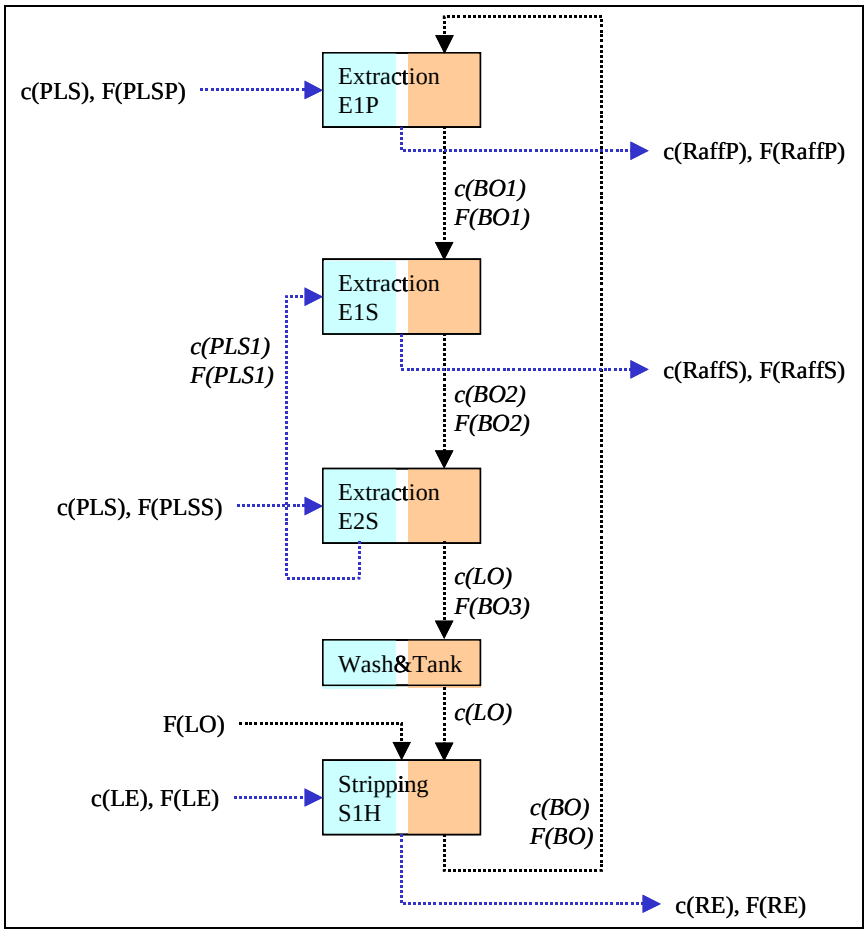

Figure 6-1: Simulation model of the copper solvent extraction process. The parallel extraction unit is marked with E1P, the first series extraction unit with E1S, and the second extraction unit with E2S. The stripping unit is marked with S1H and the organic storage tank with 'Tank'. The input variables (left) are the copper concentrations c(PLS) and c(LE) and the flow rates F(PLSP), F(PLSS), F(LO), F(LE). The state variables are the intermediate copper concentrations *c(BO), c(BO1), c(BO2), c(LO), c(PLS1)* marked with italics. The output variables (right) are the copper concentrations c(RE), c(RaffS) and c(RaffP).

The inputs of the simulator are the copper concentrations of the leach and electrolyte solutions, c(PLS) and c(LE), and the flow rates of the parallel and series leach solutions, the organic solution and the electrolyte solution, F(PLSP), F(PLSS), F(LO), F(LE). The intermediate copper concentrations are the partial leach solution c(PLS1) from the second extraction step, the barren organic concentration c(BO) from stripping, the first partial organic concentration c(BO1) from the parallel extraction step, second partial c(BO2) organic concentration from first series extraction step, and the loaded organic concentration c(LO) from the second series extraction step. The

loaded organic copper concentration is then led to the tank model, which is a pure time delay, and then to the stripping stage. The output copper concentrations from the model are the raffinate parallel and series concentrations, c(RaffP) and c(RaffS), and the rich electrolyte concentration c(RE). The input variables, state variables, output variables, parameters and constants of the simulation model are listed in Table 6-1.

Table 6-1: Input variables, state variables, output variables, parameters and coefficients of the simulation model.

Classification	Variable name	Abbreviation
Input variables	PLS Cu concentration	c(PLS)
	Lean electrolyte Cu concentration	c(LE)
	PLS parallel flow rate	F(PLSP)
	PLS series flow rate	F(PLSS)
	Organic flow rate	F(LO)
	Electrolyte flow rate	F(LE)
State variables	Partial PLS copper concentration	c(PLS1)
	First partial organic copper concentration	c(BO1)
	Second partial organic copper concentration	c(BO2)
	Loaded organic Cu concentration	c(LO)
	Barren organic Cu concentration	c(BO)
Output variables	Rich electrolyte Cu concentration	c(RE)
	Raffinate series Cu concentration	c(RaffS)
	Raffinate parallel Cu concentration	c(RaffP)
Parameters	Mass transfer param.	K_1, K_2, K_3, K_4
	Efficiencies	α_1, α_2, α_3, α_4
	Recycle correction param.	cf_1, cf_2,cf_3, cf_4
	Extraction isotherm param.	*A,B*
	Stripping isotherm param.	*C,D*
Constants	Mixer volume	V_m
	Settler volume	V_s
	Extraction time delay	*t(extr)*
	Stripping time delay	*t(strip)*

6.3.2 Overall structure of the unit process simulation model

The extraction and stripping units are modeled as a combination of mixing and plug flow models, as shown in Figure 6-2. The inputs to the mixer are the incoming aqueous and organic flow rates, F_{in}^{aq} and F_{in}^{org}, and the incoming aqueous and organic copper concentrations, c_{in}^{aq} and c_{in}^{org}. These inputs and the parameters are first led to the mixer model, where the mass transfer of copper between the phases is calculated. The resulting mixer output copper concentrations, c_{outm}^{aq} and c_{outm}^{org}, are then led to the aqueous and organic settler models. In the settler model the mixer output copper concentrations and the flow rates are delayed. The outputs of the mixer-settler unit model are the aqueous and organic copper concentrations, c_{outs}^{aq} and c_{outs}^{org} , and the flow rates F_{outs}^{aq} and F_{outs}^{org}. The tank model is a pure time delay (Equation 7-5).

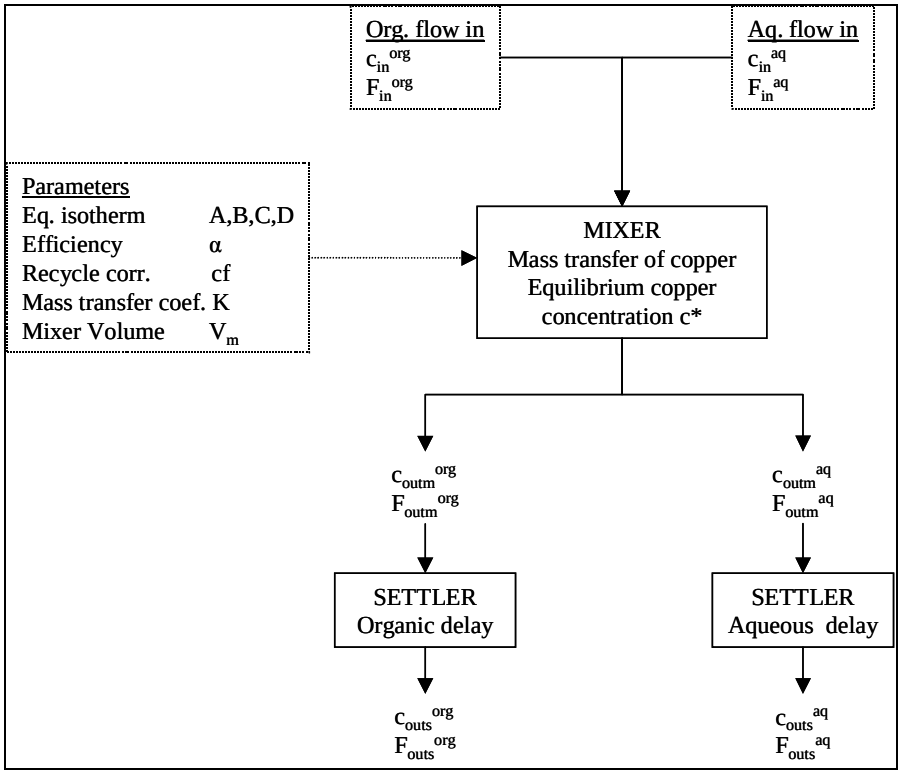

Figure 6-2: Overall structure of the mixer-settler model.

6.3.3 Detailed structure of the unit process simulation model

The structure of the mixer-settler model is illustrated in more detail in Figure 6-3 with the equations for the stripping unit. The calculation is based on the dynamic models of the plant presented in Chapter 6.2. The parameters are calculated from the offline data according to the equations presented in Chapters 4.2 and Chapter 4.3.

In the mixer model the incoming online copper concentrations, c_{in}, and online flow rates, F_{in}, are first led to the aqueous to organic ratio (A/O) dynamics filter (1/(as+1)), which describes the slowness of the phase ratio change in the mixer. Next, the equilibrium copper concentration c^{aq*} is calculated according to Equation 6-7. The calculation of the equilibrium copper concentration requires measurements of the copper concentration, c_{inm}, and flow rate, F_{inm}, together with the parameters of the equilibrium isotherm (*C,D* Equation 4-22), the efficiency (α Equation 4-23) and the recycle corrected organic to aqueous ratio (*cf* Equation 4-25). Since the equilibrium value does not change immediately, the equilibrium value is filtered with (1/(bs+1)). The filtering enhances the numerical convergence of the integration of the mass transfer equations. The mass transfer in the stripping unit between the organic and the aqueous phases is calculated according to Equation 6-21 and Equation 6-22. The inputs and parameters for this calculation are the copper concentrations c_{inm} and flow rates F_{inm}, the equilibrium copper concentration c^{aq}*, the mixer volumes for the organic and aqueous phases (V_{mix}^{org} Equation 4-37 and V_{mix}^{aq} Equation 4-38), and the mass transfer coefficient (*K* Equation 4-36).

The settler model is a pure time lag for the organic and aqueous phases. The organic copper concentration c_{outm}^{org} and flow rate F_{inm}^{org} from the mixer model are delayed according to Equation 6-25, where the time delay is calculated on the basis of Equation 4-37. The aqueous copper concentration c_{outm}^{aq} and flow rate F_{inm}^{aq} from the

mixer model are delayed according to Equation 6-24, where the time delay is calculated on the basis of Equation 4-38.

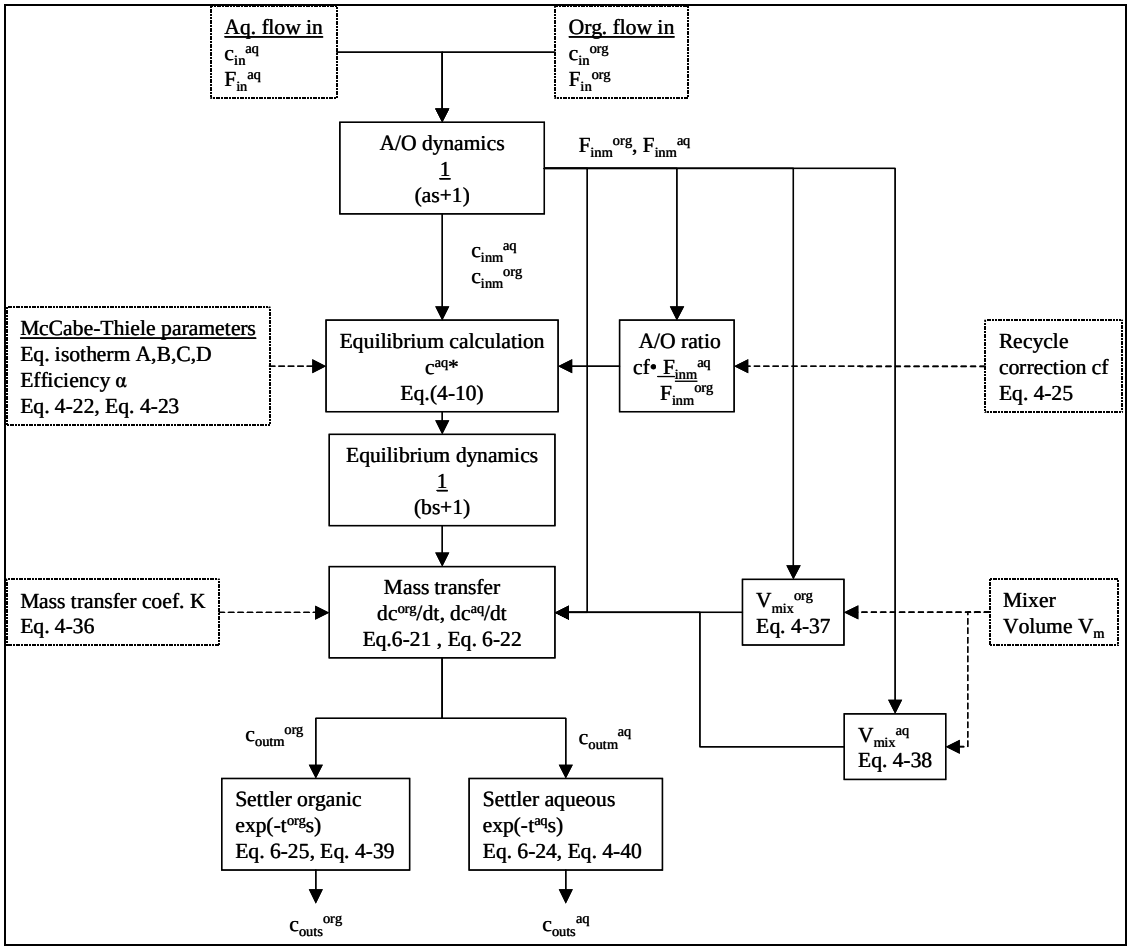

Figure 6-3: Detailed structure of the mixer-settler model with equations for the stripping unit. The input variables and parameters are marked with dashed rectangles. Calculations are marked with solid rectangles.

The inputs and outputs of each mixer-settler unit model are listed in Table 6-2, and the equations of the parameter estimation and the dynamic calculations in Table 6-3.

Table 6-2: The inputs and outputs of each mixer-settler unit model.

Classification	Variable	E1P	E1S	E2S	S1H
Inputs	c^{aq}	c(PLS) (t)	c(PLS1) (t)	c(PLS) (t)	c(LE) (t)
	c^{org}	c(BO) (t)	c(BO1) (t)	c(BO2) (t)	c(LO) (t)
	F^{aq}	F(PLSP) (t)	F(PLSS) (t- t_3)	F(PLSS) (t)	F(LE) (t)
	F^{org}	F(LO) (t-t_4)	F(LO) (t-t_4-t_1)	F(LO) (t-t_4-t_1-t_2)	F(LO) (t)
Outputs	c^{aq}	C(RaffP)	C(RaffS)	C(PLS1)	C(RE)
	c^{org}	C(BO1)	C(BO2)	C(LO)	C(BO)
	F^{aq}	F(PLSP) (t-t_1)	F(PLSS) (t- t_3-t_2)	F(PLSS) (t-t_3)	F(LE) (t-t_4)
	F^{org}	F(LO) (t-t_4-t_1)	F(LO) (t-t_4-t_1-t_2)	F(LO) (t-t_4-t_1-t_2-t_3)	F(LO) (t-t_4)

Table 6-3: The equations of the parameter estimation and dynamic calculation of each mixer-settler unit model.

Classification	Equation name	E1P	E1S	E2S	S1H
Parameters Estimations	Equilibrium isotherm *A,B, C,D*	Eq. 7-2	Eq. 7-2	Eq. 7-2	Eq. 7-4
	Efficiency α	Eq. 4-23	Eq. 4-23	Eq. 4-23	Eq. 4-23
	Recycle correction *cf*	Eq. 4-25	Eq. 4-25	Eq. 4-25	Eq. 4-25
	Mass transfer coef. *K*	Eq. 4-36	Eq. 4-36	Eq. 4-36	Eq. 4-36
	Mixing volume aq. V_{mix}^{aq}	Eq. 4-38	Eq. 4-38	Eq. 4-38	Eq. 4-38
	Mixing volume org. V_{mix}^{org}	Eq. 4-37	Eq. 4-37	Eq. 4-37	Eq. 4-37
	Settler delay aq. t^{aq}	Eq. 4-40	Eq. 4-40	Eq. 4-40	Eq. 4-40
	Settler delay org. t^{org}	Eq. 4-39	Eq. 4-39	Eq. 4-39	Eq. 4-39
Dynamic Calculations	Equilibrium calculation	Eq. 4-3 & Eq. 4-4	Eq. 4-3 & Eq. 4-4	Eq. 4-3 & Eq. 4-4	Eq. 4-10
	Mass transfer aq.	Eq. 6-10	Eq. 6-13	Eq. 6-16	Eq. 6-21
	Mass transfer org.	Eq. 6-9	Eq. 6-12	Eq. 6-15	Eq. 6-22
	Settler aq.	Eq. 6-18	Eq. 6-19	Eq. 6-19	Eq. 6-24
	Settler org.	Eq. 6-20	Eq. 6-20	Eq. 6-20	Eq. 6-25

7 SIMULATION RESULTS OF THE COPPER SOLVENT EXTRACTION MODEL

The aim of this chapter is to verify the dynamic models by comparing the simulated data to the industrial data. The input data are presented in Section 7.1. The parameters are estimated for the equilibrium state models and dynamic models in Section 7.2. The simulation results are presented for two industrial data sets in Section 7.3.

7.1 Input data for the simulation study

The input data for the simulation studies include two data sets. The online inputs consist of PLS and lean electrolyte copper concentrations, and flow rates for the two PLS streams, organic solution and electrolyte solution. The offline inputs for the parameter estimations include measurements of the pH of the PLS solution, acidity of the electrolyte solution, reagent volume of the organic solution, and six aqueous and four organic intermediate copper concentrations (Table 5-1). The online measurements of the copper concentrations and flow rates, together with extrapolated offline measurements of the pH, acidity and reagent volume per cent in the organic solution, are illustrated in the following.

The online copper concentrations, extrapolated offline measurements and flow rates of the first data set are presented in Figure 7-1 and in Figure 7-2. This data set is characterized by three slow wave types of change in the PLS grade and an almost constant decrease in the pH of PLS, together with bigger step changes in the flow rates, as shown in Figure 7-1 and Figure 7-2. Especially interesting periods are the flow rate changes during sampling period [800, 1100] and [2000, 2300], and changes in the lean electrolyte concentration during sampling period [1300 – 1600].

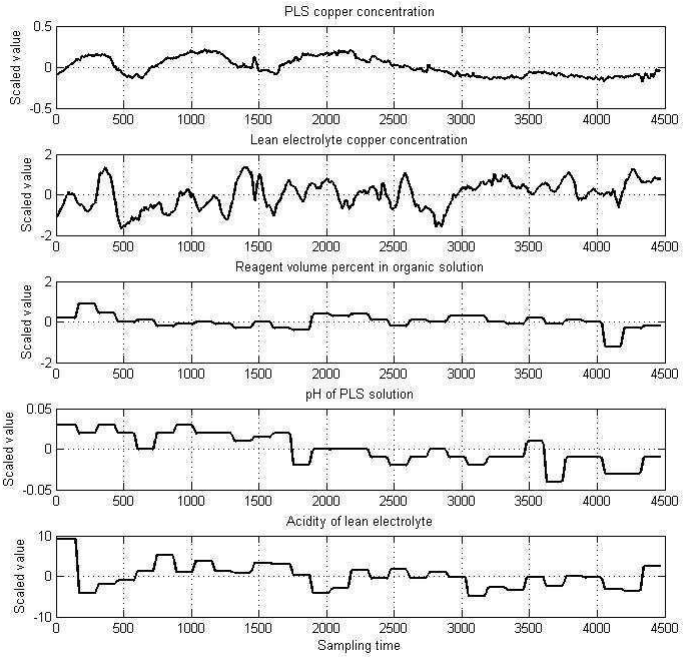

Figure 7-1: PLS and lean electrolyte copper concentrations, reagent volume per cent in the organic solution, pH of the PLS solution and acidity of the electrolyte solution.

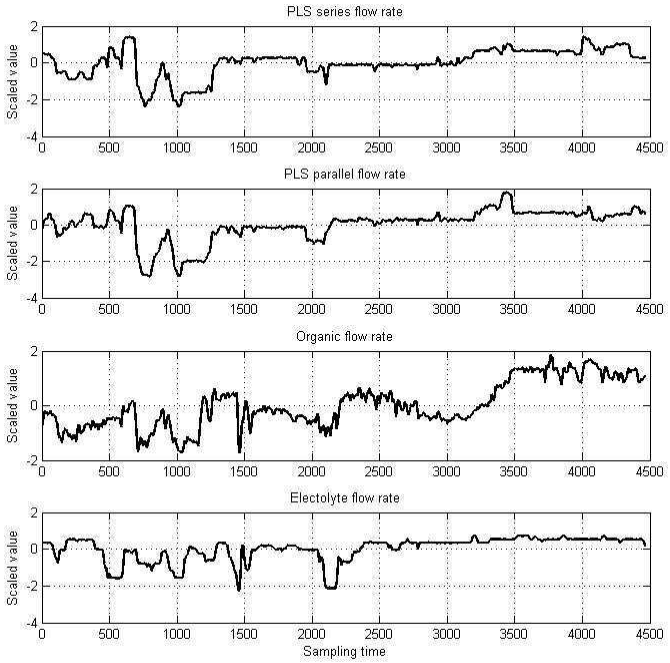

Figure 7-2: Flow rates of the PLS series, PLS parallel, organic solution and electrolyte solution.

The online copper concentrations, extrapolated offline measurements and flow rates of the second data set are presented in Figure 7-3 and Figure 7-4. This data set is characterized by a slow rise in both the PLS copper concentration and reagent volume

per cent in the organic solution after sampling time 1000. The lean electrolyte concentration change considerably during the whole period, and there is a decrease in the flow rates around sampling period [2200 – 2500].

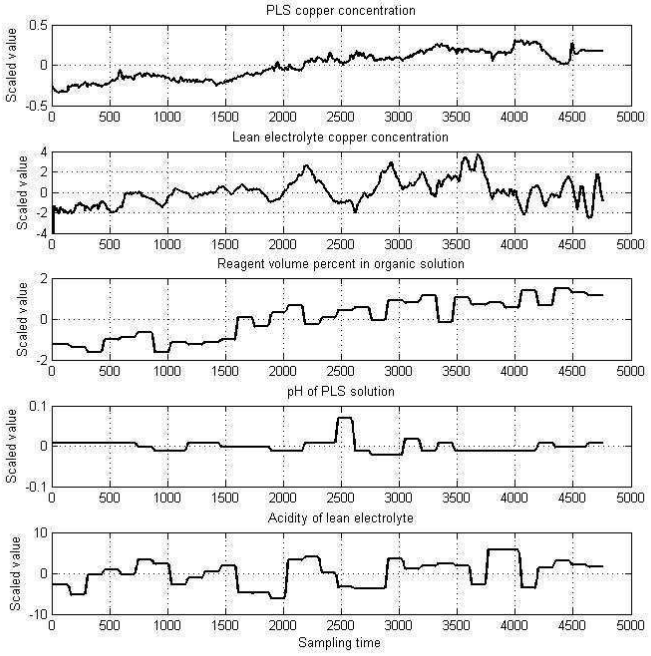

Figure 7-3: PLS and lean electrolyte copper concentrations, reagent volume per cent in the organic solution, pH of the PLS solution and acidity of the electrolyte solution.

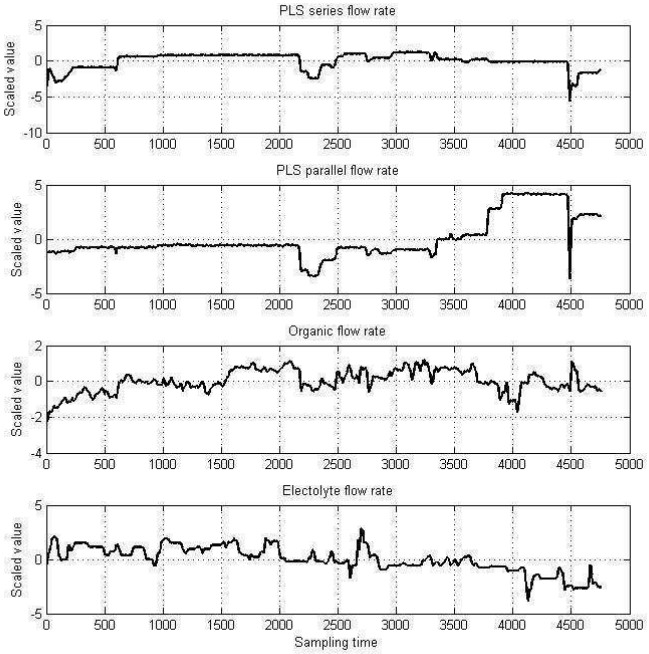

Figure 7-4: Flow rates of the PLS series, PLS parallel, organic solution and electrolyte solution.

7.2 Estimation of the simulation model parameters

The parameters for the steady state and dynamic model structures are estimated in this section. The parameter estimation for the equilibrium state model, based on the McCabe-Thiele diagram approach, is first presented. The parameters of the extraction and stripping equilibrium isotherms are determined in Section 7.2.1. The parameters for the efficiencies and the recycle corrections are estimated in Section 7.2.2. Finally, the parameters for the dynamic structures of the copper solvent extraction model are estimated in Section 7.2.3.

7.2.1 Estimation of the equilibrium isotherm parameters

The first aim of this section is to determine the constant parameters for the extraction and stripping equilibrium models on the basis of the nominal equilibrium isotherm models, and the experimental and simulated equilibrium isotherm data. The second aim is to determine the equilibrium isotherm parameters for the first and second test data period.

7.2.1.1 Estimation of the constant parameters of the equilibrium isotherm model

The basic structure for the extraction equilibrium isotherm between the organic (y) and aqueous (x) copper concentration consists of squares of the reagent volume per cent (vol) and the pH level (pH) with the reagent specific constant ϕ and the inverse reaction constant φ, and is defined as follows:

$$c^{org} = \frac{Ac^{aq}}{B + c^{aq}} = \frac{c(R)^2 \cdot c^{aq}}{c(H^+)^2 / K_e + c^{aq}} = \frac{\phi(vol)^2 \cdot c^{aq}}{\varphi(10^{-pH})^2 + c^{aq}} \quad \textbf{(7-1)}$$

For the modeling there are 144 data points from 18 simulated equilibrium isotherms, and for validation 2 data sets with 16 data points. The variables are the initial aqueous and organic concentrations (x_0 and y_0), the reagent volume percent in the organic solution (vol), the pH of the solution, and the equilibrium values for the aqueous and organic concentrations. In order to get a good fit for the equilibrium isotherm over the whole operating range, the criterion applied in model fitting is minimization of the absolute error sum between the measurements and model predictions.

The following model structure describes adequately well the extraction equilibrium data:

$$c^{org} = \frac{\phi(vol) \cdot c^{aq}}{\varphi(H^+)^2 (c^{org}{}_0 / c^{aq}{}_0) + c^{aq}} \quad \textbf{(7-2)}$$

The constant parameters are [ϕ=0.51 φ=253.80]. The model fit is good, the absolute error sum is 2.77, and measurement and the predicted points overlap very well, as can be seen from Figure 7-5.

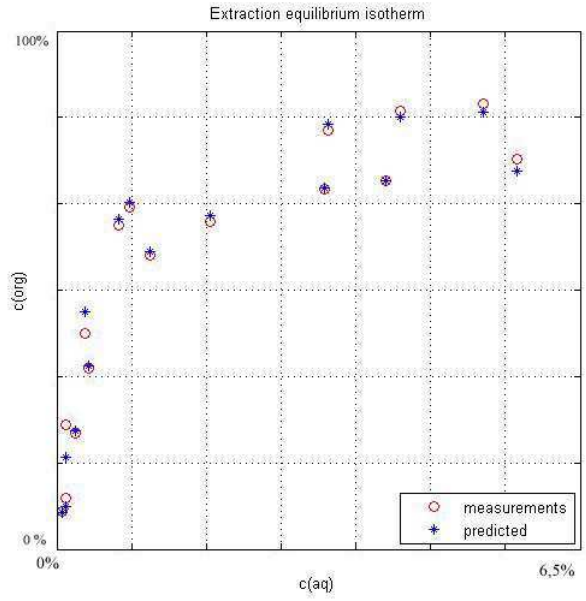

Figure 7-5: Validation datapoints (o) and predicted data points (*) of the extraction equilibrium isotherm.

The basic structure for the stripping equilibrium isotherm consists of squares of the reagent volume per cent (vol) and acidity (acid) with the reagent specific constant ϕ and the inverse reaction constant ϖ, and the estimation error term ε. The stripping equilibrium isotherm is defined as follows:

$$c^{org} = C \cdot c^{aq} + D = \frac{c(R)^2 \cdot c^{aq}}{c(H^+)^2 / K_S} + \varepsilon = \frac{\phi (vol)^2 \cdot c^{aq}}{\omega (acid)^2} + \varepsilon \qquad \textbf{(7-3)}$$

The simulated modeling data for the stripping equilibrium isotherm include 165 data points, with 24 data points close to the normal operating conditions. The model validation data include two real isotherms measured in the plant, including a total of 6 data points. The variables are the initial concentration of the aqueous solution (x_0), the reagent volume per cent in the organic solution (vol), the acidity of the solution (acid), and the equilibrium values for the aqueous and organic concentrations (x and y).

The following model structure with the parameter values [ϕ/ϖ=0.48, ψ=0. 75, ζ=-0.04] describes adequately well the stripping equilibrium data:

$$c^{org} = \frac{\phi}{\omega}\left[\frac{(vol)}{(acid)}\right]^{\psi} \cdot c^{aq} + \zeta x_0 \qquad \textbf{(7-4)}$$

The model has adequate fit to the measurements, as can be seen from Figure 7-6.

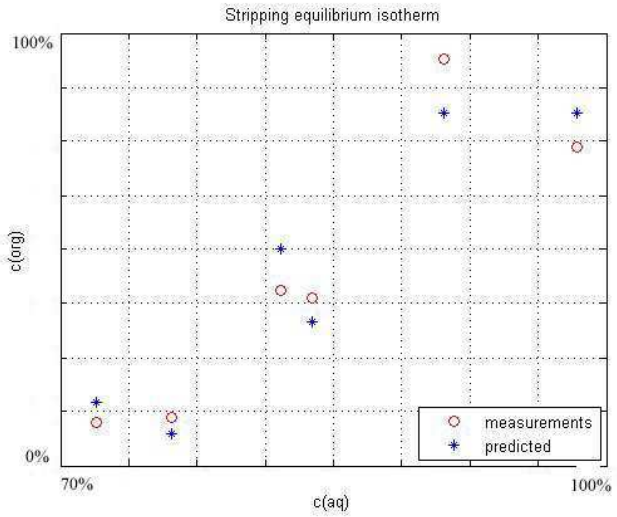

Figure 7-6: Validation data points (o) and predicted data points (*) of the stripping equilibrium isotherm.

7.2.1.2 Estimation of the equilibrium isotherm parameters

The constant equilibrium isotherm parameters are determined from the available laboratory equilibrium measurement set, including 8 data points for the extraction equilibrium isotherm curve and 3 data points for the stripping equilibrium isotherm line.

The varying equilibrium isotherm parameters are calculated from Equation 7-2 and Equation 7-4 on the basis of the reagent volume per cent in the organic solution, pH of the PLS solution and acidity of the electrolyte solution, as well as the initial values of the input concentrations in the aqueous and organic phases.

The changes in the equilibrium isotherm parameters for the first test period are shown in Figure 7-7. The isotherm parameter *A* decreases and *B* increases during the test period, leading to a lower extraction potential of copper from the PLS solution to the organic solution.

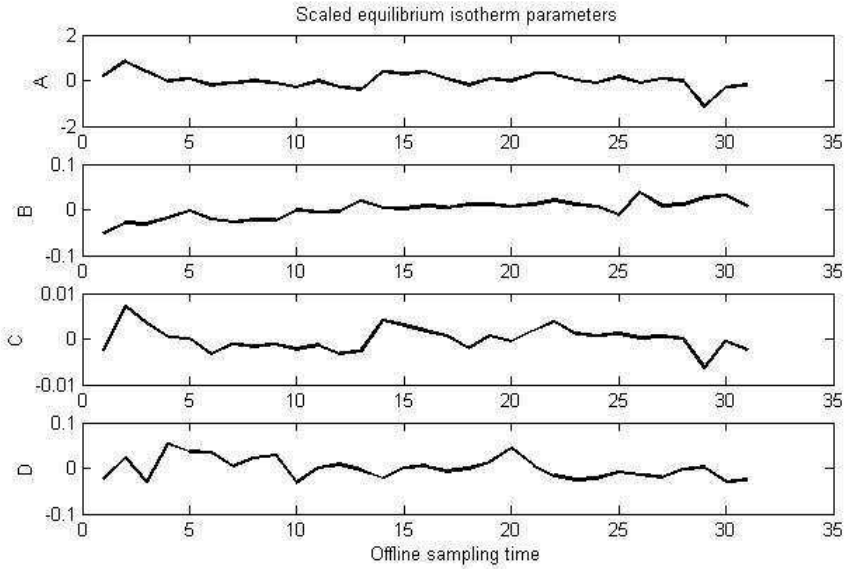

Figure 7-7: Scaled values of the varied equilibrium isotherm parameters: A and B for extraction, and C and D for stripping for the first test period.

The changes in the equilibrium isotherm parameters in the second test period are shown in Figure 7-8. In the figure the isotherm parameter *A* increases significantly during the test period, leading to a higher extraction potential of copper from the PLS solution to the organic solution.

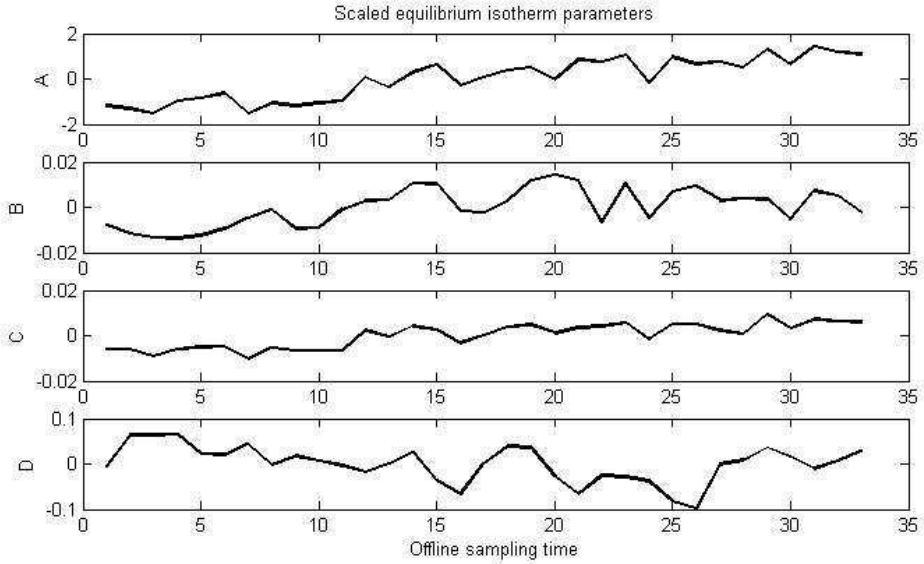

Figure 7-8: Scaled values of the varied equilibrium isotherm parameters: A and B for extraction, and C and D for stripping for the second test period.

7.2.2 Estimation of the efficiency and recycle correction parameters

The aim of this section is to determine the efficiency and recycle correction parameters for the constant parameter and varied parameter approaches. The efficiency of a mixer-settler unit is defined in Equation 4-23 and the recycle correction in Equation 4-25.

Both of the two available offline measurement data sets included around 35 data points. The plant operation was assumed to be stable, with small daily variation. As a result it was therefore also assumed that the offline copper concentration measurements, average flow rates and estimated equilibrium isotherms would represent the steady state of the process.

In the varied parameter approach, the efficiency and recycle correction parameters are calculated directly on the basis of the offline measurements, and no optimization is necessary to fit the parameters.

In the constant parameter approach, optimization is necessary to fit the parameters to the offline data sets. The optimization for the parameter estimation is explained in detail in the following.

An optimization model is constructed on the basis of the equilibrium state models presented in Section 6.1. The parameter estimation is based on minimizing the error between the equilibrium state model outputs and the measurements, listed in Table 7-1. If the steady state assumption is valid, then with optimal parameters all the error measures approach zero.

Table 7-1: Inputs, outputs, estimated parameters and error measures for all four unit processes.

Stage	Inputs and constant parameters	Outputs	Estimated parameters	Error measure
EP	c(BO),c(PLS), F(PLSP),F(LO), A,B	c_{est}(BO1), c_{est}(RaffP)	α_{EP},cf_{EP}	c(RaffP)-c_{est}(RaffP)
E1S	c_{est}(BO1), c(PLS1), F(PLSS),F(LO), A,B	c_{est}(BO2), c_{est}(RaffS)	α_{E1},cf_{E1}	c(RaffS)-c_{est}(RaffS)
E2S	c_{est}(BO2), c(PLS), F(PLSS),F(LO), A,B	c_{est}(LO), c_{est}(PLS1)	α_{E2},cf_{E2}	c(PLS1)-c_{est}(PLS1) c(LO)-c_{est}(LO)
S	c_{est}(LO), c(LE), F(LE),F(LO), C,D.	c_{est}(BO), c_{est}(RE)	α_S,cf_S	c(RE)-c_{est}(RE) c(BO)-c_{est}(BO)

It is assumed that the parameters are different for the two offline data sets. Therefore, both are optimized separately with the Matlab *lsqcurvefit* algorithm for nonlinear curve-fitting. The cost function aims to minimize the error measures presented in Table 7-1. In order to minimize the recycle loop effects, the errors between the offline measured and estimated copper concentrations of the barren organic (c(BO)) and partial PLS (c(PLS1)) concentrations are weighted more in the cost function than the errors between the offline measured and estimated copper concentrations of the rich electrolyte (c(RE)) and loaded organic (c(LO)). The cost function is defined as follows:

$$Cost = 10\sum_{i=1}^{N}\left|c(BO)_{meas}(i) - c(BO)_{est}(i)\right| + 10\sum_{i=1}^{N}\left|c(PLS1)_{meas}(i) - c(PLS1)_{est}(i)\right| + \sum_{i=1}^{N}\left|c(RE)_{meas}(i) - c(RE)_{est}(i)\right| + \sum_{i=1}^{N}\left|c(LO)_{meas}(i) - c(LO)_{est}(i)\right| \quad \textbf{(7-5)}$$

In order to demonstrate the approach, the errors for the second data set are illustrated in Figure 7-9 and the average absolute error sums are given in Table 7-2.

The error sums are not exactly zero, which implies that the steady state assumption is not fulfilled in the constant parameter approach. However, considering the possible inaccuracy of the offline measurements, the fit is sufficient. Thus, the constant efficiency approach is tested in the simulation study.

Table 7-2: Average absolute errors for the different copper concentrations.

Error sum	**c(RaffP)**	**c(RaffS)**	**c(PLS1)**	**c(LO)**	**c(RE)**	**c(BO)**
	0.0565	0.0961	0.0794	0.3117	0.4692	0.1612

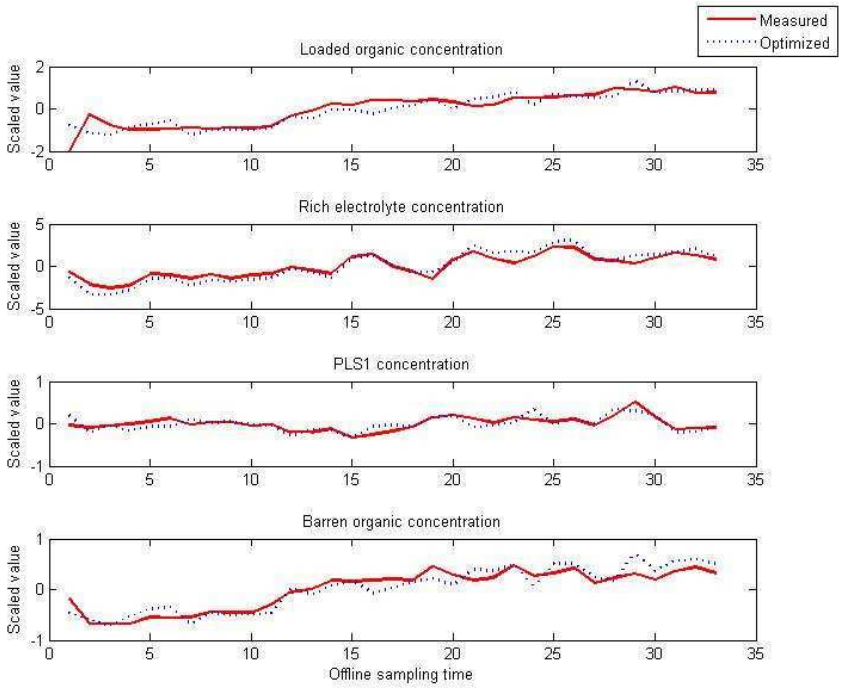

Figure 7-9: The scaled values of the loaded organic, rich electrolyte, partial PLS and barren organic copper concentrations; measured (red, solid) and estimated (blue, dotted) for the second data set.

7.2.2.1 Efficiency and recycle correction parameters for the first test period

The constant efficiency and recycle correction parameters are optimized for the first offline test data set. The parameter values are shown in Table 7-3.

Table 7-3: Efficiencies and recycle corrections for nominal (NOM) and changing equilibrium isotherm (I) models.

Model	α_{EP}	α_{E1}	α_{E2}	α_{S}	cf_{EP}	cf_{E1}	cf_{E2}	cf_{S}
(NOM)	0.9591	1.0036	0.8892	0.8351	0.9728	1.1951	0.9854	0.9523
(I)	0.9710	1.0670	0.7900	0.8432	0.9787	1.0720	0.8836	0.9171

The varied efficiency and recycle correction parameters are calculated from the first offline data set. The parameter values for the first test period are shown in Figure 7-10 and Figure 7-11. All the parameters are close to 1, although larger variation occurs

simultaneously with very high or low reagent volume per cent points. This is natural since the efficiency is strongly dependent on the equilibrium isotherm. The parameters for stripping do not change significantly, since the equilibrium isotherm parameters are relatively stable, as can be seen from Figure 7-10.

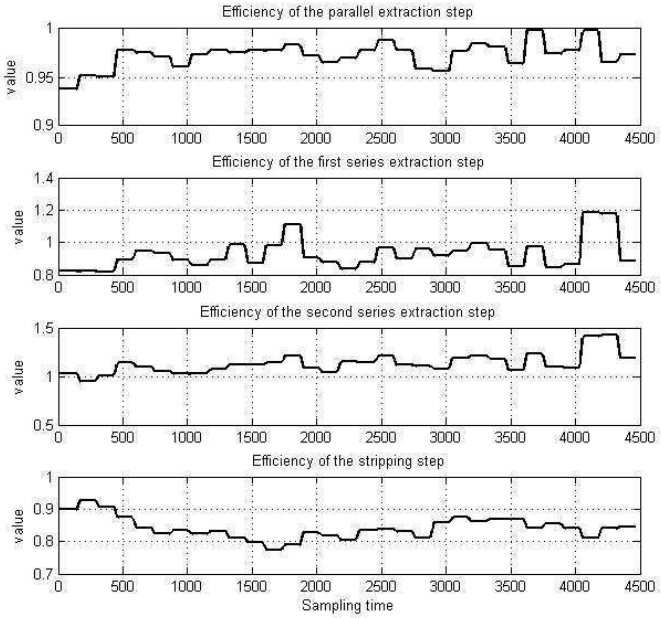

Figure 7-10: Varied efficiencies for the extraction and stripping stages.

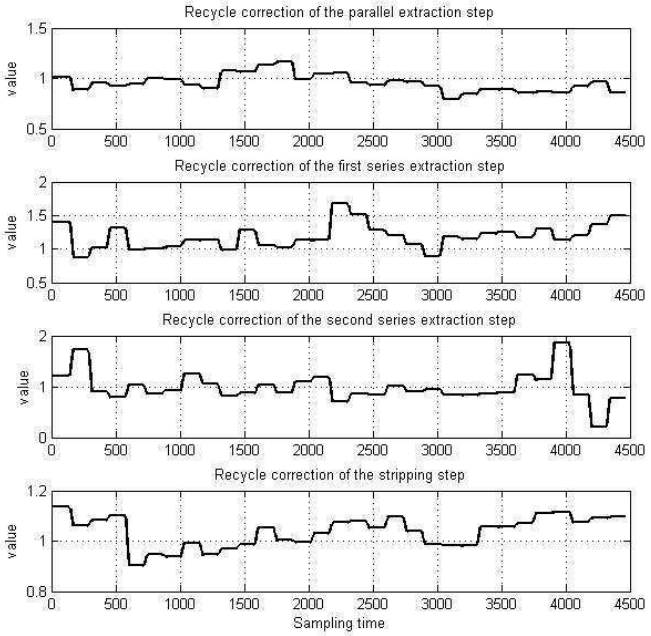

Figure 7-11: Estimated recycles for the extraction and stripping stages.

7.2.2.2 Efficiency and recycle correction parameters for the second test period

The constant efficiencies and recycle correction parameters are optimized for the second test data period. The parameter values are presented in Table 7-4. The efficiency evaluation with the constant equilibrium isotherm is a challenging task due to the significant changes in the real equilibrium isotherm. With the varied equilibrium isotherms the optimization of the efficiency parameters is better, although the efficiencies seem to change as the equilibrium isotherm parameter changes.

Table 7-4: Efficiencies and recycle corrections for nominal (nom) and changing equilibrium isotherm (I) models.

Model	α_{EP}	α_{E1}	α_{E2}	α_{S}	cf_{EP}	cf_{E1}	cf_{E2}	cf_{S}
(NOM)	0.9421	0.9478	0.9577	0.8783	1.0738	1.2738	1.0388	1.1299
(I)	1.0859	0.6655	1.0157	0.9242	1.0519	1.3181	0.9401	1.0195

The varied efficiency and recycle correction parameters are calculated for the second test data set. The parameter values are shown in Figure 7-12 and Figure 7-13. The efficiencies are slightly lower than for the first test data set, and there is much more variation in the recycle correction parameters, due to sudden drops in the flow rates and concentrations.

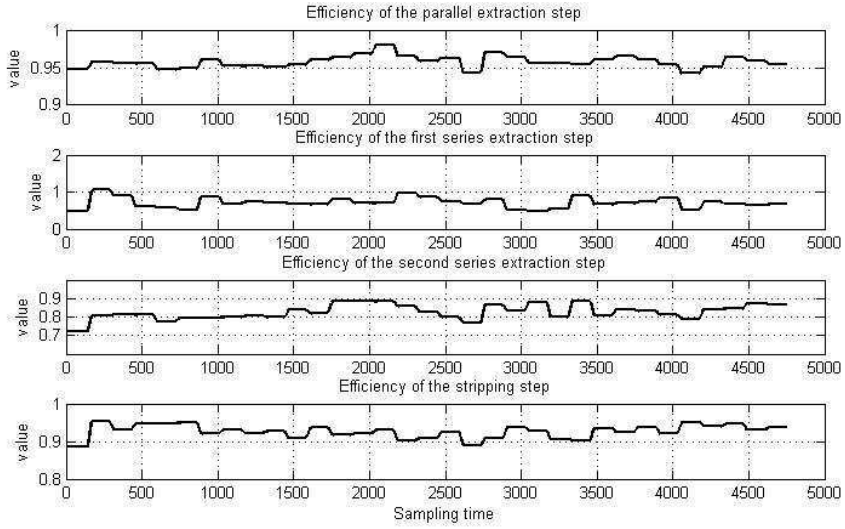

Figure 7-12: Varied efficiencies for the extraction and stripping stages.

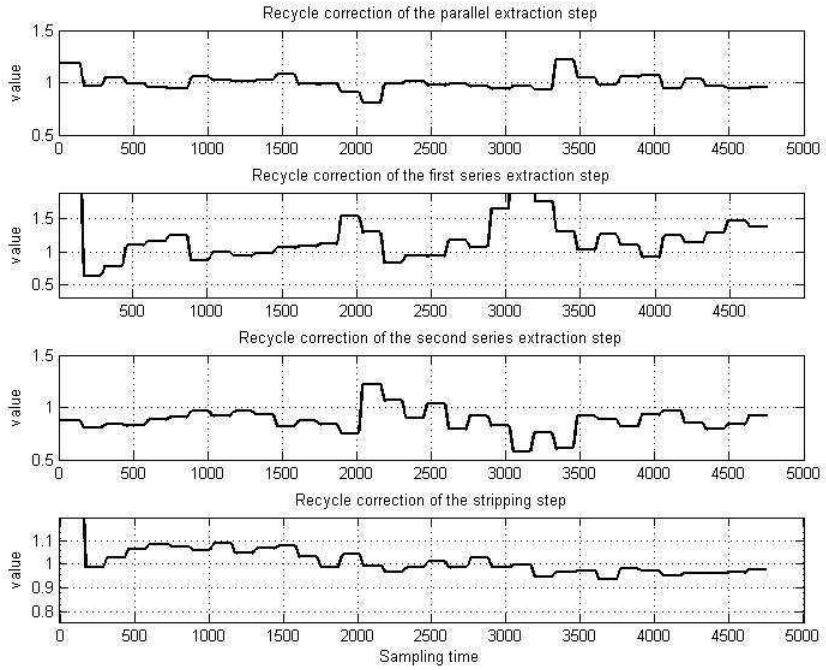

Figure 7-13: Estimated recycles for the extraction and stripping stages.

7.2.3 Estimation of the other parameters

Estimation of the mass transfer parameter *K* for the dynamic model, and constants for the dynamics of the phase ratio change and the equilibrium changes, as well as the time delay constants, are presented in this section.

The mass transfer parameter *K* is calculated on the basis of Equation (4-36). The constant parameter is estimated on the basis of the average offline measurement values. For the varied parameter approach, the mass transfer parameter is estimated from the offline measurements.

Changes in the organic and aqueous flow rates invert the aqueous to organic ratio and subsequently the interfacial area for the copper mass transfer in the mixers. The new balance between the phases does not settle immediately. As no measurements of the phenomenon are available, in this study it is therefore assumed that the change follows first order dynamics with a time constant of 2 sampling times (filter (1/(2s+1)).

The change in the equilibrium value is not immediate due to the reaction kinetics. Since measurements are not available (or even possible because this is a purely theoretical issue), it is assumed that the change follows first order dynamics with a time constant of 2 sampling times (filter (1/(2s+1)).

The time delay of the mixer-settler combination is estimated on the basis of the mean flow rate and the volume of the settler, as defined for an organic solution in Equation 4-39 and an aqueous solution in Equation 4-40. The organic tank time delay is combined with the time delay of the wash stage. The organic phase was approximated to consume half of the total volume in the wash stage settler.

$$t_{\tan k}^{org} = \frac{V^{org}}{F^{org}} = \frac{V_{\text{tank}} + 0.5 \cdot V_s}{F^{org}} \quad \textbf{(7-6)}$$

The time delays of the plug flow models for the settlers and the organic storage tank are calculated on the basis of the volumes and average flow rates. The time delays of the first and second test periods are presented in Table 7-5.

Table 7-5: Time delays of the plug flow model parts for the first test period. The unit is one sampling time.

Test period	Extraction, organic	Extraction, aqueous	Stripping, organic	Stripping, aqueous	Organic storage tank+wash stage
1	1.4	1.4	1.6	1.6	1.6
2	1.3	1.3	1.8	1.8	1.8

7.3 Simulation results

The aim of this section is to choose the best model structure to describe the dynamic behaviour of an industrial copper solvent extraction process. The model structures with different parametrization approaches and the verification indices are presented in Section 7.3.1. The simulation performances for the first and second test periods are then described in Section 7.3.2 and Section 7.3.3. Finally, the simulation performance is studied in detail in Section 7.3.4.

7.3.1 Model structures and methods for the simulation study

The models are constructed with different combinations of constant and varied parameters. For the nominal model (NOM) all the parameters are constant. For the equilibrium isotherm model structure (I) the equilibrium isotherm model parameters are varied, i.e. estimated from the offline process data. For the equilibrium isotherm and efficiency model (EI), the equilibrium isotherm, efficiency and recycle correction parameters are varied on the basis of the offline process data. The effect of the mass transfer coefficient adaptation is tested with a model that included adaptation in all the parameters (EKI).

The simulation model is constructed in the Matlab Simulink environment, and integrated with the ode15s algorithm. The two test data sets consist of online and offline measurements, which are first filtered with the method described in Section 5.2.1. The parameters are first calculated offline and then the simulation is run through, starting from the first measurement values, i.e. not from the steady state.
The verification consists of visual examination of the models ability to follow process trends, and two residual indices: the average absolute error (aae) and integral of the absolute error (iae), both of which are calculated as a percentage of the nominal value of the variable.
The total results of each model structure are compared with a scaled sum of the errors. The error for each output copper concentration is divided by the corresponding error of the nominal model, as follows:

$$total_j = \sum_{i=1}^{5} \frac{e_{i,j}}{e_{i,NOM}} \quad \textbf{(7-7)}$$

Since there are five outputs, the total error sum for the nominal model is 5.

7.3.2 Simulation performance for the first test period

The input data and the parameters of the first test period are described in Chapters 7.1 and 7.2.

The statistical results for the first test period are presented in Table 7-6 and Table 7-7. In the tables, the columns represent the different model structures. The first five rows present the error sums for each output copper concentration, and the sixth row the total sum for each column.

The results clearly show that adaptation of the equilibrium isotherm parameters improves the result. Adding the efficiency parameter adaptation decreases the residuals even more for all the other variables, except for the loaded organic copper concentration. Adding the mass transfer parameter does not improve the result and, therefore, the visual model comparison is performed only for the nominal (NOM), equilibrium isotherm (I), and equilibrium isotherm with efficiency (EI) varied models.

Table 7-6: Average absolute error percentage for the different models.

aae	NOM	I	EI	EKI
c(LO)	3.06	2.74	3.24	3.25
c(BO)	4.00	4.86	3.04	3.06
c(RE)	1.43	1.32	1.25	1.25
c(RaffS)	39.67	18.38	15.53	15.57
c(RaffP)	21.86	7.45	5.76	5.76
total	5	3.84	3.35	3.36

Table 7-7: Average integral of absolute error for the different models.

	NOM	I	EI	EKI
c(LO)	0.31	0.28	0.32	0.33
c(BO)	0.18	0.22	0.13	0.14
c(RE)	0.64	0.60	0.57	0.57
c(RaffS)	0.11	0.05	0.04	0.04
c(RaffP)	0.08	0.03	0.02	0.02
total	5	3.89	3.26	3.35

For the rich electrolyte copper concentration the changes are well predicted with all the models, although at the beginning and end of the test period there is a clear difference. The good fit to the model can be explained by the dependence on the lean electrolyte concentration, which causes a similar effect in all the models. The deviation at the end is caused by analyzer calibration around sampling time 2800.

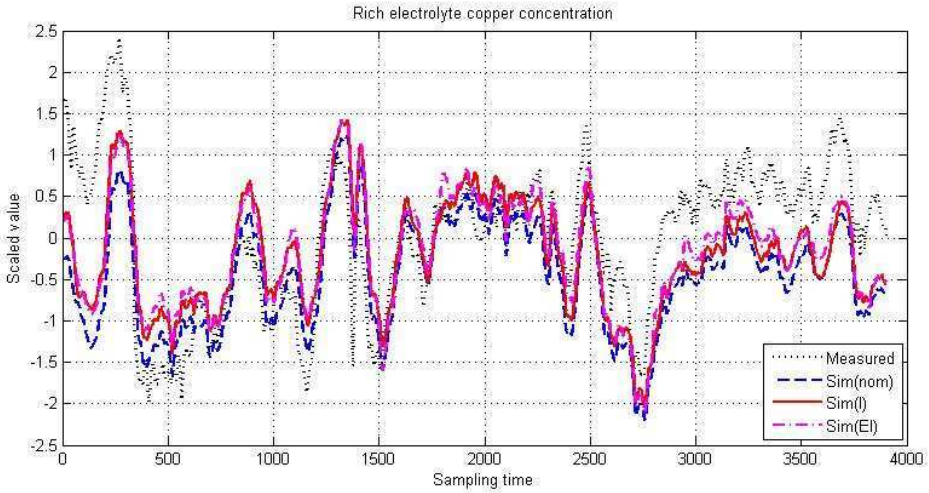

Figure 7-14: Rich electrolyte copper concentration; measured (dotted, black), nominal (nom) model (dashed, blue), equilibrium isotherm parameter varied (I) model (solid, red), and equilibrium isotherm and efficiency parameter varied (EI) model (dash dotted, magenta).

The loaded organic copper concentration was extremely noisy before filtering, and the reliability of the filtered measurements was not very good either. Therefore, for this test period the trends are more important. The model with adaptation in only the equilibrium isotherm parameters best fits the industrial data. However, the organic copper concentrations generally should have similar trends, and here the barren organic copper concentration measurement was more reliable. Therefore, the model with both parameters varied might be the best one, since it fits best to the trends in the barren organic copper concentrations, as presented in Figure 7-16. The rise in the level at 2800 due to analyzer calibration cannot be captured by any of the models.

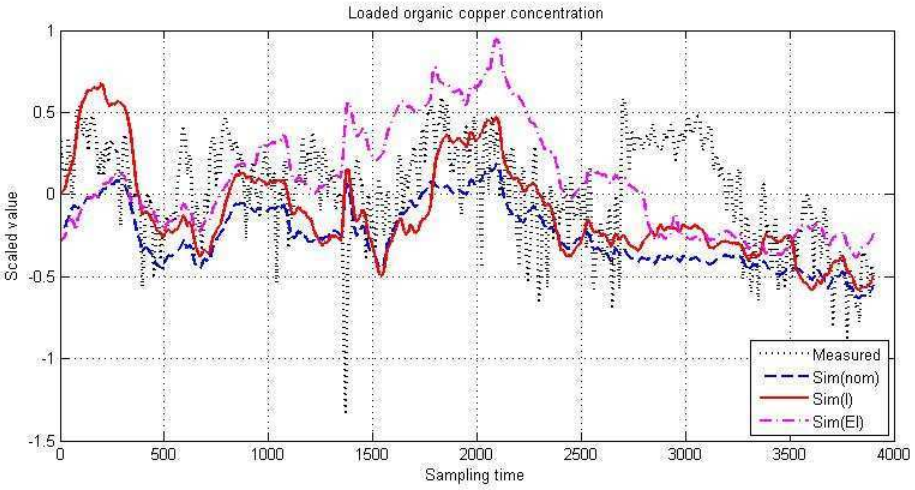

Figure 7-15: Loaded organic copper concentration; measured (dotted, black), nominal (nom) model (dashed, blue), equilibrium isotherm parameter varied (I) model (solid, red), and equilibrium isotherm and efficiency parameter varied (EI) model (dash dotted, magenta).

The fit of the EI model to the barren organic data trends is relatively good, whereas the nominal model has the worst fit. The model with adaptation in only the equilibrium isotherm model (I) is also slightly off the trends. The efficiency and recycle correction parameter adaptation clearly helps to capture this un-modeled phenomenon.

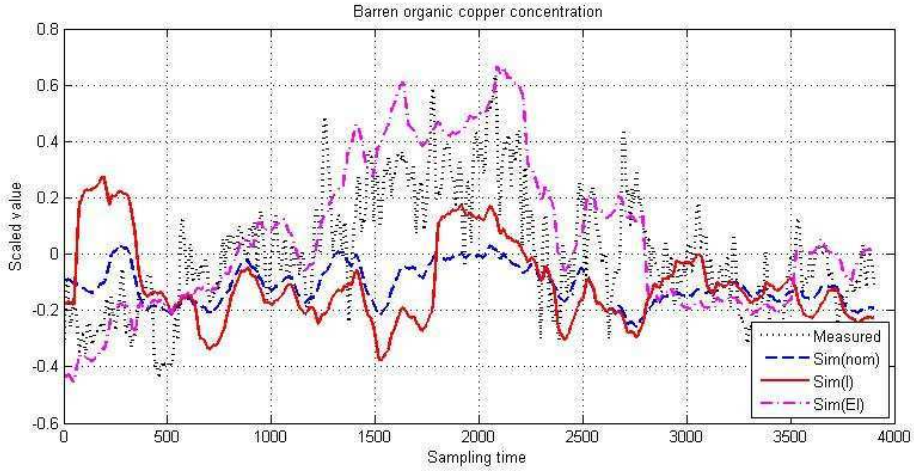

Figure 7-16: Barren organic copper concentration; measured (dotted, black), nominal (nom) model (dashed, blue), equilibrium isotherm parameter varied (I) model (solid, red), and equilibrium isotherm and efficiency parameter varied (EI) model (dash dotted, magenta).

The prediction accuracy of the raffinate series copper concentration is dependent on the chain of three extraction stages, and the predictions of all the models in the middle of the period deviate from the measurement. The trend in the nominal model is different from that for the measurements, although the level change is corrected by including adaptation in the equilibrium isotherms. The adaptation of the efficiencies increases the fit to the data, as can be seen for example during sampling period [300, 1000].

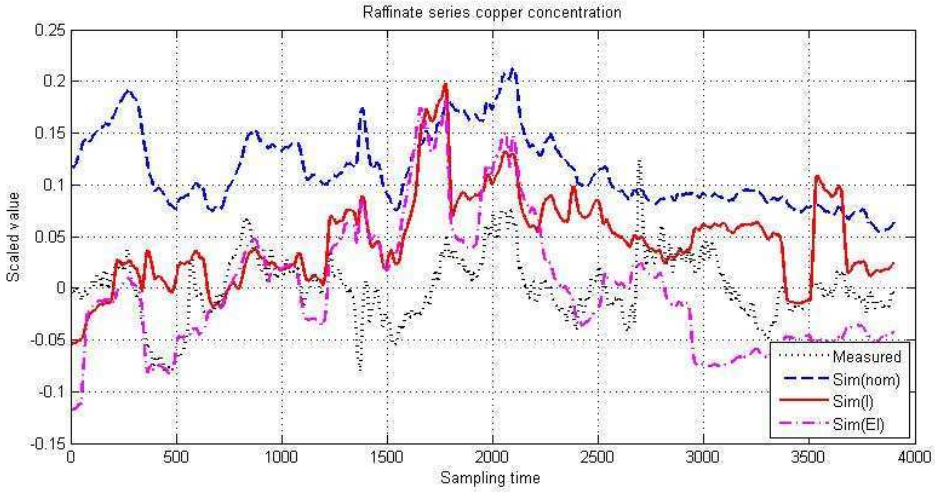

Figure 7-17: Raffinate series copper concentration; measured (dotted, black), nominal (nom) model (dashed, blue), equilibrium isotherm parameter varied (I) model (solid, red), and equilibrium isotherm and efficiency parameter varied (EI) model (dash dotted, magenta).

For the raffinate parallel copper concentration the nominal model has different level than the measurements, but the trends are similar. The level is corrected by introducing adaptation to the equilibrium isotherm parameters, and the fit is further increased with the efficiency parameter adaptation.

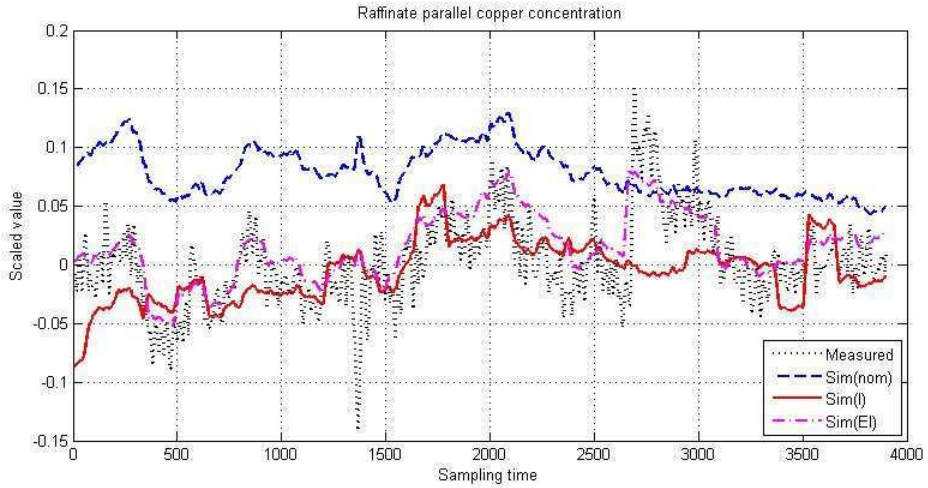

Figure 7-18: Raffinate parallel copper concentration; measured (dotted, black), nominal (nom) model (dashed, blue), equilibrium isotherm parameter varied (I) model (solid, red), and equilibrium isotherm and efficiency parameter varied (EI) model (dash dotted, magenta).

The model with adaptation in both the equilibrium isotherm and efficiency parameters described the industrial data the best. The model fit to the industrial data was adequate. The model follows the main trends caused by flow rate, concentration and chemical changes. In order to get more confidence in the model, the second data set was tested with the same model structures.

7.3.3 Simulation performance for the second test period

The input data and the parameters of the second test period are described in Chapters 7.1 and 7.2.

The statistical results for the second test period are presented in Table 7-8 and

Table 7-9. In the tables, the columns represent the different model structures. The first five rows present the error sums for each output copper concentration, and the sixth row the total sum for each column.

The results clearly imply that including adaptation in both the equilibrium isotherm and efficiency parameters is necessary. Adaptation of the mass transfer coefficient does not improve the predictions and is therefore not necessary. With the EI model the average absolute error percentages are at a satisfactory level for the electrolyte and organic copper concentrations and, considering the noise level of the raffinate copper concentrations, the raffinate predictions are very good.

Table 7-8: Average absolute error percentage for the different models.

aae	NOM	I	EI	EKI
c(LO)	5.26	5.40	1.30	1.30
c(BO)	6.87	5.15	1.67	1.67
c(RE)	1.85	1.69	1.42	1.42
c(RaffS)	41.84	38.79	8.94	8.94
c(RaffP)	19.13	47.68	6.03	6.01
total	5	6.11	1.79	1.79

Table 7-9: Average integral of absolute error for the different models.

iae	NOM	I	EI	EKI
c(LO)	0.60	0.62	0.15	0.15
c(BO)	0.29	0.22	0.07	0.07
c(RE)	0.86	0.79	0.66	0.66
c(RaffS)	0.30	0.28	0.06	0.06
c(RaffP)	0.06	0.14	0.02	0.02
total	5	5.98	1.79	1.79

Figure 7-19 shows the process data and the model predictions for the rich electrolyte copper concentration. The prediction with the nominal model (NOM) gives excellent results for rich electrolyte copper concentration. Increasing the modeling level decreases the result for the rich electrolyte, but drastically improves the results for the other variables. The best prediction ability for the latter part of the test period is gained with adaptation in both the equilibrium isotherm parameters and efficiency parameters.

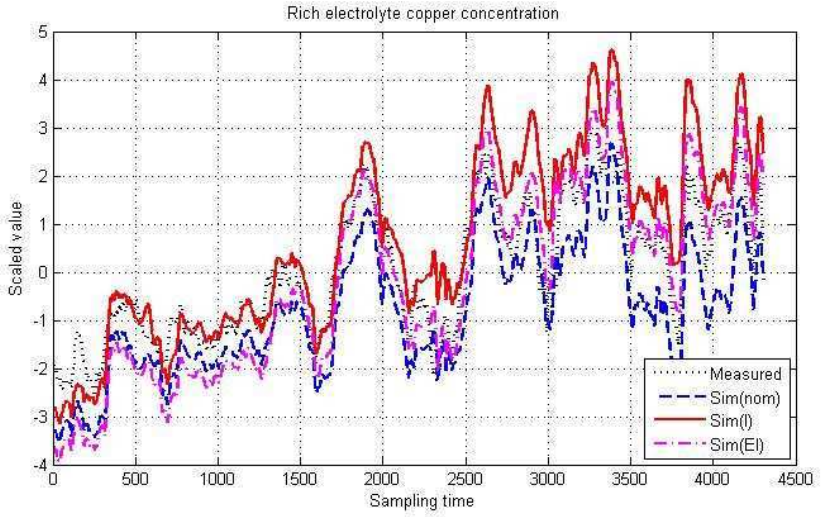

Figure 7-19: Rich electrolyte copper concentration; measured (dotted, black), nominal (nom) model (dashed, blue), equilibrium isotherm parameter varied (I) model (solid, red), and equilibrium isotherm and efficiency parameter varied (EI) model (dash dotted, magenta).

Figure 7-20 presents the process data and model predictions for the loaded organic copper concentration. The constant parameter approach to the model loaded organic copper concentration is not successful because the change in the organic copper level is due to the increase in the reagent volume per cent in the organic solution. The varied equilibrium isotherm model (I) successfully predicts the change, but the level is not correct due to the constant efficiencies of the extraction stages. The fit of the equilibrium isotherm and efficiency parameter model (EI) predictions match well the loaded organic copper concentration measurements. This experiment clearly demonstrates the need to change both the equilibrium isotherm and efficiency parameters simultaneously.

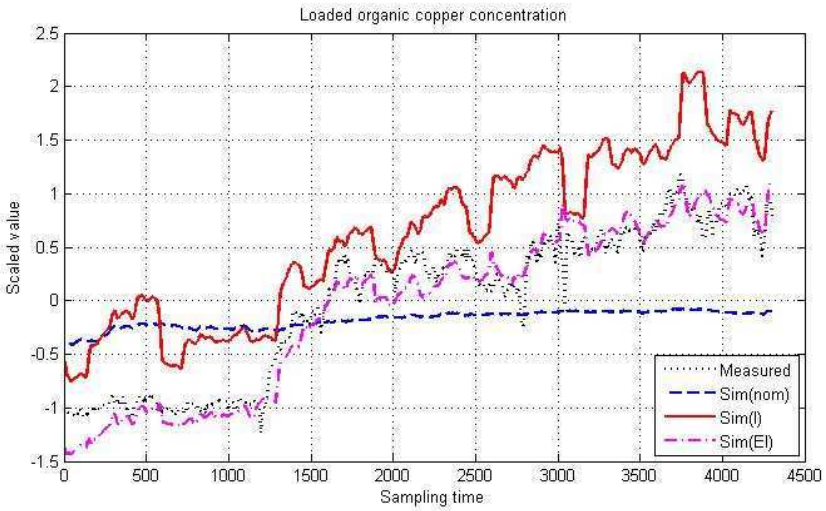

Figure 7-20: Loaded organic copper concentration; measured (dotted, black), nominal (nom) model (dashed, blue), equilibrium isotherm parameter varied (I) model (solid, red), and equilibrium isotherm and efficiency parameter varied (EI) model (dash dotted, magenta).

The barren organic copper concentration measurements and model predictions are presented in Figure 7-21. The quality of the barren organic copper concentration predictions are very similar to that of the loaded organic copper concentrations. The constant parameter model (NOM) cannot adapt to the change in the reagent volume per cent. The equilibrium isotherm model (I) sufficiently well predicts the changes, and the (EI) model even better. Adaptation in the equilibrium isotherm and efficiency parameters is clearly necessary.

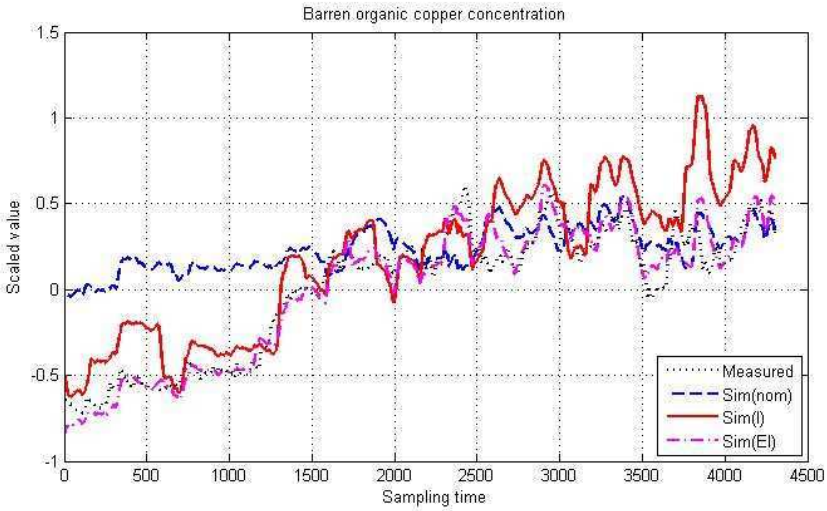

Figure 7-21: Barren organic copper concentration; measured (dotted, black), nominal (nom) model (dashed, blue), equilibrium isotherm parameter varied (I) model (solid, red), and equilibrium isotherm and efficiency parameter varied (EI) model (dash dotted, magenta).

Figure 7-22 presents the process data and the model predictions for the raffinate series copper concentration. The raffinate series predictions suffer drastically from the deviations between the true and utilized equilibrium isotherm and efficiency parameters. The constant extraction isotherm parameters give too high an extraction

rate, which pushes the raffinate to the minimum allowed level, as can be seen for the nominal (NOM) and equilibrium isotherm model (I) experiments. The predictions with varied efficiency and equilibrium isotherm parameters are very reasonable and match well with the measurement data.

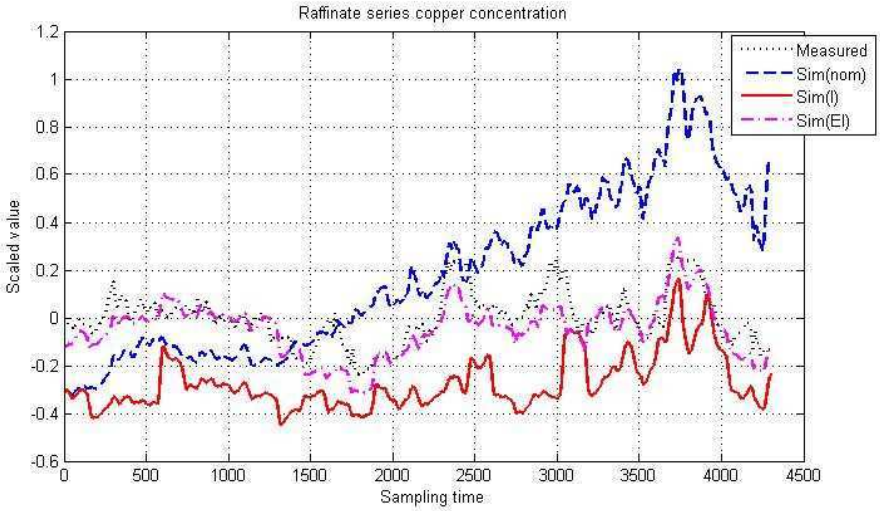

Figure 7-22: Raffinate series copper concentration; measured (dotted, black), nominal (nom) model (dashed, blue), equilibrium isotherm parameter varied (I) model (solid, red), and equilibrium isotherm and efficiency parameter varied (EI) model (dash dotted, magenta).

Figure 7-23 presents the process data and the model predictions for the raffinate parallel copper concentration. The quality of the raffinate parallel copper concentration predictions is similar to the quality of the raffinate series copper concentration predictions. Due to the change in the reagent level in the organic solution, nominal model prediction fails. For the equilibrium isotherm varied model (I) the efficiency is too high, and the raffinate level is almost at the minimum value possible. This is therefore corrected by adding adaptive efficiency. The match between the measurements and the varied (EI) model are relatively good.

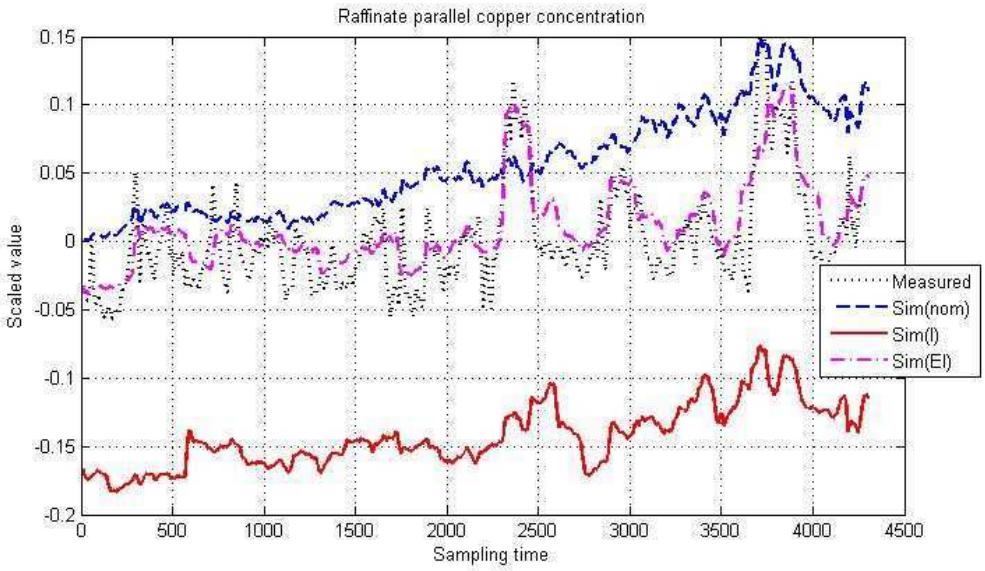

Figure 7-23: Raffinate parallel copper concentration; measured (dotted, black), nominal (nom) model (dashed, blue), equilibrium isotherm parameter varied (I) model (solid, red), and equilibrium isotherm and efficiency parameter varied (EI) model (dash dotted, magenta).

The interplay between the equilibrium isotherm and the efficiency is demonstrated by the organic and raffinate copper concentrations: the changes in the reagent volume per cent induce a change in the equilibrium. The equilibrium isotherm adaptation is thus necessary and, on the basis of the experiments, adaptation of the efficiencies is crucial. The average absolute error percentages are reasonably good for all the measurements with the (EI) model: less than 2% for the electrolyte and organic copper concentrations, and less than 10% for the less reliable raffinate copper concentrations.

7.3.4 Simulation performance under input changes

The simulation performance is further evaluated with five examples with distinct changes in the input variables. The examples are chosen from the two test data sets. The simulation performance is evaluated with input flow rate changes in Section 7.3.4.1, then with a change in the input copper concentrations in Section 7.3.4.2, and, finally, with a change in the reagent volume per cent in the organic solution in Section 7.3.4.3.

7.3.4.1 Simulation performance under input flow rate changes

During sampling period [800, 1100] in the first data set, the flow rates are first raised and then lowered again. This causes a clear effect in the process, as shown for the rich electrolyte copper concentration in Figure 7-24 and for the raffinate parallel copper concentration in Figure 7-25. Detailed analysis of the figures of the rich electrolyte and raffinate parallel copper concentrations during this time reveal that the simulations follow the trend, although the smaller variations in the data are not captured by any of the models. The residual might be due to measurement noise or to unmodeled phenomena in the process, like rapid changes in the reagent volume and pH, both of which are measured only offline.

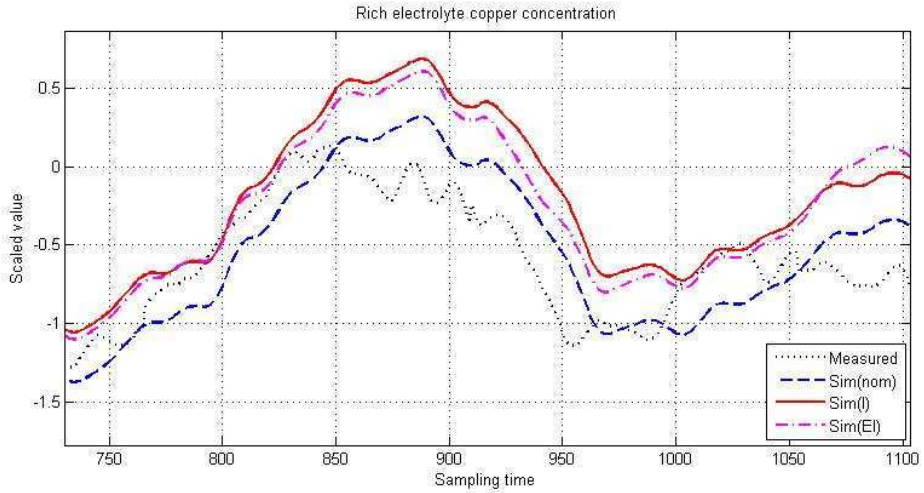

Figure 7-24: Rich electrolyte copper concentration for sampling period [800, 1100] in the first data set; measured (dotted, black), nominal (nom) model (dashed, blue), equilibrium isotherm parameter varied (I) model (solid, red), and equilibrium isotherm and efficiency parameter varied (EI) model (dash dotted, magenta).

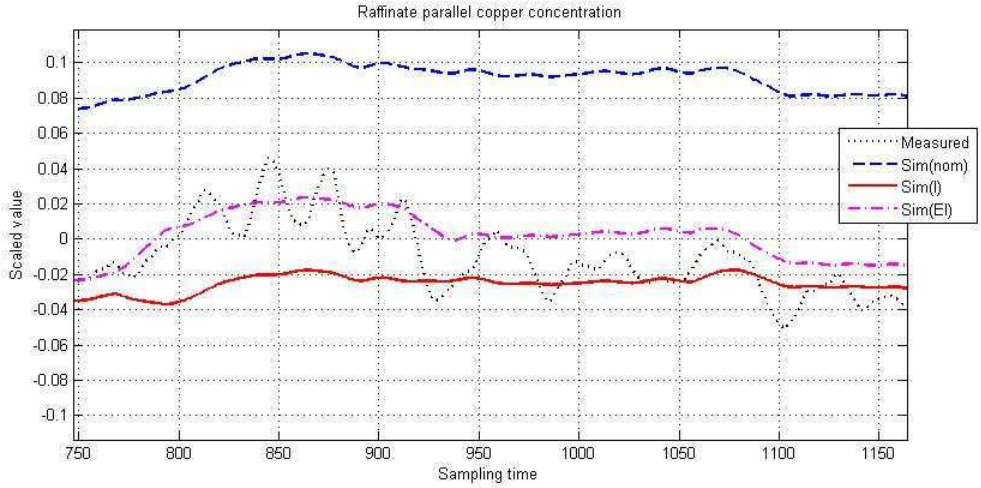

Figure 7-25: Raffinate parallel copper concentration for sampling period [800, 1100] in the first data set; measured (dotted, black), nominal (nom) model (dashed, blue), equilibrium isotherm parameter varied (I) model (solid, red), and equilibrium isotherm and efficiency parameter varied (EI) model (dash dotted, magenta).

During sampling period [1800, 2100] in the first data set there is a downward peak in the PLS and organic flow rates, and during sampling period [2000, 2300] there is a downward peak in the electrolyte flow. These changes cause peaks in the rich electrolyte and raffinate parallel copper concentrations, as illustrated in Figure 7-26 and Figure 7-27.

For the rich electrolyte copper concentration the downward step in the electrolyte flow rate causes a downward peak around sampling time 2100. The upward steps in the organic flow rate and the electrolyte flow rate cause oscillations between [2100 - 2350] in the rich electrolyte copper concentration, and a larger downward peak around 2300. All the models follow the changes well, the model with adaptation in the isotherm and efficiency parameters (EI) having the best fit.

The flow rate changes in the PLS parallel and series flow rates and the organic flow rate cause a mild upward peak in the raffinate parallel copper concentration around sampling period [2000, 2100]. The models adequately follow the trends.

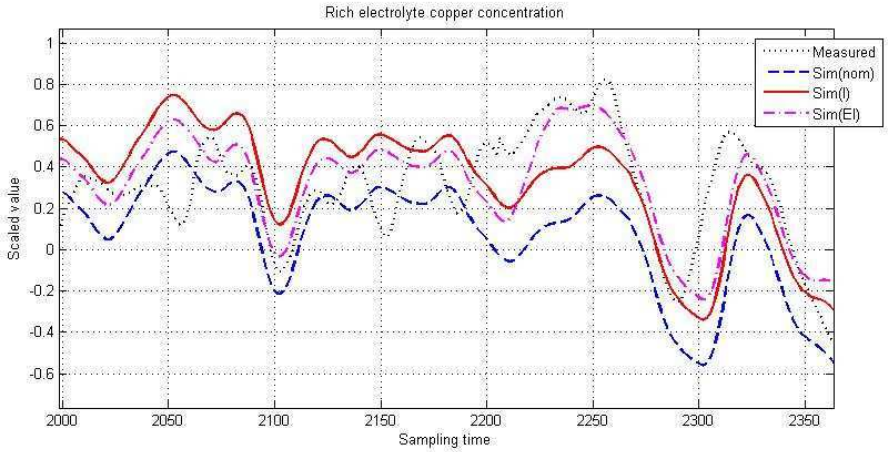

Figure 7-26: Rich electrolyte copper concentration for sampling period [2000 - 2300] in the first data set; measured (dotted, black), nominal (nom) model (dashed, blue), equilibrium isotherm parameter varied (I) model (solid, red), and equilibrium isotherm and efficiency parameter varied (EI) model (dash dotted, magenta).

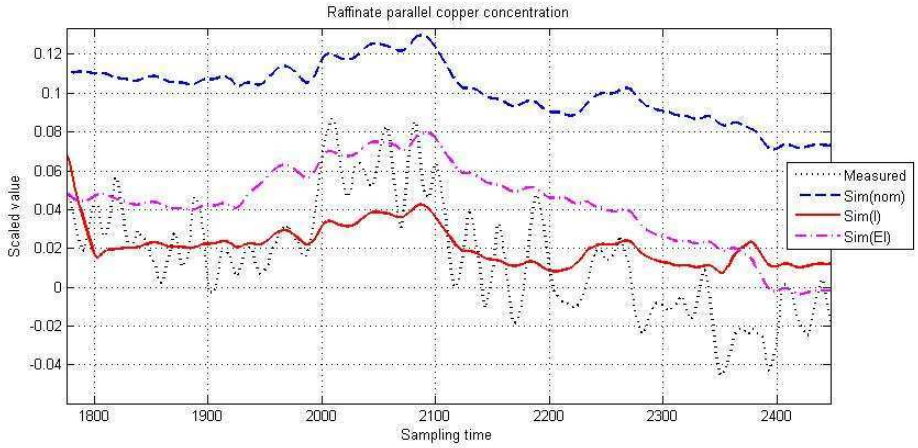

Figure 7-27: Raffinate parallel copper concentration for sampling period [2000 - 2300] in the first data set; measured (dotted, black), nominal (nom) model (dashed, blue), equilibrium isotherm parameter varied (I) model (solid, red), and equilibrium isotherm and efficiency parameter varied (EI) model (dash dotted, magenta).

A drop in the flow rates around sampling period [2200, 2500] in the second data set causes a downward step in the rich electrolyte copper concentration and an upward peak in the raffinate series copper concentration, as illustrated in Figure 7-28 and Figure 7-29. The rich electrolyte copper concentration trends are the best followed by the model structure with adaptation in both the equilibrium isotherm and efficiency (EI), although the other models follow the flow rate changes adequately well, too.

The upward peak in the raffinate series concentration between sampling period [2300 - 2450] is best followed by the model structure with adaptation in both the equilibrium isotherm and efficiency (EI). The nominal model structure has similar trends to the

measurement data, but the level is well above the raffinate series copper concentration measurements. The model structure with adaptation in the equilibrium isotherm parameters (I) dampens the upward peak.

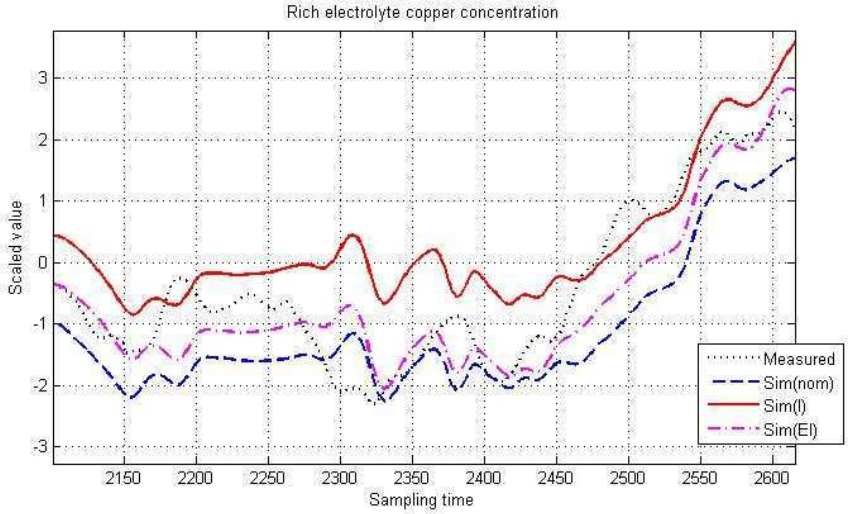

Figure 7-28: Rich electrolyte copper concentration for sampling period [2100, 2600] in the second data set; measured (dotted, black), nominal (nom) model (dashed, blue), equilibrium isotherm parameter varied (I) model (solid, red), and equilibrium isotherm and efficiency parameter varied (EI) model (dash dotted, magenta).

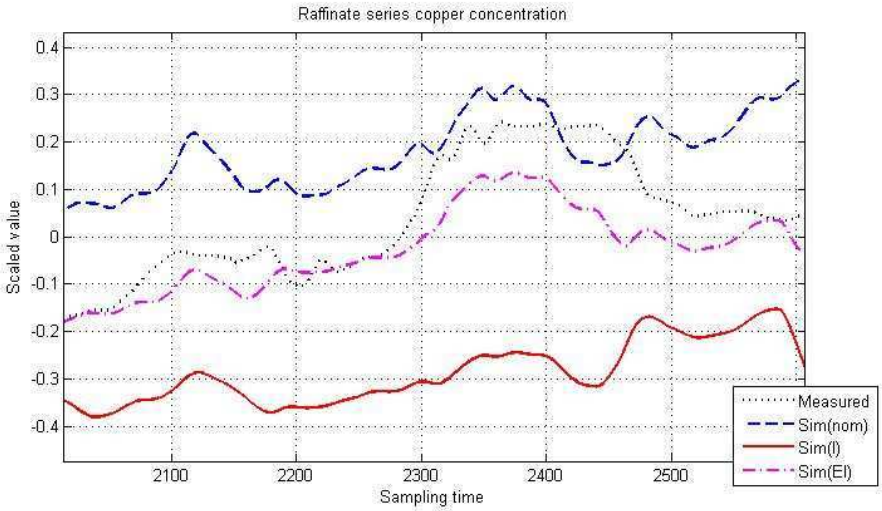

Figure 7-29: Raffinate series copper concentration for sampling period [2100, 2600] in the second data set; measured (dotted, black), nominal (nom) model (dashed, blue), equilibrium isotherm parameter varied (I) model (solid, red), and equilibrium isotherm and efficiency parameter varied (EI) model (dash dotted, magenta).

7.3.4.2 Simulation performance under input copper concentration changes

During sampling period [1300 - 1600] in the first data set there is a peak in the lean electrolyte copper concentration. The effect on the rich electrolyte and raffinate parallel copper concentrations are illustrated in Figure 7-30 and Figure 7-31. The peaks in the rich electrolyte copper concentration are followed with a small lag (~20

sampling times) by all the model structures. The lean electrolyte copper concentration change does not have any significant effect on the raffinate parallel copper concentration, and the copper concentration remains at the same level with only small variations. The best model structures are those with varied parameters of the equilibrium isotherm (I) and the equilibrium isotherm with efficiency (EI). The downward peak around sampling time 1350 is not explained by any of the models.

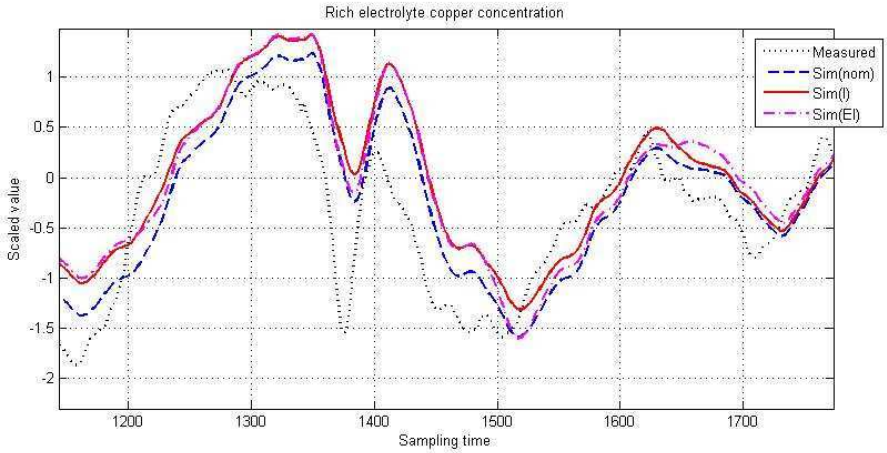

Figure 7-30: Rich electrolyte copper concentration for sampling period [1200, 1700] in the first data set; measured (dotted, black), nominal (nom) model (dashed, blue), equilibrium isotherm parameter varied (I) model (solid, red), and equilibrium isotherm and efficiency parameter varied (EI) model (dash dotted, magenta).

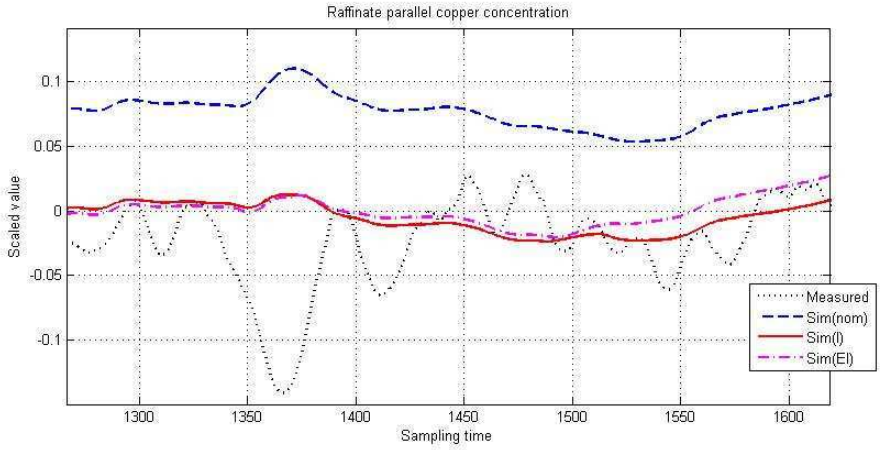

Figure 7-31: Raffinate parallel copper concentration for sampling period [800, 1100] in the first data set; measured (dotted, black), nominal (nom) model (dashed, blue), equilibrium isotherm parameter varied (I) model (solid, red), and equilibrium isotherm and efficiency parameter varied (EI) model (dash dotted, magenta).

7.3.4.3 Simulation performance under disturbances

There is a change in the reagent volume per cent in the organic solution starting around sampling time 1200. This causes significant changes in the loaded organic and rich electrolyte copper concentrations, as presented in Figure 7-32 and Figure 7-33.

In this case, the importance of adaptation of the equilibrium isotherm and the efficiency parameters is highlighted in the loaded organic copper concentration. The

model structures with adaptation in the equilibrium parameters (I) and adaptation in both the equilibrium isotherm and efficiency (EI) follow the rising trend in the loaded organic copper concentration, but are lagged by about 50 sampling times from the beginning of the change. This is due to the delay in the offline measurement of the reagent volume per cent in the organic solution. The best model structure is the one with adaptation in both the equilibrium isotherm and efficiency (EI).

For the rich electrolyte copper concentration the rise in the reagent volume per cent in the organic solution does not have as drastic an effect as for the loaded organic copper concentration. This is due to the smaller changes in the linear stripping equilibrium isotherm. All the model structures follow well the rich electrolyte copper concentration trends.

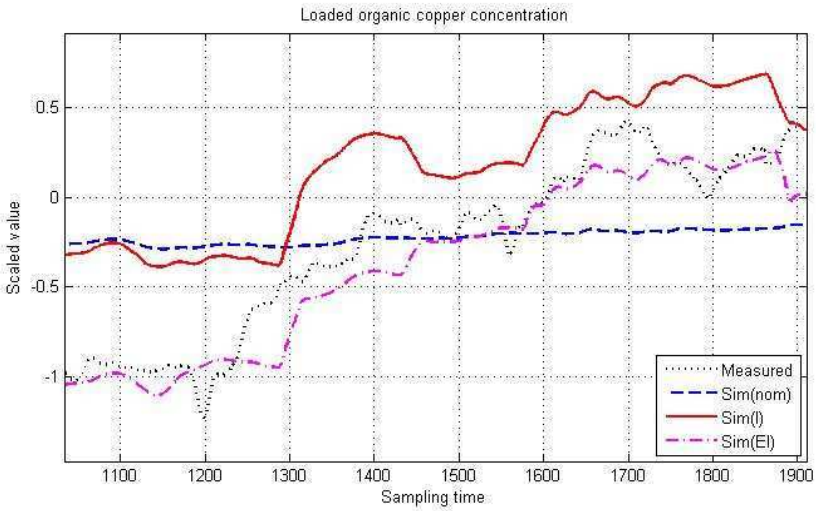

Figure 7-32: Loaded organic copper concentration for sampling period [1100, 1900] in the second data set; measured (dotted, black), nominal (nom) model (dashed, blue), equilibrium isotherm parameter varied (I) model (solid, red), and equilibrium isotherm and efficiency parameter varied (EI) model (dash dotted, magenta).

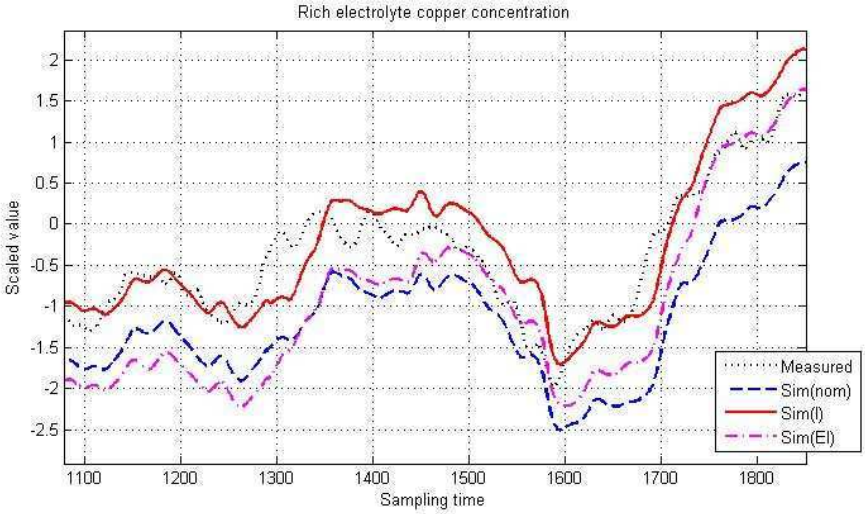

Figure 7-33: Rich electrolyte copper concentration for sampling period [1100, 1900] in the second data set; measured (dotted, black), nominal (nom) model (dashed, blue), equilibrium isotherm parameter varied (I) model (solid, red), and equilibrium isotherm and efficiency parameter varied (EI) model (dash dotted, magenta).

7.4 Concluding remarks

The dynamic models were tested with two data sets representing the normal operation of the industrial case copper solvent extraction plant. The effect of parameter adaptation was studied using different parametrization approaches and by comparing the results to the nominal case.

The models followed the output copper concentration trends smoothly for the major input changes in the flow rates and copper concentrations, and the residuals between the simulated values and measurements were sufficiently small. The changes in the reagent volume per cent in the organic solution were only followed by the model structure with adaptation in the equilibrium isotherm parameters. A further increase in

the simulation performance was gained by using adaptation in the efficiency and recycle correction parameters. This underlines the necessity of adaptation, especially for the extraction process in the equilibrium isotherm, efficiency and recycle correction parameters. Adaptation of the mass transfer parameter did not significantly affect the results, and thus the constant mass transfer parameters are used in the further studies.

The smaller peaks in the measurement data were not explained by any of the models. This might be due to measurement noise or to modeling inaccuracies. The modeling is unable to describe rapid changes in the reagent volume per cent in the organic solution and the pH level, because both of these are measured only offline. Adaptation to the changes in the reagent volume per cent in the organic solution and pH level is also lagged due to the offline measurement delay.

The model with adaptation in both equilibrium isotherm parameters and efficiency parameters (EI) was chosen for further studies due to better overall results and a model structure that gives more information about the process state. The efficiency parameters describe the unit process efficiencies that seldom are 100% in industrial plants. Thus, these parameters could be used to give indication of the performance of the plant.

Variations not captured by this (EI) model can be due to inaccuracy of the data and process upsets that are can not measured (formation of crud/emulsion, heavy rain). Therefore, the operating conditions of the process should be verified before applying the model.

The model can be applied to similar copper solvent extraction plants using mixer-settlers by modifying the flow configuration between the mixer-settlers, and by adapting the equilibrium isotherm, efficiency and recycle correction parameters.

8 LINEAR MODELS OF THE COPPER SOLVENT EXTRACTION PROCESS

The aim of this chapter is to study the linearity of the dynamic process models and to develop linear process models for further control purposes. The linearity of the dynamic process models, i.e. the applicability of the superposition principle, is first studied in Section 8.1, and the order of the linearized models then determined in Section 8.2. Finally, the dynamic process models are linearized to state space and transfer function forms, and the linear model predictions compared to the industrial data in Section 8.3.

8.1 Linearity of the dynamic models

The constraints of extraction and stripping (equilibrium isotherms) cause nonlinearities in the seemingly linear combination of several mixing – plug flow sub-models. Therefore it is essential to study the severity of the nonlinearities and to determine whether such nonlinearities are small enough to enable linear controllers to be used to control the process efficiently.

According to Glad and Ljung (2000), the outputs of a linear system are the weighted sum of the past and present input values at all times. A linear system has the following properties: invariance under scaling, additivity and frequency fidelity. The combination of the two first properties is the superposition principle, which is tested in this study.

The output variables in this study are the rich electrolyte and loaded organic copper concentrations. The input variables are the PLS and lean electrolyte copper concentrations, the PLS series and parallel, organic and electrolyte flow rates, and the reagent volume per cent in the organic solution. The operating points for the study are DP1 from the beginning of the first data set, and DP4 from the beginning of the second data set, as described in Section 5.2.2. The input changes were chosen to be ±5% of the nominal value, which is the maximum input variable change according to the plant variation study described in Section 5.2.3.

8.1.1 Scaling invariance

Invariance under scaling is studied by comparing the responses of the outputs with input changes of different magnitudes, for example a change of 5% of the nominal value of the input variable. The response is calculated as the difference between the output at time t and the output before the change in the input at time 0, divided by the magnitude of the input change at time 1. Thus the response G between input u and output y is calculated as follows:

$$G(t) = \frac{y(t) - y(0)}{u(1) - u(0)} \qquad \textbf{(8-1)}$$

The scaling invariance applies if there are no nonlinearities or asymmetries. The system has nonlinearity if the responses (at time t) for the input changes of different magnitudes and the same sign, for example +1% and +5%, are different. The system has asymmetry if the absolute value of the gains (at time t) with input changes of the same opposite signs and same magnitude, for example -5% and +5%, are different.

The nonlinearity and asymmetry are evaluated by calculating the percentual absolute difference between the +5% steady state gain and the steady state gains with different input change magnitudes. The scaling invariance applies adequately if the nonlinearity and asymmetry of the responses are mild.

The scaling invariance is tested at the chosen operating points DP1 and DP4 by introducing ±1%, ±5%, and ±10% changes to all the seven input variables of the dynamic process models and then collecting the responses of the output variables, rich electrolyte and loaded organic copper concentrations. A maximum change of ±10% is tested in order to get more confidence about the results.

The steady state gains, i.e. the gains after the maximum response is reached, are first determined. The steady state gains for each input-output variable pair are compared in order to determine whether there are any nonlinearities or asymmetries. The responses for each input-output variable pair are then plotted in order to confirm the results for the whole time range.

8.1.1.1 Rich electrolyte copper concentration

The steady state gains of the rich electrolyte copper concentration at the first operating point DP1 are presented in Table 8-1. For most of the input variables the gains are relatively similar between the positive and negative input steps, but for the organic flow rate F(LO) and reagent volume per cent (vol) there are asymmetries of less than 20%, and mild nonlinearities of around 20%.

Table 8-1: Steady state gains for rich electrolyte copper concentration responses at operating point DP1.

C(RE)	F(PLSS)	F(PLSP)	F(LO)	F(LE)	c(PLS)	c(LE)	vol
+1%	0.1452	0.1320	0.0189	-0.5347	3.1491	0.9819	0.0215
+5%	0.1448	0.1313	0.0177	-0.5149	3.1337	0.9816	0.0196
+10%	0.1441	0.1303	0.0164	-0.4920	3.1108	0.9811	0.0176
-1%	-0.1455	-0.1323	-0.0196	0.5452	-3.1561	-0.9821	-0.0226
-5%	-0.1459	-0.1330	-0.0212	0.5675	-3.1686	-0.9825	-0.0249
-10%	-0.1463	-0.1338	-0.0237	0.5980	-3.1823	-0.9829	-0.0286

The responses of the rich electrolyte copper concentration to the step input changes at the first operating point DP1 are presented in Figure 8-1 and Figure 8-2. The responses appear to be linear with first order plus time delay dynamics, except for the F(LO) response, which is of the second order with zero plus time delay type. The PLS and electrolyte copper concentrations, c(PLS) and c(LE), together with the electrolyte flow rate, F(LE), have the largest impact on the rich electrolyte copper concentration.

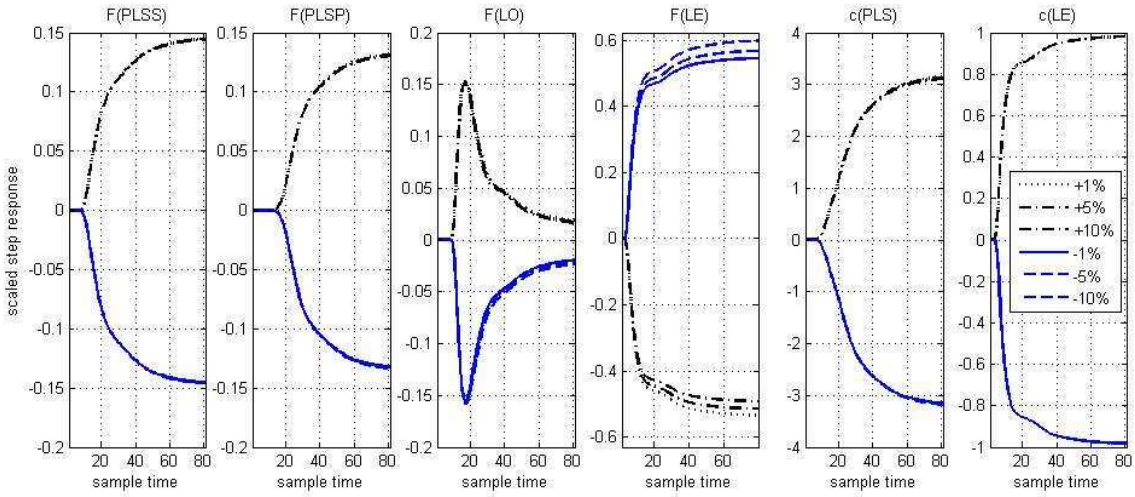

Figure 8-1: Responses of the rich electrolyte copper concentration to input changes in F(PLSS), F(PLSP), F(LO),F(LE), c(PLS),and c(LE) at operating point DP1.

The response to reagent volume per cent change is especially interesting with inverse dynamics, as can be seen from Figure 8-2. Since the exact time dynamics of reagent volume blending to the organic solution are not known, blending is assumed to be instant. At this operating point DP1, the effect of an increasing reagent volume per cent is small for a rich electrolyte copper concentration. The inverse effect is due to the increase in the organic solution copper concentration via the organic recycle between the stripping and extraction steps.

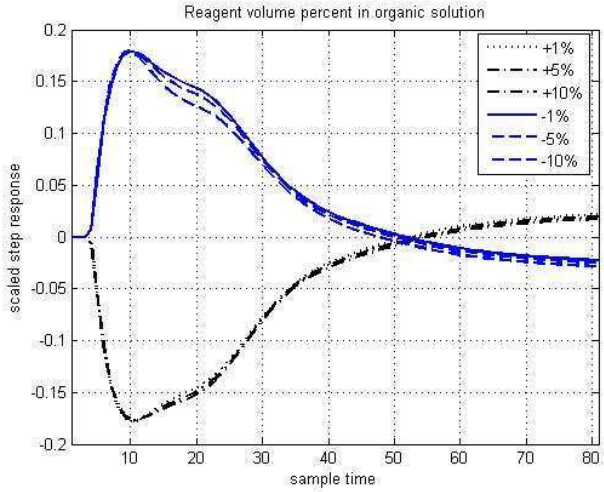

Figure 8-2: Responses of the rich electrolyte copper concentration to input changes in the reagent volume per cent at operating point DP1.

The steady state gains for the rich electrolyte copper concentration at the second operating point DP4 are shown in Table 8-2. The gains are relatively similar between the positive and negative input steps, except for the organic flow rate F(LO) and reagent volume per cent where there are high asymmetries of up to 50%, and mild nonlinear behaviour of up to 35%. For the change in the PLS copper concentration the asymmetry and nonlinearity are around 10%.

Table 8-2: Steady state gains for rich electrolyte copper concentration responses at operating point DP4.

C(RE)	F(PLSS)	F(PLSP)	F(LO)	F(LE)	c(PLS)	c(LE)	Vol%
+1%	0.0853	0.0955	0.0886	-0.5472	2.8758	0.9626	0.1087
+5%	0.0821	0.0933	0.0782	-0.5274	2.7236	0.9614	0.0956
+10%	0.0782	0.0905	0.0675	-0.5046	2.5287	0.9599	0.0821
-1%	-0.0869	-0.0966	-0.0944	0.5576	-2.9487	-0.9632	-0.1160
-5%	-0.0900	-0.0987	-0.1070	0.5798	-3.0833	-0.9643	-0.1320
-10%	-0.0936	-0.1012	-0.1246	0.6099	-3.2249	-0.9657	-0.1545

The responses of the rich electrolyte copper concentration to the input step changes at operating point DP4 are presented in Figure 8-3 and Figure 8-4. The responses mainly follow the first order plus time delay dynamics, except for the organic flow rate, F(LO), which is of the second order with zero plus time delay type. The PLS and electrolyte copper concentrations, c(PLS) and c(LE), and the electrolyte flow rate, F(LE), have the greatest effect on the rich electrolyte copper concentration.

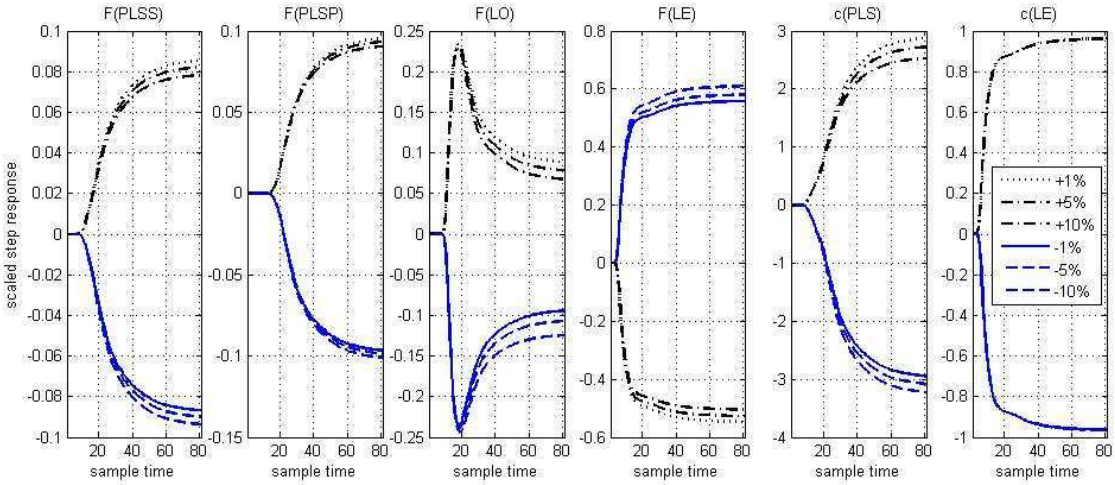

Figure 8-3: Responses of the rich electrolyte copper concentration to input changes in F(PLSS), F(PLSP), F(LO),F(LE), c(PLS),and c(LE) at operating point DP4.

The response to a change in the reagent volume per cent is especially interesting with inverse dynamics, as can be seen from Figure 8-4. The effect of increasing the reagent volume per cent at operating point DP4 is larger than at the first operating point (DP1). However, decreasing the reagent volume per cent results in decreased stripping after the increased stripping period, as at the first operating point for the rich electrolyte copper concentration. The inverse effect is due to the increase in the organic solution copper concentration via the organic recycle between the stripping and extraction steps.

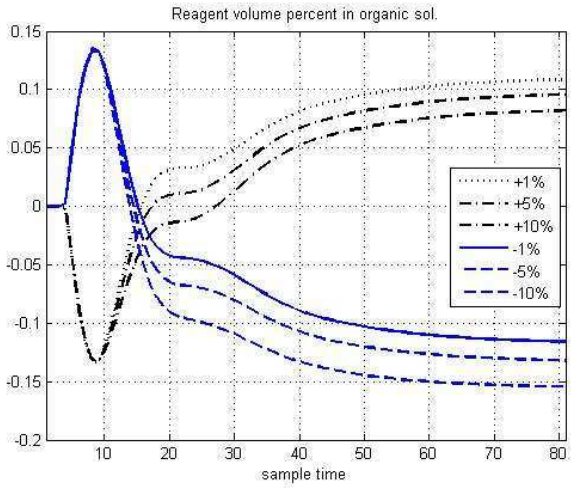

Figure 8-4: Responses of the rich electrolyte copper concentration to input changes in the reagent volume per cent at operating point DP4.

8.1.1.2 Loaded organic copper concentration

The steady state gains for the loaded organic copper concentrations at the first operating point DP1 are presented in Table 8-3. The gains are relatively similar, except for the organic and electrolyte flow rates, F(LO) and F(LE), and the reagent volume per cent, for which the asymmetry and nonlinearity are about 10%.

Table 8-3: Steady state gains for loaded organic copper concentration responses at operating point DP1.

C(RE)	F(PLSS)	F(PLSP)	F(LO)	F(LE)	c(PLS)	c(LE)	Vol%
+1%	0.0997	0.0909	-0.1492	-0.0516	2.1661	0.0858	0.1529
+5%	0.0994	0.0904	-0.1442	-0.0497	2.1556	0.0855	0.1510
+10%	0.0990	0.0897	-0.1384	-0.0475	2.1401	0.0852	0.1489
-1%	-0.0999	-0.0912	0.1518	0.0526	-2.1708	-0.0859	-0.1539
-5%	-0.1002	-0.0916	0.1572	0.0546	-2.1793	-0.0861	-0.1561
-10%	-0.1005	-0.0922	0.1642	0.0575	-2.1886	-0.0864	-0.1594

The responses of the loaded organic copper concentration to the input step changes at operating point DP1 are presented in Figure 8-5 and Figure 8-6. All the step responses follow first order plus time delay dynamics. The main affecting inputs are the PLS copper concentration and organic flow rate, c(PLS) and F(LO), and the reagent volume percent.

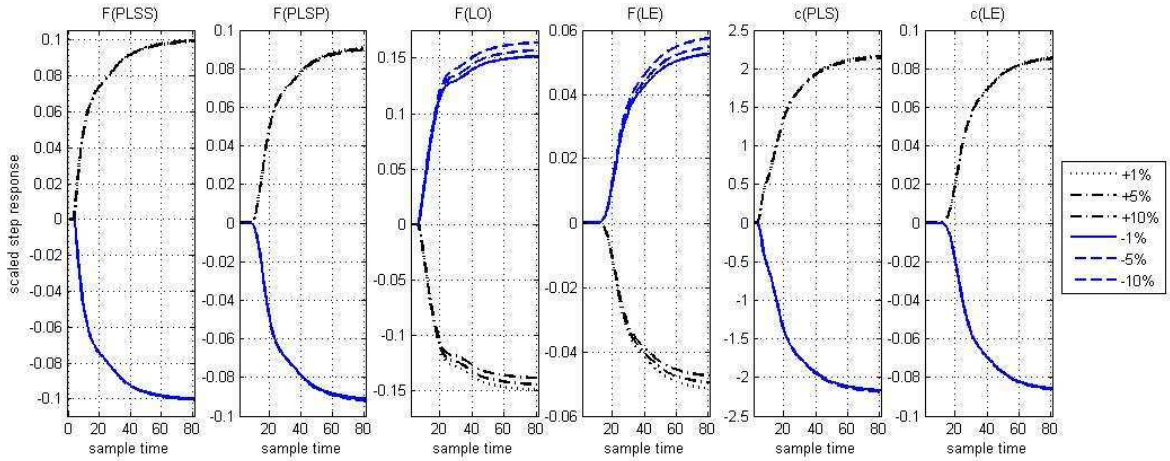

Figure 8-5: Responses of the loaded organic copper concentration to input changes in F(PLSS), F(PLSP), F(LO),F(LE), c(PLS),and c(LE) at operating point DP1.

The response of a change in the reagent volume per cent at operating point DP1 has a larger effect than a change in the organic flow rate, as can be seen from Figure 8-6 and Figure 8-5. The response is relatively linear and symmetric, with dynamics of a higher order plus time delay form. An increasing reagent volume per cent in the organic solution increases the organic copper concentration due to the larger copper ion complexation potential.

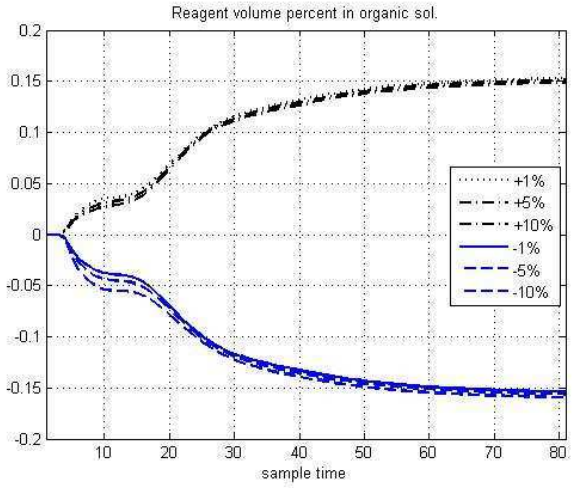

Figure 8-6: Responses of the loaded organic copper concentration to input changes in the reagent volume per cent at operating point DP1.

The steady state gains for the loaded organic copper concentrations at the second operating point DP4 are presented in Table 8-4. The gains are relatively linear, and the asymmetries and nonlinearities are weak, between 10% and 20%, for the organic and electrolyte flow rates, F(LO) and F(LE), and the reagent volume percent.

Table 8-4: Steady state gains for loaded organic copper concentration responses at operating point DP4.

C(RE)	F(PLSS)	F(PLSP)	F(LO)	F(LE)	c(PLS)	c(LE)	Vol%
+1%	0.0678	0.0761	-0.1781	-0.0419	2.2897	0.0682	0.2166
+5%	0.0653	0.0743	-0.1789	-0.0405	2.1683	0.0673	0.2059
+10%	0.0622	0.0721	-0.1782	-0.0390	2.0118	0.0661	0.1947
-1%	-0.0691	-0.0770	0.1773	0.0426	-2.3476	-0.0687	-0.2225
-5%	-0.0716	-0.0786	0.1747	0.0440	-2.4542	-0.0696	-0.2354
-10%	-0.0745	-0.0806	0.1696	0.0460	-2.5661	-0.0707	-0.2533

The responses of the loaded organic copper concentration to the input step changes at operating point DP1 are presented in Figure 8-7 and Figure 8-8. As at operating point DP1, the step responses all seem to be of a first order plus time delay form. The main affecting inputs are the PLS copper concentration and the organic flow rate, c(PLS) and F(LO), and the reagent volume percent.

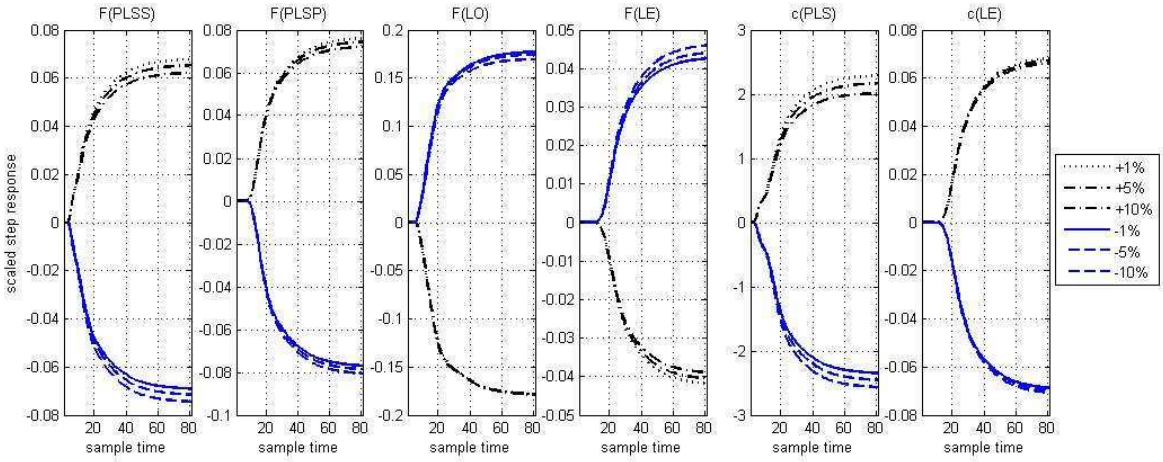

Figure 8-7: Responses of the loaded organic copper concentration to input changes in F(PLSS), F(PLSP), F(LO),F(LE), c(PLS),and c(LE) at operating point DP4.

The response of the reagent volume per cent change is slightly larger than the change in the organic flow rate, as can be seen from Figure 8-8 and Figure 8-7. The response is weakly nonlinear (15%) and asymmetric (20%), with dynamics of higher order plus time delay. Increasing the reagent volume per cent in the organic solution naturally increases the organic copper concentration due to the larger copper ion complexation potential.

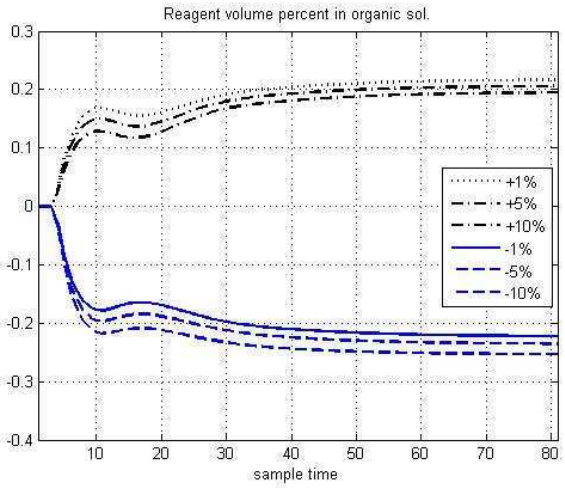

Figure 8-8: Responses of the loaded organic copper concentration to input changes in the reagent volume per cent at operating point DP4.

8.1.2 Additivity

Additivity is tested by changing two or more inputs at the same time and comparing the output change to the sum of the output changes from experiments in which one input is changed at a time. For example, for the loaded organic copper concentration, simultaneous changes in the PLS series flow rate and the PLS copper concentration (combo) are compared to the sum of the loaded organic copper concentration changes (sum) for the separate experiments in which the PLS series flow rate and the PLS copper concentration are changed. This is denoted as:

$$combo = c(LO)\big|_{F(PLSS)+c(PLS)}$$
$$sum = c(LO)\big|_{F(PLSS)} + c(LO)\big|_{c(PLS)} \qquad \textbf{(8-2)}$$

Additivity of the responses of the rich electrolyte and loaded organic copper concentration is studied at operating point DP4 with 5% step changes to the input variables. Since the number of all possible input combinations is relatively high, only the most common cases, with changes in two inputs at the same time are studied. The collected outputs are compared to the sum of outputs from separate 5% input step change experiments. The tested input combinations are:

- both PLS series and parallel flow rates, F(PLSS) and F(PLSP)
- PLS series flow rate and organic flow rate, F(PLSS) and F(LO)
- organic and electrolyte flow rate, F(LO) and F(LE)
- PLS series flow rate and PLS copper concentration, F(PLSS) and c(PLS)
- organic flow rate and electrolyte copper concentration, F(LO) and c(LE)
- electrolyte flow rate and electrolyte copper concentration, F(LE) and c(LE)
- organic flow rate and PLS copper concentration, F(LO) and c(PLS)

8.1.2.1 Rich electrolyte copper concentration

The differences between the response combinations and sums for the rich electrolyte copper concentration at operating point DP4 are numerically evaluated in Table 8-5. These differences are transformed into percentages by dividing the difference with the total response change, as shown in Table 8-6. The differences are less than 0.06% of the nominal value of the rich electrolyte copper concentration, which implies that the additivity principle is applying very well. The responses are almost identical from the summed outputs and the input change combinations, as illustrated for the input changes in the PLS series and parallel flow rates in Figure 8-9.

Table 8-5: Differencies between the gains of the outputs of combined input changes and sum of separate input changes for rich electrolyte copper concentration responses in operating point DP4.

cRE)	**+5% -5%**	**-5% +5%**	**+5% +5%**	**-5% -5%**
F(PLSS)&F(PLSP)	0.0143	0.0143	-0.0149	-0.0132
F(PLSS)&F(LO)	-0.0319	-0.0244	0.0275	0.0307
F(LO)&F(LE)	0.0113	0.0126	-0.0098	-0.0144
F(PLSS)&c(PLS)	0.0194	0.0232	-0.0257	-0.0146
F(LO)&c(LE)	-0.0110	-0.0135	0.0117	0.0131
F(LE)&c(LE)	-0.0043	-0.0053	0.0046	0.0050
F(LO)&c(PLS)	-0.0387	-0.0590	0.0503	0.0512

Table 8-6: Percentual differencies between the gains of the outputs of combined input changes and sum of separate input changes for rich electrolyte copper concentration responses in operating point DP4.

c(RE)	**+5% -5%**	**-5% +5%**	**+5% +5%**	**-5% -5%**
F(PLSS)&F(PLSP)	-	-	3.78%	2.89%
F(PLSS)&F(LO)	-	-	7.80%	8.51%
F(LO)&F(LE)	1.52%	1.77%	2.25%	3.44%
F(PLSS)&c(PLS)	7.34%	10.04%	4.29%	2.04%
F(LO)&c(LE)	0.74%	0.95%	0.67%	0.75%
F(LE)&c(LE)	0.20%	0.24%	0.44%	0.50%
F(LO)&c(PLS)	9.78%	30.35%	8.36%	8.48%

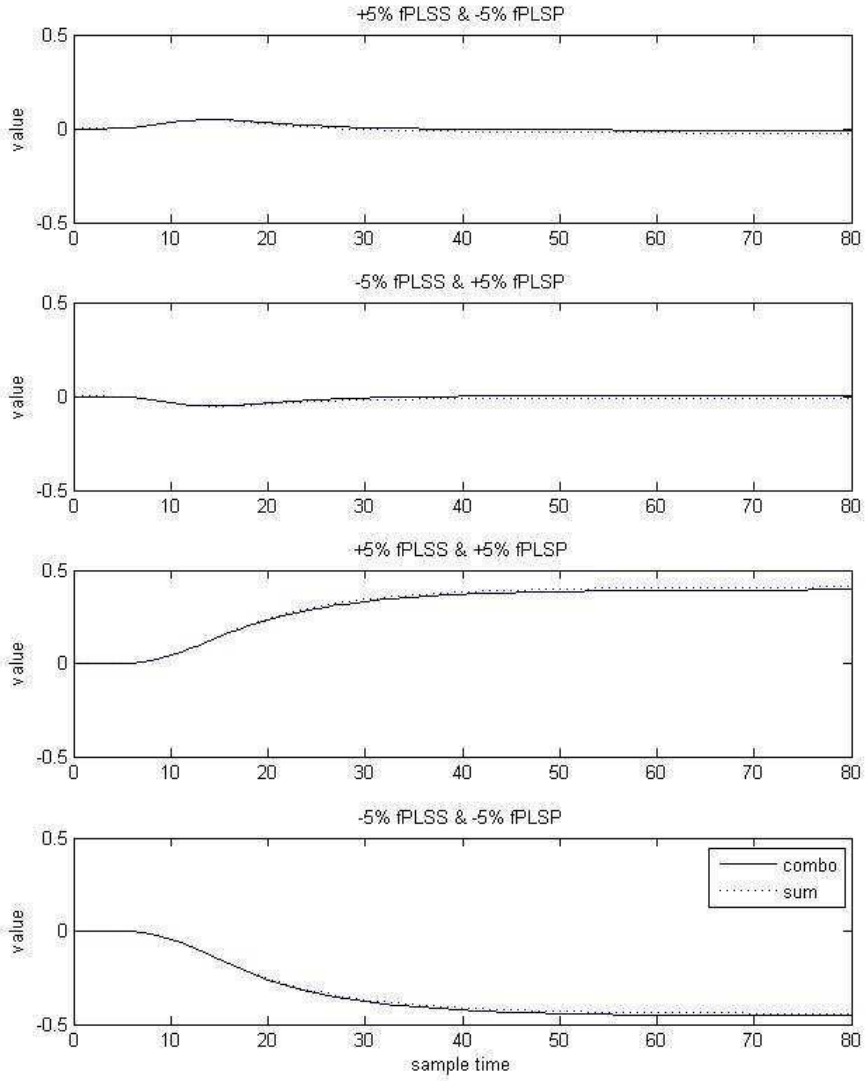

Figure 8-9: Responses of the rich electrolyte copper concentration to 5% changes in the series and parallel PLS flow rates, F(PLSS) and F(PLSP). Response from simultaneous input changes in solid curves (combo), and the sum of responses from separate experiments with dashed curves (sum).

8.1.2.2 Loaded organic copper concentration

The differences between the response combinations and sums for the loaded organic copper concentration at operating point DP4 are numerically evaluated in Table 8-7. The differences are transformed into percentages by dividing the difference by the total response change, as shown in Table 8-8. The differences are less than 0.2% of the nominal value of the loaded organic copper concentration, and thus the additivity principle is applying well for the loaded organic copper concentration. The responses are almost identical for the summed outputs and the input change combinations, as presented in Figure 8-10 for input changes in the PLS series flow rate and organic flow rate.

Table 8-7: Differencies between the gains of the outputs of combined input changes and sum of separate input changes for loaded organic copper concentration responses in operating point DP4.

c(LO)	**+5% -5%**	**-5% +5%**	**+5% +5%**	**-5% -5%**
F(PLSS)&F(PLSP)	0.0113	0.0113	-0.0119	-0.0104
F(PLSS)&F(LO)	-0.0193	-0.0114	0.0144	0.0176
F(LO)&F(LE)	0.0049	0.0054	-0.0044	-0.0060
F(PLSS)&c(PLS)	0.0154	0.0184	-0.0204	-0.0116
F(LO)&c(LE)	-0.0102	-0.0134	0.0109	0.0129
F(LE)&c(LE)	-0.0016	-0.0019	0.0017	0.0018
F(LO)&c(PLS)	-0.0136	-0.0336	0.0243	0.0250

Table 8-8: Percentual differencies between the gains of the outputs of combined input changes and sum of separate input changes for loaded organic copper concentration responses in operating point DP4.

c(LO)	**+5% -5%**	**-5% +5%**	**+5% +5%**	**-5% -5%**
F(PLSS)&F(PLSP)	-	-	3.79%	2.89%
F(PLSS)&F(LO)	4.52%	2.37%	11.70%	13.23%
F(LO)&F(LE)	2.02%	2.15%	1.27%	1.83%
F(PLSS)&c(PLS)	7.34%	10.04%	4.30%	2.04%
F(LO)&c(LE)	2.41%	3.45%	6.34%	7.01%
F(LE)&c(LE)	0.99%	1.21%	2.35%	2.64%
F(LO)&c(PLS)	1.97%	5.67%	-	-

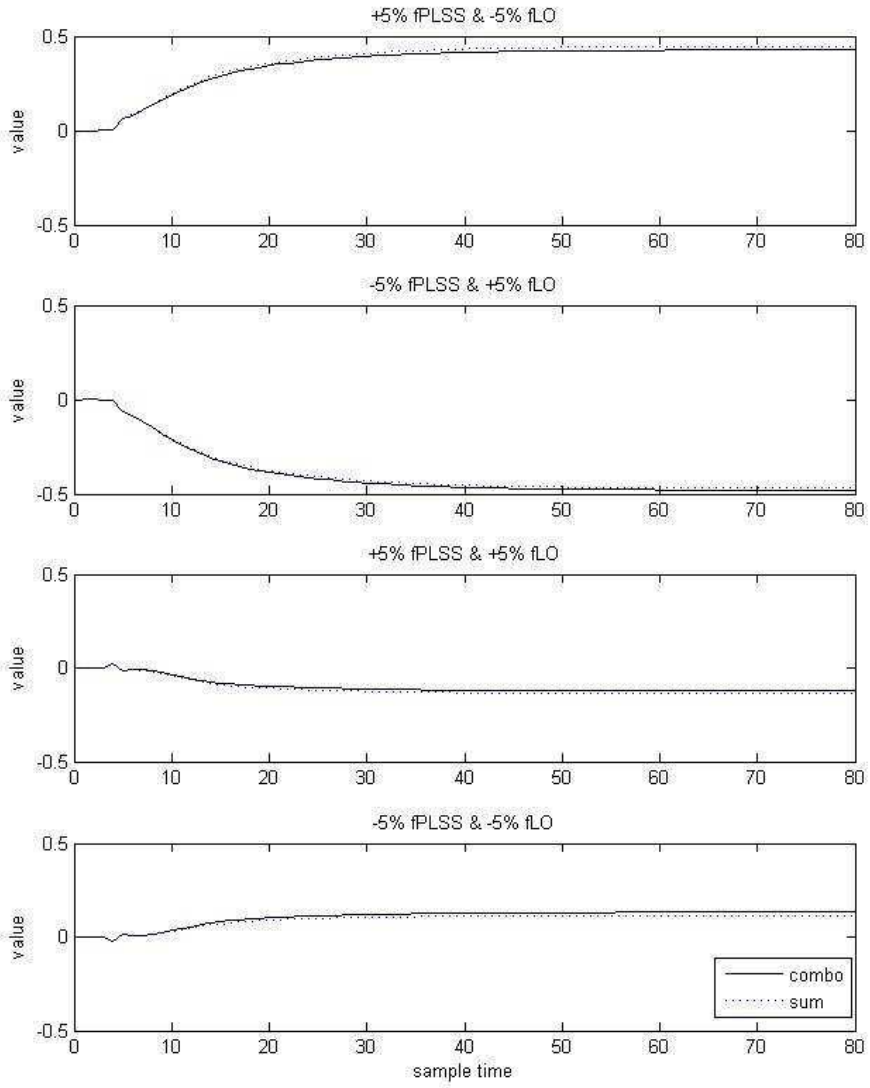

Figure 8-10: Responses of the loaded organic copper concentration to 5% changes in the PLS series and organic flow rates, F(PLSS) and F(LO). Response from simultaneous input changes in solid curves (combo), and the sum of responses from separate experiments with dashed curves (sum).

8.1.3 Summary of the linearity study

The linearity of the dynamic models at both operating points DP1 and DP4 is studied. The scaling invariance and additivity are sufficiently applicable for both output variables, i.e. the rich electrolyte and loaded organic copper concentrations. In the scaling invariance study the asymmetry between the positive and negative changes is less than 20% on the average. The steady state gain difference for changes with the same sign is less than 20% on the average, and thus the process is only weakly nonlinear. Since the controllers will keep the process around its desired operating point, the nonlinearities will not seriously affect the controller performance.

On the basis of the responses, the following suggestion for linearization to the transfer function form can be made: *the models should be formulated to be of the first order*

plus time delay form, except for the organic flow rate response to the rich electrolyte copper concentration and all the reagent volume per cent responses, which are of the second order with zero plus time delay form.

8.2 Determining the order of the linearized process models

Since the dynamic model has proved to be adequately linear, the minimum order for the linear state space model has to be determined. Each mixer-settler model is first formulated in the first order plus time delay transfer function, and the sub-models are then combined according to the case plant flowsheet. The models are combined in order to present the output copper concentrations as a linear combination of the input variables. The order of the state space models is determined on the basis of these models.

8.2.1 Linear model of one unit process

Due to the severe nonlinearities of the dynamic process model (multiplications and divisions of the input variables), the linear model of the output copper concentrations is assumed to be a linear function of the two input concentrations and two input flow rates. It is assumed that the dynamics in one unit process follows the first order plus time delay form, as follows:

$$c_{out}^{org}(s)=\frac{h_{11}\cdot e^{-h_{13}s}}{h_{12}s+1}c_{in}^{org}(s)+\frac{h_{21}\cdot e^{-h_{23}s}}{h_{22}s+1}c_{in}^{aq}(s)+\frac{h_{31}\cdot e^{-h_{33}s}}{h_{32}s+1}F_{in}^{org}(s)+\frac{h_{41}\cdot e^{-h_{43}s}}{h_{42}s+1}F_{in}^{aq}(s) \tag{8-3}$$

Assume that changes in the input concentration cause responses with identical time dynamics, but different gains. The responses for the input flow rate changes are also assumed to behave similarly, but with different gains. This yields:

$$\begin{aligned}c_{out}^{org}(s)&=\frac{h_{11}\cdot e^{-h_{13}s}}{h_{12}s+1}c_{in}^{org}(s)+\frac{h_{21}\cdot e^{-h_{23}s}}{h_{22}s+1}c_{in}^{aq}(s)+\frac{h_{31}\cdot e^{-h_{33}s}}{h_{32}s+1}F_{in}^{org}(s)+\frac{h_{41}\cdot e^{-h_{43}s}}{h_{42}s+1}F_{in}^{aq}(s)\\&\approx\frac{e^{-h_{13}s}}{h_{12}s+1}\left[h_{11}\cdot c_{in}^{org}(s)+h_{21}\cdot c_{in}^{aq}(s)\right]+\frac{e^{-h_{33}s}}{h_{32}s+1}\left[h_{31}\cdot F_{in}^{org}(s)+h_{41}\cdot F_{in}^{aq}(s)\right]\end{aligned} \tag{8-4}$$

Assume that the time delays can be Pade approximated as follows:

$$e^{-h_{13}s}\approx\frac{1-\frac{h_{13}}{2}s}{1+\frac{h_{13}}{2}s}=\frac{2-h_{13}s}{2+h_{13}s} \tag{8-5}$$

Now the output copper concentrations can be formulated as follows:

$$c_{out}^{org}(s) \approx \frac{2-h_{13}s}{2+h_{13}s}\frac{1}{h_{12}s+1}\left[h_{11}\cdot c_{in}^{org}(s)+h_{21}\cdot C_{in}^{aq}(s)\right]+\frac{2-h_{33}s}{2+h_{33}s}\frac{1}{h_{32}s+1}\left[h_{31}\cdot F_{in}^{org}(s)+h_{41}\cdot F_{in}^{aq}(s)\right] \quad (8\text{-}6)$$

8.2.2 Linear model of the copper solvent extraction process

In this section the linear models of the unit processes are combined according to the plant flow sheet presented in Figure 5-1. The plant consists of four unit processes, and an organic storage tank and a wash stage for the organic solution.

For simplicity, in the derivation of the linear plant model, the first order plus time delay (FOPTD) models are marked with h_i, as follows:

$$c_{out}^{org}(s) = h_1(s)c_{in}^{org}(s)+h_2(s)c_{in}^{aq}(s)+h_3(s)F_{in}^{org}(s)+h_4(s)F_{in}^{aq}(s) \quad (8\text{-}7)$$

As the volume of the tank is significantly smaller than that of one settler, in the following analysis the organic tank and the organic phase of the wash stage are approximated with a constant organic time delay (θ).

Since the output flow rates from settlers S1H, E1P, E1S and E2S, marked as F(BO), F(BO1), F(BO2), F(PLS1), are not measured, they have to be approximated from the flow rates and equipment volumes. In the process the mixer and settler volumes are approximately constant, and the maximum deviation from the normal operating point during process changes is about 5%. The mixers and settlers are identical and the organic surface depths are very similar in each settler. Assume that the flow rate is approximately constant and the settler aqueous and organic volumes are not changing, then the time delays in the mixer-settlers for the organic (θ) and aqueous (δ) phases are approximately constant. Now the missing flow rate measurements can be expressed as:

$$F(BO)(s) = F(LO)\cdot e^{-\theta s} \quad (8\text{-}8)$$

$$F(BO1)(s) = F(LO)\cdot e^{-2\theta s} \quad (8\text{-}9)$$

$$F(BO2)(s) = F(LO)\cdot e^{-3\theta s} \quad (8\text{-}10)$$

$$F(PLS1)(s) = F(PLSS)\cdot e^{-\delta s} \quad (8\text{-}11)$$

The detailed models for each of the unit process are first developed, and these models are then combined to model the output copper concentrations of rich electrolyte and loaded organic as functions of the measured input variables.

The output copper concentrations of the first extraction unit process E1P are formulated as follows:

$$c(BO1)(s) = h_1(s)c(BO)(s) + h_2(s)c(PLS)(s) + h_3(s)F(BO)(s) + h_4(s)F(PLSP)(s) \quad (8\text{-}12)$$

$$c(RaffP)(s) = u_1(s)c(BO)(s) + u_2(s)c(PLS)(s) + u_3(s)F(BO)(s) + u_4(s)F(PLSP)(s) \quad (8\text{-}13)$$

The output copper concentrations of the second extraction unit process E1S are formulated as follows:

$$c(BO2)(s) = f_1(s)c(BO1)(s) + f_2(s)c(PLS1)(s) + f_3(s)F(BO1)(s) + f_4(s)F(PLS1)(s) \quad (8\text{-}14)$$

$$c(RaffS)(s) = v_1(s)c(BO1)(s) + v_2(s)c(PLS1)(s) + v_3(s)F(BO1)(s) + v_4(s)F(PLS1)(s) \quad (8\text{-}15)$$

The output copper concentrations of the third extraction unit process E2S are formulated as follows:

$$c(LO)(s) = g_1(s)c(BO2)(s) + g_2(s)c(PLS)(s) + g_3(s)F(BO2)(s) + g_4(s)F(PLSS)(s) \quad (8\text{-}16)$$

$$c(PLS1)(s) = k_1(s)c(BO2)(s) + k_2(s)c(PLS)(s) + k_3(s)F(BO2)(s) + k_4(s)F(PLSS)(s) \quad (8\text{-}17)$$

The output copper concentrations of the stripping unit process S1H are formulated as follows:

$$c(BO)(s) = j_1(s)c(LO)(s) + j_2(s)c(LE)(s) + j_3(s)F(LO)(s) + j_4(s)F(LE)(s) \quad (8\text{-}18)$$

$$c(RE)(s) = p_1(s)c(LO)(s) + p_2(s)c(LE)(s) + p_3(s)F(LO)(s) + p_4(s)F(LE)(s) \quad (8\text{-}19)$$

Now the output concentrations of loaded organic c(LO) and rich electrolyte c(RE) can be expressed as a combination of Equations 8-15 – 8-26 as follows:

$$
\begin{aligned}
&c(LO)(s)=\frac{1}{1-f_2(s)k_1(s)-g_1(s)f_1(s)h_1(s)j_1(s)}\cdot\\
&\Big[c(PLS)(s)\big[g_1(s)f_2(s)k_2(s)+g_1(s)f_1(s)h_2(s)+(1-f_2(s)k_1(s))g_2(s)\big]\\
&+c(LE)(s)\big[g_1(s)f_1(s)h_1(s)j_2(s)\big]\\
&+F(LO)(s)\Big[g_1(s)f_2(s)k_3(s)e^{-3\theta s}+g_1(s)f_3(s)e^{-2\theta s}+g_1(s)f_1(s)h_3(s)e^{-\theta s}\\
&+g_1(s)f_1(s)h_1(s)j_3(s)+(1-f_2(s)k_1(s))g_3(s)e^{-3\theta s}\Big]\\
&+F(PLSS)(s)\Big[g_1(s)f_2(s)k_4(s)+g_1(s)f_4(s)e^{-\delta s}+(1-f_2(s)k_1(s))g_4(s)\Big]\\
&+F(PLSP)(s)\big[g_1(s)f_1(s)h_4(s)\big]\\
&+F(LE)(s)\big[g_1(s)f_1(s)h_1(s)j_4(s)\big]\Big]
\end{aligned}
\tag{8-20}
$$

$$
\begin{aligned}
&c(RE)(s)=\frac{p_1(s)}{1-f_2(s)k_1(s)-g_1(s)f_1(s)h_1(s)j_1(s)}\cdot\\
&\Big[c(PLS)(s)\big[g_1(s)f_2(s)k_2(s)+g_1(s)f_1(s)h_2(s)+(1-f_2(s)k_1(s))g_2(s)\big]\\
&+c(LE)(s)\big[g_1(s)f_1(s)h_1(s)j_2(s)\big]\\
&+F(LO)(s)\Big[g_1(s)f_2(s)k_3(s)e^{-3\theta s}+g_1(s)f_3(s)e^{-2\theta s}+g_1(s)f_1(s)h_3(s)e^{-\theta s}\\
&+g_1(s)f_1(s)h_1(s)j_3(s)+(1-f_2(s)k_1(s))g_3(s)e^{-3\theta s}\Big]\\
&+F(PLSS)(s)\Big[g_1(s)f_2(s)k_4(s)+g_1(s)f_4(s)e^{-\delta s}+(1-f_2(s)k_1(s))g_4(s)\Big]\\
&+F(PLSP)(s)\big[g_1(s)f_1(s)h_4(s)\big]\\
&+F(LE)(s)\big[g_1(s)f_1(s)h_1(s)j_4(s)\big]\Big]\\
&+p_2(s)c(LE)(s)+p_3(s)F(LO)(s)+p_4(s)F(LE)(s)
\end{aligned}
\tag{8-21}
$$

Using Equations 8-11 – 8-13, the organic recycle term, consisting of the term $f_2(s)k_2(s)$, is caused by the PLS recycle in the series extraction units and term $g_1(s)f_1(s)h_1(s)j_1(s)$ by the loaded organic recycle through all the unit processes, can be analyzed, as follows:

$$
\begin{aligned}
&\frac{1}{1-f_2(s)k_1(s)-g_1(s)f_1(s)h_1(s)j_1(s)}\\
&=\frac{1}{1-\dfrac{f_{21}\cdot e^{-f_{23}s}}{f_{22}s+1}\cdot\dfrac{k_{21}\cdot e^{-k_{23}s}}{k_{22}s+1}-\dfrac{g_{11}\cdot e^{-g_{13}s}}{g_{12}s+1}\dfrac{f_{11}\cdot e^{-f_{13}s}}{f_{12}s+1}\dfrac{h_{11}\cdot e^{-h_{13}s}}{h_{12}s+1}\dfrac{j_{11}\cdot e^{-j_{13}s}}{j_{12}s+1}}
\end{aligned}
$$

$$
=\frac{1}{1-\dfrac{1}{f_{12}s+1}\cdot\dfrac{2-f_{13}s}{2+f_{13}s}\left[\dfrac{f_{21}\cdot k_{21}}{k_{22}s+1}\cdot\dfrac{2-k_{23}s}{2+k_{23}s}-\dfrac{g_{11}\cdot f_{11}}{g_{12}s+1}\cdot\dfrac{h_{11}}{h_{12}s+1}\cdot\dfrac{j_{11}}{j_{12}s+1}\cdot\dfrac{2-(g_{13}+h_{13}+j_{13})s}{2+(g_{13}+h_{13}+j_{13})s}\right]}
$$

$$= \frac{(f_{12}s+1)(2+f_{13}s1)(k_{22}s+1)(2+k_{23}s)(g_{12}s+1)(h_{12}s+1)(j_{12}s+1)(2+(g_{13}+h_{13}+j_{13})s)}{\left[(f_{12}s+1)(2+f_{13}s1)(k_{22}s+1)(2+k_{23}s)(g_{12}s+1)(h_{12}s+1)(j_{12}s+1)(2+(g_{13}+h_{13}+j_{13})s)\right.}$$
$$+(2-f_{13}s)\cdot\left[f_{21}k_{21}(2-k_{23}s)(g_{12}s+1)(h_{12}s+1)(j_{12}s+1)(2+(g_{13}+h_{13}+j_{13})s)\right]$$
$$\left.-(2-f_{13}s)\cdot\left[g_{11}f_{11}h_{11}j_{11}(k_{22}s+1)(2+k_{23}s)(2-(g_{13}+h_{13}+j_{13})s)\right]\right] \quad (8\text{-}22)$$

The order of the numerator is 8 and the orders of the denominator terms are 8, 6 and 4. If the organic recycle term can be neglected, from Equations (8-27) and (8-28), then the highest denominator orders for the loaded organic copper concentration are [6 8 8 6 6 8] and for the rich electrolyte concentration [8 10 10 8 8 10], with the corresponding inputs [c(PLS), c(LE), F(PLSS), F(PLSP), F(LO), F(LE)]. If the recycle (Equation 8-29) of the highest denominator order of 8 is included, then the highest denominator order is 16 for loaded organic and 18 for rich electrolyte. Thus, for the state-space model identification, model orders of between 6 and 18 should be tested.

8.3 Identification of the linear models

The aim of this section is to linearize the dynamic process models to state space (SS) and first or higher order plus time delay transfer function (TF) forms. The state space model matrices and transfer function model parameters are first identified from the modeling data using the Matlab system identification toolbox (Ljung, 2006), and the models are then verified by applying the inputs of the verification data sets to the linear models and comparing the linear model outputs to the outputs of the verification data sets.

The output variables are the rich electrolyte, loaded organic copper concentrations, c(RE) and c(LO). The input variables are the flow rates of the PLS series, PLS parallel, organic and electrolyte, F(PLSS), F(PLSP), F(LO) and F(LE), the copper concentrations of PLS and lean electrolyte, c(PLS) and c(LE), and the reagent volume per cent in the organic solution, vol.

The models are identified from the simulated data because the industrial data does not have enough excitation for model indentification. The modeling data are created with dynamic process models by introducing a pseudo random binary signal, PRBS (Söderström and Stoica, 1989, pp.96 –97), with an amplitude of ± 5%, bandwidth [0 0.1] and length 4000 samples to all the 7 input channels. The input-output data are collected and subspace identification performed (for the N4SID identification algorithm, see Ljung, 2006).

The state space models (SS) with 2 - 24 states are identified from the PRBS data separately for both outputs. Each state-space model is identified separately, model order reduction techniques are not used. The state space model for the loaded organic and rich electrolyte copper concentrations, c(LO) and c(RE), is defined as follows:

$$\dot{x} = M_1 x + M_2 \begin{bmatrix} F(PLSS) & F(PLSP) & F(LO) & F(LE) & c(PLS) & c(LE) & vol \end{bmatrix}^T$$
$$\begin{bmatrix} c(LO) & c(RE) \end{bmatrix}^T = M_3 x + M_4 \begin{bmatrix} F(PLSS) & F(PLSP) & F(LO) & F(LE) & c(PLS) & c(LE) & vol \end{bmatrix}^T$$

(8-23)

, where the number (n) of states x determines the order of the coefficient matrices $M_1 \in R^{n \times n}$, $M_2 \in R^{n \times 7}$, $M_3 \in R^{2 \times n}$.

Matrix M_4 in this case is [0] since there are no direct effects from the inputs to the outputs. (Ljung, 1987, pp. 82-86)

The transfer function model (TF) parameters are identified from the PRBS data separately for both outputs. The transfer function model forms are predetermined on the basis of the step responses (Section 8.1.1). Most of the submodels are of the first order plus time delay form. The more complex dynamics are modeled as second order with zero plus time delay. The transfer function models for loaded organic and rich electrolyte copper concentrations, c(LO) and c(RE), are of the following form:

$$\begin{bmatrix} c(LO) & c(RE) \end{bmatrix}^T = G_{p,tot} \begin{bmatrix} F(PLSS) & F(PLSP) & F(LO) & F(LE) & c(PLS) & c(LE) & vol \end{bmatrix}^T$$

$$G_{p,tot}^T = \begin{bmatrix} \frac{a_{11}e^{-c_{11}s}}{b_{11}s+1} & \frac{a_{21}e^{-c_{21}s}}{b_{21}s+1} \\ \frac{a_{12}e^{-c_{12}s}}{b_{12}s+1} & \frac{a_{22}e^{-c_{22}s}}{b_{22}s+1} \\ \frac{a_{13}e^{-c_{13}s}}{b_{13}s+1} & \frac{a_{23}\left(d_{23}s+1\right)e^{-c_{23}s}}{\left(b_{231}s+1\right)\left(b_{232}s+1\right)} \\ \frac{a_{14}e^{-c_{14}s}}{b_{14}s+1} & \frac{a_{24}e^{-c_{24}s}}{b_{24}s+1} \\ \frac{a_{15}e^{-c_{15}s}}{b_{15}s+1} & \frac{a_{25}e^{-c_{25}s}}{b_{25}s+1} \\ \frac{a_{16}e^{-c_{16}s}}{b_{16}s+1} & \frac{a_{26}e^{-c_{26}s}}{b_{26}s+1} \\ \frac{a_{17}e^{-c_{17}s}}{b_{17}s+1} & \frac{a_{27}\left(-d_{27}s+1\right)e^{-c_{27}s}}{(b_{271}s+1)(b_{272}s+1)} \end{bmatrix}$$

(8-24)

where a_{ij}, b_{ij}, c_{ij} and d_{ij} are scalar constants.

The models are tested and verified with three different data sets. The first validation data set "Valid1" is created by introducing ± 5% input steps, one at a time, to the simulator inputs and the input-output data are collected. The operating point for the validation data set is the same as for the modeling data set. The second validation data set "Valid2" is created by introducing the industrial input data to the simulator, and collecting the input-output data. The third validation data set "Valid3" consists of the industrial input-output data.

The model performances are compared to each other using the fit index. The fit index is the percentage of output variations that is reproduced by the model: the higher the

percentage, the better the fit. The fit index is especially suitable when the comparison is performed at one operating point. (Matlab system identification toolbox: Ljung, 2006).

$$fit = \left[1 - \frac{norm\left(Y_{meas} - Y_{\text{model}}\right)}{norm\left(Y_{meas} - \bar{Y}_{meas}\right)} \right] \cdot 100\% \qquad \textbf{(8-25)}$$

where Y_{meas} is the measured value, $\bar{Y}_{meas}$ is the average value of the measured outputs, Y_{model} is the model value. The fit index values are between [-100 100].

8.3.1 Linear models for rich electrolyte copper concentration

The models of the rich electrolyte copper concentration are identified at two operating points, the first at DP1 and the second at DP4. At both operating points, the transfer function model for the rich electrolyte copper concentration included five first order plus time delay and two second order with zero plus time delay submodels. The state space models have 2,3,4,5,6,7,8,10,12,14, 16, 18, 20, 21 and 24 states. The fits of the linearized models to the validation data sets are presented in Table 8-9.

The state space models identified at the first operating point DP1 with 16, 20 and 21 states are not successful. The fit of the linear models to the step data (Valid1 DP1) and to the mechanistic model output data (Valid 2 DP1) are good with the transfer function model and the state space models with more than 6 states. The linear model fit to the industrial data (Valid 3 DP1) is slightly poorer. For the transfer function model and the state space the models linearized at operating point DP4, the fits with more than 4 states are very good on all the validation data sets (Valid1 DP4, Valid2 DP4 and Valid3 DP4). The best model structures are the transfer function model and the state space models with 8 and 10 states.

Table 8-9: Model fits to the rich electrolyte copper concentration responses to the 5% input steps (Valid 1) at DP1 and DP4, to mechanistic model outputs (Valid2) with the inputs of the first and second industrial data set, and to the first and second industrial data set (Valid3).

model structure for c(RE)	Valid1 DP1	Valid2 DP1	Valid3 DP1	Valid1 DP4	Valid2 DP4	Valid3 DP4
Transfer function (Eq. 8-30)	89.64	79.34	27.19	90.26	87.54	40.67
State space 2 order	67.51	69.7	20.36	76.08	78.59	52.39
State space 3 order	62.89	57.94	23.33	62.15	81.67	37
State space 4 order	59.07	53.23	28.59	56.05	76.39	52.09
State space 5 order	70.33	70.2	20.35	71.27	81.9	48.15
State space 6 order	68.17	66.8	25.87	66.93	80.46	50.21
State space 7 order	87.37	75.35	14.29	88.27	86.68	37.88
State space 8 order	91.7	72.96	13.21	89.15	86.23	36.96
State space 10 order	90.9	76.92	16.7	92.58	86.98	38.15
State space 12 order	90.66	78.03	17.74	92.08	85.32	33.41
State space 14 order	92.75	75.77	15.97	91.95	85.03	32.65
State space 16 order	-	-	-	90.43	84.02	30.85
State space 18 order	91.91	75.11	17.22	90.54	83.64	30.2
State space 20 order	-	-	-	90.59	83.68	30.33
State space 21 order	-	-	-	91.36	84.77	32.4

State space 24 order	90.36	74.73	18.64	90.87	83.89	30.58

Compared to the rich electrolyte copper concentration measurements of the first industrial data set (Valid3 DP1), the linear transfer function and eight order state space models follow well the dynamics of the process, as can be seen from Figure 8-11.

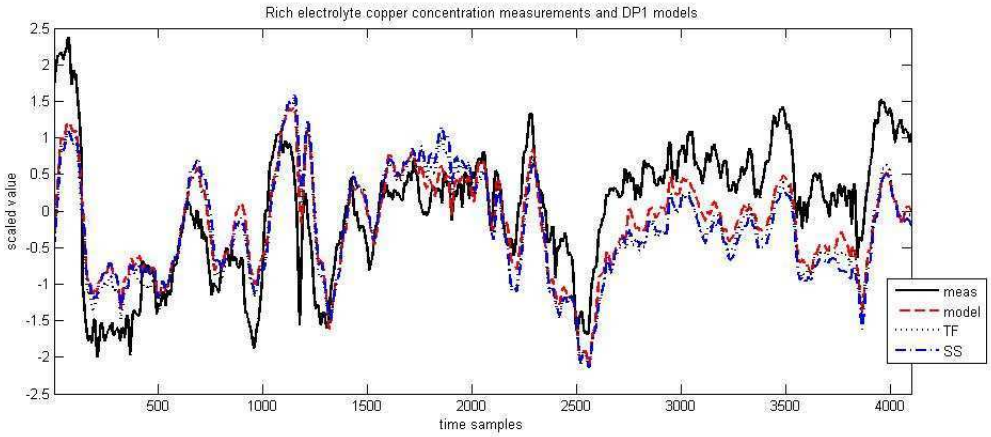

Figure 8-11: Rich electrolyte copper concentration; measurement of the first industrial data set (solid), mechanistic model (dashed), transfer function model (dotted), and eight order state space model (dash dotted).

The rich electrolyte copper concentration measurements of the second industrial data set (Valid3 DP4) are well followed by the linearized models, as can be seen from Figure 8-12. The dynamics are very similar to the process and the mechanistic model data, with a slight difference in the end of the data set.

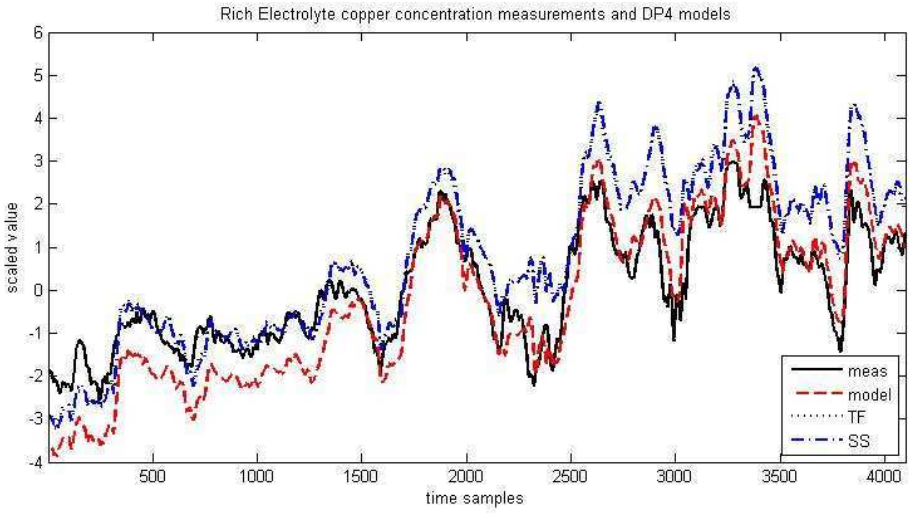

Figure 8-12: Rich electrolyte copper concentration; measurement of the second industrial data set (solid), mechanistic model (dashed), transfer function model (dotted), and eight order state space model (dash dotted).

8.3.2 Linear models for loaded organic copper concentration

The models of the loaded organic concentration are identified at two operating points, the first at DP1 and the second at DP4. At both operating points, the transfer function model for loaded organic copper concentration included only the first order plus time delay submodels, as presented in Equation 8-30. The model state space models identified have 2,3,4,5,6,7,8,10,12,14, 16, 18, 20, 21 and 24 states. The fits of the linear models to the validation data sets are presented in Table 8-10.

At the first operating point DP1, the state space models with 20 and 21 states are not successful. The fit indices of the linear models to the first two validation data sets (Valid1 DP1 and Valid2 DP1) are adequate. The fits to the first industrial data set (Valid3 DP1), that has only small changes, are worse than for the second data set (Valid3 DP4), that has a considerable level change. The best models linearized at the first operating point DP1 are the transfer function model and the state space models with more than 7 states.

At the second operating point DP4, the state space models with 12, 21 and 24 states are not successful. The fit of the transfer function model and the state space models with more than 4 states are very good on all the validation data sets (Valid1 DP4, Valid2 DP4 and Valid3 DP4). At the second operating point the best model structures are the transfer function model and the state space models with 8 and 10 states.

Table 8-10: Model fits to the loaded organic copper concentration responses to the 5% input steps (Valid1) at DP1 and DP4, mechanistic model outputs (Valid2) with the inputs of the first and second industrial data set, and to the first and second industrial data set (Valid 3).

model structure for c(LO)	Valid1 DP1	Valid2 DP1	Valid3 DP1	Valid1 DP4	Valid2 DP4	Valid3 DP4
Transfer function (Eq. 8-30)	93.82	39.23	4.837	88.44	74.4	62.34
State space 2 order	60.01	31.27	16.05	40.49	64.35	63.55
State space 3 order	55.71	30.59	16.22	56.36	45.08	48.03
State space 4 order	51.47	30.6	16.47	48.98	34.71	37.18

State space 5 order	52.79	30.04	16.77	79.05	68.91	63.95
State space 6 order	57.84	36.2	15.63	76.3	68.51	63.6
State space 7 order	67.72	39.72	13.09	77.92	66.98	63.61
State space 8 order	75.42	41.6	10.24	81.7	71.3	63.38
State space 10 order	75.43	40.69	10.45	82.65	71.28	63.56
State space 12 order	73.91	41.69	10.39	-	-	-
State space 14 order	74.6	41.72	9.783	81.45	70.95	63.88
State space 16 order	75.42	41.71	9.271	79.88	70.5	64.13
State space 18 order	76.12	40.26	10.43	76.82	68.4	63.64
State space 20 order	-	-	-	78.76	69.34	63.85
State space 21 order	-	-	-	-	-	-
State space 24 order	73.97	40.26	12.01	-	-	-

At the first operating point DP1, the linearized models follow the trends of the dynamic process models (Valid2 DP1) with a slight difference between the levels. The process data (Valid3 DP1) for the loaded organic copper concentration are of poor quality, but the state space model was relatively successful in following the trends. The eight order state space model is closer to the mechanistic model, as can be seen from Figure 8-13.

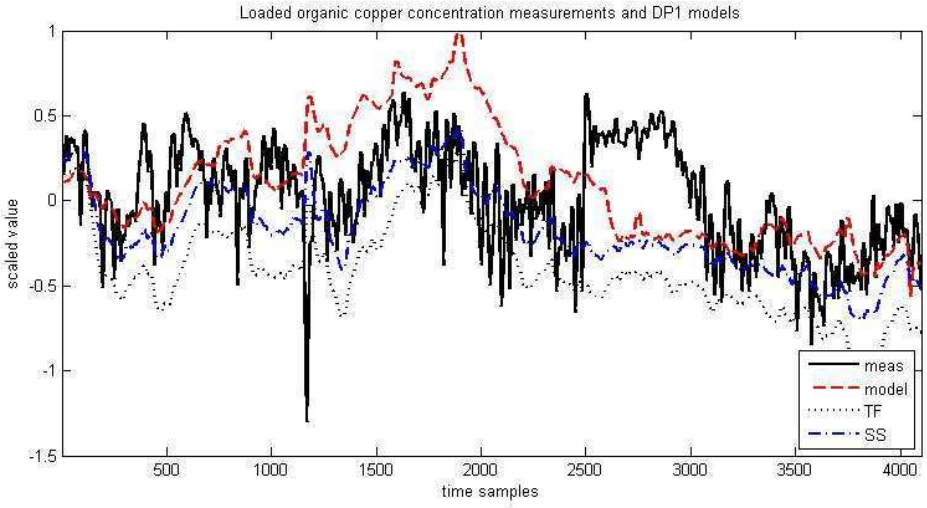

Figure 8-13: Loaded organic copper concentration; measurement (solid), mechanistic model (dashed), transfer function model (dotted), and eight order state space model (dash dotted).

At the second operating point DP4, the transfer function outputs and the outputs of the state space model with eight states are plotted against the second industrial data set (Valid3 DP4) with reasonably good fit, as can be seen in Figure 8-14. The value of the loaded organic copper concentration changes much faster with the dynamic process models than with the linear models, but the final level is reached relatively successfully with all the models. The linearized models have the same dynamic changes as the mechanistic models, but they slightly lack the level adaptation for the loaded organic copper concentration.

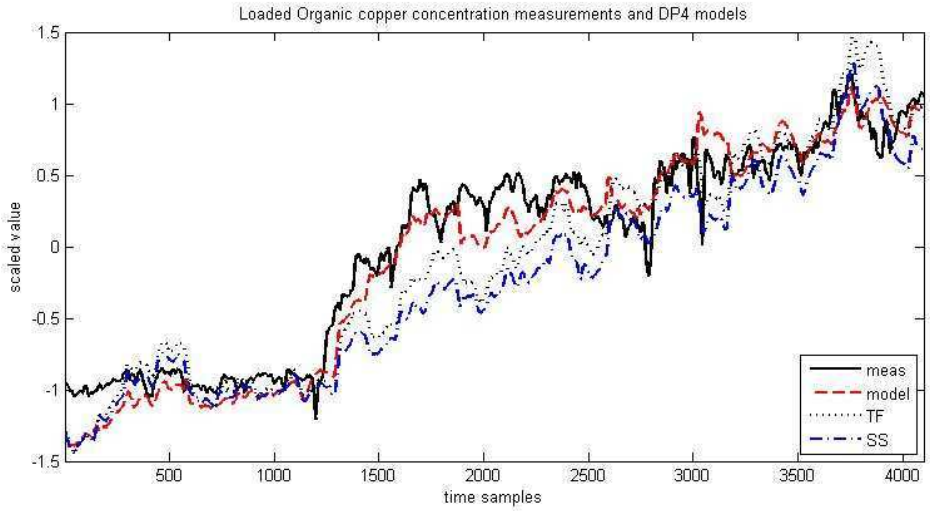

Figure 8-14: Loaded organic copper concentration; measurement (solid), mechanistic model (dashed), transfer function model (dotted), and eight order state space model (dash dotted).

8.4 Concluding remarks

The scaling invariance was sufficiently applicable and the additivity very applicable for the output responses of the dynamic models, and thus the superposition principle is adequately applicable for the models. Therefore, the linear model structures were assumed to be accurate enough to approximate the dynamic behaviour of the process.

The dynamic process models were linearized to transfer function and state space model forms. The linear model order derivation resulted in a theoretical minimum of 6 - 18 orders for the state space model, assuming that each unit process behaves as a first order plus time delay model, and approximating the dead times with the first order Pade transformation. The responses of the scaling invariance study revealed that suitable transfer function models would be of the first order plus time delay and second order with zero plus time delay form.

The linear models were identified using a subspace identification algorithm. The modeling data were created by introducing pseudo random binary signals to the dynamic process models and then collecting the input-output data. The linear models were validated against three different data sets, one input step change response data set, one simulated data set, and one industrial data set. The model linearization was successful for the rich electrolyte and loaded organic copper concentrations. The best model structures were transfer function models and state space models of 8 and 10 orders, which will be used in the further studies.

9 DESIGN OF THE CONTROL STRATEGIES AND OPTIMIZATION FOR THE COPPER SOLVENT EXTRACTION PROCESS

The aim of this chapter is to describe the design of the control structure, present the single-input single-output and multi-input multi-output control strategies, and develop optimization for the industrial plant. The control system design is based on the systematic analysis of the dynamics of the copper solvent extraction process.

The control aims and current control strategy of the industrial plant are described in Section 9.1, and the proposed control structure presented in Section 9.2. The stability, state controllability and observability of the plant are analyzed in Section 9.3. The input-output pairing of the manipulated and controlled variables is performed by means of relative gain array analysis, as described in Section 9.4. The single-input single-output and multi-input multi-output control strategies are designed on the basis of this analysis in Section 9.5. The structure of the dynamic simulator with the controllers is presented in Section 9.6. Finally, the optimization algorithm, based on the chosen pairing of the controlled and manipulated variables, is presented in Section 9.7.

9.1 Control objectives and the current control strategy of the case copper solvent extraction plant

Maximization of copper production is the main goal of the control strategy in the copper solvent extraction and electrowinning plant. The control strategy in the plant for solvent extraction is to keep the flow rates as high as possible in order to maximize copper mass flow through the process. The control strategy in the plant for the electrowinning process is to keep the current amperages as high as economically possible in order to maximize the copper cathode production.

In the copper solvent extraction process, the regulatory control level of the automation system consists of PID loops for the flow rates. Higher control levels do not exist. The operators choose the flow rate setpoints that keep the process within the target values. The metallurgists give target values for the lean electrolyte copper concentrations once a week. The flow rates have restrictions due to the maximum pumping capacities, and the aqueous to organic flow ratios maintaining the phase continuities in the mixers.

Maximum production is not achieved with the current control strategy. The long time delays between the control actions and the responses in the key process variables, complex interactions and cause-effect relationships make control of the process a very challenging task for a human operator. Therefore the control actions are very conservative and the process is in a suboptimal state for most of the time. The current control strategy also lacks real time optimization that would enable steering the process to the optimal operating point.

9.2 Proposed control structure for the case copper solvent extraction plant

The problems of the current control strategy could be avoided by careful control strategy design and implementation of an advanced control system. The objectives of the control system are to enable running the process at the optimal operating point, decrease the plant variation and speed up adaptation to the changing process conditions, thus increasing the copper production. The control strategy is designed on the basis of the proposed control hierarchy and the control structure analysis.

The proposed control hierarchy is illustrated in Figure 9-1. The hierarchy for the copper solvent extraction plant is developed on the basis of the process operational knowledge and classification of the controlled and manipulated variables. In this thesis the optimization and stabilizing control levels are developed. The lower levels of the hierarchy already exist at the plant.

An optimization algorithm is developed in order to maximize the production of the copper solvent extraction process. The optimization level provides optimal setpoints of the controlled variables for the supervisory control level.

The stabilizing control level consists of a multi-input multi-output controller or several single-input single-output controllers that attempt to keep the controlled variables at given setpoints. The supervisory control levels provide setpoints of the manipulated variables for the basic control level.

In the copper solvent extraction process the basic control level consists of the flow rate PID loops, which keep the flow rates at the given setpoints. The basic control level gives valve opening signals to the final control elements, i.e. the actuators of the flow control valves at the instrumentation level. The instrumentation level consists of the final control elements, actuators, transmitters and sensors. The measurement information from the instrumentation level is transmitted to the control levels. The industrial copper solvent extraction process is located below the instrumentation level.

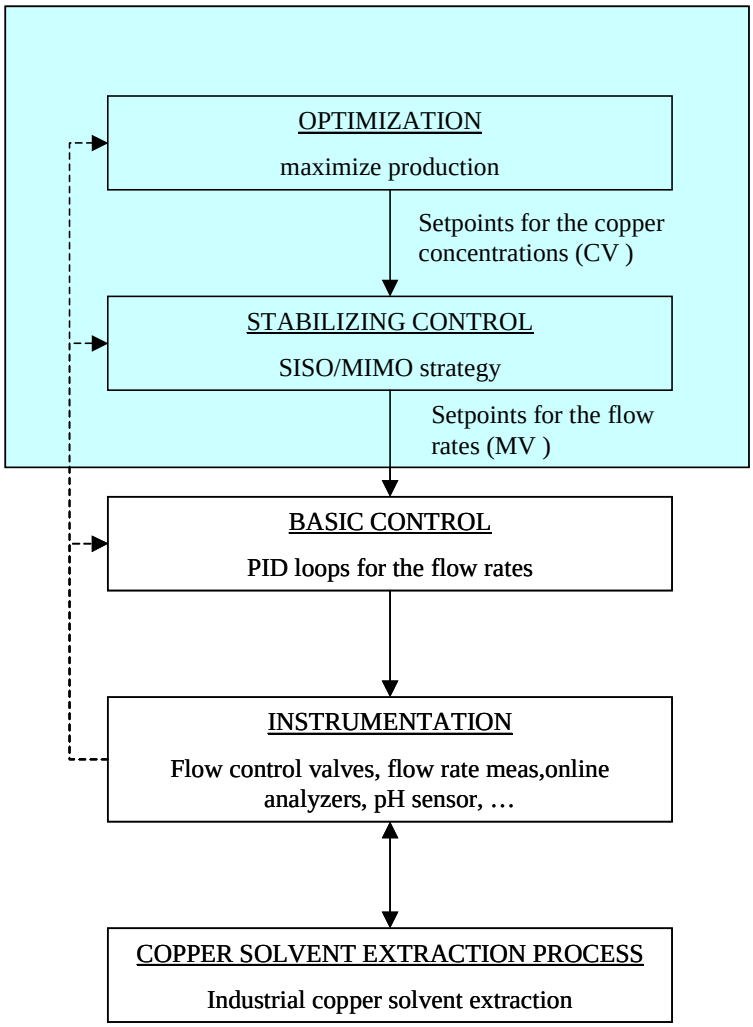

Figure 9-1: Proposed control hierarchy for the copper solvent extraction process. The optimization layer provides the setpoints of the controlled variables to the supervisory control level. The stabilizing control level is based on a single-input single-output or multi-input multi-output control strategy. The stabilizing control level provides the setpoints of the manipulated variables to the regulatory control level. The basic control level gives signals to the final control elements at the instrumentation level. The measurement information is led from the instrumentation level to all the upper levels.

The possible *controlled variables* (CV) are the outputs of the extraction, the loaded organic and raffinate copper concentrations, and the outputs of stripping, and the rich electrolyte and barren organic copper concentrations. Since only rich electrolyte solution enters the electrowinning process, the rich electrolyte copper concentration is chosen as the primary controlled variable. The raffinate copper concentration measurements are unreliable, as stated in Chapter 5.2, and thus the loaded organic copper concentration is chosen as the secondary controlled variable.

The available *manipulated variables* (MV) are the flow rates of PLS, organic and electrolyte, F(PLSS), F(PLSP), F(LO) and FLE).

The measured *disturbance variables* (DV) are the PLS and lean electrolyte concentrations and the total PLS flow rate, and the unmeasured disturbance is the change in reagent volume per cent in the organic solution and pH changes in PLS and acidity changes in the electrolyte solution.

The restrictions are the organic to aqueous ratio, which is related to phase continuity, pumping capacity, and the organic level in the tanks. The process, together with a classification of the controlled, manipulated and disturbance variables, is presented in Figure 9-1.

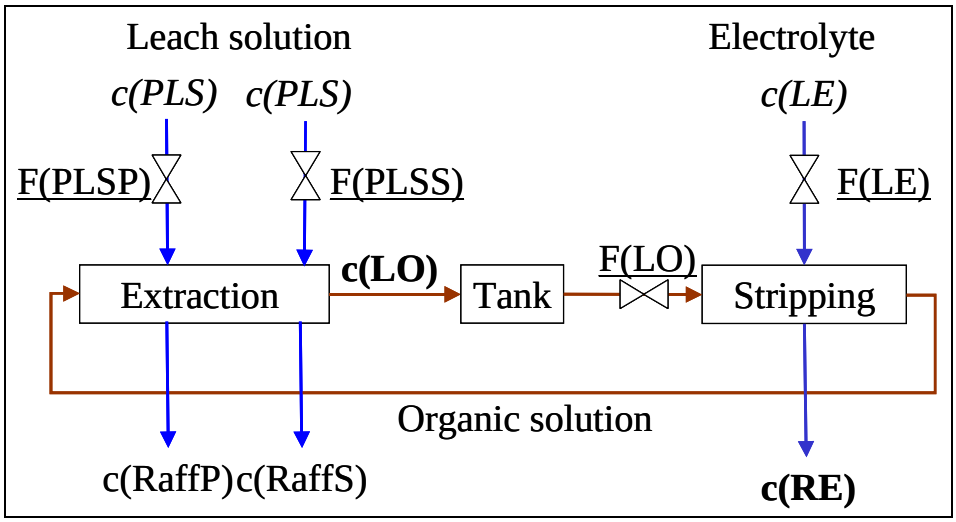

Figure 9-2: Solvent extraction process. Controlled variables (CV) are marked in bold, manipulated variables (MV) underlined, and disturbance variables marked in italics.

9.3 State controllability, state observability and stability

In order to design a control strategy, the state controllability, observability and stability have to be studied. The transfer function matrices are first transformed into state space form:

$$\begin{aligned} \dot{x} &= M_1 x + M_2 u \\ y &= M_3 x + M_4 u \end{aligned} \qquad \textbf{(9-1)}$$

where x are states, u inputs and y outputs. In this notation, n is the number of states, m the number of inputs and p the number or outputs. The order of the coefficient matrices are defined as $M_1 \in R^{n \times n}$, $M_2 \in R^{n \times m}$, $M_3 \in R^{p \times n}$ and $M_4 \in R^{p \times m}$.

The observability matrix is determined as:

$$Obs^T = \begin{bmatrix} M_3 \\ M_3 M_1 \\ M_3 M_1^{\,2} \\ \vdots \\ M_3 M_1^{\,n-1} \end{bmatrix} \qquad \textbf{(9-2)}$$

If the rank (column rank) of the observability matrix is the same as the number of states n, then the system is state observable. (Ogata, 1987, Skogestad and Postlethwaite, 2005, p.131)

The state controllability matrix is determined as:

$$Co = \begin{bmatrix} M_2 & M_1 M_2 & M_1^2 M_2 & \cdots & M_1^{n-1} M_2 \end{bmatrix} \quad \textbf{(9-3)}$$

If the rank (row rank) of the controllability matrix is the same as the number of states *n*, then the system is state controllable. (Ogata, 1987, Skogestad and Postlethwaite, 2005, p.128)

Controllability and observability conditions are directly related to the cancellation of poles and zeros in the corresponding transfer functions.

In order to study whether the system is input-output controllable, the condition number of the system has to be low (less than 10), i.e. the directionality of the system is desired to be weak (Skogestad and Postlethwaite, 2005). The condition number is calculated as the ratio of the maximum and minimum singular values of the system at different frequencies.

The stability is studied by plotting the Nyquist plot of all the controlled variable – manipulated variable transfer function pairs. If the –1 point is not circled, then the subsystem is stable.

For the transfer function model linearized at the operating point DP1 (DP1TF), the observability and controllability were studied by comparing the row rank of the observability matrix and column rank of the controllability matrix to the number of states of the state space system. Since the ranks and number of states were equal, the linear model is state observable and state controllable. The condition number, presented in Figure 9-3, is below 5 for the studied frequency range [0, 0.2] and, thus, the system is input-output controllable. The stability requirement with a P controller can also be met; as can be seen from Figure 9-5, all the curves are on the right hand side of the point -1. (For the Nyquist analysis with the PI controllers, see Section 10.2)

For the transfer function model linearized at the operating point DP4 (DP4TF), the observability and controllability were studied by comparing the row rank of the observability matrix and column rank of the controllability matrix to the number of states of the state space system. Since the ranks and number of states were equal, the linear model is state observable and state controllable. The condition number, presented in Figure 9-4 is below 9 over the studied frequency range [0, 0.2] and, thus, the system is input-output controllable. The stability requirement with a P controller can also be met; as can be seen from Figure 9-6, all the curves are on the right hand side of the point -1. (For the Nyquist analysis with the PI controllers, see Section 10.2)

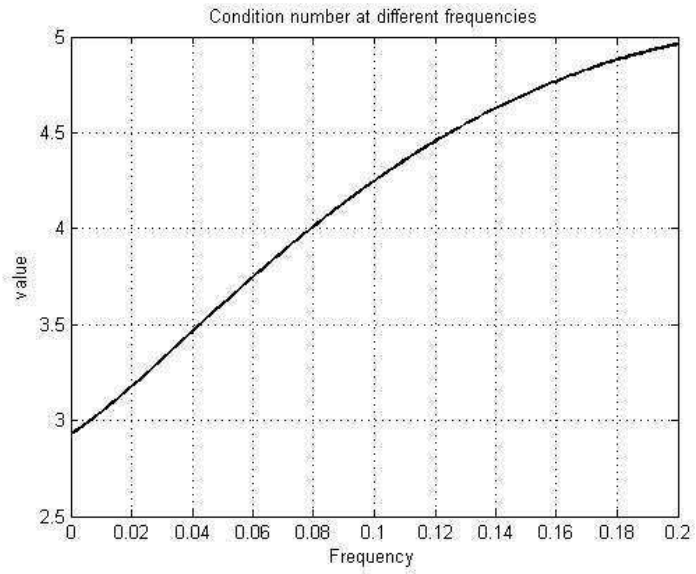

Figure 9-3: Condition number at different frequencies for the transfer function matrix linearized at the first operating point DP1.

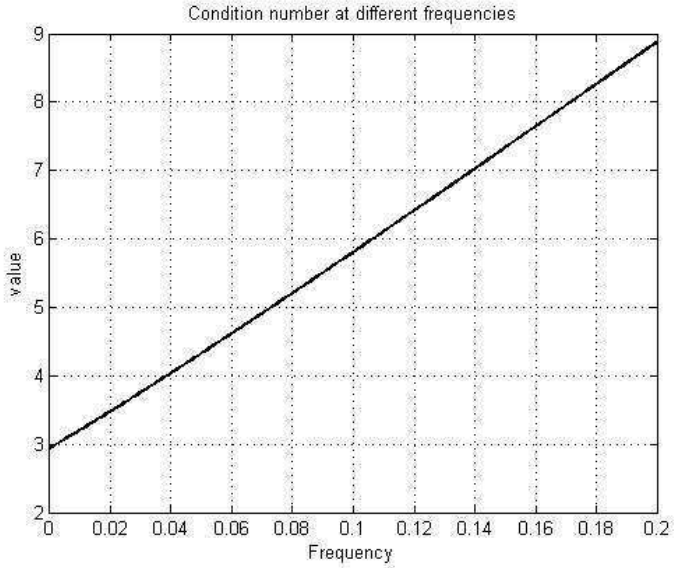

Figure 9-4: Condition number at different frequencies for the transfer function matrix linearized at the second operating point DP4.

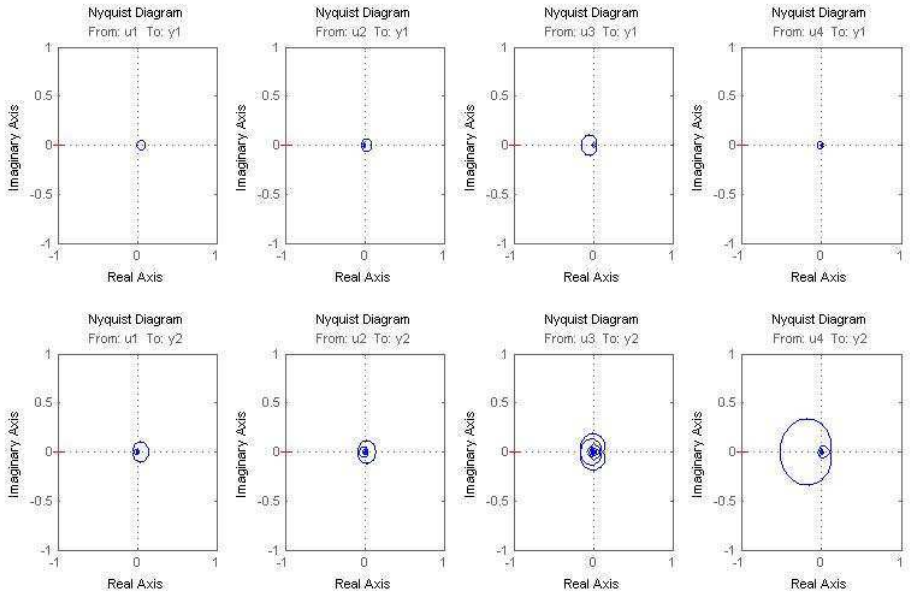

Figure 9-5: Nyquist plots of the controlled variable-manipulated variable pairs of the transfer function model linearized at operating point DP1. The controlled variable on the first row is the loaded organic copper concentration, c(LO), and on the second row the rich electrolyte copper concentration, c(RE). The manipulated variables on the columns are: first PLS series flow rate, F(PLSS), second PLS parallel flow rate, F(PLSP), third organic flow rate, F(LO), and fourth electrolyte flow rate, F(LE).

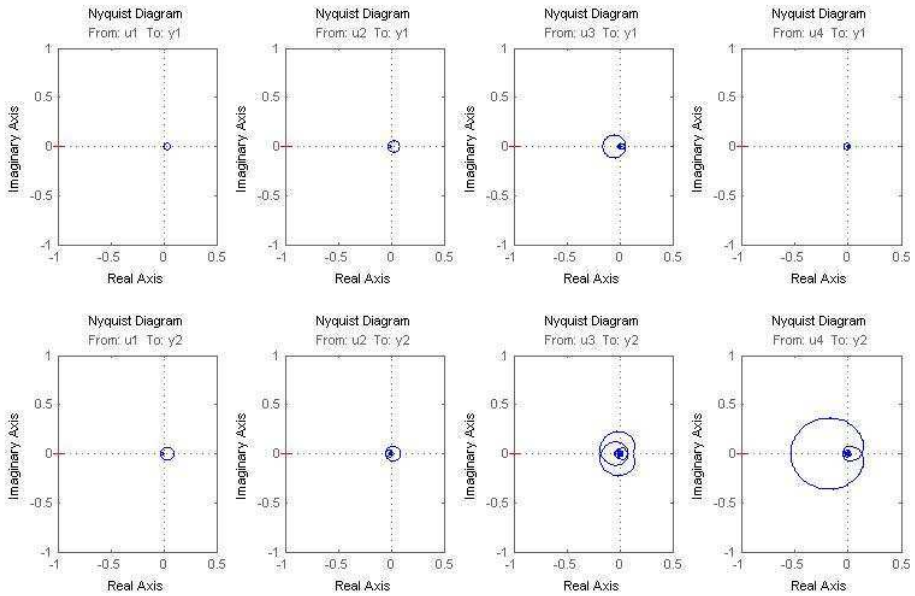

Figure 9-6: Nyquist plots of the controlled variable-manipulated variable pairs of the transfer function model linearized at operating point DP4. The controlled variable on the first row is the loaded organic copper concentration, c(LO), and on the second row the rich electrolyte copper concentration, c(RE). The manipulated variables on the columns are: first PLS series flow rate, F(PLSS), second PLS parallel flow rate, F(PLSP), third organic flow rate, F(LO), and fourth electrolyte flow rate, F(LE).

Since the linear model of the plant is state controllable, state observable and the system with P controllers would be stable, the control strategy can be designed and

tested with the following steps: pairing the controlled and manipulated variables, designing SISO and MIMO controllers for the stabilizing control level and optimizing the algorithm for the optimization level, and implementing and testing these strategies.

9.4 Pairing the controlled and manipulated variables

In order to design single-input single-output controllers, the optimal controller and manipulated variable pairing has to be determined. Bristol's Relative Gain Array is one of the most common methods to investigate loop interactions and to choose pairing for the controlled and manipulated variables. [Ogunnaike, 1994 ,Glad and Ljung, 2004, Seborg et al., 2004, Skogestad and Postlethwaite, 2005]

The basic RGA matrix is calculated by first evaluating the process transfer function, *G*, at the selected frequency ω. Then, this gain matrix, *M*, is element-wise multiplied by the transpose of its inverse matrix (Hadamard or Schur product marked with ×), and the resulting RGA matrix is analyzed.

$$M = G(\omega) \tag{9-4}$$

$$RGA(M) = M \times \left(M^{-1}\right)^{T} \tag{9-5}$$

If there are more inputs than outputs, or vice versa, then the gain matrix becomes non-square, and the inverse operation is replaced by a pseudo-inverse operation. Skogestad and Postlethwaite (2005) suggest discarding the columns or rows with a sum of the RGA elements of far less than one. In other cases RGA should be performed for square sub-matrices.

According to Ogunnaike (1994), the pairing of the input u_j with output y_i is possible if the RGA_{ij} value is above 0.5 and not too much larger than 1. The optimum value is 1, which means that there are no interactions from the other inputs with the considered input. The closer the value is to 0, the less the input affects the output and the bigger the interactions are with other outputs. The higher the RGA_{ij} value, the more the other loops oppose the effect from the input u_i to the output y_j. Pairing with negative RGA values is highly unrecommendable, because the open-loop and closed-loop gains have opposite signs; the other inputs are more dominant to the output, and also the effect of the other loops has the opposite effect. To verify the pairing, Glad and Ljung (2004) suggest evaluation of RGA at other typical frequencies.

In this study, the pairing of the controlled variables (loaded organic and rich electrolyte copper concentrations, c(LO) and c(RE)), with the manipulated variables PLS series and parallel, organic and electrolyte flow rates, F(PLSS), F(PLSP), F(LO), F(LE), was first analyzed using a full non-square matrix RGA for both transfer function matrices at frequencies $\omega \in [0, 1/5]$. Analysis of the first controlled variable, the loaded organic copper concentration c(LO), at the two operating points DP1 and DP5 are presented in Figure 9-7 and Figure 9-8, respectively. The analysis of the second controlled variable, the rich electrolyte copper concentration c(RE), at the two operating points DP1 and DP5 are presented in Figure 9-9 and Figure 9-10.

For the loaded organic copper concentration the pairing at lower frequencies ($\omega<0.1$) favours the organic flow rate, F(LO), for both cases. For the first case, where the analysis is performed with the transfer function matrix linearized at the operating

point DP1, at higher frequencies (ω>0.1) the pairing with the PLS series flow rate, F(PLSS), becomes more favourable, as illustrated in Figure 9-7. However, the RGA values for the organic flow rate pairing do not fall below 0, so this pairing is still valid over the frequency range.

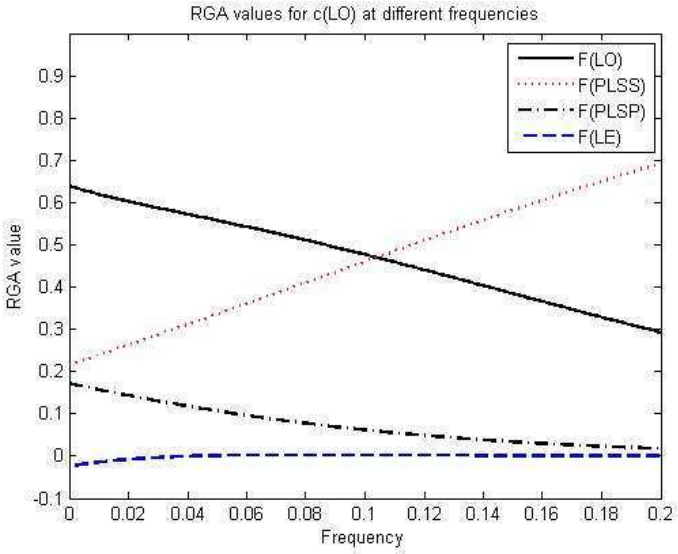

Figure 9-7: The RGA values for the loaded organic copper concentration, c(LO), pairing with the organic flow rate, F(LO), PLS series flow rate, F(PLSS), PLS parallel flow rate, F(PLSP) and electrolyte flow rate, F(LE), at frequencies ω=0 … 0.2. The analysis is performed with the transfer function matrix linearized at the operating point DP1.

The pairing favours the organic flow rate, F(LO), in the second case, where the analysis is performed with the transfer function matrix linearized at the operating point DP4, as illustrated in Figure 9-8. The RGA values for this pairing are above 0.6 for the whole frequency range.

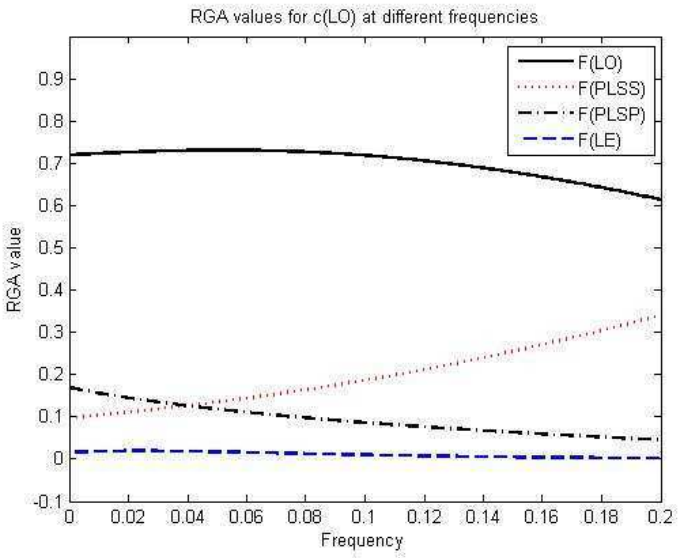

Figure 9-8: The RGA values for the loaded organic copper concentration, c(LO), pairing with the organic flow rate, F(LO), PLS series flow rate, F(PLSS), PLS parallel flow rate, F(PLSP) and electrolyte flow rate, F(LE), at frequencies ω=0 … 0.2. The analysis is performed with the transfer function matrix linearized at the operating point DP4.

For the rich electrolyte copper concentration, the RGA analysis favours pairing with the electrolyte flow rate. The RGA values for this pairing are above 0.9 at all frequencies, as illustrated in Figure 9-9 and Figure 9-10.

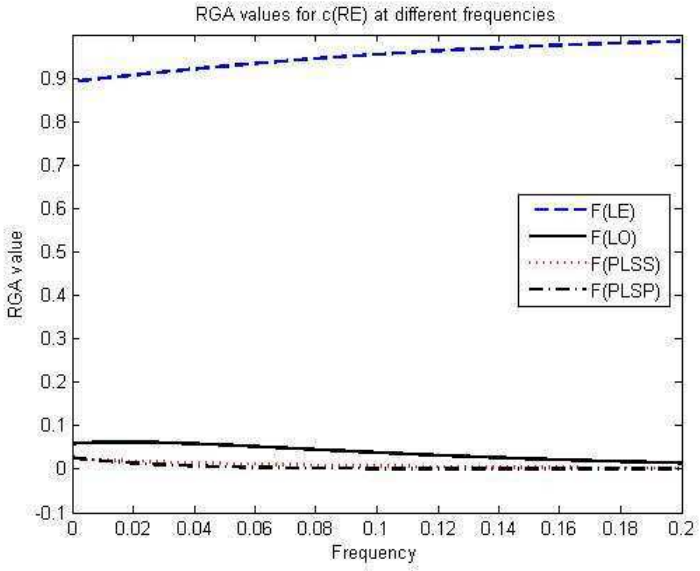

Figure 9-9: The RGA values for the rich electrolyte copper concentration, c(RE), pairing with the organic flow rate, F(LO), PLS series flow rate, F(PLSS), PLS parallel flow rate, F(PLSP) and electrolyte flow rate, F(LE), at frequencies ω=0 … 0.2. The analysis is performed with the transfer function matrix linearized at the operating point DP1.

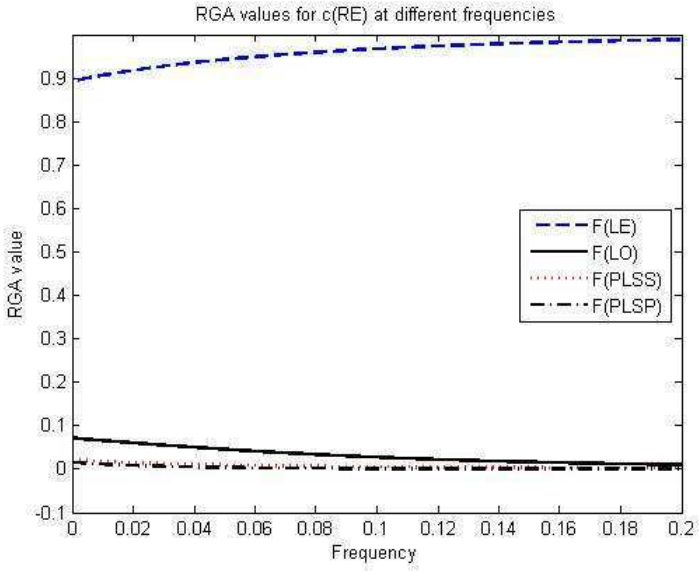

Figure 9-10: The RGA values for the rich electrolyte copper concentration, c(RE), pairing with the organic flow rate, F(LO), PLS series flow rate, F(PLSS), PLS parallel flow rate, F(PLSP) and electrolyte flow rate, F(LE), at frequencies ω=0 … 0.2. The analysis is performed with the transfer function matrix linearized at the operating point DP4.

On the basis of this analysis, the favourable pairing of the controlled and manipulated variables is the loaded organic copper concentration with the organic flow rate, c(LO)-F(LO), and the rich electrolyte copper concentration with the electrolyte flow rate, c(RE)-F(LE).

This pairing is further studied by performing RGA for the [c(LO),c(RE)]x [F(LO),F(LE)] square matrices at frequencies $\omega = 0, 1/20, 1/10, 1/5$. The RGA values are presented in Table 9-1. The 1-2 pairing values, calculated for the c(LO)-F(LO)

and c(RE)-F(LE) pairs, are close to one at all the studied frequencies. Therefore, the pairing between the loaded organic copper concentration with the organic flow rate, c(LO)-F(LO), and the rich electrolyte copper concentration with the electrolyte flow rate, c(RE)-F(LE) is chosen for the control strategy development.

Table 9-1: RGA coefficients for 1-2 pairing on the basis of the transfer function matrix linearized at the operating points DP1 and DP4.

1-2 pairing/ Frequency ω	[c(LO),c(RE)]x [F(LO),F(LE)], DP1	[c(LO),c(RE)]x [F(LO),F(LE)], DP4
0	0.9549	0.9471
1/20	0.9584	0.9681
1/10	0.9726	0.9831
1/5	0.9906	0.9960

9.5 Proposed control strategies for the case copper solvent extraction plant

A single-input single-output control strategy and comparable multi-input multi-output control strategy are designed on the basis of the RGA analysis. These strategies are alternatives for the supervisory control level in the proposed control hierarchy presented in Section 9.2. In the single-input single-output control strategy, the first control loop consists of the loaded organic copper concentration, c(LO), which is controlled by manipulating the organic flow rate, F(LO). The second control loop consists of the rich electrolyte copper concentration, c(RE), which is kept at the setpoint by manipulating the electrolyte flow rate, F(LE). PI controllers are used for the single-input single output strategy.

The additional manipulated variables, PLS flow rates, F(PLSS) and F(PLSP), are considered as measured disturbances. The feedforward controllers are constructed to compensate for changes in the PLS and lean electrolyte concentrations, c(PLS) and c(LE), and PLS series and parallel flow rates, F(PLSS) and F(PLSP), as shown Figure 2-1. The feedforward compensators are of lead-lag type. The parametrization of the lead-lag compensators is described in Chapter 10.1.

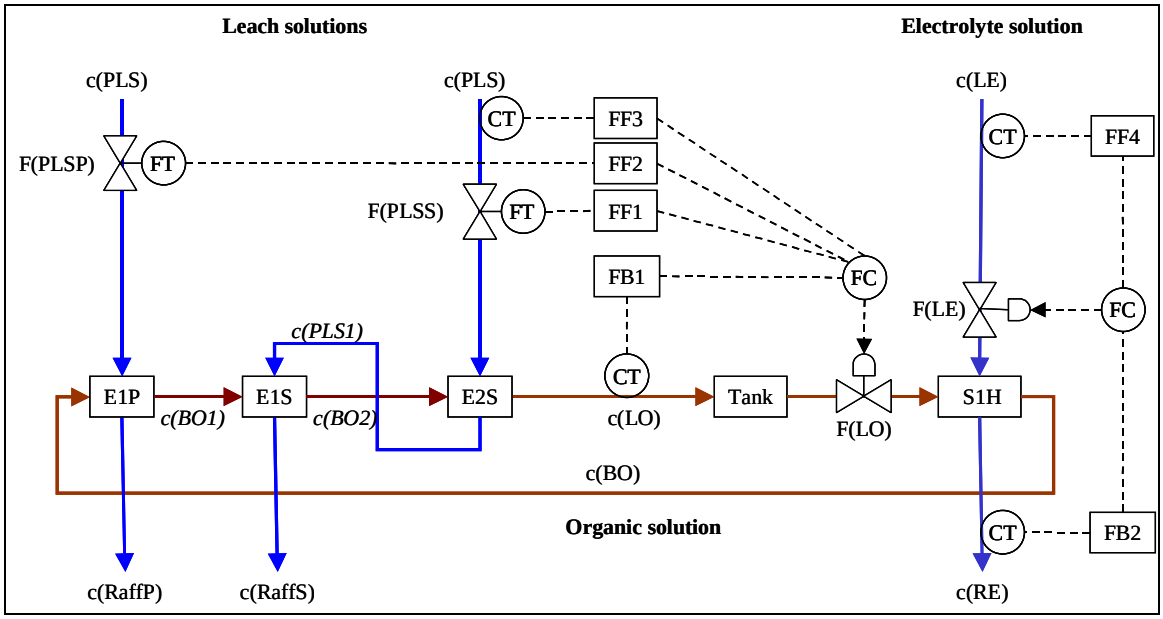

Figure 9-11: Control strategy: the loaded organic copper concentration, c(LO), is feedback controlled (FB1) with the organic flow F(LO). The rich electrolyte copper concentration, c(RE), is feedback controlled (FB2) with the electrolyte flow, F(LE). The disturbances are compensated with feedforward controllers, for PLS series flow, F(PLSS) with FF1, for PLS parallel flow, F(PLSP), with FF2, for PLS copper concentration, c(PLS), with FF3, and for the lean electrolyte copper concentration, c(LE) with FF4.

The multi-input multi-output control strategy utilizes the same controlled, manipulated and disturbance variable structure, but the controlled variables are changed by manipulating both the organic and electrolyte flow rates by means of the model predictive controller. The difference between the single input-single output and multi-input multi-output control strategies is illustrated in Figure 9-12.

Compensation of input concentration disturbances and set-point tracking of the loaded organic and rich electrolyte concentrations is done by changing the organic and electrolyte flow rates. A change in the flow rates changes the organic to aqueous ratio in the mixers and, as a result, changes the output concentration of the process. An effective way to compensate the concentration disturbances would be to change the reagent volume per cent in the organic solution but, due to the lack of instrumentation and measurements, this is not currently a realizable approach.

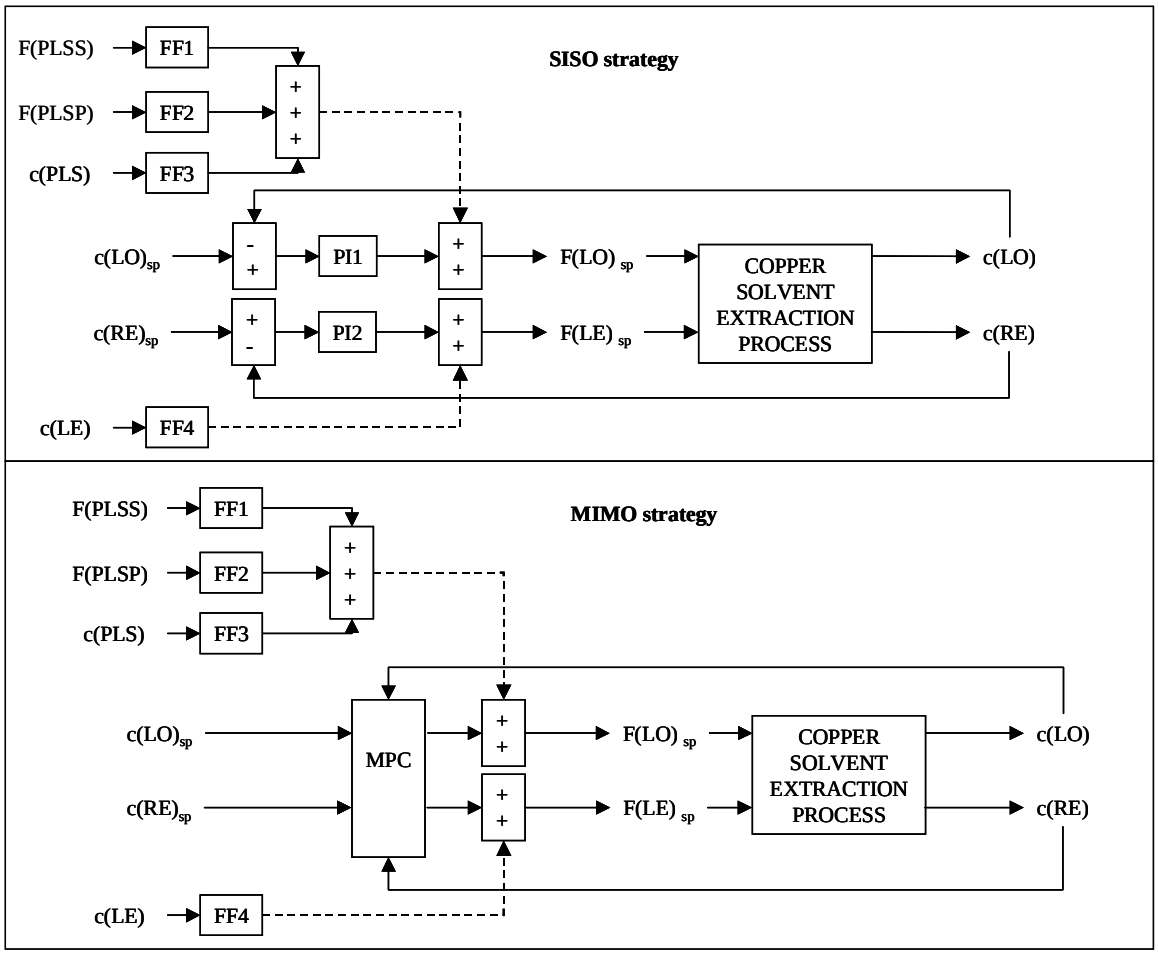

Figure 9-12: The single-input single-output (SISO) and multi-input multi-output (MIMO) control strategies. The SISO strategy utilizes two PI controllers marked with PI1 and PI2, and the MIMO strategy utilizes model predictive controller, marked with MPC. The additional feedforward compensators are marked with FF. The setpoints are marked with the subscript sp.

9.6 Structure of the dynamic simulator with the controllers

The simulation model, presented in Section 6.3, in Figure 6-1, is modified when the controllers are used. The values of the manipulated variables, i.e. the organic and electrolyte flow rate measurements, are determined by summing up the controller and feedforward compensator outputs. This is illustrated in Figure 9-13, where two PI controllers and four feedforward controllers are added to the simulation model. The PI controllers continue the output on the basis of the error between the setpoint and the measured value of the controlled variable. The feedforward compensators compare the difference between the nominal and the measured value of the disturbance variables.

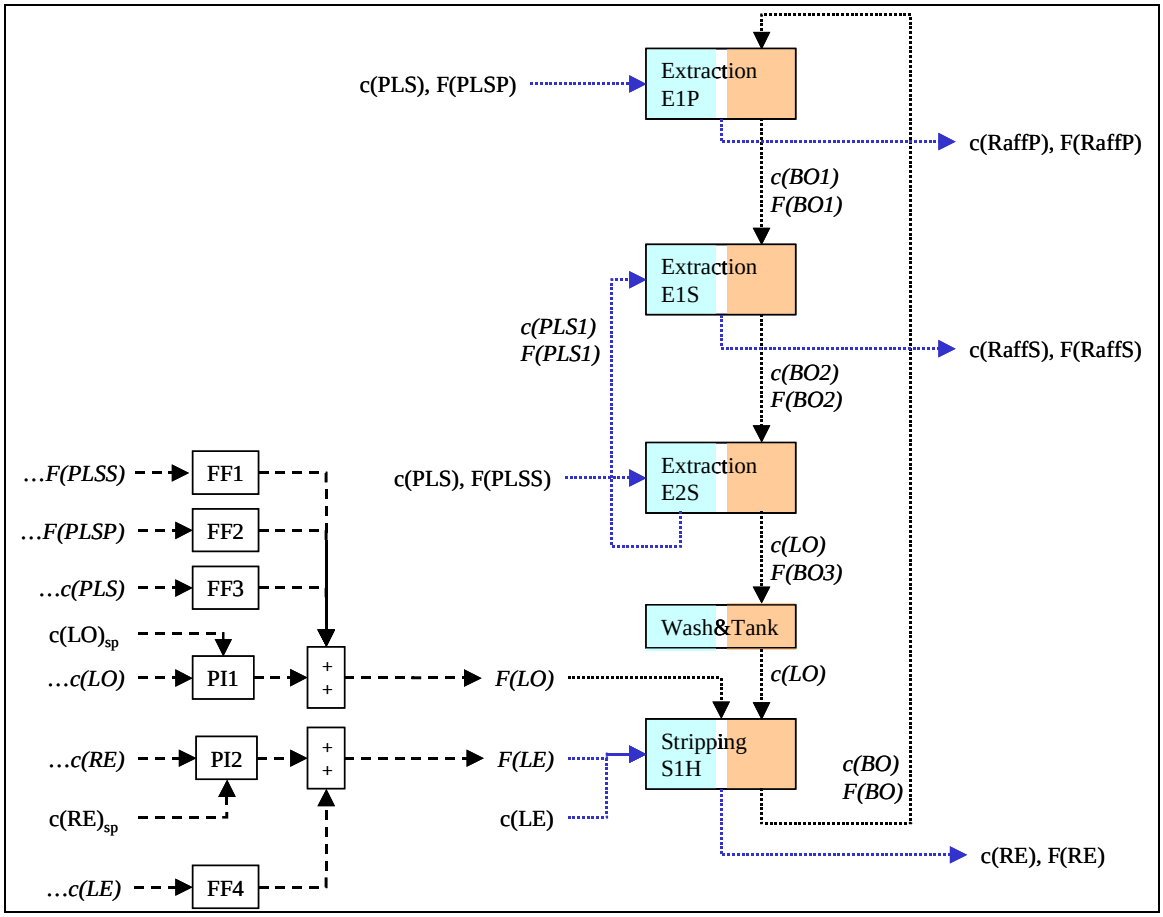

Figure 9-13: Simulation model of the case copper solvent extraction process with two PI controllers (PI1 and PI2) and four feedforward compensators (FF1, FF2, FF3, FF4). The manipulated variables are the organic and electrolyte flow rates, F(LO) and F(LE). The inputs to the PI controllers PI1 and PI2 are the measurements (…c) and the setpoints (sp). In the feedforward compensators the measurements (...c and …F) are compared to the nominal values of these variables.

9.7 Optimization of the industrial case process

The optimization provides setpoints of the controlled variables for the controllers, and is the local optimization level of the proposed control hierarchy, presented in Section 9.2. The setpoints of the controlled variables and the optimal values of the manipulated variables are determined by solving the linear optimization problem with the constraints (for linear optimization, see Kreyzig, 1999, Hillier and Liebermann, 2001). The controlled, manipulated and disturbance variables, as well as the parameters of the optimization problem, are presented in Table 9-2. The optimal values of the controlled and manipulated variables are calculated on the basis of the values of the disturbance variables and the optimization parameters.

Table 9-2: Manipulated, controlled and disturbance variables, and the parameters of the optimization problem.

Classification	Variable name	Abbreviation
Controlled variables	Loaded organic copper concentration	c(LO)
	Rich electrolyte copper concentration	c(RE)
Manipulated variables	Organic flow rate	F(LO)
	Electrolyte flow rate	F(LE)
Disturbance variables	PLS series flow rate	F(PLSS)
	PLS parallel flow rate	F(PLSP)
	PLS copper concentration	c(PLS)
	Lean electrolyte copper concentration	c(LE)
	Reagent volume percent	vol
Parameters	Minimum O/A ratio in extraction	β_1
	Maximum O/A ratio in stripping	β_2
	Steady state gains for rich electrolyte copper concentration	w_i
	Steady state gains for loaded organic copper concentration	r_i

Continuous direct measurement of the production does not exist due to the nature of the electrowinning process (in electrowinning process copper cathodes are grown for one week in electrolysis cells, and weighted only after they are taken out of the cells). , thus the production is estimated from the copper concentrations and flow rates of the rich and lean electrolyte solutions.

The maximization of production, i.e. the copper mass flow out of the copper solvent extraction process, can be formulated mathematically as the difference in the copper concentration between the rich and lean electrolytes, multiplied by the electrolyte flow rate, as follows:

$$P = \left[c(RE) - c(LE)\right] F(LE) \qquad \textbf{(9-6)}$$

The restrictions of the optimization problem are the aqueous to organic ratios in the mixers. In the extraction part the mixers are assumed to run aqueous continuously, i.e. the major phase is aqueous, and therefore the organic to aqueous ratio has to be below β_1 (<1). In the stripping part, the mixers are assumed to run organic continuously with an organic to aqueous ratio of above β_2 (>1). These restrictions can be formulated for the extraction as follows:

$$\frac{F(LO)}{F(PLSS)} \le \beta_1 \quad \frac{F(LO)}{F(PLSP)} \le \beta_1 \qquad \textbf{(9-7)}$$

and for the stripping as follows:

$$\frac{F(LO)}{F(LE)} \geq \beta_2 \qquad \textbf{(9-8)}$$

The optimization problem can be presented with the controlled, manipulated and disturbance variables by assuming that the transfer function models of the plant represent the steady state of the process adequately well, as asserted in Chapter 8. Now the rich electrolyte copper concentration can be presented as:

$$c(RE) = w_1F(PLSS) + w_2F(PLSP) + w_3F(LO) - w_4F(LE) + w_5c(PLS) + w_6c(LE) + w_7vol \qquad \textbf{(9-9)}$$

and the loaded organic copper concentration as:

$$c(LO) = r_1F(PLSS) + r_2F(PLSP) - r_3F(LO) - r_4F(LE) + r_5c(PLS) + r_6c(LE) + r_7vol \qquad \textbf{(9-10)}$$

The constants, w_i and r_i, are positive, and represent the absolute values of the steady state gains of the transfer function models for the loaded organic and rich electrolyte copper concentrations.

On the basis of these equations (9-9) and (9-10), the profit function (Equation 9-7) can be expressed using the manipulated and disturbance variables as follows:

$$\big[c(RE) - c(LE)\big]F(LE) = \begin{bmatrix} w_1F(PLSS) + w_2F(PLSP) + w_3F(LO) \\ +w_5c(PLS) - (1 - w_6)c(LE) + w_7vol \end{bmatrix} F(LE) - w_4F(LE)^2 \qquad \textbf{(9-11)}$$

The maximization of this equation requires a maximum value for the organic flow rate, F(LO). The maximum values of the manipulated flow rates can be derived from the restrictions of the optimization problem. The organic flow rate has a maximum restriction in relation to the minimum of the PLS flow rates. Since a maximum value is desired for the organic flow rate, Equation (9-7) yields:

$$F(LO)_{opt} = \beta_1 \cdot \min\big\{F(PLSS), F(PLSP)\big\} \qquad \textbf{(9-12)}$$

The electrolyte flow rate, F(LE), has an optimum point, which can be calculated by setting the derivative of the profit function (9-11) to zero. The derivative is taken in relation to the electrolyte flow rate. Using the optimal organic flow rate, $F(LO)_{opt}$, Equation (9-12) yields:

$$F(LE)_{opt} = \frac{-1}{2w_4}\Big[w_1F(PLSS) + w_2F(PLSP) + w_3F(LO)_{opt} + w_5c(PLS) - (1 - w_6)c(LE) + w_7vol\Big] \qquad \textbf{(9-13)}$$

This is the optimal value for the electrolyte flow rate if the maximum electrolyte flow rate limitation is not exceeded, as required in Equation 9-8. The maximum for the electrolyte flow rate is smaller than the optimum organic flow rate divided by β_2:

$$F(LE)_{optF} = \min\left\{F(LE)_{opt}, \frac{1}{\beta_2}F(LO)_{opt}\right\} \qquad \textbf{(9-14)}$$

Now the setpoints for the rich electrolyte and loaded organic copper concentration can be formulated on the basis of the optimum manipulated variables, the disturbance variables and optimization parameters, as follows:

$$c(RE)_{sp} = \begin{array}{l} w_1F(PLSS) + w_2F(PLSP) + \beta_1 w_3 F(PLS)_{\min} - w_4F(LE)_{optF} \\ +w_5c(PLS) + w_6c(LE) + w_7 vol \end{array} \quad \textbf{(9-15)}$$

$$c(LO)_{sp} = \begin{array}{l} r_1F(PLSS) + r_2F(PLSP) - \beta_1 r_3 F(PLS)_{\min} - r_4F(LE)_{optF} \\ +r_5c(PLS) + r_6c(LE) + r_7 vol \end{array} \quad \textbf{(9-16)}$$

where the minimum of the PLS flow rates is marked as $F(PLS)_{min}$.

The maximal production can be calculated by substituting Equations (9-13) and (9-15) to Equation (9-6) as follows:

$$\left[c(RE)_{sp} - c(LE)\right]F(LE)_{opt} = \begin{bmatrix} w_1F(PLSS) + w_2F(PLSP) \\ +\beta_1 w_3 F(PLS)_{\min} - w_4F(LE)_{optF} \\ +w_5c(PLS) - (1-w_6)c(LE) + w_7 vol \end{bmatrix} F(LE)_{optF} \quad \textbf{(9-17)}$$

These setpoints are used as input to the control algorithms (see Chapter 9.5.). The numerical results of the optimization, i.e. the setpoints, are presented in Chapter 12.

10 TESTING OF THE SISO CONTROL STRATEGY FOR THE COPPER SOLVENT EXTRACTION PROCESS

The aim of this chapter is to describe the tuning and testing of the single input-single output (SISO) control strategy in the simulation environment (see Chapter 6). The controller tuning, based on the single-input single-output control structure described in Chapter 9, is first presented in Section 10.1. The stability of the process with the controllers is studied with Nyquist criterion in Section 10.2, and the control loop interactions in Section 10.3. Finally, the controller performance is tested against input disturbances in Section 10.4 and setpoint changes in Section 10.5.

10.1 Tuning of the PI controllers and the feedforward compensators

PI controllers were chosen for the single input – single output strategy owing to their simplicity and wide use in the industry. Since the manipulated variables are flow rates with considerable noise, both controllers will be implemented without the D term, in PI form.

Assume that the controlled variable-manipulated variable interaction can be presented as a first order plus time delay transfer function form:

$$G_p(s) = \frac{K_p}{\tau_p s + 1} e^{-\alpha_p s} \qquad \textbf{(10-1)}$$

the parameters for the PI controller of the following form:

$$G_C = K_C \left(1 + \frac{1}{T_i s} \right) \qquad \textbf{(10-2)}$$

can be derived with the internal model control (IMC) tuning rules. The IMC structure has only one parameter, λ, to be changed during the tuning procedure. The gain K_c and the integration time T_i are now determined as follows (Ogunnaike and Ray, 1994, pp. 539):

$$K_C = \frac{2\tau_p + \alpha_p}{2\lambda K_p} \qquad \textbf{(10-3)}$$

$$T_i = \tau_p + 0.5 \cdot \alpha_p \qquad \textbf{(10-4)}$$

with the restriction that

$$\lambda > 1.7 \cdot \alpha_p \qquad \textbf{(10-5)}$$

The PI controllers were tuned starting from the smallest possible value for λ, and then increasing the value until adequate performance was reached for both set-point tracking and disturbance rejection. The coefficients of the PI2 controller in the faster loop, FB2, were tuned first by keeping the FB1 loop open. The coefficients of the PI1

controllers in the FB1 loop were then tuned by keeping the FB2 loop open and, finally, both loops were closed and the coefficients were fine tuned.

The aim of the feedforward controllers is to compensate the effect of the measured disturbances before they affect the process behaviour. Assuming first order plus time delay model form for the controlled variable – disturbance variable interactions, then:

$$G_d(s) = \frac{K_d}{\tau_d s + 1} e^{-\alpha_d s} \qquad \textbf{(10-6)}$$

The feedforward compensator can be designed by using the CV-DV model and the CV-MV model as follows (Åström and Wittenmark, 1997, p. 234, Ogunnaike and Ray, 1994, pp. 571-572):

$$G_{FF}(s) = -\frac{G_d(s)}{G_p(s)} = -\frac{K_d}{K_p}\frac{1+\tau_p s}{1+\tau_d s} e^{-(\alpha_d - \alpha_p)s} \approx K_{ff}\left(\frac{1+\tau_p s}{1+\tau_d s}\right) \qquad \textbf{(10-7)}$$

The FF controllers were added one by one on the top of the FB controllers, and the coefficients were tuned.

The SISO control structure with two PI controllers and four feedforward compensators does not take into account the interactions, and the control actions are not limited by rate or magnitude.

10.2 Stability of the process with the PI controllers

The stability of the process with the controllers is studied by plotting the transfer function combination of the PI controller and the process into the complex plane. The process is here represented by the transfer function of the loaded organic copper concentration – organic flow rate, c(LO) – F(LO), for the first feedback loop, and by the transfer function of the rich electrolyte copper concentration – electrolyte flow rate, c(RE) – F(LE), for the second feedback loop. The transfer functions are presented in Section 8.3, and the controllers in Section 10.1 earlier. The open loop transfer function for both feedback loops is of the following form:

$$G_{OL} = G_c \cdot G_p = \frac{K_c(T_i s + 1)}{T_i s} \cdot \frac{K_p \cdot e^{-\alpha_p s}}{\tau_p s + 1} \qquad \textbf{(10-8)}$$

The Nyquist stability criterion is used to determine whether the process with PI controllers is stable (Ogunnaike and Ray, 1994, p.543, Skogestad and Postlethwaite, 2005). The Nyquist plots are illustrated in Figure 10-1 for the process linearized at the first operating point DP1, and in Figure 10-2 for the process linearized at the second operating point DP4. Since all the transfer function plots are on the right hand side of the –1 point, the process with the PI controllers is stable, and there is a gain margin of about 2.5 for all the PI controllers.

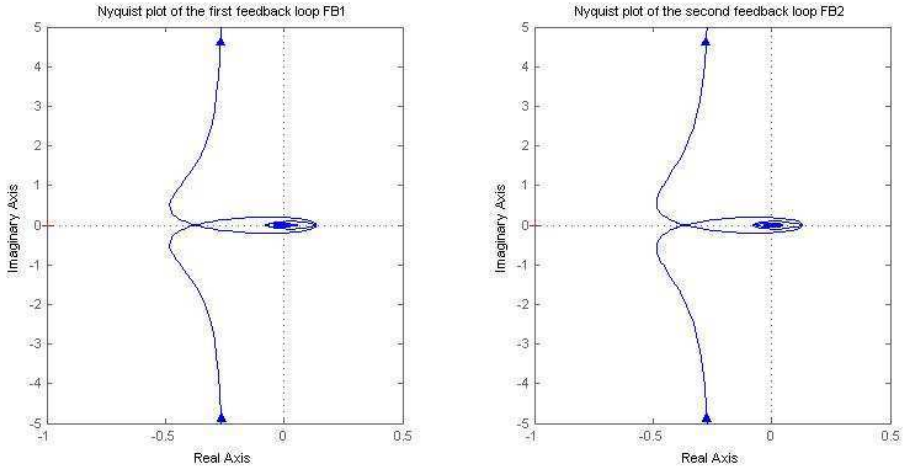

Figure 10-1: Nyquist plots of the first (left) and second (right) feedback loop for the transfer function model linearized at the first operating point DP1.

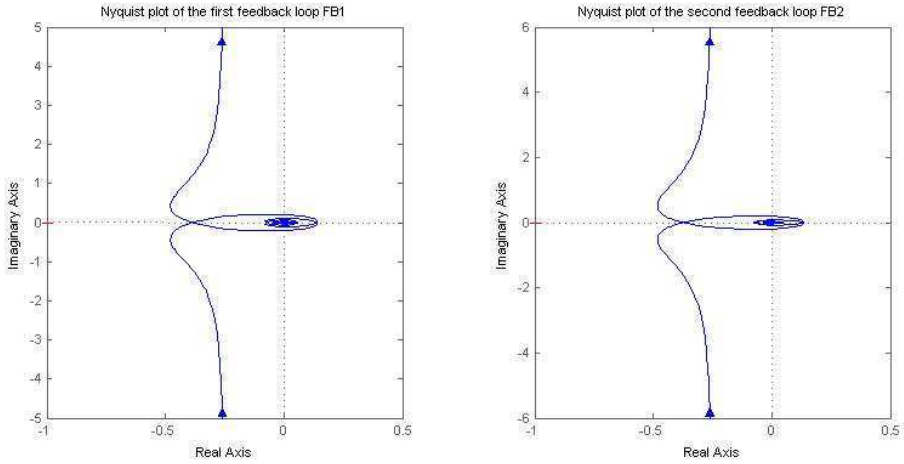

Figure 10-2: Nyquist plots of the first (left) and second (right) feedback loop for the transfer function model linearized at the second operating point DP4.

In order to take into account the effects of the loop interactions, MIMO Nyquist stability criteria are also tested, as suggested by Skogestad and Postlethwaite (2005). The determinant of the identity matrix plus the open loop transfer function with the controllers, *det(I+L(s))* should not make any encirclements of the origin if L(s) is stable. In this case we have a 2×2 system G_p, with a diagonal controller G_c. The open loop transfer function is defined as follows:

$$L(s) = G_p G_c = \begin{pmatrix} G_{p11} & G_{p12} \\ G_{p21} & G_{p22} \end{pmatrix} \begin{pmatrix} G_{c1} & 0 \\ 0 & G_{c2} \end{pmatrix} = \begin{pmatrix} G_{p11}G_{c1} & G_{p12}G_{c2} \\ G_{p21}G_{c1} & G_{p22}G_{c2} \end{pmatrix} \quad \textbf{(10-9)}$$

Now the determinant is defined as follows:

$$\det(1+L(s)) = \det\begin{pmatrix} 1+G_{p11}G_{c1} & G_{p12}G_{c2} \\ G_{p21}G_{c1} & 1+G_{p22}G_{c2} \end{pmatrix} = \left(1+G_{p11}G_{c1}\right)\left(1+G_{p22}G_{c2}\right) - G_{p12}G_{c2}G_{p21}G_{c1} \quad \textbf{(10-10)}$$

The determinant was calculated for the transfer functions with first order pade approximations for the time delays, as defined in Equation (8-13). The Nyquist plots for the transfer functions determined at the first and second operating points are presented in Figure 10-3 and in Figure 10-4, respectively. Since neither of them encircle the origin, the process with controllers is stable.

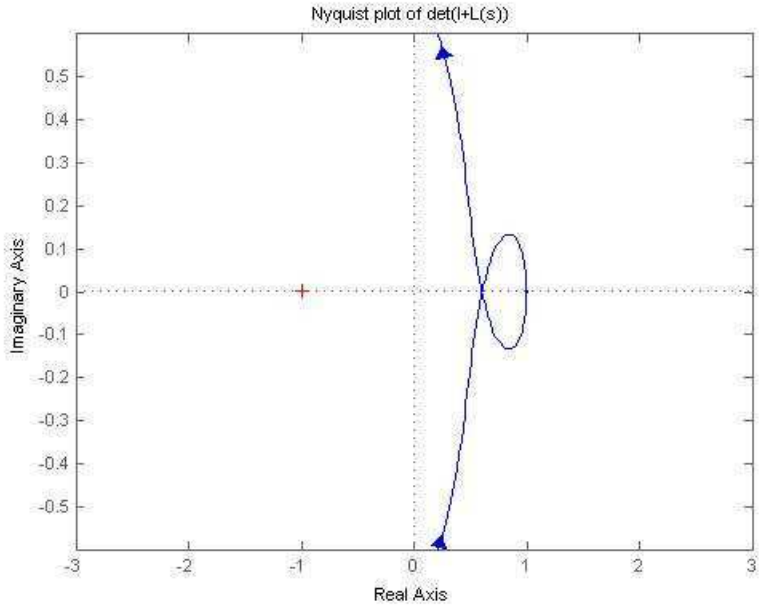

Figure 10-3: Nyquist plots of det (I+L(s)) for the transfer function model linearized at the first operating point DP1.

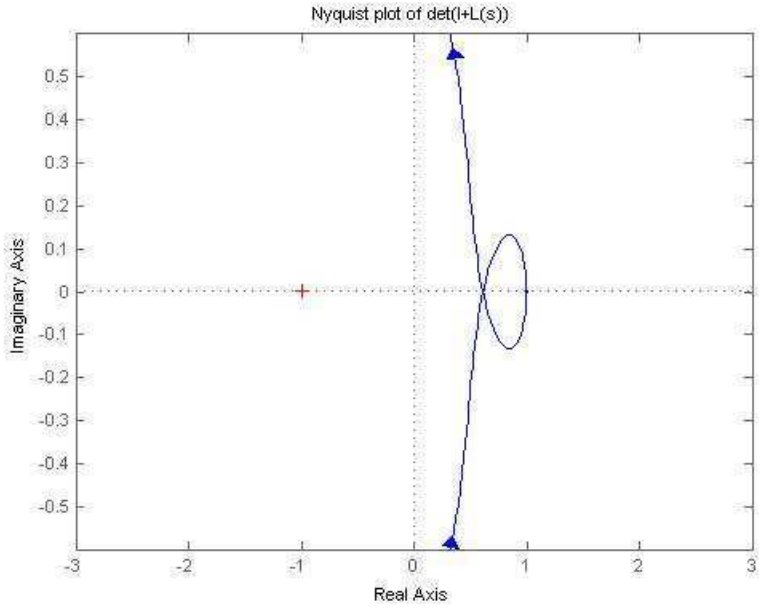

Figure 10-4: Nyquist plots of det (I+L(s)) for the transfer function model linearized at the second operating point DP4.

10.3 Feedback loop interactions

In order to determine whether it was necessary to add decouplers to the control strategy, the interactions on the feedback loops were studied. This was done by closing one of the control loops while keeping the other loop open. The responses to the open loop output variable were studied by comparing the case with both loops open and the other loop closed.

10.3.1 Interactions with the closed loop FB1

The interactions under closed FB1 loop were determined by plotting the responses of the 5% changes in the input variables to the rich electrolyte copper concentration (output of the FB2 loop).

At operating point DP1, the interactions between the input changes and the rich electrolyte copper concentration under the closed FB1 loop were not strong, as can be seen from Figure 10-5. The differences between the open loop and FB1 loop responses are around 20% for the PLS flow rates and copper concentration. The interaction is minimal for the lean electrolyte copper concentration. The setpoint change in the loaded organic copper concentration causes a second order with zero type of response to the rich electrolyte copper concentration, settling to a constant level after 70 sample times. The interaction is not strong, and therefore a decoupler is not necessary.

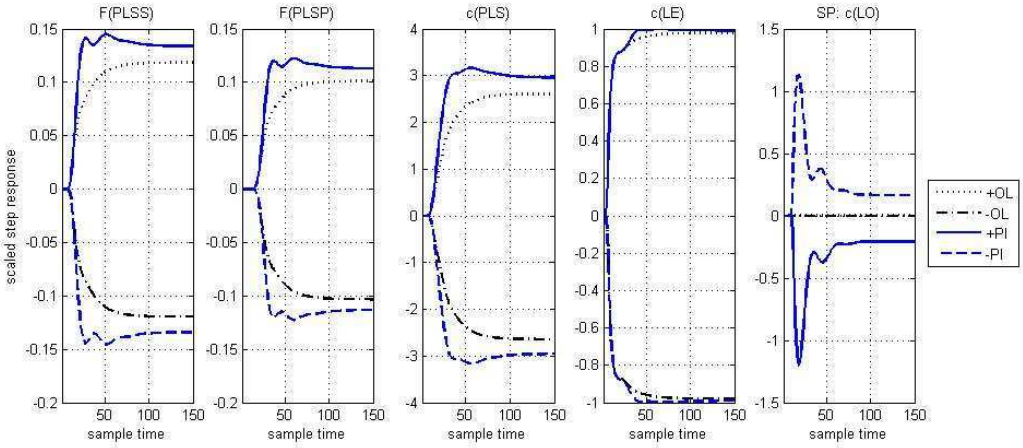

Figure 10-5: Responses of the rich electrolyte copper concentration to ±5% changes in F(PLSS), F(PLSP), c(PLS), c(LE) and setpoint of the c(LO) with open control loops (OL) and under a closed FB1 control loop (PI).

The interactions at operating point DP4 for the rich electrolyte copper concentration were stronger than the interactions at operating point DP1. The interaction between loop FB1 and the rich electrolyte copper concentration was significant. When the FB1 loop was closed, the responses to 5% changes in the PLS series and parallel flow rates, F(PLSS) and F(PLSP), and PLS copper concentration, c(PLS), were almost twice as large as those with both control loops open. The FB1 loop had almost no effect on the response to the change in the lean electrolyte copper concentration c(LE), as can be seen from Figure 10-6. When FB1 loop was closed, a 5% change in the c(LO) setpoint caused a significant and very asymmetric change in the rich electrolyte copper concentration, c(RE), via manipulations in the loaded organic flow rate, F(LO). Therefore, a decoupler could be included in the control strategy.

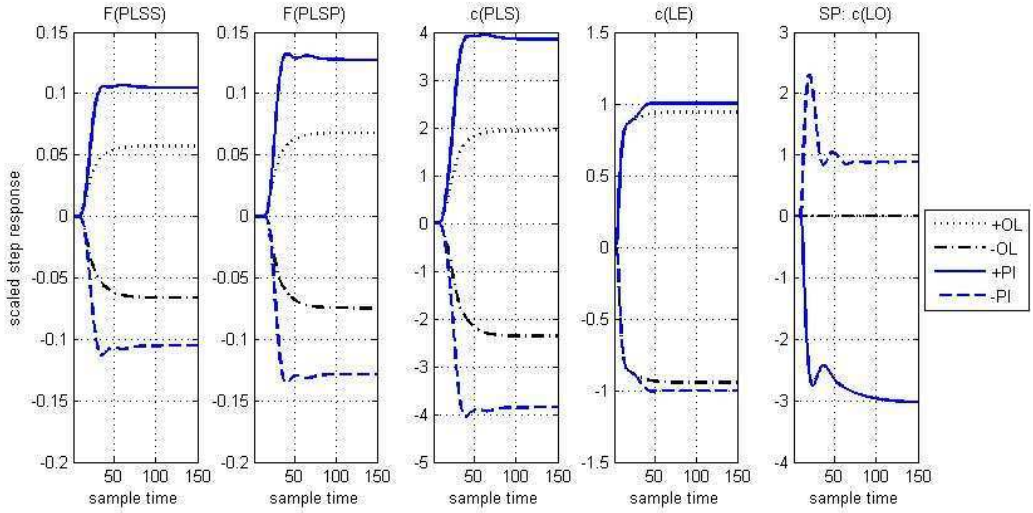

Figure 10-6: Responses of the rich electrolyte copper concentration to ±5% changes in F(PLSS), F(PLSP), c(PLS), c(LE) and setpoint of the c(LO) with open control loops (OL) and under a closed FB1 control loop (PI).

10.3.2 Interactions with the closed loop FB2

The interactions under the closed FB2 loop were determined by plotting the responses of the 5% changes in the input variables to the loaded organic copper concentration (output of the FB1 loop).

At operating point DP1, the interaction between loop FB2 and the loaded organic copper concentration was relatively small in DP1. When the FB1 loop was closed, the responses to the 5% changes in the PLS series and parallel flow rates, F(PLSS) and F(PLSP), and PLS copper concentration, c(PLS), were less than 20% smaller than the responses with the open control loops. The FB1 loop decreased the effect of the change in the lean electrolyte copper concentration c(LE), but turned it into an inverse response, as can be seen from Figure 10-7. When the FB2 loop was closed, a 5% change in the c(RE) setpoint caused as large an effect as the changes PLS in the series flow rate to the loaded organic copper concentration, c(LO). Because the interactions of the FB2 loop are relatively small, a decoupler is not necessary.

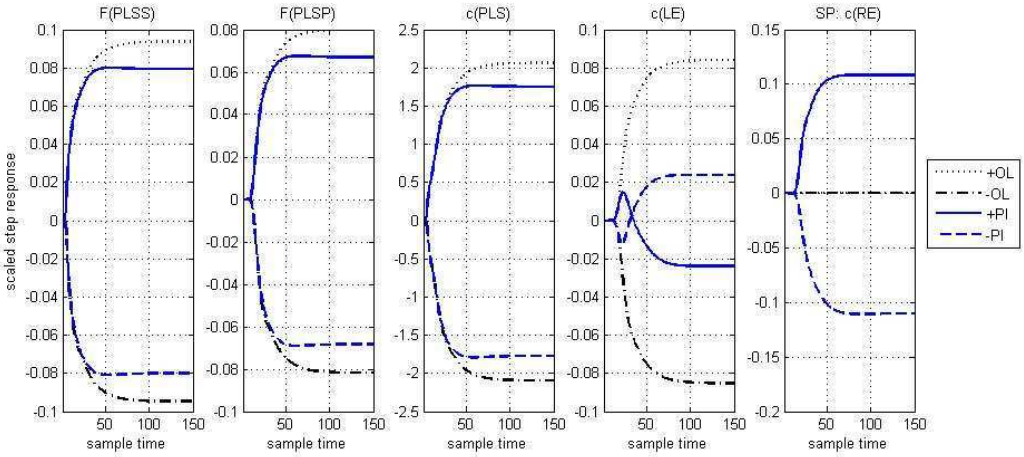

Figure 10-7: Responses of the load organic copper concentration to ±5% changes in F(PLSS), F(PLSP), c(PLS), c(LE) and setpoint of the c(RE) with open control loops (OL) and under a closed FB2 control loop (PI).

The interaction between loop FB2 and the loaded organic copper concentration was relatively small at operating point DP4. When the FB1 loop was closed, the responses to the 5% changes in the PLS series and parallel flow rates, F(PLSS) and F(PLSP), and PLS copper concentration, c(PLS), were similar to the responses with open control loops. The FB1 loop decreased the effect of the change in the lean electrolyte copper concentration c(LE), but turned it into an inverse response, as can be seen from Figure 10-8. When the FB2 loop was closed, a 5% change in the c(RE) setpoint caused as large an effect as the changes in the flow rate to the loaded organic copper concentration, c(LO). Because the interactions of the FB2 loop are relatively small, a decoupler is not necessary.

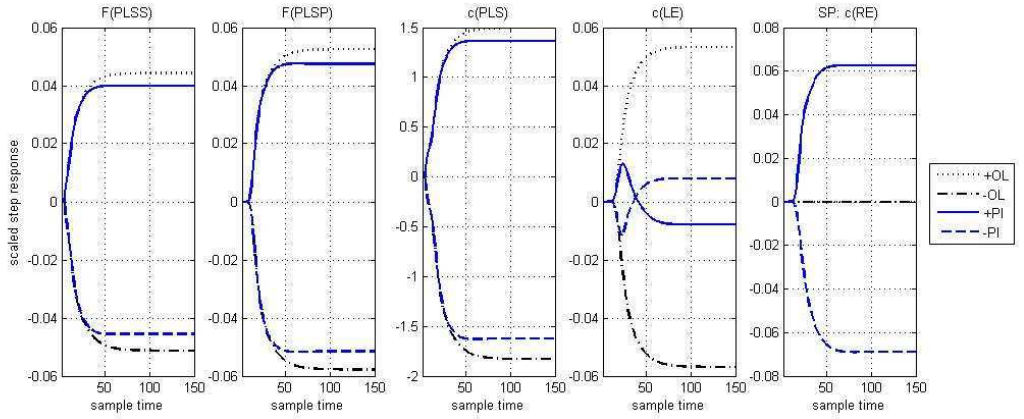

Figure 10-8: Responses of the load organic copper concentration to ±5% changes in F(PLSS), F(PLSP), c(PLS), c(LE) and setpoint of the c(RE) with open control loops (OL) and under a closed FB2 control loop (PI).

10.4 Disturbance rejection

The aim in this section is to test the disturbance rejection performances of the single-input single-output controllers. The following controller combinations were used in this study:

- open loop (OL), no controllers
- only the first PI controller (FB1)
- only the second PI (FB2)
- both of the two PI controllers (PI)
- both of the two PI controllers with four feedforward compensators (PIFF)

Testing was performed by introducing ±5% changes to the following the inputs and input combinations one at a time:

- PLS series flow rate, F(PLSS)
- PLS parallel flow rate F(PLSP)
- PLS copper concentration, c(PLS)
- lean electrolyte copper concentration, c(LE)
- simultaneous with different signs for the PLS series flow rate and PLS copper concentration, F(PLSS)&c(PLS)
- simultaneous with same signs for the PLS parallel flow rate and PLS copper concentration, F(PLSP)&c(PLS)
- simultaneous for the PLS copper concentration and electrolyte copper concentration c(PLS)&c(LE)

The measure used to compare the controller combinations was the integral of the absolute error (IAE) between the constant setpoints of the controlled variables and the outputs of the controlled variables under control. The results for the loaded organic copper concentration are presented in Section 10.4.1 and for the rich electrolyte copper concentration are presented in Section 10.4.2.

10.4.1 Loaded organic copper concentration

Disturbance rejection performances with different control schemes for the loaded organic copper concentration in operating points DP1 and DP4 are elaborated in this section with numerical and visual examples.

The disturbance rejection results evaluated in the first operating point DP1 are presented in Table 10-1, Figure 10-9, Figure 10-10 and Figure 10-11.

The disturbance rejection with the first PI controller (FB1) was very good. Opening the FB1 loop and adding the second PI controller (FB2) decreases the performance to a similar level as for the open loop case (OL). The disturbance rejection performance was increased when both loops were closed (PI), and further improved by adding the feedforward compensators (PIFF), as can be seen from Table 10-1.

Table 10-1: The integral of absolute error (IAE) for loaded organic copper concentration with disturbances at the first operating point.

	F(PLSS)	F(PLSP)	c(PLS)	c(LE)	F(PLSS) &c(PLS)	F(PLSP) &c(PLS)	c(PLS) &c(LE)
c(LO) OL iae	66.5	57.7	134.3	57.9	200.5	191.7	76.4
c(LO) FB1iae	10.2	8.7	20.6	8.3	30.8	29.3	12.3
c(LO) FB2iae	56.4	48.4	114.3	17.3	170.4	162.4	130.3
C(LO) PIiae	9.1	7.8	18.4	4.1	27.6	26.2	21.0
C(LO) PIFFiae	4.0	1.9	7.1	2.6	9.9	7.1	7.2

In the following visual analysis the open loop responses are compared to the PI-controller performance with both loops closed (PI), and to the performance of the two PI-control loops with four feedforward compensators.

The disturbances in the PLS series at sampling period [0, 1000] and parallel at sampling period [1000, 2000] flow rates, F(PLSS) and F(PLSP), were adequately rejected with the PI controllers. Adding the feedforward compensators fastens the disturbance rejection and considerably decreases the effect of the disturbance, as shown in Figure 10-9.

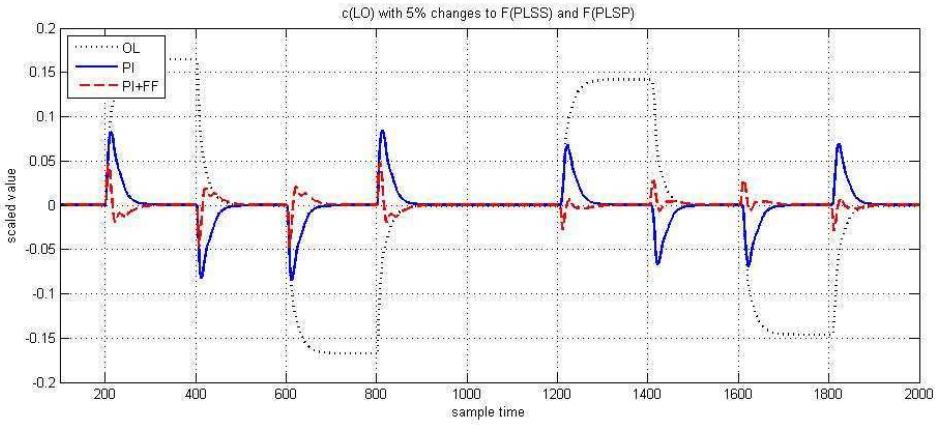

Figure 10-9: Loaded organic copper concentration with a +5% change in F(PLSS) and F(PLSP), under open loop control (OL), PI controllers (PI), and PI controllers with feedforward compensators (PIFF) at the first operating point.

Similar results are obtained for the PLS copper concentration, c(PLS) at sampling period [2000, 3000]. The lean electrolyte copper concentration disturbances at sampling period [3000, 4000] are satisfactorily rejected with both PI controllers and additional feedforward compensators, as can be seen from Figure 10-10:

Figure 10-10: Loaded organic copper concentration with a +5% change in c(PLS) and c(LE), under open loop control (OL), PI controllers (PI), and PI controllers with feedforward compensators (PIFF) at the first operating point.

The disturbance combinations are as effectively rejected as the single disturbances, especially with the feedforward compensators, as can be noted from Figure 10-11 and Table 10-1.

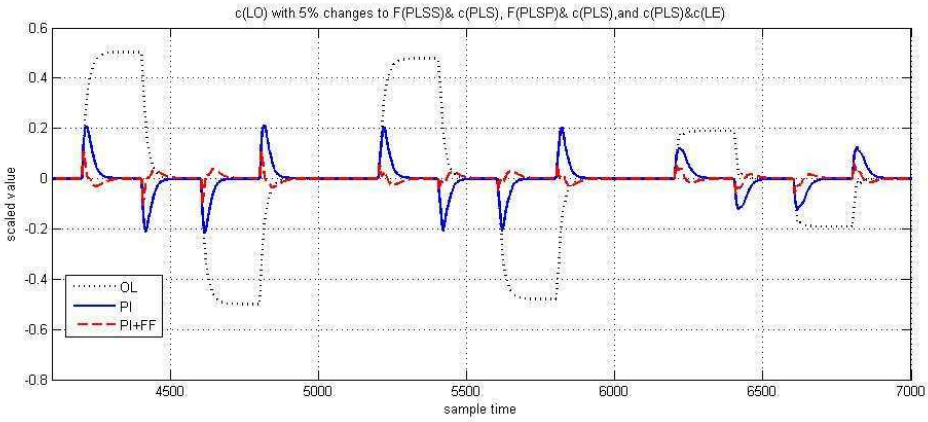

Figure 10-11: Loaded organic copper concentration with a +5% change in c(PLS)&F(PLSS), c(PLS)&F(PLSP), and c(PLS)&c(LE), under open loop control (OL), PI controllers (PI), and PI controllers with feedforward compensators (PIFF) at the first operating point.

The disturbance rejection results evaluated at the second operating point DP4 are presented in Table 10-2, Figure 10-12, Figure 10-13 and Figure 10-14.

Disturbance rejection with the first PI controller (FB1) was very good. Opening the FB1 loop and closing the FB2 loop (FB2) decreases the performance to a similar level as for the open loop case (OL). The disturbance rejection performance was increased with both loops closed (PI), and further improved by adding the feedforward compensators (PIFF), as can be seen from Table 10-2.

Table 10-2: The integral of absolute error (IAE) for loaded organic copper concentration with disturbances at the second operating point.

	F(PLSS)	F(PLSP)	c(PLS)	c(LE)	F(PLSS) &c(PLS)	F(PLSP) &c(PLS)	c(PLS) &c(LE)
c(LO) OL iae	45.2	49.2	105.8	36.7	149.9	154.0	69.3
c(LO) FB1iae	4.7	5.6	12.0	4.0	16.9	17.6	8.0
c(LO) FB2iae	40.4	44.2	95.1	6.3	134.4	138.3	100.2
C(LO) PIiae	4.4	5.0	10.8	1.9	15.1	15.8	11.0
C(LO) PIFFiae	2.1	1.4	4.5	0.6	6.4	5.2	4.2

In the following visual analysis the open loop responses are compared to the PI-controller performance with both loops closed (PI), and to the performance of the two PI-control loops with four feedforward compensators.

The ±5% disturbances to the PLS series and parallel flow rates were effectively rejected with the PI controllers, as can be seen from Figure 10-12. Even better performance was gained by adding feedforward compensators to the control system. For example, with a +5% change in F(PLSS) the integral of the absolute error for open loop control is 45.2, whereas PI control decreases the index to 4.4 and PI control with feedforward compensator down to 2.2. For a PLS parallel flow rate disturbance the rejection is even better: with PI controllers the IAE index decreases from 49.2 to 5.0. Adding the feed forward compensators improves the index to 1.4.

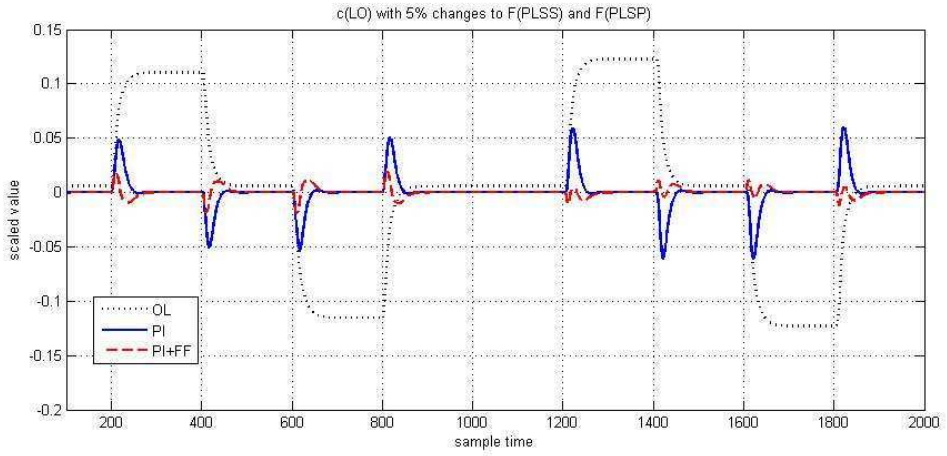

Figure 10-12: Loaded organic copper concentration with a +5% change in F(PLSS) and F(PLSP), under open loop control (OL), PI controllers (PI), and PI controllers with feedforward compensators (PIFF) at the second operating point.

The disturbances in the copper concentrations of PLS and lean electrolyte are rejected satisfactorily, as can be seen from Figure 10-13. Adding the feedforward compensators decreases the IAE index for the PLS change from 10.8 to 4.5, and for the lean electrolyte copper concentration from 1.9 to 0.6.

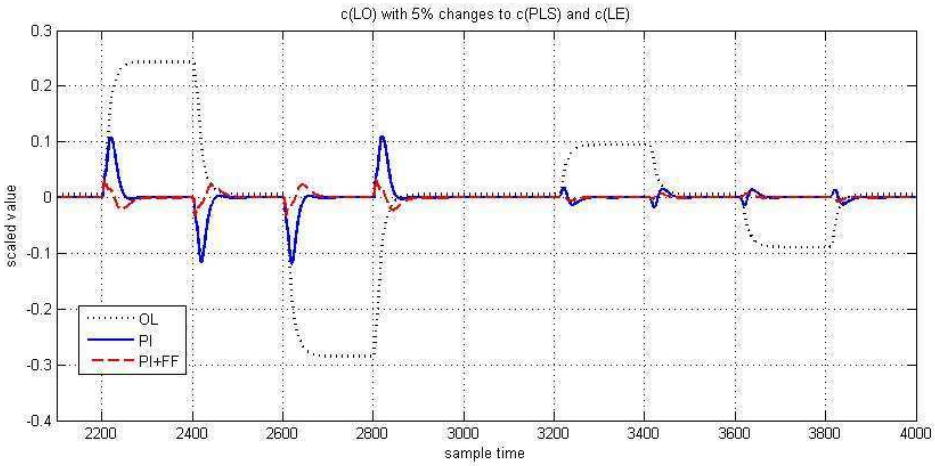

Figure 10-13: Loaded organic copper concentration with a +5% change in c(PLS) and c(LE), under open loop control (OL), PI controllers (PI), and PI controllers with feedforward compensators (PIFF) at the second operating point.

The rejection of multiple disturbances is as successful as for single disturbances, as can be seen from Figure 10-14. The PI control is relatively good, but adding feedforward controllers especially well rejected the effect of the disturbances.

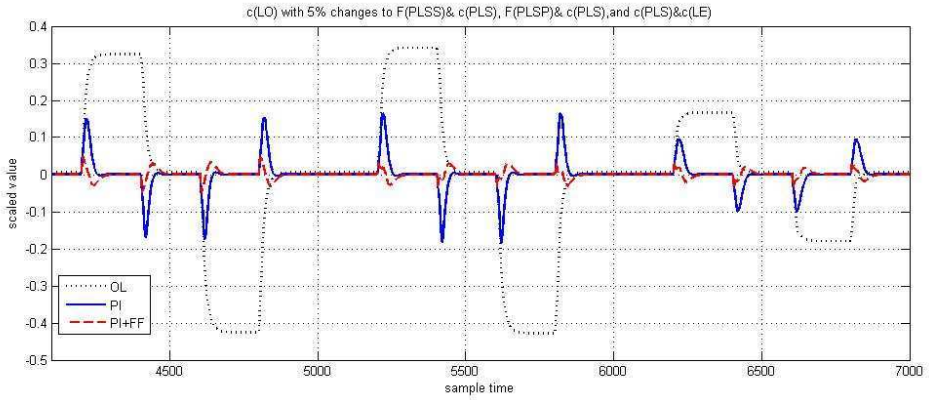

Figure 10-14: Loaded organic copper concentration with a +5% change in c(PLS)&F(PLSS), c(PLS)&F(PLSP), and c(PLS)&c(LE), under open loop control (OL), PI controllers (PI), and PI controllers with feedforward compensators (PIFF) at the second operating point.

10.4.2 Rich electrolyte copper concentration

Disturbance rejection performances with different control schemes for the rich electrolyte copper concentration at operating points DP1 and DP4 are elaborated in this section with numerical and visual examples.

The disturbance rejection results evaluated at the first operating point DP1 are presented in Table 10-3, Figure 10-15, Figure 10-16 and Figure 10-17.

At the first operating point the disturbance rejection with the second PI controller (FB2) was excellent. Opening the FB2 loop and closing the FB1 loop (FB1) decreases the performance to a similar level as for the open loop case (OL). The setpoint tracking performance with both control loops closed (PI) was slightly worse than with the FB2 loop alone due to the interactions, especially for the disturbance rejection of the changes in the PLS flow rate and copper concentration. Thus, adding the

feedforward compensators (PIFF) improved the result considerably for the lean electrolyte copper concentration disturbance, as can be seen from Table 10-3.

Table 10-3: The integral of absolute error (IAE) for the rich electrolyte copper concentration with disturbances at the first operating point.

	F(PLSS)	F(PLSP)	c(PLS)	c(LE)	F(PLSS) &c(PLS)	F(PLSP) &c(PLS)	c(PLS) &c(LE)
c(RE) OLiae	83.9	72.8	169.7	669.1	253.3	242.1	506.7
c(RE) FB1iae	97.4	83.1	196.4	680.0	293.5	279.5	491.0
c(RE) FB2iae	5.9	5.1	12.0	40.7	17.9	17.1	34.3
C(RE) PIiae	8.0	6.8	16.0	40.8	24.0	22.8	31.0
C(RE) PIFFiae	7.7	5.9	15.4	7.4	22.7	21.1	19.5

In the following visual analysis the open loop responses are compared to the PI-controller performance with both loops closed (PI), and to the performance of the two PI-control loops with four feedforward compensators.

The feedforward compensators fasten the disturbance rejection, although they cause higher peaks than the PI controllers alone, as shown for the PLS flow rate disturbances, F(PLSS) and F(PLSP), in Figure 10-15. The deviation from the setpoint is smaller with feedforward compensators, as shown in Table 10-3.

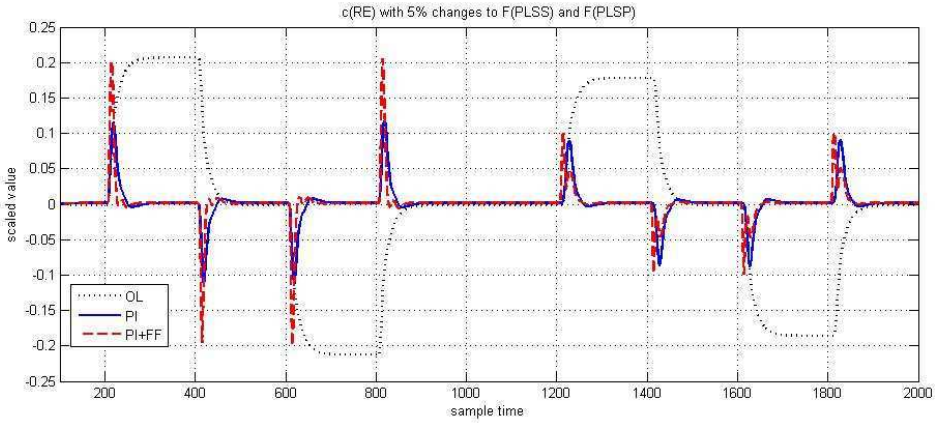

Figure 10-15: Rich electrolyte copper concentration with a +5% change in F(PLSS) and F(PLSP), under open loop control (OL), PI controllers (PI), and PI controllers with feedforward compensators (PIFF) at the first operating point.

For the PLS copper concentration, c(PLS) at sampling period [2000, 3000], the disturbance rejection performance is similar to the previous ones. The lean electrolyte copper concentration disturbance rejection at sampling period [3000, 4000], however, is significantly improved with the feedforward compensation, as shown in Figure 10-16.

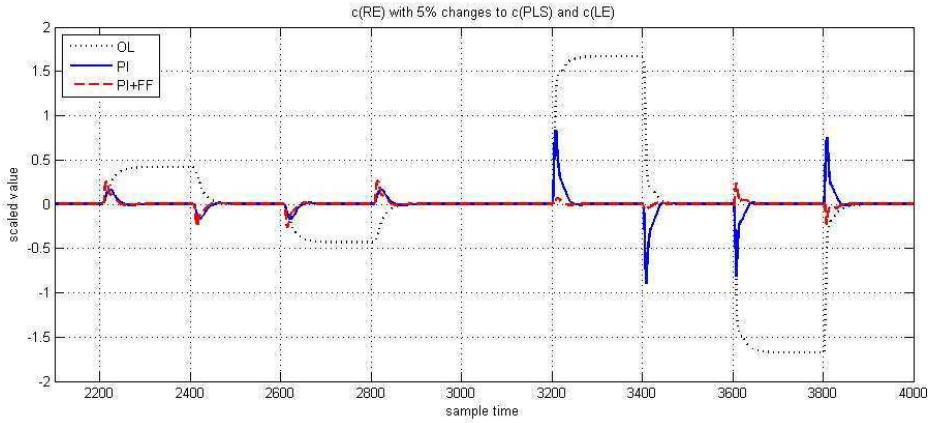

Figure 10-16: Rich electrolyte copper concentration with a +5% change in c(PLS) and c(LE), under open loop control (OL), PI controllers (PI), and PI controllers with feedforward compensators (PIFF) at the first operating point.

The simultaneous disturbances are most effectively rejected by adding the feedforward compensators with the PI controllers, as can be seen from Figure 10-17.

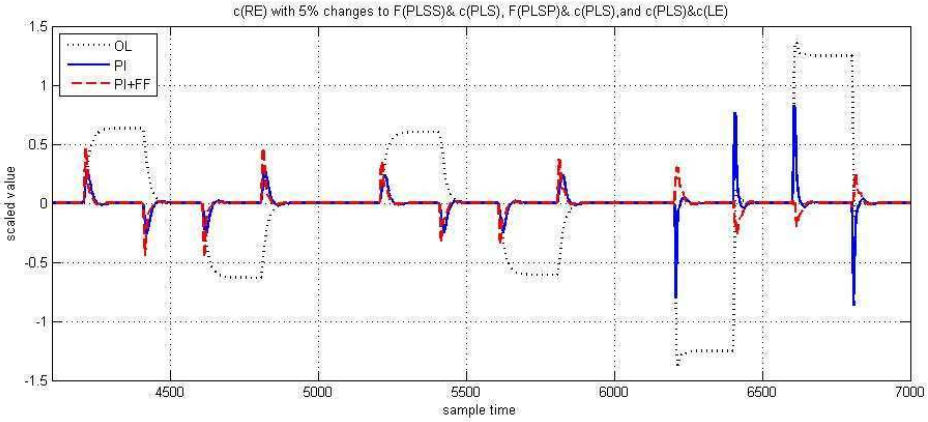

Figure 10-17: Rich electrolyte copper concentration with a +5% change in c(PLS)&F(PLSS), c(PLS)&F(PLSP), and c(PLS)&c(LE), under open loop control (OL), PI controllers (PI), and PI controllers with feedforward compensators (PIFF) at the first operating point.

The disturbance rejection results evaluated in the second operating point DP4 are presented in Table 10-4, Figure 10-18, Figure 10-19 and Figure 10-20.

The disturbance rejection with the second PI controller (FB2) was excellent. Opening the FB2 loop and closing the FB1 loop (FB1) has a drastic effect on the disturbance rejection due to high interaction between the loops and, for some cases, the performance drops to worse levels than for the open loop case (OL). The setpoint tracking performance with both control loops closed (PI) was worse than the FB2 loop alone due to the interactions. Thus, adding the feedforward compensators (PIFF) improved the result considerably for the lean electrolyte copper concentration disturbance, as can be seen from Table 10-4.

Table 10-4: The integral of absolute error (IAE) for rich electrolyte copper concentration with disturbances at the second operating point.

	F(PLSS)	F(PLSP)	c(PLS)	c(LE)	F(PLSS) &c(PLS)	F(PLSP) &c(PLS)	c(PLS) &c(LE)
c(RE) OLiae	58.4	63.6	136.8	628.4	193.9	199.1	499.8
c(RE) FB1iae	100.2	115.4	247.3	667.2	347.2	362.5	434.3
c(RE) FB2iae	3.2	3.5	7.5	35.1	10.5	10.8	31.9
C(RE) PIiae	6.5	7.5	15.8	36.4	22.3	23.3	34.8
C(RE) PIFFiae	6.9	7.0	15.9	5.9	22.3	22.9	16.5

In the following visual analysis the open loop responses are compared to the PI-controller performance with both loops closed (PI), and to the performance of the two PI-control loops with four feedforward compensators.

The feedforward compensators fasten the disturbance rejection, although causing higher peaks than the PI controllers alone, as shown for the PLS flow rate disturbances F(PLSS) at sampling period [0, 1000] and for F(PLSP) at sampling period [1000, 2000] in Figure 10-18.

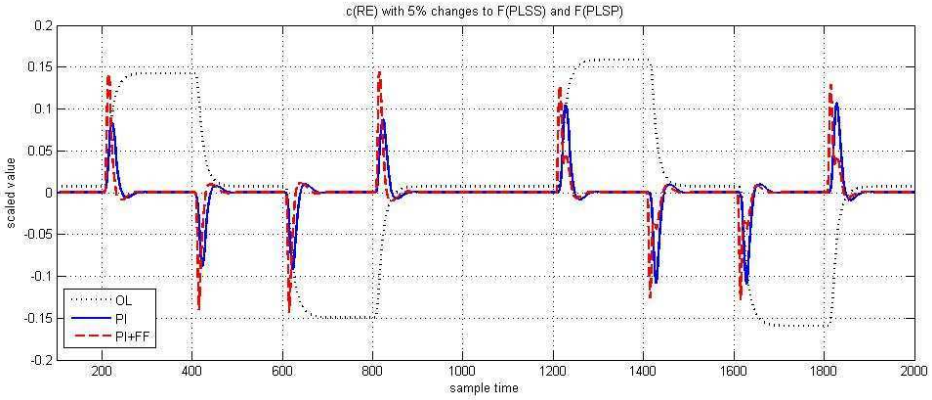

Figure 10-18: Rich electrolyte copper concentration with a +5% change in F(PLSS) and F(PLSP), under open loop control (OL), PI controllers (PI), and PI controllers with feedforward compensators (PIFF) at the second operating point.

The disturbance rejection performance for the PLS copper concentration c(PLS) at sampling period [2000, 3000] is similar to the previous ones. The lean electrolyte copper concentration disturbance rejection at sampling period [3000, 4000], however, is significantly improved with the feedforward compensation, as shown in Figure 10-19.

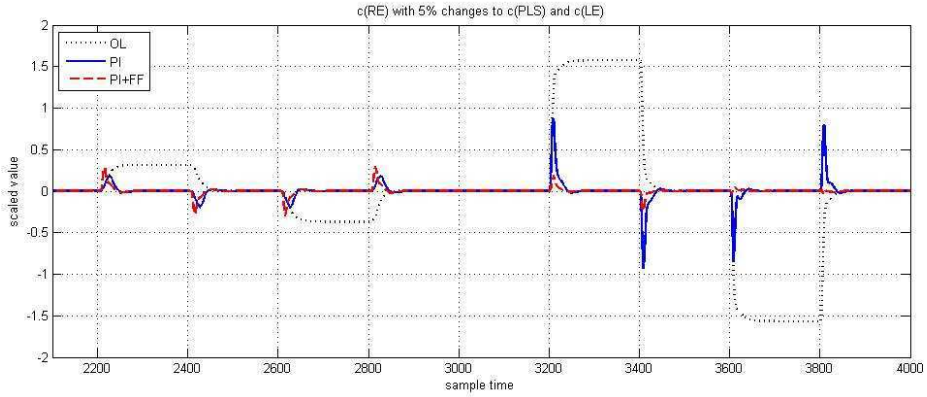

Figure 10-19: Rich electrolyte copper concentration with a +5% change in c(PLS) and c(LE), under open loop control (OL), PI controllers (PI), and PI controllers with feedforward compensators (PIFF) at the second operating point.

The simultaneous disturbances are rejected the best by adding the feedforward compensators with the PI controllers, as can be seen from Figure 10-20, and Table 10-4.

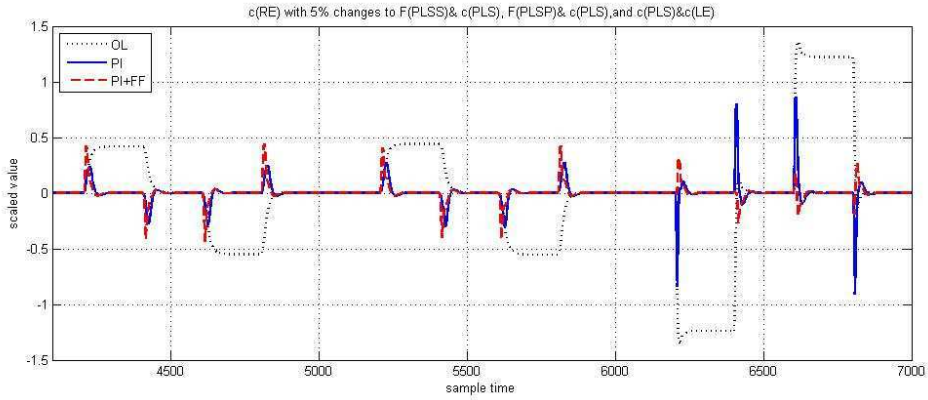

Figure 10-20: Rich electrolyte copper concentration with a +5% change in c(PLS)&F(PLSS), c(PLS)&F(PLSP), and c(PLS)&c(LE), under open loop control (OL), PI controllers (PI), and PI controllers with feedforward compensators (PIFF) at the second operating point.

10.5 Setpoint tracking

The aim in this section is to test the disturbance rejection performances of the single-input single-output controllers. The following controller combinations were used in this study:

- open loop (OL), no controllers
- only the first PI controller (FB1)
- only the second PI (FB2)
- both of the two PI controllers (PI)
- both of the two PI controllers with four feedforward compensators (PIFF)

Testing was performed by introducing ±5% changes to the setpoints of the controlled variables and their combination:

- loaded organic copper concentration, c(LO)
- rich electrolyte copper concentration, c(RE)
- simultaneous with the same signs for the loaded organic copper concentration and rich electrolyte copper concentration, c(LO)&c(RE)

The measure used to compare the controller combinations was the integral of the absolute error (IAE) between the setpoints of the controlled variables and the outputs of the controlled variables under control. The results for the loaded organic copper concentration are presented in Section 10.5.1 and for the rich electrolyte copper concentration in Section 10.5.2.

10.5.1 Loaded organic copper concentration

The setpoint tracking performances with different control schemes for the loaded organic copper concentration at operating points DP1 and DP4 are elaborated in this section with numerical and visual examples.

The setpoint tracking performances at the first operating point DP1 are numerically presented in Table 10-5 for all the controller combinations, and illustrated in Figure 10-21 for the open loop (OL), two PI controller (PI) and two PI controllers with four feedforward compensators (PIFF).

The setpoint tracking with the FB1 controller (FB1) was excellent. Opening the FB1 loop and closing the FB2 loop (FB2) decrease the performance to a similar level as for the open loop case (OL). The setpoint tracking performance was minimally decreased by closing both loops (PI). The feedforward controllers obviously do not affect the setpoint tracking performance, as shown in Table 10-5.

Table 10-5: The integral of absolute error (IAE) for the loaded organic copper concentration with setpoint tracking at the first operating point.

	c(LO)	**c(RE)**	**c(LO) &c(RE)**
c(LO) OL iae	191.4	0.0	191.4
c(LO) FB1iae	29.1	0.0	29.1
c(LO) FB2iae	191.4	99.0	117.6
C(LO) PIiae	30.8	15.7	30.2
C(LO) PIFFiae	30.8	15.7	30.2

Tracking of the loaded organic copper concentration changes at sampling period [7000, 8000] is slightly sluggish. The more realistic case with a simultaneous change in the loaded organic and rich electrolyte copper concentration setpoints at sampling period [9000, 10000] results in far tighter control with a 10% overshoot, as can be seen from Figure 10-21. The changes in the rich electrolyte copper concentration setpoint at sampling period [8000, 9000] cause peaks of less than 20% due to the interactions between the control loops.

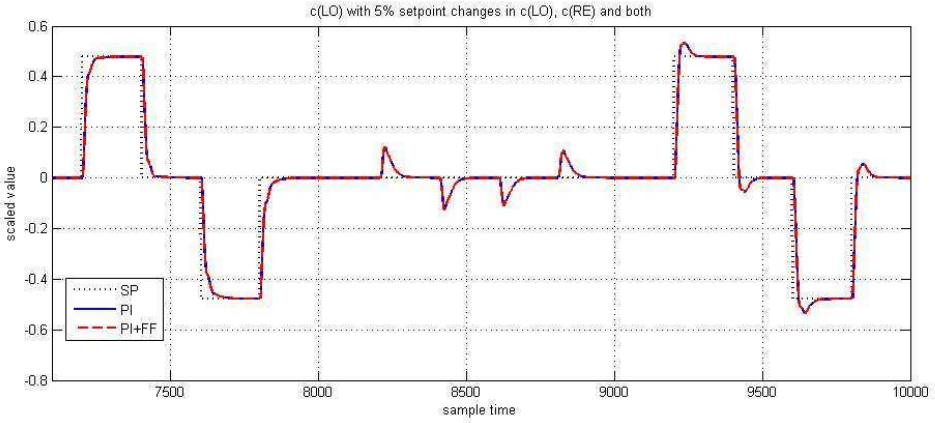

Figure 10-21: Loaded organic copper concentration with +5% changes in c(LO) setpoint, c(RE) setpoint, and simultaneously to both setpoints, under open loop control (OL), PI controllers (PI), and PI controllers with feedforward compensators (PIFF) at the first operating point.

The setpoint tracking performances at the second operating point DP4 are numerically presented in Table 10-6 for all the controller combinations, and illustrated in Figure 10-22 for the open loop (OL), two PI controller (PI) and two PI controllers with four feedforward compensators (PIFF).

The setpoint tracking with the first PI controller (FB1) was excellent. Opening the FB1 loop and adding the second PI controller (FB2) decrease the performance to a similar level as for the open loop case (OL). The setpoint tracking performance was minimally decreased by closing both loops (PI). Adding the feedforward compensators (PIFF) did not affect the performance, as can be seen from Table 10-6.

Table 10-6: The integral of absolute error (IAE) for the loaded organic copper concentration with set point tracking at the second operating point .

	c(LO)	**c(RE)**	**c(LO) &c(RE)**
c(LO) OL iae	212.0	0.0	212.0
c(LO) FB1iae	33.7	0.0	33.7
c(LO) FB2iae	212.0	58.7	167.0
C(LO) PIiae	32.5	6.4	33.1
C(LO) PIFFiae	32.5	6.4	33.1

The setpoint tracking for the loaded organic copper concentration is successful with both PI controllers. If the controller was more aggressive, this would result in disturbances in the rich electrolyte copper concentration. Changes in the rich electrolyte copper concentration setpoint cause only small disturbances, although in normal operation both setpoints are either raised or decreased simultaneously. The setpoint tracking during the simultaneous setpoint changes results in slightly more aggressive responses, as can be seen from Figure 10-22.

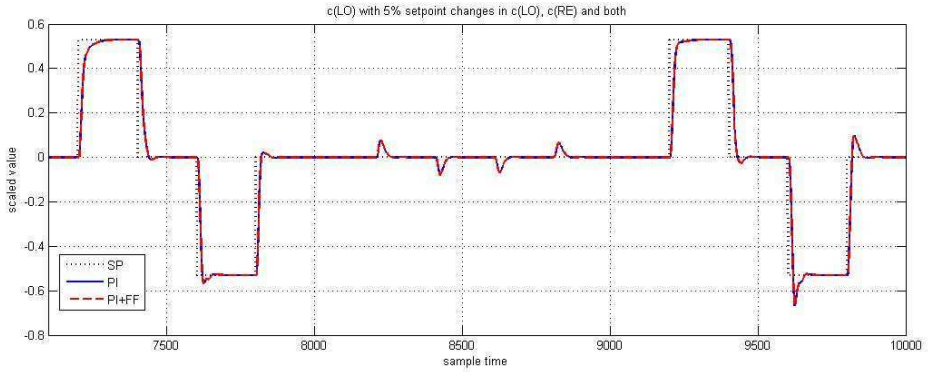

Figure 10-22: Loaded organic copper concentration with +5% changes in c(LO) setpoint, c(RE) setpoint, and simultaneously to both setpoints, under open loop control (OL), PI controllers (PI), and PI controllers with feedforward compensators (PIFF) at the second operating point.

10.5.2 Rich electrolyte copper concentration

Setpoint tracking performances with the different control schemes for the rich electrolyte copper concentration at operating points DP1 and DP4 are elaborated in this section with numerical and visual examples.

The setpoint tracking performances at the first operating point with different controllers are presented in Table 10-7 and Figure 10-23. The setpoint tracking with the FB2 controller (FB2) was excellent. Opening the FB2 loop and closing the FB1 loop (FB1) decrease the performance to a similar level as for the open loop case (OL).

The setpoint tracking performance with both control loops closed (PI) improved the result compared to the FB1 case, as can be seen from Table 10-7.

Table 10-7: The integral of absolute error (IAE) for the rich electrolyte copper concentration with set point tracking at the first operating point.

	c(LO)	**c(RE)**	**c(LO) &c(RE)**
c(RE) OLiae	0.0	906.0	906.0
c(RE) FB1iae	66.6	906.0	972.6
c(RE) FB2iae	0.0	63.1	63.1
C(RE) PIiae	19.9	64.4	81.5
C(RE) PIFFiae	19.9	64.4	81.5

The setpoint change for the loaded organic copper concentration c(LO) at sampling period [7000, 8000] causes small peaks of less than 20% in the rich electrolyte copper concentration due to the control loop interactions. The tracking of the setpoint changes in the rich electrolyte copper concentration c(RE) is is adequately fast and effective in the single change at sampling period [8000, 9000] and the simultaneous change at sampling period [9000, 10000] cases, as can be observed from Figure 10-23.

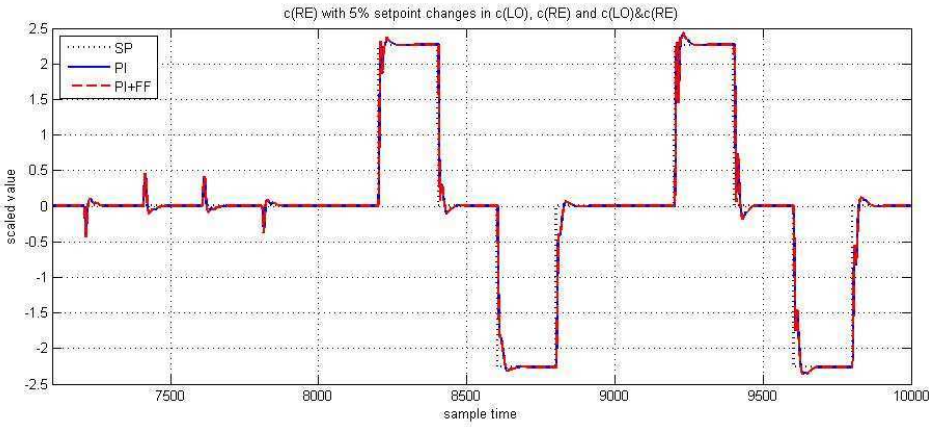

Figure 10-23: Rich electrolyte copper concentration with +5% changes in c(LO) setpoint, c(RE) setpoint, and simultaneously to both setpoints, under open loop control (OL), PI controllers (PI), and PI controllers with feedforward compensators (PIFF) at the first operating point.

The setpoint tracking performances at the second operating point DP4 with different controllers are presented in Table 10-8 and in Figure 10-24.

The setpoint tracking with the second PI controller (FB2) was excellent. Opening the FB2 loop and closing the FB1 loop (FB1) have a drastic effect on disturbance rejection due to the high interaction between the loops and, for some cases, the performance drops to worse levels than for the open loop case (OL). The setpoint tracking performance with both control loops closed (PI) improved the result compared to the FB1 loop closed, as shown in Table 10-8.

Table 10-8: The integral of absolute error (IAE) for the rich electrolyte copper concentration with disturbances and set point tracking at the second operating point.

	c(LO)	c(RE)	c(LO) &c(RE)
c(RE) OLiae	0.0	892.0	892.0
c(RE) FB1iae	423.4	892.0	1315.4
c(RE) FB2iae	0.0	56.8	56.8
C(RE) PIiae	38.9	60.8	94.2
C(RE) PIFFiae	38.9	60.8	94.2

The setpoint change for the loaded organic copper concentration c(LO) at sampling period [7000, 8000] causes peaks of about 35% in the rich electrolyte copper concentration due to the high loop interactions. The tracking of the setpoint changes in the rich electrolyte copper concentration c(RE) is adequately fast and effective in the single change at sampling period [8000, 9000]. The simultaneous setpoint change in the loaded organic copper concentration at sampling period [9000, 10000] causes slightly more oscillating behaviour, despite the adequately good setpoint tracking, as can be seen from Figure 10-24.

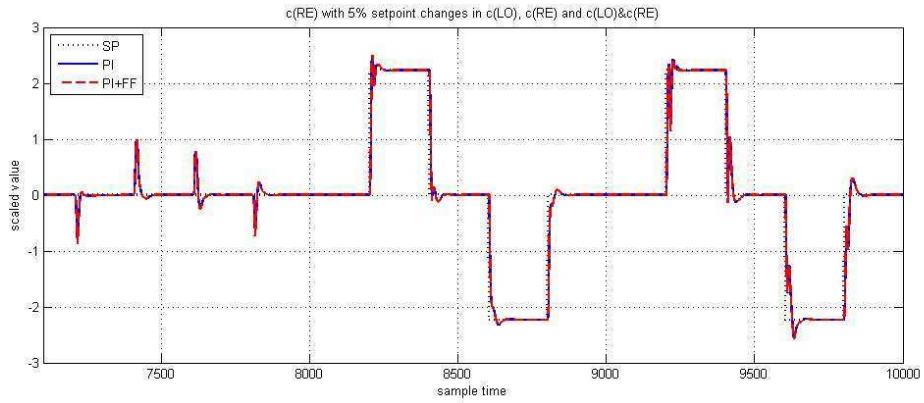

Figure 10-24: Rich electrolyte copper concentration with +5% changes in c(LO) setpoint, c(RE) setpoint, and simultaneously to both setpoints, under open loop control (OL), PI controllers (PI), and PI controllers with feedforward compensators (PIFF) at the second operating point.

10.6 Concluding remarks

The two PI controllers and the four feedforward compensators were tuned on the basis of the linear transfer function models. The control loop interactions were mild for the first control loop, but the second loop had larger interactions for the transfer function model linearized at operating point DP4. Since the other transfer function model did not have strong interactions, no decouplers were added.

The setpoint tracking performance of the PI controllers was studied with step changes to the setpoints of the controlled variables, firs one at a time and then with simultaneous step changes. The PI controller performed very well for the setpoint tracking. The disturbance rejection was tested with several step changes to the

disturbance variables, one at a time and simultaneously. The changes in the copper concentrations and flow rates were well rejected with the PI controllers. Adding the feedforward compensators improved the disturbance rejection significantly, by around 50 – 70% for the loaded organic copper concentration with the disturbances in the PLS copper concentration and flow rates, and by around 80% for the rich electrolyte copper concentration with the disturbance in the lean electrolyte copper concentration.

11 TESTING OF THE MIMO CONTROL STRATEGY FOR THE COPPER SOLVENT EXTRACTION PROCESS

The aim of this chapter is to describe the tuning and testing of the multi-input multi-output controller (MIMO) in the simulation environment (see Chapter 6). The basic principles of the model predictive controller are introduced in Section 11.1. The controller tuning, based on the multi-input multi-output control structure (eight order linear state space model) presented in Chapter 9, is described in Section 11.2. Finally, the model predictive controller performance is tested against input disturbances in Section 11.3 and setpoint changes in Section 11.4.

11.1 Introduction to model predictive control

Model predictive control (MPC) refers to a class of control algorithms in which a dynamic process model is used to predict and optimize process performance. The cost function to be minimized has the following form:

$$J = \sum_{i=n_1}^{n_2} \gamma_{yi} \left[y_r(k+d+i) - \hat{y}(k+d+i \mid k) \right]^2 + \sum_{j=1}^{n_u} \gamma_{uj} \Delta u^2 (k-1+j) \qquad \textbf{(11-1)}$$

where y_r is the reference trajectory, $\hat{y}$ is the output prediction and u is the input value, k is the present moment and d is the discrete dead time. The tuning parameters are the prediction horizon (n_2-n_1), the control horizon n_u, and the weights γ_y and γ_u. The output weight γ_y is punishing the error between the output and the reference trajectory, and γ_u is punishing the changes in the manipulated variable.

The current control action is obtained by solving, online at each sampling time, a finite horizon open-loop optimal control problem using the current state as the initial state. The optimization yields an optimal control sequence, and the first control in this sequence is applied to the plant.

All the MPC methods share the following four basic elements. The process model is used to predict the future outputs of the process. The future outputs are compared to the reference trajectory, and the future errors and the costs of the control actions to be made are optimized. Both the cost function and constraints are considered in the optimization. The future inputs are calculated, and the next control action is performed. The strategy and philosophy of the implementation of the elements differs between the different methods, but the general structure follows the scheme presented in Figure 11-1. (Camacho and Bordons 1999, Henson, 1998, Mayne, 2000, Rawlings, 2000, Maciejovski, 2002).

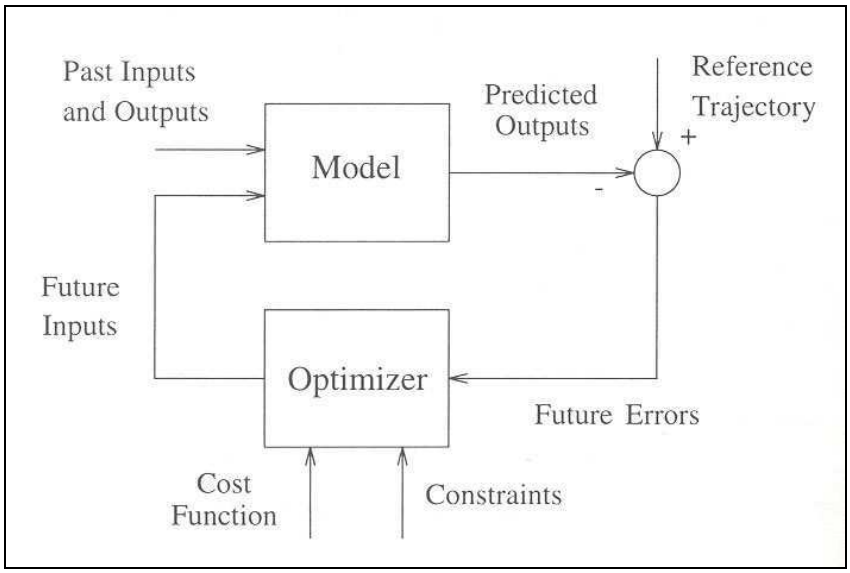

Figure 11-1: The general strategy of MPC. (Camacho and Bordons 1999).

The first MPC techniques were developed in the 1970s because conventional single-loop controllers were unable to satisfy the increasingly stringent performance requirements. MPC is well suited for high performance control of constrained multivariable processes. The current generation of industrial model predictive controllers is based on the assumption of process linearity, because this simplifies model development and controller design. The empirical dynamic models are identified from test data, and the stability of the tuning is assured by testing the scheme with closed-loop simulations. (Morari and Lee, 1999, Qin and Badgwell, 2003)

MPC technology has been used extensively in the refining and petrochemical industries. During the past decade MPC strategies have also been applied to other areas. Adaptation was one of the motivations for MPC, and there is a strong market incentive for a self-tuning model predictive controller. (Mayne, 2000, Qin and Badgwell, 2003).

11.2 Tuning of the model predictive controller

Due to the long time delays in the process, a model predictive control algorithm was chosen as the multi-input-multi-output controller. The controller is based on the eight order state space model identified from the simulated data, as presented in Chapter 8. The plant is described in Chapter 5 and illustrated in Figure 5-1. The control strategy is presented in Chapter 9 and illustrated in Figure 9-11 and Figure 9-12. The control strategy includes two controlled variables: the loaded organic and rich electrolyte concentrations, c(LO) and c(RE); two manipulated variables: the loaded organic and lean electrolyte flow rates, F(LO) and F(LE); and four disturbance variables: the PLS and lean electrolyte copper concentrations, c(PLS) and c(LE), and the PLS series and parallel flow rates F(PLSS) and F(PLSP). The model predictive controller performance is compared to that of the PI controller by using the same structure of manipulated, disturbance and controlled variables.

In this work the Matlab MPC toolbox was used. The tuning of the model predictive controller was performed by changing the following parameters (in Equation 11-1):

prediction horizon (n_2-n_1), control horizon (n_u), and cost function weights for the controlled variable weights (γ_y) and manipulated variable rate weights (γ_u). Hard constraints were not assigned. The initial choices for the parameters were the following: the prediction horizon was the longest settling time of the manipulated variable-controlled variable pairs, and the control horizon was longer than the longest dead time of the manipulated variable-controlled variable pairs. The rich electrolyte copper concentration had a larger weight than the loaded organic copper concentration in order to emphasize the importance of the end product quality. The manipulated variable rate weights were tuned to avoid large changes and oscillating behaviour. For the fine tuning of the horizons and weights, minimization of the iae index was used. In the following sections the disturbance rejection and setpoint tracking performance of the model predictive controller is compared to that of the PI controllers.

11.3 Disturbance rejection

The aim in this Section is to test the disturbance rejection performances of the multi-input multi-output controller and to compare the performance to the single-input single-output controllers performances. The following controller combinations were used in this study:

- open loop (OL), no controllers
- both of the two PI controllers (PI) (see Section 10.1)
- both of the two PI controllers with four feedforward compensators (PI+FF) (see Section 10.1)
- model predictive controller (MPC)
- model predictive controller with four feedforward compensators (MPC+FF)

The testing was done by introducing ±5% changes into the following the inputs and input combinations one at a time:

- PLS series flow rate, F(PLSS)
- PLS parallel flow rate, F(PLSP)
- PLS copper concentration, c(PLS)
- lean electrolyte copper concentration, c(LE)
- simultaneous with different signs for the PLS series flow rate and PLS copper concentration, F(PLSS)&c(PLS)
- simultaneous with same signs for the PLS parallel flow rate and PLS copper concentration, F(PLSP)&c(PLS)
- simultaneous for the PLS copper concentration and electrolyte copper concentration c(PLS)&c(LE)

The measure used to compare the controller combinations was the integral of the absolute error (IAE) between the constant setpoints of the controlled variables and the outputs of the controlled variables under control. The results for the loaded organic copper concentration are presented in Section 11.3.1 and for the rich electrolyte copper concentration are presented in Section 11.3.2.

11.3.1 Loaded organic copper concentration

The rejection of disturbances in the loaded organic copper concentration at the first operating point DP1 with different control schemes is elaborated in the following section, with numerical and visual examples in Table 11-1, Figure 11-2, Figure 11-3 and Figure 11-4.

he results obtained with the model predictive controller were better for disturbance rejection than with the PI controllers, as can be seen from Table 11-1. With the feedforward compensators, the PI controllers performed better in rejecting the F(PLSS), F(PLSP) and c(PLS) disturbances.

Table 11-1: The integral of absolute error (IAE) for the loaded organic copper concentration with disturbances and set point tracking at the first operating point.

	F(PLSS)	**F(PLSP)**	**c(PLS)**	**c(LE)**	**F(PLSS) &c(PLS)**	**F(PLSP) &c(PLS)**	**c(PLS) &c(LE)**
c(LO) OL	66.5	57.7	134.3	57.9	200.5	191.7	76.4
c(LO) PI	9.1	7.8	18.4	4.1	27.6	26.2	21.0
c(LO) PI+FF	4.0	1.9	7.1	2.6	9.9	7.1	7.2
c(LO) MPC	7.2	6.1	14.3	7.1	21.4	20.4	20.3
c(LO) MPC+FF	4.2	2.2	8.0	2.0	11.4	9.1	8.7

In the following visual analysis the PI-controllers performance is compared to that of the model predictive controller (MPC). The open loop responses are also presented.

The flow rate disturbances in PLS series F(PLSS) at sampling period [0, 1000], and in PLS parallel F(PLSP) at sampling period [1000, 2000], are rejected with the MPC faster than with PI controllers, as shown in Figure 11-2.

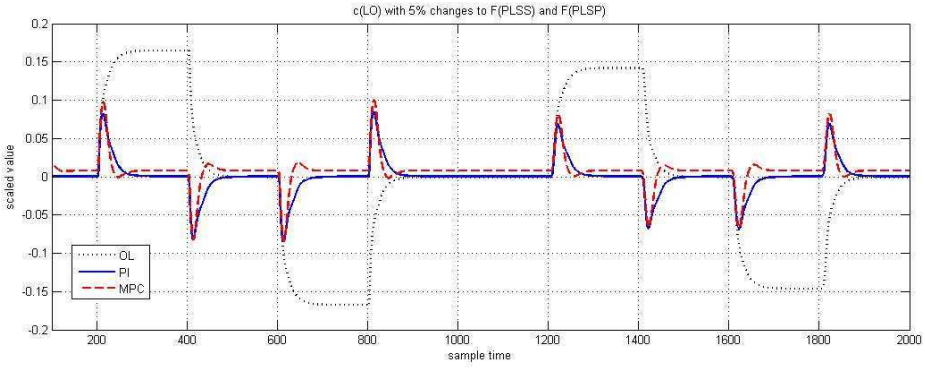

Figure 11-2: Loaded organic copper concentration with a +5% change in F(PLSS) and F(PLSP), under open loop control (OL), PI controllers (PI), and model predictive controller (MPC) at the first operating point.

As with the PLS flow rate disturbances, the PLS copper concentration disturbance at sampling period [2000, 3000] is more effectively rejected with MPC than with PI controllers. However, a disturbance in the lean electrolyte copper concentration causes larger changes in the loaded organic copper concentration with MPC than with PI controllers, as shown in Figure 11-3. This is due to the MPC tuning, which favours

disturbance rejection in the rich electrolyte copper concentration over the loaded organic copper concentration.

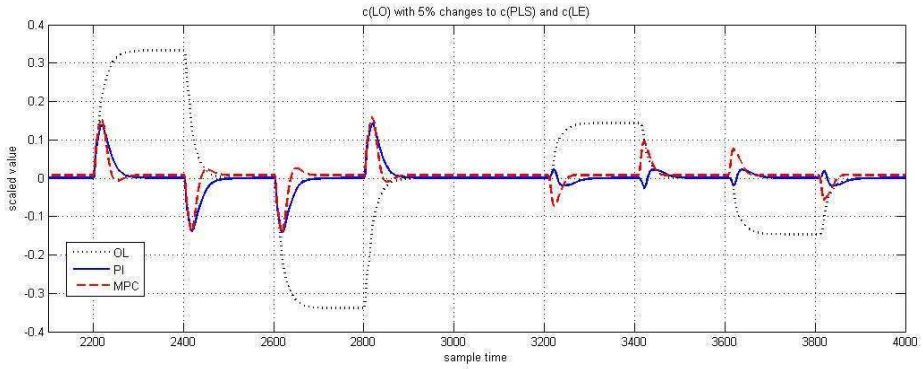

Figure 11-3: Loaded organic copper concentration with a +5% change in c(PLS) and c(LE), under open loop control (OL), PI controllers (PI), and model predictive controller (MPC) at the first operating point.

All the combined disturbances are rejected more effectively with MPC than with PI controllers, as can be seen from Figure 11-4. For the last combination of PLS and lean electrolyte copper concentration disturbances at sampling period [6000, 7000], MPC has a lower integral of the absolute error value than PI controllers (IAE 20.3 and 21.0 correspondingly), as shown in Table 11-1.

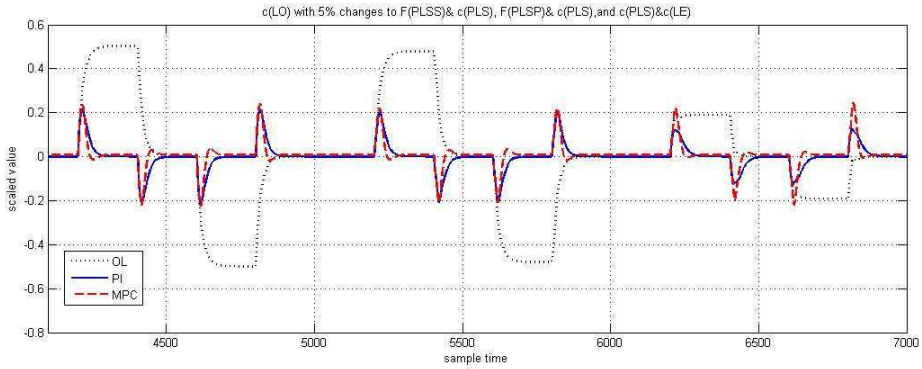

Figure 11-4: Loaded organic copper concentration with a +5% change in c(PLS)&F(PLSS), c(PLS)&F(PLSP), and c(PLS)&c(LE), under open loop control (OL), PI controllers (PI), and model predictive controller (MPC) at the first operating point.

11.3.2 Rich electrolyte copper concentration

The rejection if disturbances in the rich electrolyte copper concentration at operating point DP1 with different control schemes is elaborated in the following section, with numerical and visual examples in Table 11-2 and Figure 11-5.

The disturbance rejection for the rich electrolyte copper concentration is clearly better with MPC than with PI controllers, as presented in Table 11-2. Addition of the feedforward controller for the lean electrolyte copper concentration improves the disturbance rejection characteristics for MPC. The other feedforward compensators slightly worsen the result for the rich electrolyte copper concentration but, on the other hand, the result for the loaded organic copper concentration is significantly improved.

Table 11-2: The integral of absolute error (IAE) for the rich electrolyte copper concentration with disturbances at the first operating point.

	F(PLSS)	F(PLSP)	c(PLS)	c(LE)	F(PLSS) &c(PLS)	F(PLSP) &c(PLS)	c(PLS) &c(LE)
c(RE) OL	83.9	72.8	169.7	669.1	253.3	242.1	506.7
C(RE) PI	8.0	6.8	16.0	40.8	24.0	22.8	31.0
C(RE) PI+FF	7.7	5.9	15.4	7.4	22.7	21.1	19.5
C(RE) MPC	2.4	1.9	3.3	28.5	5.6	4.9	29.5
C(RE) MPC+FF	4.9	2.9	6.7	5.5	11.2	9.5	8.9

In the following visual analysis the PI-controllers performance is compared to that of the model predictive controller (MPC). The open loop responses are also shown.

The PLS series and parallel flow rate disturbances F(PLSS) at sampling period [0, 1000], and F(PLSP) at sampling period [1000, 2000], are rejected more effectively with MPC than with PI controllers, as is illustrated in Figure 11-5.

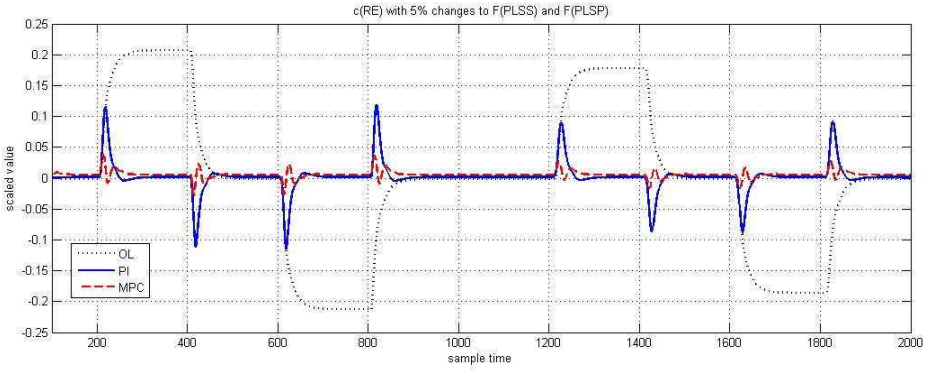

Figure 11-5: Rich electrolyte copper concentration with a +5% change in F(PLSS) and F(PLSP), under open loop control (OL), PI controllers (PI), and model predictive controller (MPC) at the first operating point.

The disturbances in the PLS copper concentration c(PLS) at sampling period [2000, 3000], and the lean electrolyte copper concentration, c(LE) at sampling period [3000, 4000], are especially well rejected with MPC, as shown in Figure 11-6. The performance for the PLS copper concentration with MPC is four times better than with PI controllers (IAE 3.3 and 16.0 correspondingly), and the for lean electrolyte copper concentration almost twice as good (IAE 28.5 and 40.8 correspondingly).

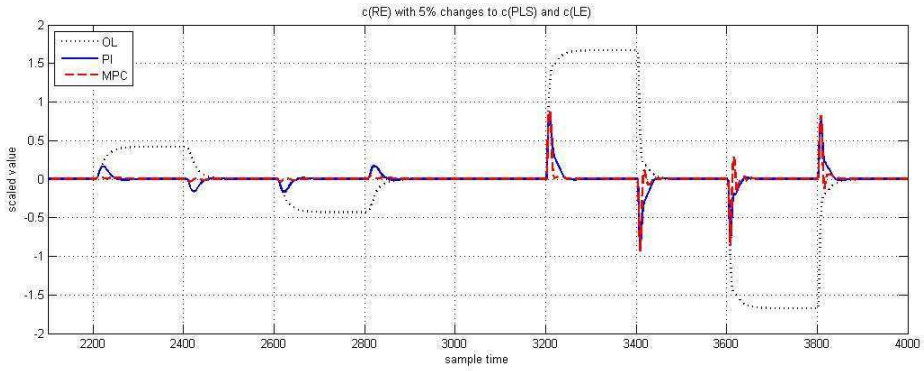

Figure 11-6: Rich electrolyte copper concentration with a +5% change in c(PLS) and c(LE), under open loop control (OL), PI controllers (PI), and model predictive controller (MPC) at the first operating point.

The simultaneous disturbances are rejected far better with MPC than with PI controllers, as can be seen from Figure 11-7, and Table 11-2.

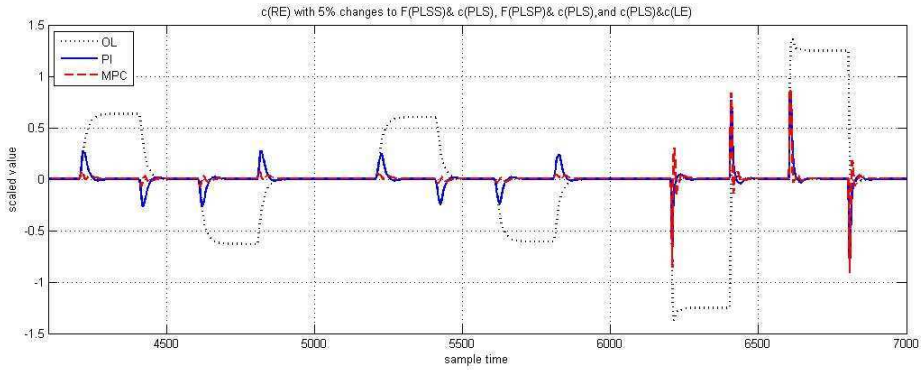

Figure 11-7: Rich electrolyte copper concentration with a +5% change in c(PLS)&F(PLSS), c(PLS)&F(PLSP), and c(PLS)&c(LE), under open loop control (OL), PI controllers (PI), and model predictive controller (MPC) at the first operating point.

11.4 Setpoint tracking

The aim in this section is to test the disturbance rejection performances of the single-input single-output controllers. The following controller combinations were used in this study:

- open loop (OL), no controllers
- both of the two PI controllers (PI) (see Section 10.1)
- both of the two PI controllers with four feedforward compensators (PI+FF) (see Section 10.1)
- model predictive controller (MPC)
- model predictive controller with four feedforward compensators (MPC+FF)

The testing was performed by introducing ±5% changes in the setpoints of the controlled variables and their combination:

- loaded organic copper concentration, c(LO)
- rich electrolyte copper concentration, c(RE)

- simultaneous with the same signs for the loaded organic copper concentration and rich electrolyte copper concentration, c(LO)&c(RE)

The measure used to compare the controller combinations was the integral of the absolute error (IAE) between the setpoints of the controlled variables and the outputs of the controlled variables under control. The results for the loaded organic copper concentration are presented in Section 11.4.1 and for the rich electrolyte copper concentration are presented in Section 11.4.2.

11.4.1 Loaded organic copper concentration

The loaded organic copper concentration setpoint tracking performance at operating point DP1 with different control schemes is elaborated in the following section, with numerical and visual examples in Table 11-3 and Figure 11-8.

The results obtained with the model predictive controller were better for setpoint tracking than with the PI controllers, as can be seen from Table 11-3. The controller interaction is significantly decreased with MPC; for example, the setpoint tracking of the rich electrolyte copper concentration c(RE) has a value of 4.8 with MPC and of 15.7 with PI controllers. Within the MPC structure the rich electrolyte copper concentration setpoint tracking had a higher coefficient than the loaded organic copper concentration, and thus here the loop interaction counteracts the good result for the loaded organic copper concentration.

Table 11-3: The integral of absolute error (IAE) for the loaded organic copper concentration with set point tracking at the first operating point.

	c(LO)	**c(RE)**	**c(LO) &c(RE)**
c(LO) OL	191.4	0.0	191.4
c(LO) PI	30.8	15.7	30.2
c(LO) PI+FF	30.8	15.7	30.2
c(LO) MPC	25.7	4.8	29.1
c(LO) MPC+FF	25.6	4.9	28.9

Adaptation to the new loaded organic setpoint [7000 8000] is fast with only small overshoot. The simultaneous setpoint change for both of the controlled variables results in similar responses between the MPC and PI controller. However, as can be seen from the previous table, MPC is slightly better than the PI controllers (29.1 and 30.2 correspondingly). The effect of the rich electrolyte copper concentration setpoint change is also far smaller with the model predictive controller than with the PI controllers (IAE 4.8 and 15.7, respectively).

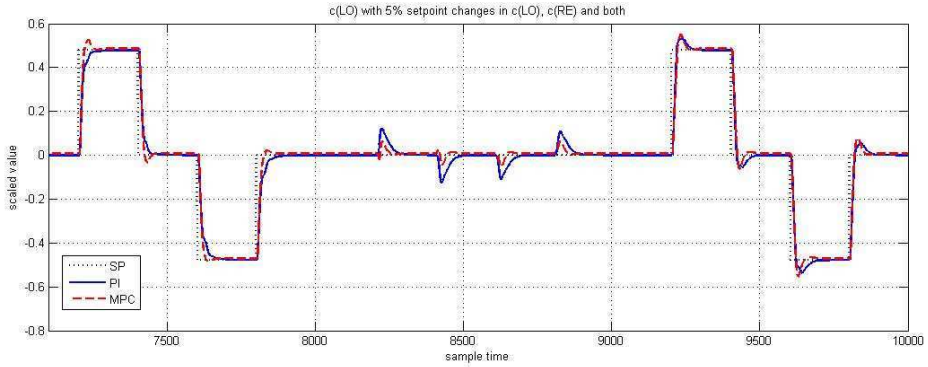

Figure 11-8: Loaded organic copper concentration with a +5% changes in c(LO) setpoint, c(RE) setpoint, and simultaneously to both setpoints, under open loop control (OL), PI controllers (PI), and model predictive controller (MPC) at the first operating point.

11.4.2 Rich electrolyte copper concentration

The rich electrolyte copper concentration setpoint tracking performance at operating point DP1 with different control schemes is elaborated in the following section, with numerical and visual examples in Table 11-4 and Figure 11-9.

The disturbance rejection for the rich electrolyte copper concentration is clearly better with MPC than with PI controllers, as presented in Table 11-4. The control loop interactions during setpoint changes is more effectively handled with MPC than with PI controllers: for example, during a change in the setpoint of the loaded organic copper concentration, c(LO), the integral of the absolute error (IAE) index is three times smaller with MPC than with PI controllers (7.7 and 19.9, respectively). During the setpoint change in both controlled variables, c(LO)&c(RE), the IAE index is also significantly smaller than with the PI controllers (IAE 58.4 and 81.5, respectively).

Table 11-4: The integral of absolute error (IAE) for the rich electrolyte copper concentration with set point tracking at the first operating point.

	c(LO)	**c(RE)**	**c(LO) &c(RE)**
c(RE) OL	0.0	906.0	906.0
C(RE) PI	19.9	64.4	81.5
C(RE) PI+FF	19.9	64.4	81.5
C(RE) MPC	7.7	58.5	58.4
C(RE) MPC+FF	8.1	58.4	58.0

The setpoint tracking is more effective with MPC than with PI controllers, as illustrated in Figure 11-9. The loaded organic copper concentration setpoint tracking [7000 8000] causes a smaller disturbance to the rich electrolyte copper concentration with MPC than with PI control (IAE 7.7 and 19.9, respectively). The change in the setpoint of the rich electrolyte copper concentration at sampling period [8000, 9000] is varied faster with MPC than with PI controllers (IAE 58.5 and 64.4, respectively).

MPC performs especially well with the simultaneous setpoint change in both controlled variables: the IAE index is 58.4, whereas for PI controllers the index is 81.5.

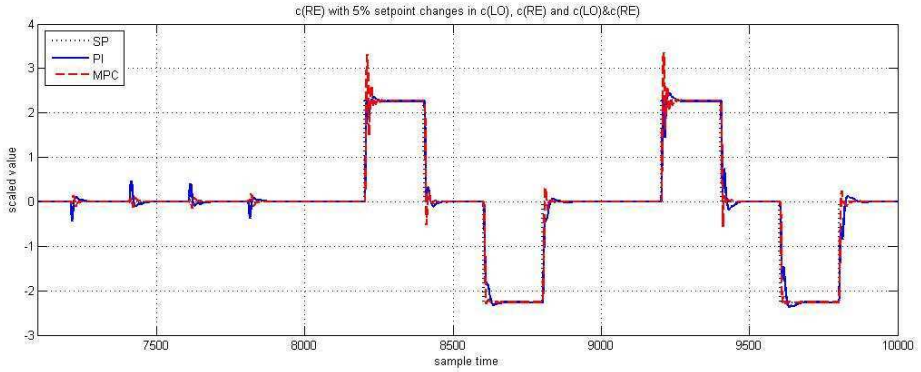

Figure 11-9: Rich electrolyte copper concentration with +5% changes in c(LO) setpoint, c(RE) setpoint, and simultaneously to both setpoints, under open loop control (OL), PI controllers (PI), and model predictive controller (MPC) at the first operating point.

11.5 Concluding remarks

The model predictive controller was chosen for the multi input – multi output controller due to its good dead time handling and clearly comparable structure with the single input-single output control strategy. The MPC was designed on the basis of the eight order state space model. Setpoint tracking and disturbance rejection were tested with the same input variable changes as for the PI controllers. As expected, MPC significantly improved the setpoint tracking and disturbance rejection performance compared to PI controllers. Adding the feedforward compensator of the lean electrolyte copper concentration improved the disturbance rejection performance for the rich electrolyte copper concentration, whereas the other feedforward compensators did not perform as well with the MPC. However, MPC was able to minimize the control loop interactions, and the overall performance was better than with PI controllers. Therefore the model predictive controller will be the preferred controller for the further studies.

12 COMPARISON OF THE CONTROL STRATEGIES FOR THE COPPER SOLVENT EXTRACTION PROCESS

In this chapter the benefits of control are verified by comparing the single-input single-output and multi-input multi-output control strategies against the manual control strategy of the plant in the simulation environment (see Chapter 6) with industrial process data. The strategy for the comparison is presented in Section 12.1. The total production with the different control strategies is compared in Section 12.2, and the variation in the key process indicators in Section 12.3.

12.1 Strategy for the comparison of the control strategies

In order to verify the benefits of the proposed single-input single-output and multi-input multi-output control strategies, the performances of the proposed control strategies are compared to that of the manual control strategy of the copper solvent extraction plant. The control strategies are compared to each other on the basis of the average copper production, and the average absolute error around the setpoints on the basis of the simulated and measured outputs.

The average production is determined as follows:

$$prod = \frac{\sum_{i=1}^{N} \left(c(RE)(i) - c(LE)(i) \right) \cdot F(LE)(i)}{N} \qquad \textbf{(12-1)}$$

where N is the total number of samples.

The average absolute error between the output copper concentration c and the setpoint c_{sp} is calculated as follows:

$$AAE = \frac{\sum_{i=1}^{N} \left| c_{sp}(i) - c(i) \right|}{N} \qquad \textbf{(12-2)}$$

The industrial measurements represent the manual control strategy. The setpoints for the controlled variables are determined as the one-day moving average of the corresponding industrial online measurement.

The inputs to the simulator with the controllers for the single-input single-output and multi-input-multi-output control strategies are the industrial measurements and varied parameters for the equilibrium isotherm, efficiencies and recycle correction, as described in Chapter 7. The PI controllers and feedforward (FF) compensators described in Chapter 10, and the model predictive controller (MPC) with the feedforward compensator for the lean electrolyte copper concentration described in Chapter11, are utilized. The setpoints for the controlled variables are determined by solving the optimization problem with the offline process data, as described in Section 9.7.

In the optimization, the minimum and maximum flow rates of the industrial data are considered as additional constraints. Also the organic to aqueous ratios are determined

on the basis of the maximum value for the extraction and the minimum value for the stripping from the industrial data.

No assumptions are made about the operation of the electrowinning, but the lean electrolyte copper concentration measurements are used as such. Such an assumption might affect the control results negatively, since the rich electrolyte control loop has to do extra work to stabilize the disturbances in the lean electrolyte copper concentration. If an electrowinning model existed, the electrolyte copper concentrations could be stabilized at the desired levels.

The control results are presented for the production increase in Section 12.2 and for the variation decrease in Section 12.3.

12.2 Comparison of the total production with different control strategies

The production increase with the different control strategies compared to manual control is presented in Table 12-1. For the first test data set, the production was increased by almost 5% and for the second data set by around 2.8%. It should be noted that since the SISO (PI control) and MIMO (MPC) control strategies have the same setpoints, the production increases are expected to be rather similar.

Table 12-1: The production increase with the different control strategies compared to the manual control strategy.

	Production First test data set	**Production second test data set**
PI	+4.93%	+2.77%
PI+FF	+4.92%	+2.81%
MPC	+4.93%	+2.78%
MPC+FF	+4.93%	

For the first data set, the production under the PI controllers with the feedforward compensator is presented in Figure 12-1, and under MPC control with the c(LE) feedforward compensator in Figure 12-2. The production is clearly higher and has less variation compared to that for the manual operating practice. The visual comparison shows that the model predictive controller also causes less variation in the production compared to the PI controllers with the feedforward compensators.

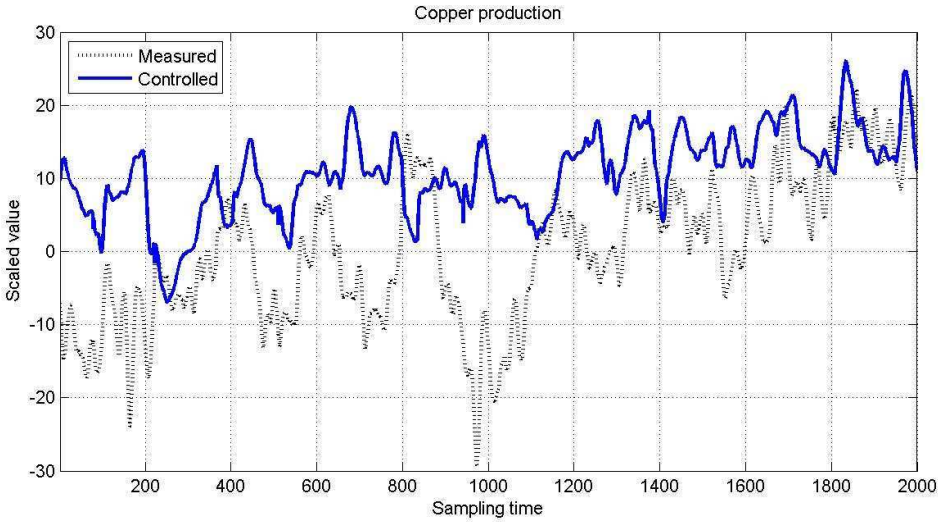

Figure 12-1: Copper production for the first test data set: industrial measurement (dotted) and PI+FF controlled in the simulation environment (solid).

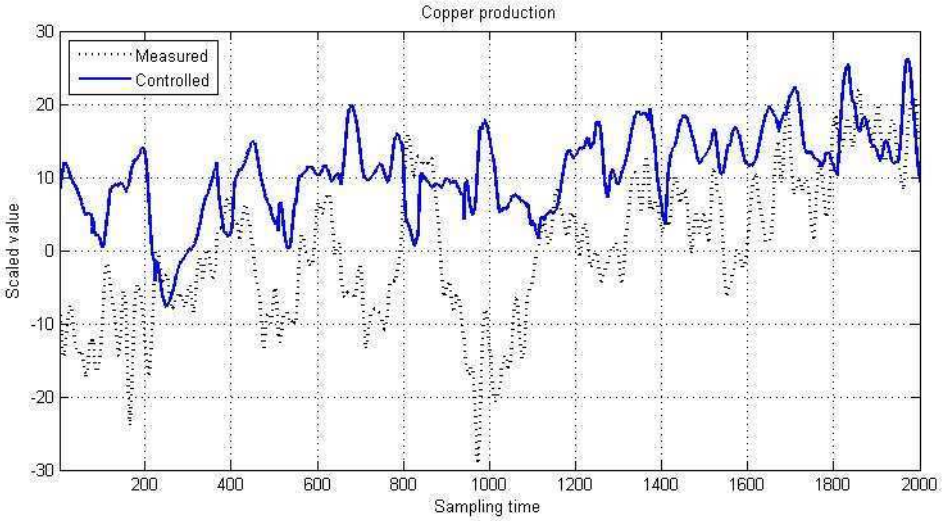

Figure 12-2: Copper production for the first test data set: industrial measurement (dotted) and MPC+FF controlled in the simulation environment (solid).

For the second data set, the production is more stable with the MPC controller, as shown in Figure 12-4, compared to the PI controlled production presented in Figure 12-3. However, the production under MPC has more small variation, whereas the production with PI controllers has slower dynamics.

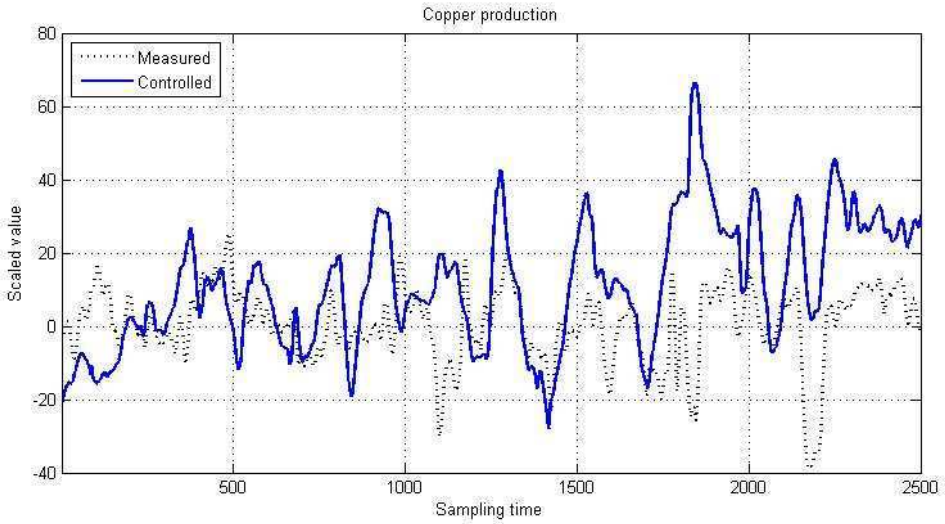

Figure 12-3: Copper production for the second test data set: industrial measurement (dotted) and PI controlled in the simulation environment (solid).

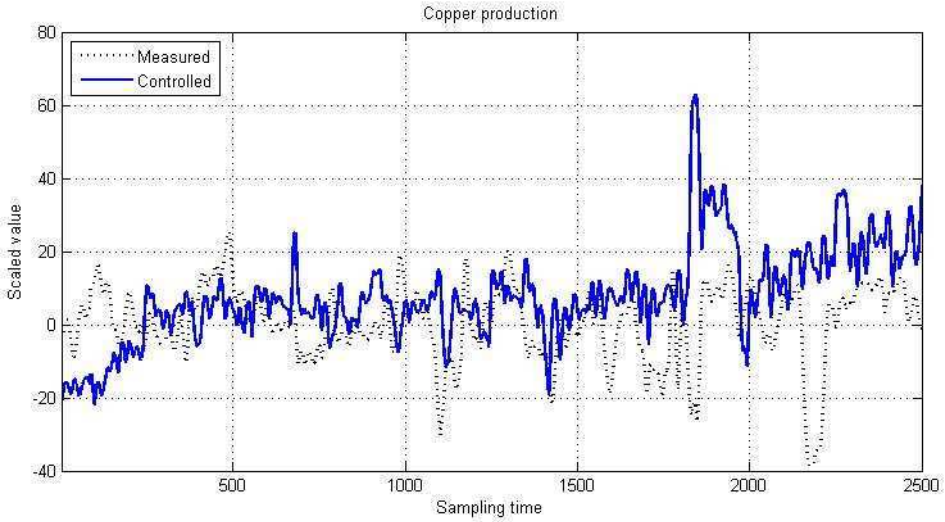

Figure 12-4: Copper production for the first test data set: industrial measurement (dotted) and MPC controlled in the simulation environment (solid).

12.3 Comparison of the process variation with different control strategies

The decrease in variation with the different control strategies for the loaded organic and rich electrolyte copper concentrations are presented in Section 12.3.1 and in Section 12.3.2.

12.3.1 Variation of the loaded organic copper concentration

The decrease in variation in the loaded organic copper concentration with the different control strategies is shown in Table 12-2. The PI controllers and MPC were almost as good at decreasing the average absolute error by about 71% for the first data set. Adding the feedforward compensators decreased the average absolute error between the measurement and the setpoint, especially for the PI control strategy, to 80%. For the second data set, both the PI controllers and MPC were almost as good at

decreasing the average absolute error by around 30-40% for the loaded organic copper concentration. Adding the feedforward compensators decreased the average absolute error for the PI control strategy to 38% for the loaded organic copper concentration.

Table 12-2: The variation decrease for the loaded organic copper concentration with the different control strategies compared to the manual control strategy.

	AAE c(LO) First test data set	**AAE c(LO) second test data set**
PI	-71.09%	-30.17%
PI+FF	-80.43%	-37.78%
MPC	-71.20%	-37.03%
MPC+FF	-73.49%	

For the first test data set, the PI controller with the feedforward compensators better tracks the setpoint for the loaded organic copper concentration, as shown in Figure 12-5, than the MPC with the feedforward compensator, as presented in Figure 12-6. The optimization for this data set reduces the setpoint of the loaded organic copper concentration to a lower level than the measurement, but the flow rate is higher and therefore more copper is transferred from the pregnant leach solution to the organic solution.

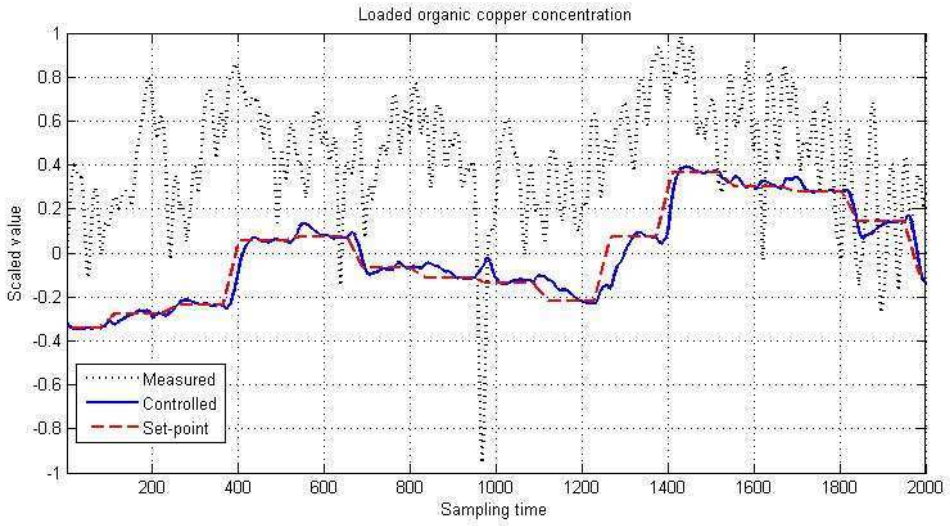

Figure 12-5: Loaded organic copper concentration for the first test data set: industrial measurement (dotted, black), PI+FF controlled in the simulation environment (solid, blue), and setpoint (red, dashed).

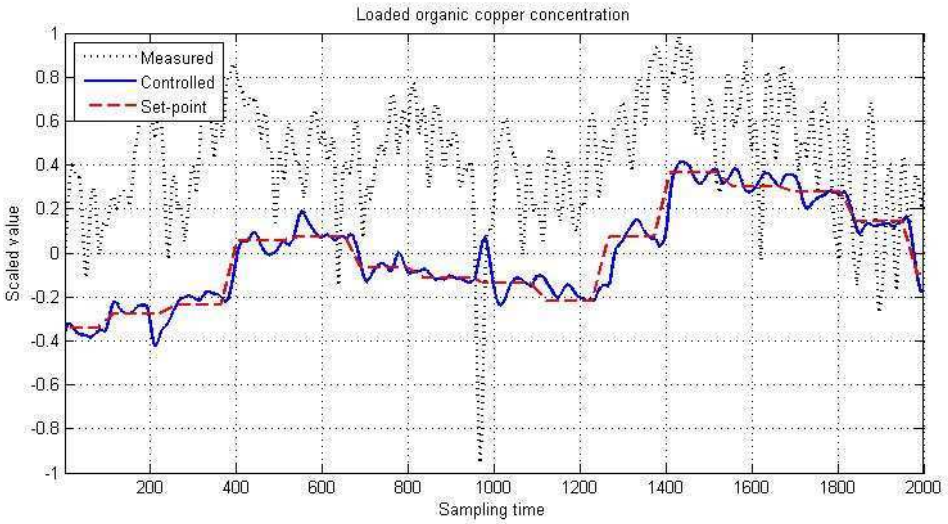

Figure 12-6: Loaded organic copper concentration for the first test data set: industrial measurement (dotted, black), MPC+FF controlled in the simulation environment (solid, blue), and setpoint (red, dashed).

For the second test data set, the setpoint tracking performance of both controllers are good for the loaded organic copper concentration, as illustrated for PI controllers in Figure 12-7 and for the MPC in Figure 12-8. The setpoint is slightly lower than the industrial measurement and the organic flow rate therefore higher in order to achieve higher copper extraction.

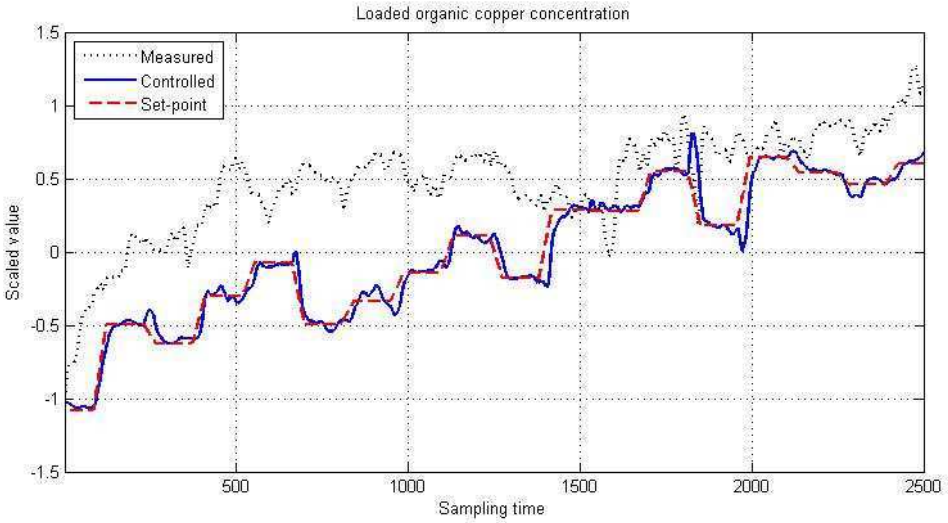

Figure 12-7: Loaded organic copper concentration for the second test data set: industrial measurement (dotted, black), PI controlled in the simulation environment (solid, blue), and setpoint (red, dashed).

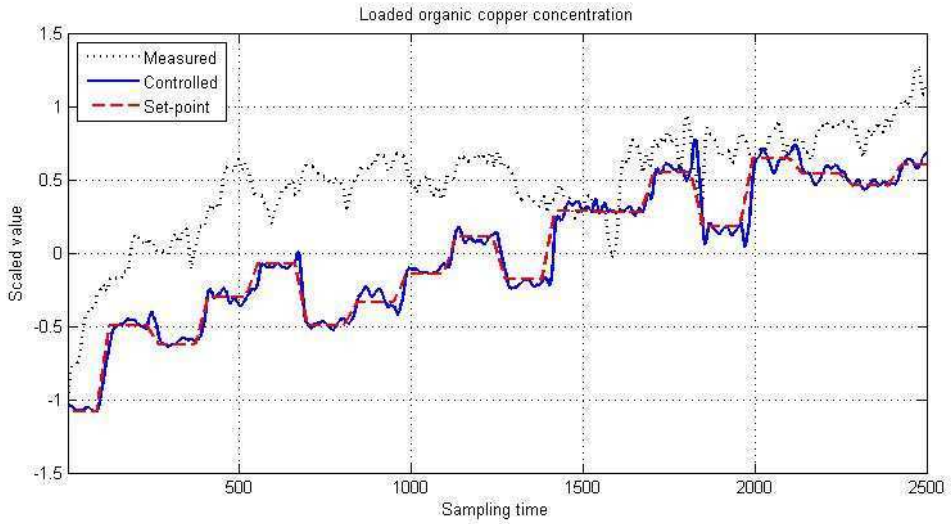

Figure 12-8: Loaded organic copper concentration for the second test data set: industrial measurement (dotted, black), MPC controlled in the simulation environment (solid, blue), and setpoint (red, dashed).

12.3.2 Variation of the rich electrolyte copper concentration

The decrease in variation in the rich electrolyte copper concentration with the different control strategies is shown in Table 12-3. The PI controllers and MPC are almost as good at decreasing the average absolute error by about 80% for both data sets. Within the first data set, adding the feedforward compensators decreases the average absolute error between the measurements and the setpoints, especially for the PI control strategy, up to 80%. Within the second data set, adding the feedforward compensators decreased the average absolute error for the PI control strategy to 80% for the rich electrolyte copper concentration.

Table 12-3: The variation decrease for the rich electrolyte copper concentration with the different control strategies compared to the manual control strategy.

	AAE c(RE) First test data set	**AAE c(RE) second test data set**
PI	-75.15%	-70.61%
PI+FF	-84.11%	-82.17%
MPC	-81.33%	-78.74%
MPC+FF	-91.75%	

For the first test data set, the setpoint tracking for the rich electrolyte copper concentration is more effective with the MPC with feedforward compensator, as shown in Figure 12-10, than with the PI controllers with feedforward compensators, as presented in Figure 12-9. The rich electrolyte copper concentration setpoint is higher than the measurement, but the flow rate is slightly lower.

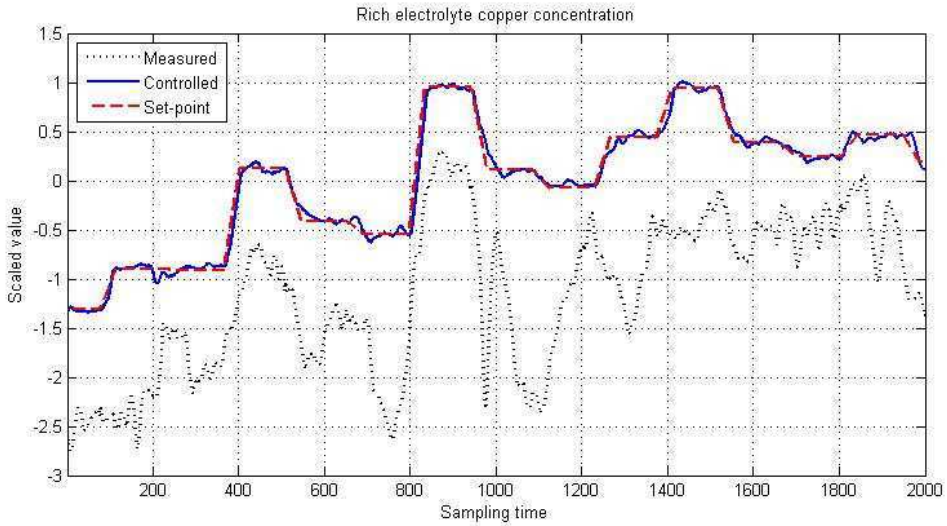

Figure 12-9: Rich electrolyte copper concentration for the first test data set: industrial measurement (dotted, black), PI+FF controlled in the simulation environment (solid, blue), and setpoint (red, dashed).

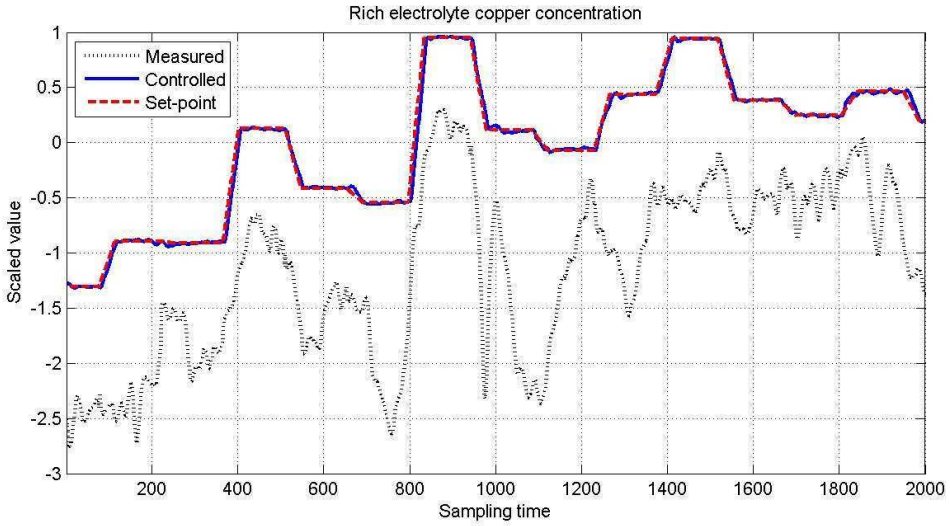

Figure 12-10: Rich electrolyte copper concentration for the first test data set: industrial measurement (dotted, black), MPC+FF controlled in the simulation environment (solid, blue), and setpoint (red, dashed).

For the second test data set, the rich electrolyte copper concentration setpoint tracking is successful with both controllers, as shown for PI controllers in Figure 12-11 and for MPC in Figure 12-12. The setpoint is almost at the same level as the measurement. For this data set, the maximum flow rate constraints restrict the increase in production.

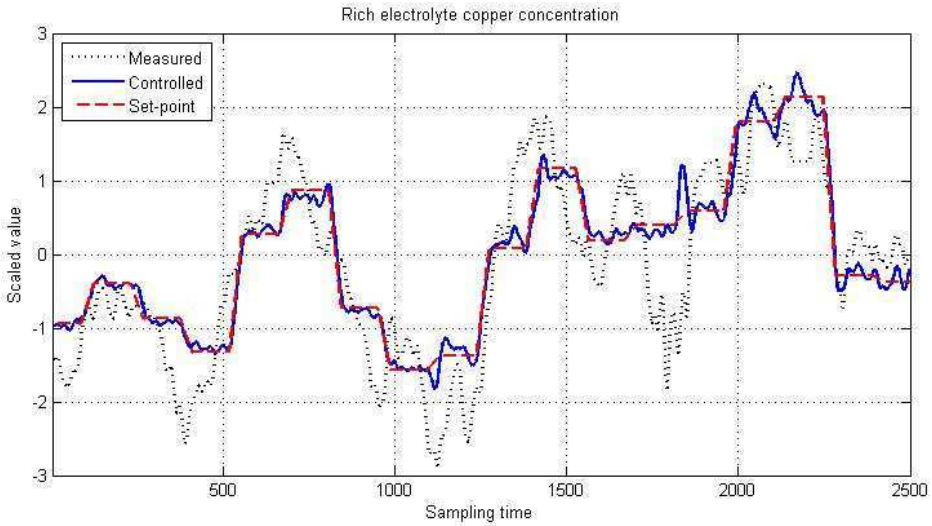

Figure 12-11: Rich electrolyte copper concentration for the second test data set: industrial measurement (dotted, black), PI controlled in the simulation environment (solid, blue), and setpoint (red).

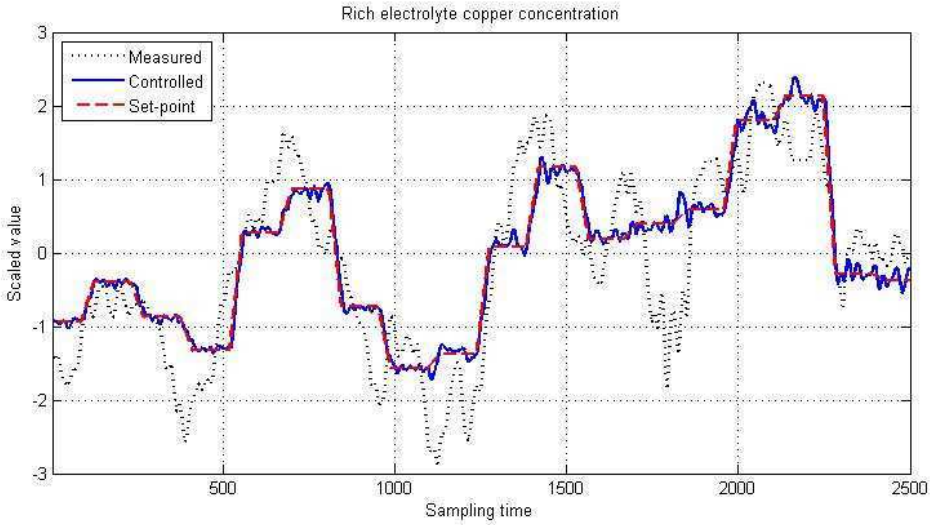

Figure 12-12: Rich electrolyte copper concentration for the second test data set: industrial measurement (dotted, black), MPC controlled in the simulation environment (solid, blue), and setpoint (red).

12.4 Concluding remarks

The control strategies were compared to the manual operating practice of the industrial copper solvent extraction plant. The production was raised by up to 5% for the first data set, and on the average by 3% for the second data set. The variation around the setpoints was decreased for the rich electrolyte copper concentration by 70 – 90%, and for the loaded organic copper concentration by between 30 – 80%. The performance increase was slightly higher with the MPC than with the PI controllers. Adding the feedforward controllers improved the setpoint tracking performance for the PI controllers especially.

The results could be improved by adding an electrowinning model that would provide more realistic lean electrolyte copper concentrations for the solvent extraction model. By stabilizing the rich electrolyte copper concentration, the lean electrolyte copper concentration would also have less variation and the production could be increased.

13 SUMMARY OF THE MODELING AND CONTROL RESULTS FOR THE COPPER SOLVENT EXTRACTION PROCESS

A mechanistic model has been developed to describe the dynamic behaviour of an industrial copper solvent extraction process. The model consists of a combination of steady state and dynamical models. The models consider only the mass transfer of copper, which is the main phenomenon in the industrially utilized mixer-settler equipment. The McCabe-Thiele diagram based approach was chosen for the equilibrium state model due to the availability of the required measurements and its wide industrial and academic acceptance. The dynamic models were based on modified ideal mixing and plug flow assumptions. The dynamic mixing models utilize the equilibrium state models to determine the equilibrium values.

The novelty of the modeling lies in the combination of these models. The mechanistic model framework is general, and can be extended to represent the behaviour of any industrial copper solvent extraction plant.

The mechanistic model structure was modified to represent the case process plant configuration and a process simulator was constructed. The model parameters were fitted to the offline data, which were assumed to represent the steady state of the process. Verification of the mechanistic models was carried out with two industrial online data sets. The different model structures were tested in the simulation environment, and the structure with the varied equilibrium and efficiency parameters was found to fit the industrial data the best.

For control development purposes, the mechanistic models were linearized around two operating points. The linear transfer function and state space models followed adequately well the trends in the industrial data sets. The single input-single output controllers were designed on the basis of the transfer function models. The linearized system was found to be observable and controllable. The controlled variable – manipulated variable pairing was performed using the relative gain array (RGA). The PI controllers were designed and tested for setpoint tracking and disturbance rejection at the two operating points with very successful results.

The model predictive control structure was chosen for the multi input - multi output controller due to its good time delay handling and popularity in a range of other industrial applications. The MPC was designed on the basis of the eight order state space model. The setpoint tracking and disturbance rejection performance of the model predictive controller was improved compared to that of the the PI controllers.

The controllers' performances were compared to the manual control practice in the simulation environment with two industrial data sets. The benefits of the control system were verified by comparing the variation in the controlled variables and the copper tonnes produced. An optimization algorithm was developed to give the setpoints for the SISO and MIMO controllers. With the PI controllers the variation in the rich electrolyte copper concentration was decreased by 70-80%, and with MPC the decrease was around 80 - 90% on the average. The copper mass production was increased by about 3-5% with both types of controllers.

14 CONCLUSIONS

Novel dynamic models and a novel simulation tool for the industrial copper solvent extraction process have been developed in this work. The models facilitate studies on the dynamic behaviour and development of control system for industrial copper solvent extraction plants. The model structure is divided into unit processes, and therefore can be easily modified to represent different plant configurations. With the dynamic models the cause and effect relationships of the process can be easily illustrated, and an understanding of the process principles taught. A simulator, based on the dynamic models, could be used as an operator's training tool and as a plant optimization tool.

The dynamic models are necessary for the development of a control system. In this work, two novel control strategies have been designed. The single input-single output and multi input – multi output control strategies on the stabilizing control level, and the optimization algorithm on the optimization level, were based on linearized process models. Due to the simple controller structures based on phenomenological process models, the control system should be easily accepted by industrial partners. Testing the control system in the simulation environment showed a significant increase in the performance and profitability of the operation. This greatly encourages the testing of the control system in an industrial plant.

In the future, the solvent extraction models could be extended by modeling the mixer as series of two or more mixing units and adding back-mixing models for the settlers. In most of the copper solvent extraction plants the mixer is series of two to three mixing units and this addition might increase the accuracy of the modeling. The settler time delays could be set to be time variant, and the model parameters could be estimated from the online measurements directly.

Since the operating data from industrial plants has often problems with accuracy/ non-existents of some measurements, it would be beneficial to use a pilot plant to collect data, especially online data of variables that in this study were available only offline. Thus, for further model development it is suggested to collect data from a well instrumented pilot plant under normal operating conditions in different operating points. Including online measurement copper concentrations, pH, acidity and reagent volume percent from all the unit processes of the plant would enhance the modeling as well as the control.

The dynamic solvent extraction model should be combined with a dynamic electrowinning model. This would enable even more realistic studies of the process chain behaviour, and enable real time optimization of a network of several solvent extraction and electrowinning processes. Since electrowinning is a more complicated process than solvent extraction, a simple approach, such as adaptive data based models, could provide the easiest basis for further modeling and control studies.

One critical issue in industrial copper solvent extraction plants is the control of the impurity level, for example of iron, manganese and chloride levels. Since an x-ray analyzer is also able to measure concentration of these species, the impurities could be added to the control system. Dynamic models that include the different mass transfer paths of each species should therefore be developed.

A ratio controller for the parallel and series PLS flow should be added to the control structure in order to optimize copper extraction from the total available PLS. If an

electrowinning model is added, a new control structure should be designed. For the combined model the electric current in electrowinning should be an additional manipulated variable. Model predictive control could be a convenient control algorithm for the combined system due to the good interaction and time delay handling properties. Application of nonlinear model predictive control could further enhance the control performance due to the ability to explicitly take into account the process nonlinearities. However, the performance of the nonlinear MPC algorithm should be compared to the performance of the linear MPC algorithm to justify the development and maintenance costs associated with industrial use of a more complex process model.

With the dynamic models, the simulation tool and the control system, a plant-wide operator support system can be developed and the performance and profitability of an industrial copper solvent extraction process significantly improved.

15 REFERENCES

Abdeltawab, A.A., Nii, S., Kawaizumi, F., and Takahashi, K. (2002), Separation of La and Ce with PC-88A by counter-current mixer-settler extraction column, *Separation and Purification Technology*, **26**, pp 265-272.

Aminian, H., Bazin, C., Hodouin, D., Jacob, C., (2000), Simulation of a SX-EW pilot plant, *Hydrometallurgy*, **56**, pp. 13-31.

Aminian, H., Bazin, C. (2000), Technical note solvent extraction equilibria in copper(II)-iron(III)-LIX984 system, *Minerals Engineering*, **13**, pp. 667 – 672.

Aminian, H., Bazin, C., Hodouin, D. (1998), Residence time distriburion in SX-EW equipment, *Int. J. Miner. Process.*, **54**, pp. 235-242.

Anon (2000), The Acorga Technical Library: The McCabe-Thiele Diagram And Theoretical Design Aspects For Solvent Extraction Plants, http://www.acorga.com/htdocs/pdf/mc.pdf, ref. 5.10.2006.

Aromaa, J. (1990), Hydrometallurgian perusteet – teoriaa ja prosessi esimerkkejä (fin), TKK-V-KORR-9, TKK OFFSET, Espoo, 134 pp.

Åström, K.J. and Wittenmark, B., *Computer-Controller Systems – Theory and Design*, 3rd Ed., Prentice Hall Inc., New Jersey, pp. 230 - 237 (557).

Bartos, P.J.(2002), SX-EW copper and the technology cycle, *Resources Policy*, **28**, pp. 85-94.

Bazin, C., Hodouin, D., Zouadi, M. (2005), Data reconciliation and equilibrium constant estimation: Application to copper solvent extraction, *Hydrometallurgy*, **80**, pp. 43-53.

Bergh, L.G., Lucic, E.M., and Zuleta, F. (2006), Supervisory control project of a copper solvent extraction pilot plant, *In: Proceedings of the IFAC workshop MMM'2006 – Automation in Mining, Mineral and Metal Industry*, (eds. Cierpisz, S., Miskiewicz, K., Heyduk, A.), Cracow, IFAC, pp.127-131.

Bergh, L.G., and Yianatos, J.B. (2001), Current Status and Limitations of Copper SX/EW Plants Control, *Minerals Engineering*, **14**, pp. 975 – 985.

Bergh, L.G., Jämsä-Jounela, S.-L., Hodouin, D., (2001) , State of the art in copper hydrometallurgic processes control, *Control Engineering Practice*, **9,** pp. 1007-1012.

Biswas, A.K., and Davenport, W.G. (1994), Extractive metallurgy of copper, 3rd ed., Pergamon, Oxford, pp. 500.

Camacho, E.F., Bordons, C. (1999), *Model Predictive Control*, Springer-Verlag, London 1999, pp. 280.

Doungdeethaveeratana, D. and Sohn, H.Y. (1998), Solvent extraction equilibria in the $CuSO_4$-H_2SO_4-H_2O-LIX860-kerosene system, *Minerals Engineering*, **11**, pp. 821-826.

Edelstein, D.L. (2004), Copper (in Minerals Year Book), http://minerals.usgs.gov/minerals/pubs/commodity/copper/coppemyb04.pdf , ref 13.11.2006.

Flintoff, B. (1993), Process control in hydrometallurgy, *In: Proceedings of the International Symposium on Modelling, Simulation and Control of Hydrometallurgical Processes*, (eds. V.G. Papangelakis, G.P. Demopoulos), Montreal, p. 175-190.

Galvez, E.D., Vega, C.A., Swaney, R.E., Cisternas, L.A. (2004), Design of solvent extraction circuit schemes, *Hydrometallurgy*, **74**, pp. 19–38.

Glad, T., and Ljung, L. (2000), *Control Theory, Multivariable and Nonlinear Methods*, Taylor & Francis, London, pp. 27, 219, 308 (467).

Habashi, F. (1999), The future of extractive metallurgy, *CIM Bulletin*, **92**, pp.161-165.

Hayes, P. (1993), *Process Principles in Minerals & Material Production*, Hayes Publishing co, Brisbane, 730pp.

Henson, M. A. (1998), Nonlinear model predictive control: current status and future derections, *Computers and Chemical Engineering*, **23**, pp. 187 – 202.

Hillier, F.S. and Lieberman, G.J. (2001), *Introduction to operations research*, 7th ed. McGraw-Hill, Boston, pp. 24-42 (1214).

Hodouin, D., Jämsä-Jounela, S. -L., Carvalho, M. T. and Bergh, L.(2001), State of the art and challenges in mineral processing control, *Control Engineering Practice*, **9**, pp. 995-1005

Hodouin, D., Bazin, C., Gagnon, E., and Flament, F. (2000), Feedforward-feedback predictive control of a simulated flotation bank, *Powder Technology*, **108**, pp. 173 – 179.

Hoh Y.C., Ju, S.J. and Chiu T.M. (1989), Effect of internal recycle on mixer-settler performance, Hydrometallurgy, 23, pp. 105-118.

Hughes, D., Saloheimo, K.(2000), On-stream analysis in copper SX-EW processes, *Preprints of the IFAC Workshop on Future Trends in Automation in Mineral and Metal Processing*, eds. S.-L. Jämsä-Jounela, E. Vapaavuori, Helsinki, pp. 361-366.

Hyvärinen, O., Hämäläinen, M. (2005), HydroCopper((TM)) - a new technology producing copper directly from concentrate, *Hydrometallurgy*, **77**, pp. 61-65.

Ingham, J., Dunn, I.J., Heinzle, E., Prenosil, J.E., (1994), *Chemical Engineering Dynamics - Modelling with PC Simulation*, VCH Verlagsgesellschaft mbH, Weinham, pp. 166 – 193 (701).

Jenkins, J., Davenport, W.G., Kennedy, B., Robinson, T., (1999), Electrolytic copper – leach, solvent extraction and electrowinning world operating data, In: *Proceedings of the Copper 99 – Cobre 99 International Conference – Volume IV*, (eds. Young, S.K., Dreisinger, D.B. Hackl, R.P. , Dixon D.G.), Phoenix, TMS, Warrendale, pp. 493-566.

Jämsä-Jounela, S.-L., (2001), Current status and future trends in the automation of mineral and metal processing, *Control Engineering Practice* **9**, pp. 1021-1035.

Katajainen, E., (1998), Multivariable correlation analysis of a solvent extraction process, Master's Thesis, Helsinki University of Technology, Espoo.

Komulainen, T., Doyle, F.J., Rantala, A., Jämsä-Jounela, S.-L (2007), Control of an industrial copper solvent extraction process, *Journal of Process Control, (submitted).*

Komulainen, T., Pekkala, P., Rantala, A., Jämsä-Jounela, S.-L (2006), Dynamic modelling of an industrial copper solvent extraction process. , *Hydrometallurgy*, **81**, pp. 52-61 .

Komulainen, T., Rantala, A., Jämsä-Jounela, S.-L. (2005), Dynamic modelling of an industrial copper solvent extraction process, *In: Proceedings of the 16th IFAC World Congress* (eds. Zítek, P.), Prague, IFAC, (CD).

Kordosky, G., Virnig, M., Boley, B. (2006), Equilibrium copper strip points as a function of temperature and other operating parameters: Implications for commercial copper solvent extraction plants, Tsinghua Science and Technology, 11, pp. 160-164.

Kordosky, G., (2002), Copper recovery using leach / solvent extraction / electrowinning technology: Forty years of innovation, 2.2 million tonnes of copper annually, *In: Proceedings of the International Solvent Extraction Conference*, Johannesburg, pp. 853-862.

Kordosky, G.A., Olafson, S., and Hahn, C. (2000), Iron Control Strategies in Copper Solvent Extraction Plants, The Case for Wash Stage, *In: Proceedings of ALTA Copper-6 Conference*, Perth Australia, ALTA Metallurgical Services, (CD).

Kordosky, G.A., Olafson, S.M., Lewis, R.G., and Deffner, V.L. (1987), A State of the Art Discussion on the Solvent Extraction reagents Used for the recovery of Copper from Dilute Sulfuric Acid Leach Solutions, *Separation science and technology*, **22**, pp. 215 – 232.

Kreyzig, E. (1999), *Advanced Engineering Mathematics*, 8th ed., John Wiley & Sons Inc., New York, pp.994-1001 (1156).

Ljung, L. 2006, *System Identification Toolbox for use with Matlab – User's Guide*, 6th ed., http://www.mathworks.com/access/helpdesk/help/pdf_doc/ident/ident.pdf, The MathWorks Inc., p. 228.

Ljung, L. (1987), *System Identification, Prentice-Hall*, Inc., New Jersey, p. 519.

Maciejowski, J.M., (2002), *Predictive control with constraints*, Prentice Hall, Harlow, England, pp. 352.

MathWorks, (2006), Signal processing toolbox for use with Matlab – User's Guide, 6th ed., http://www.mathworks.com/access/helpdesk/help/pdf_doc/signal/signal_tb.pdf , The MathWorks Inc., pp. 271 (683).

Mayne, D.Q., Rawlings, J.B., Rao, C.V., Scokaert, P.O.M. (2000), Constrained model predictive control: Stability and optimality, *Automatica*, **36**, pp. 789 – 814.

McCabe, W.L., Smith, J.C., Harriot, P. (1993), Unit operations of chemical engineering, 5th Ed., McGraw-Hill Inc., New York, pp. 623-638 (1130).

Mills, A.L. (1983), *Computation and modeling techniques In*: *Handbook of solvent extraction*, (Eds. Lo, T.C., Baird, M.H.I., Hanson, C.), Wiley & Sons, New York, pp.841 – 852.

Mooiman, M.B, Sole, K.C., Kinneberg, D.J. (2005), Challenging the traditional hydrometallurgy curriculum – an industry perspective, *Hydrometallurgy*, **79**, pp. 80 – 88.

Morari, M., Lee, J.H. (1999), Model predictive control: past, present and future, *Computers and Chemical Engineering*, **23**, pp. 667 – 682.

Moskalyk, R.R., and Alfantazi, A.M. (2003), Review of copper pyrometallurgical practice: today and tomorrow, *Minerals Engineering*, **16**, pp. 893-919.

Munnik, E, Singh, H., Uys, T., Bellino, M., du Plessis, J., Fraser, K. and Harris, G.B. (2003), Development and implementation of a novel pressure leach process for the recovery of cobalt and copper at Chambishi Zambia, *The Journal of The South African Institute of Mining and Metallurgy*, **103**, pp. 1-10.

Nishihama, S., Hirai, T., Komasawa, I. (2003), Advanced liquid-liquid extraction systems for the separation of rare earth ions by combination of conversion of the metal species with chemical reaction, *Journal of Solid State Chemistry*, **171**, pp. 101-108.

Norton, G.A. and Leahy, P.P. (2006), Mineral Commodity Summaries, http://minerals.usgs.gov/minerals/pubs/mcs/2006/mcs2006.pdf , United States Government Printing Office, Washington, pp. 56-57 (202).

Nunez, E., Desbiens, A., del Villar, R. and Duchesne, C. (2006), Multivariable predictive control of a pilot flotation column: Part2: Identification and control, In: Proceedings of Mineral process modeling, simulation and control, pp. 291 – 301.

Nyman, B., Ekman, E., Kuusisto, R. and Pekkala, P., (2003) *The OutoCompact SX Approach to Copper Solvent Extraction*, JOM, pp. 27 – 30.

Ogata, K. (1987), *Discrete-time control systems*, Prentice Hall Inc., New Jersey, pp. 625-646 (984).

Ogunnaike, B.A. (1994), *Process Dynamics, Modeling and Control*, Oxford University Press Inc., New York, pp. 728 – 765 (1260).

Orfanidis, S.J. (1990), *Optimum signal processing*, 2nd ed., McGraw Hill, New York, pp. 30 – 33 (590).

Pinto, G.A., Durao, F.O., Fiuza, A.M.A., Guimaraes, M.M.B.L., Madureira, C.M.N. (2004), Design optimisation study of solvent extraction: chemical reaction,mass transfer and mixer–settler hydrodynamics, *Hydrometallurgy*, **74**, pp.131–147.

Qin S.J., Badgwell, T.A. (2003), A survey of industrial model predictive control technology, *Control engineering practice*, **11**, pp. 733-764.

Rawlings, J.B. (2000), Tutorial overview of model predictive control, *IEEE Control Systems Magazine*, **20**, pp.38-52.

Ray, W.H. (1989), Advanced Process Control, Butterworth Publishers, Boston, pp. 28-30 (376).

Ray, H.S., Sridhar, R., Abraham, K.P (1985), *Extraction of Nonferrous Metals*, Affiliated East-West Press Private Ltd, New Delhi, pp. 531.

Ritcey, G.M. (2002), Some design and operating problems encountered in solvent extraction plants, In: Proceedings of the International Solvent Extraction Conference, ISEC 2002 (eds. Sole, K.C., Cole, P.M., Preston, J.S. and Robinson, D.J.), Johannesburg, South Africal Institute of Mining and Metallurgy, pp. 871- 878.

Ritcey, G.M., Ashbrook, A.W. (1998), *Hydrometallurgical Extraction, In: Handbook of Separation Techniques for Chemical Engineers*, 2nd ed., (Ed. Schweitzer, P.A.), McGraw-Hill Inc. New York, pp.2-105 – 2-130.

Robbins, L.A. (1984), *Liquid-Liquid Extraction, In: Perry's Chemical Engineers Handbook*, 6th ed. (Eds. Perry, R.H., Green, D.W., and Maloney, J.O.), McGraw-Hill Inc, New York, pp. 15-1 – 15-20.

Robinson T, Sandoval S, Cook, P (2003), World copper solvent extraction plants: Practices and design, *JOM*, **55**, pp. A24-A26.

Rydberg, J., Musikas, C., Choppin, G.R., *Solvent extraction principles and practice*, M. Dekker, New York,2004, 584 p.

Saarenpää, T. (1992), Kuparin liuotus-uutto-elektrowinning-laitoksen mellitus (fin), Master's Thesis, Helsinki University of Technology, Espoo, p. 64.

Salem, A.B. and Sheirah, M.A. (1990), Dynamic Behavior of mixer-settlers, *The Canadian Journal of Chemical Engineering*, **68**, pp. 867 – 875.

Seborg, D. E., Edgar, T.F., Mellichamp, D. A. (2004), *Process Dynamics and Control*, 2nd ed., John Wiley & Sons Inc, pp. 713.

G.W.Seward (1999), The Acorga Technical Library: A Review of Leaching Technologies available to Process Copper Sulfide Concentrates, http://www.acorga.com/htdocs/pdf/process.copper.pdf , ref. 5.10.2006.

Söderström, T. and Stoica, P. (1989), System Identification, Prentice-Hall Inc, New York, p. 612.

Sole, K.C., Feather, A.M., Cole, P.M. (2005), Solvent extraction in southern Africa: An update of some recent hydrometallurgical developments, *Hydrometallurgy*, **78**, pp. 52-78.

Steiner, L. and Hartland, S. (1983), *Unsteady-state extraction In*: *Handbook of solvent extraction*, (Eds. Lo, T.C., Baird, M.H.I., Hanson, C.), Wiley & Sons, New York, pp.249 – 264.

Suontaka, V.; Rantala, A.; Jämsä-Jounela, S.-L., (2004),A Process Monitoring System for Copper Solvent Extraction, *In: Proceedings of the 11th IFAC Symposium on automation in mining, mineral and metal processing*, (ed. Sauter, D.), Nancy, IFAC, pp. .

Suontaka, V., Saloheimo, K., Marttila, T., Jämsä-Jounela, S.-L. (2003), A monitoring system for copper solvent extraction – electrowinning process, In: Proceedings of IFAC Workshop on New Technologies for Automation of Metallurgical Industry (ed. Wei Wang), Shanghai, IFAC, pp. 305-310.

Skogestad, S., Postlethwaite, I. (2005), Multivariable Feedback Control - Analysis and Design, 2nd, John Wiley & Sons, Chichester, p. 608.

Tetlow, Peter (2003), Crud Formation and Techniques for Crud Control, *Acorga Notes*, **9**, pp. 5 – 7.]

Vancas, M.F. (2003), Pulsed Column and Mixer-Settler Applications in Solvent Extraction, *JOM*, **55**, A43-A45.

Virnig, M.J. and Olafson, S.M. (2002), Improved Iron Scrubbing with a Wash Stage, *In: Proceedings of ALTA Copper-7 Conference*, Perth, ALTA Metallurgical Services, (CD).

Whyte, R.M., Schoeman, N. and Bowes, K.G. (2001), Processing of Konkola copper concentrates and Chingola refractory ore in a fully integrated hydrometallurgical pilot plant circuit, *The Journal of The South African Institute of Mining and Metallurgy*, **101**, pp. 427-436.

Wichterlová, J. and Rod, V. (1999), Dynamic behaviour of the mixer-settler cascade. Extractive separation of the rare earths, *Journal of Chemical Engineering Sciences*, **54**, pp. 4041 – 4051.

Wilkinson, W.L., Ingham, J. (1983), Dynamic Behaviour and Control, In: *Handbook of Solvent Extraction*, (Eds. Lo, T.C., Baird, M.H.I., Hanson, C.), Wiley & Sons, New York, pp.853 – 886.

ISBN 978-951-22-9055-0
ISBN 978-951-22-9056-7 (PDF)
ISSN 1795-2239
ISSN 1795-4584 (PDF)